BIOSTRUCTURES AS COMPOSITE MATERIALS

PROCEEDINGS OF ARO WORKSHOP

OCTOBER 23-25, 1989

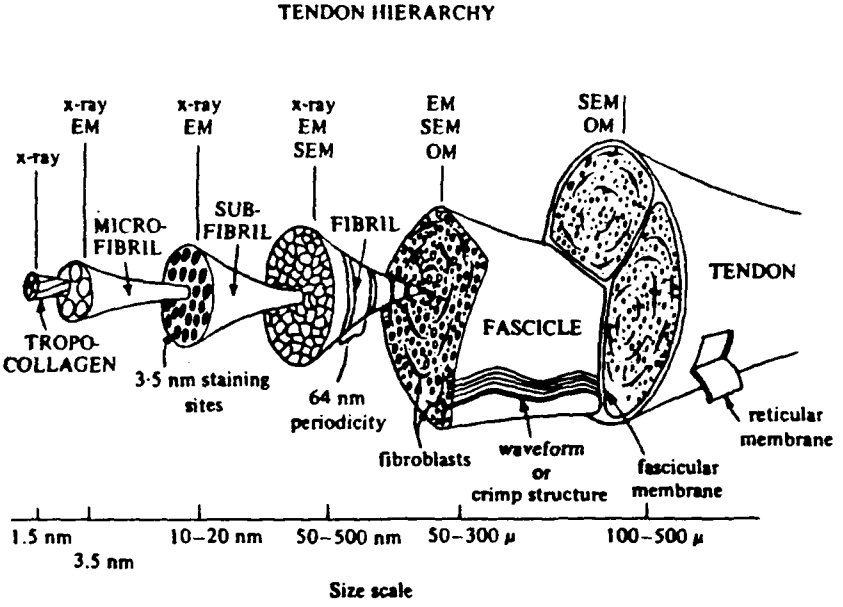

HELD AT

DEPARTMENT OF MACROMOLECULAR SCIENCE AND
CENTER FOR APPLIED POLYMER RESEARCH
CASE WESTERN RESERVE UNIVERSITY
CLEVELAND, OHIO 44106

UNCLASSIFIED
SECURITY CLASSIFICATION OF THIS PAGE

MASTER COPY - FOR REPRODUCTION PURPOSES

REPORT DOCUMENTATION PAGE

1a. REPORT SECURITY CLASSIFICATION Unclassified	1b. RESTRICTIVE MARKINGS
2a. SECURITY CLASSIFICATION AUTHORITY	3. DISTRIBUTION/AVAILABILITY OF REPORT Approved for public release; distribution unlimited.
2b. DECLASSIFICATION/DOWNGRADING SCHEDULE	
4. PERFORMING ORGANIZATION REPORT NUMBER(S)	5. MONITORING ORGANIZATION REPORT NUMBER(S) ARO 26892.1-MS-CF
6a. NAME OF PERFORMING ORGANIZATION Case-Western Reserve U 6b. OFFICE SYMBOL (If applicable)	7a. NAME OF MONITORING ORGANIZATION U. S. Army Research Office
6c. ADDRESS (City, State, and ZIP Code) Cleveland, Ohio 44106	7b. ADDRESS (City, State, and ZIP Code) P. O. Box 12211 Research Triangle Park, NC 27709-2211
8a. NAME OF FUNDING/SPONSORING ORGANIZATION U. S. Army Research Office 8b. OFFICE SYMBOL (If applicable)	9. PROCUREMENT INSTRUMENT IDENTIFICATION NUMBER DAAL03-89-G-0075
8c. ADDRESS (City, State, and ZIP Code) P. O. Box 12211 Research Triangle Park, NC 27709-2211	10. SOURCE OF FUNDING NUMBERS PROGRAM ELEMENT NO. / PROJECT NO. / TASK NO. / WORK UNIT ACCESSION NO.

11. TITLE (Include Security Classification)
Biostructures as Composite Materials

12. PERSONAL AUTHOR(S)
Eric Baer and Igbal Ahmad

13a. TYPE OF REPORT	13b. TIME COVERED	14. DATE OF REPORT (Year, Month, Day)	15. PAGE COUNT
Final	FROM 6/1/89 TO 5/31/90	March 1990	196

16. SUPPLEMENTARY NOTATION
The view, opinions and/or findings contained in this report are those of the author(s) and should not be construed as an official Department of the Army position, policy, or decision, unless so designated by other documentation.

17. COSATI CODES		
FIELD	GROUP	SUB-GROUP

18. SUBJECT TERMS (Continue on reverse if necessary and identify by block number)
Workshop; Biostructures; Composite Materials; Biomechanics; Biophysics; Materials (KT)

19. ABSTRACT (Continue on reverse if necessary and identify by block number)

Realizing the opportunities that the studies of biosystems can offer to materials scientists and engineers, and the general lack of communication between the materials scientists and the biologists, the Army Research Office organized this workshop in which active workers in the field of biomechanics and biophysics as well as materials scientists participated. The focus was on the hierarchical structures in biosystems. In addition to identifying the fundamental structural design-property relationships all the way from molecular to the engineering systems scale, participants recommended a number of areas for future research necessary to develop radically new materials and systems, in which the design principles used in nature can be utilized and perhaps even mimicked.

Raymond

20. DISTRIBUTION/AVAILABILITY OF ABSTRACT	21. ABSTRACT SECURITY CLASSIFICATION
☐ UNCLASSIFIED/UNLIMITED ☐ SAME AS RPT. ☐ DTIC USERS	Unclassified
22a. NAME OF RESPONSIBLE INDIVIDUAL	22b. TELEPHONE (Include Area Code) / 22c. OFFICE SYMBOL

DD FORM 1473, 84 MAR — 83 APR edition may be used until exhausted. All other editions are obsolete.

SECURITY CLASSIFICATION OF THIS PAGE
UNCLASSIFIED

BIOSTRUCTURES AS COMPOSITE MATERIALS

PROCEEDINGS OF ARO WORKSHOP

PROFESSOR ERIC BAER, CWRU AND DR. IGBAL AHMAD, ARO
CO-CHAIRMEN

HELD AT

CASE WESTERN RESERVE UNIVERSITY
DEPARTMENT OF MACROMOLECULAR SCIENCE AND CENTER FOR
APPLIED POLYMER RESEARCH
CLEVELAND, OHIO 44106

ON

OCTOBER 23-25, 1989

Sponsored by

U.S. Army Research Office
P.O. Box 12211
Research Triangle Park, NC 27709-2211

March 1990

TABLE OF CONTENTS

ABSTRACTS

FORWARD

During the last 20-30 years, materials science and technology have made quantum jumps in terms of developing not only superior and novel bulk materials including numerous polymers, ceramics and metallic alloys, but also designing structures both on micro and macro scale, in which heterogeneous materials are combined in a synergistic manner to achieve desirable properties. Some of these materials, for example high strength fiber reinforced polymers, have been developed to a stage where they represent a major industrial product and have been effectively used in both critical and non critical applications. Similar but less spectacular progress has been made in the case of metal matrix and ceramic matrix composites. Currently new concepts of design, fabrication and quality control of these materials to achieve specific performance capabilities, such as those required for light weight aerodynamically stable aircraft, energy efficient ground vehicles, seacraft, and for numerous civilian and military systems, are being developed by materials scientists and engineers. For these applications specific stiffness and yield strength, and fracture toughness are some of the basic properties sought. In other applications, properties such as thermal expansion coefficients, thermal and electrical conductivity, magnetic field strength, acoustic impedance, various electro-optical characteristics etc,. are the goals of the materials engineering.

On the other hand the biologists and the biophysicists have made spectacular progress in determining the structure of biosystems, including animal and plant kingdoms, and elucidating the mechanisms involved in some of the biological processes of their growth, repair and physiomechanical functions. These studies show conclusively that the principles of materials selection and the interaction of materials in complex systems that are capable of performing highly efficient useful work are

extremely advanced in nature. In comparison, the state of the art of the science and technology of materials, and the design of structural and functional systems, is almost primitive. The scientific community must now look into the biosystems to discover new concepts and principles to develop advanced materials and systems needed by mankind in the next century and beyond.

Realizing the opportunities that the studies of such biosystems can offer to materials scientists and engineers, and the general lack of communication between the materials scientists and the biologists, the Army Research Office organized this workshop in which active workers in the field of biomechanics and biophysics as well as materials scientists participated. The focus was on the hierarchical structures in biosystems. In addition to identifying the fundamental structural design-property relationships all the way from molecular to the engineering systems scale, participants recommended a number of areas for future research necessary to develop radically new materials and systems, in which the design principles used in nature can be utilized and perhaps even mimicked.

The workshop was very informal in structure and spirit. Therefore the speakers were required to submit only the extended abstracts which have been collected in this volume. A very large majority of the attendees were highly complimentary about the objectives, scope and the material presented at the workshop, and expressed the need of a follow on meeting. It was therefore decided to organize a second workshop on the same theme after about two years. For that workshop speakers will be required to submit manuscripts of their papers in advance for the purpose of a proceedings volume.

SUMMARY AND CONCLUSIONS

Dean Katz opened the workshop and enthusiastically suggested that the lessons learned from biocomposites would point to future directions for new materials systems. Four main topics were addressed at the workshop, namely: soft connective tissues, hard connective tissues and impact resistant structures, molecular self assembly, and biomimetics. Dr. Wainwright in his opening speech reviewed the collagen based structural systems, particularly the skin and muscles of sea mammals. These components are composed of essentially collagen and highly hydrated glycosaminoglycans (GAG) in ionic fluids. The molecular orientation in collagen fibrils and subsequent hierarchy of the fibrils and charge distribution provide these systems the capability of locomotion. Some of the examples of the locomotor systems given included muscular action during swimming of shark, whale and sea urchins. Dr. Wainwright emphasized the need of enhanced research activity to gain deeper understanding of the mechanisms involved in the control of charge densities in biostructures.

Drs. Baer and Hiltner described results of their ongoing studies on the structure of tendons and intervertebral discs. They demonstrated that the hierarchical structure of tendon was designed to accommodate uniaxial tensile loads. The stress-strain curves show initial increase in modulus representing gradual straightening of the wave form in the collagen fibrils. This was followed by a linear elastic region representing reversible extension of collagen. In the yield region, the fibrils experience damage because of the slippage of tropocollagen units and permanent dissociation between microfibrils byshear/slip. The fibril organization in the intervertebral disc is characterized by structural

gradients, in which alternate lamella fribrils are inclined with respect to the vertical axis of the spine. From the edge of the disc inwards to the nucleus, the lamellar angle decreases from 62º to 45º. The fibril crimp angle, on the other hand increases from 20º to 45º. This structure combined with a water transport mechanism provides the system with excellent compression, impact, creep and relaxation properties, necessary for the multifunctional performance of the spine. Professor Baer also presented a discussion on the common features of complexity which play important roles in the evolution of hierarchical structures in biosystems. He suggested three rules: 1) all biosystems are organized and involve transitions from one scale or level to the next, 2) they have compatible interactive surfaces and interfaces, and 3) the more complex a structure or architecture, the more adaptable the system becomes.

Dr. Farrel described the structure and functions of the cornea of the eye. To the amazement of many in the audience, he showed that the cornea was not homogeneous, but was composed of orientd of fibers which were thinner than one half the wave length of visible light which made them transparent with minimum dispersion.

On the subject of hard tissues, Dr. Bonfield discussed the structural organization in cortical bone. Hydroxyapatite crystallites, which reinforce collagen, are the building block of cortical bone at the nano scale level. The structural organization at the micro and macro level gives the bone the strength and the extraordinary toughness. The piezoelectric response of the bone and tendon was the topic of Dr. William's presentation in which he explained the phenomenon of electro - mechanical transduction and its significance in the maintenance and repair of tissues. Since living bone is immersed in a flowing

ionic fluid, it was suggested that streaming was responsible for the stress induced potential in wet biological tissues.

Functional adaptation is the term used to describe the ability of organisms to increase their performance capacity according to the demand. Living bone is continually undergoing the process of growth, reinforcement and reabsorption. These processes are collectively termed as remodeling. Dr. Cowan discussed the mechanisms of both the external and internal remodeling of bone, which involve changing in the bulk density and internal trabacular structure of the tissue. He presented two models for the stress adaptation process in which bone matrix (solid extracellular material plus bone cells) is modeled as a solid structure with interconnected pores; in other words a porous linear elastic solid. The extracellular fluid and blood are modeled as a single fluid. The rate of remodelling, depending on the strain, is of the order of months.

Dr. Curry presented the relationships of the structure and impact resistance of invertebrate mineralized biosystems, including mollusc shell, crab, cuticles, sea urchins, etc. He stated that in the biosystems, there was no provision for resistance to high velocity impacts. He described how the different arrangements of the plateletes of calcium carbonate or calcium phosphate with a thin interface of acidic macromolecular matter, provided mechanisms for crack deflection with great efficiency, making these systems tough, rigid and resilient. These concepts are slowly being developed to fabricate stiff composite systems with very high fracture toughness.

Dr. McElhaney explained how the boney skeleton provided a stiff framework for a variety of functions including anchoring of soft tissues, protection of soft organs from impact and other external forces. Scalp and skull offer significant protection to the brain. Rib cage protects the heart and lungs

and vertebrae protect the spinal cord. The most important demand for such structures, in addition to structural requirements, is the lightest weight possible. Dr. McElhaney described the structure of the skull in which these requirements are very well met by the design nature has used. Skull bones are composed of an inner and outer table of compact bones separated by a core of cancellous bone. The compact bone surrounds and reinforces the structure. Due to this sandwich structure, skull bone is well suited to dissipate energy in an impact through crushing of the diploe. He presented results of his study of correlations of mechanical properties with density, and the variation in the distribution of the trabacular from section to section.

Motivated by the continued interest of the Air Force in developing stronger, stiffer and lighter structures, Dr. Anderson has studied the arrangement of components of the insect cuticle of Bessburg beetle, which appear to have design requirements similar to those of some aircraft structures. SEM examination of leg, pronotum and elytra revealed that the procuticle structures were composed of layers of chitin fibers held together by a fibrous matrix. The orientation, diameter and cross-section of the fibers varied in the structures in a regular fashion. Some of the concepts emanating from this study are being validated by fabricating carbon fiber-epoxy composites with similar layups and evaluating their mechanical behavior.

Dr. Gibson summarized some of her work in the general area of the cellular structures including cork and cancellous bone. She has coauthored a book with Dr. Ashby on this subject. She stated that the compressive stress-strain curves of all the systems were similar, in that a linear elastic region followed by a stress plateau which terminated in a final sharp increase in stress at large strains. She described models and mechanical properties of honeycombs, wood and

cancellous bone, and presented energy absorption diagrams which plot the energy absorbed per unit volume against peak stress generated in an impact.

In the area of molecular self assembly, in three very interesting papers, mechanisms of evolution of collagen fibrils in biosystems were highlighted. Most of the current knowledge of assembly of proteins into fibrous structure has been gained from studies, in vitro, starting from solutions containing 'precursor' macromolecules. However, the processes in the in vivo situation, in which organization of the cell is also involved, are quite different. Dr. Veiss explained the mechanisms involved in both the intercellular assembly of actin filaments from globular actin molecules and the extracellular assembly of collagen fibrils from molecules secreted in precursor form with amino and carboxyl propeptides. In the latter case, the assembly of the fibrils depend on the cleavage of these propeptides, and the specific interactions related to correct orientation of the collagen within the filaments. Dr. Wallace discussed a quantitative model for fibril assembly of type I collagen. This model took into consideration the effects of extra-helical peptides of type I which were ignored in Flory's model of rigid rod polymers. He showed that the theoretical kinetics derived from his model agreed with the experimental results.

DOD has special interest in the development of superior prosthetic components, high strength organic fibers and impact resistant structures. Reconstitution of collagen I into prosthetic tendon, nerve conduit materials and duramater was the topic of Dr. Silver's presentation. He reported successful implantation of collagen prostheses in rabbit Achilles tendon and skull and rat sciatic nerve. Insoluble type I collagen from bovine hide was purified and reconstituted into fibers about 50 microns in diameter, which were either formed into a tow containing 250 parallel fibers (coated with collagen dispersion)

to be used as tendon prosthesis, or packed into a silicone tube (0.2 mm in diameter) for nerve prosthesis. Collagen dispersions were air dried to form a membrane 100 micron thick for duramater replacement. Dr. Kaplan briefly described some of the on going work on the characterization of spider silk, sequencing, cloning and conformational energy calculations. At Natick Labs, according to Dr. Kaplan, chitsan has been produced directly from the fungus mucor rouxii, through fermentation controls. Current efforts are addressed towards the characterization of the two key biosynthetic enzymes, namely chitin synthetase and chitin deacetylase, prior to cloning.

Dr. Thurbrikar discussed the structure and function of aortic valve which consists of three sinuses and three leaflets. The sinus wall is composed primarily of collagen, elastin and smooth muscle cells. Consequently the sinuses can expand and contract. The leaflets are thin sheets of connective tissue with dense collagen cords running parallel to the circumferential direction. This alignment makes the leaflet anisotropic. From his studies on the aortic valves of a number of animals, Dr. Thurbrikar identified the following criteria of an ideal valve: minimum valve height, minimum leaflet flexion, a prescribed leaflet coaptation and no leaflet folds. He suggested a research program to identify a suitable polymeric composite material system with appropriate biocompatibility and viscoelastic behavior, and then develop techniques to fabricate and test prototypes designed through computer aided simulation.

Giving the example of prosthetic structure to replace a section of diseased artery, Dr. Kardos emphasized that the substitute material must be compliant, capable of being reinforced anisotropically and resistant to creep under static and dynamic loading. Other requirements include non-thrombogenic and thermal and

mechanical compatibility with the section of the artery to which it would be attached.

Dr. Aksay expounded on the concept of biomimicking. He described the structure of the abalone shell, which is composed of an outer prismatic layer and an inner nacreous layer. Two types of calcium carbonates, calcite (rhombohedral; R3c) and aragonite (orthorhombic Pmnc) constitute the inorganic component of the organic-inorganic composite in prismatic and nacereous layers, respectively. He reported 180 MPa and 7.0 MPa $m^{1/2}$ for the fracture strength and fracture toughness of the nacreous layer. The high value of fracture toughness was explained to be due to efficient crack blunting, branching and deflection, and a layer pull out mechanisms provided by the unique design of the composite structure. Cracks tend to advance predominantly in the organic layers, involving sliding of calcium carbonate layers and bridging of the organic ligaments. He then described his studies of mimicking of this structure in a boron carbide-aluminum cermet laminated composite. This composite has a layer thickness of 10 micron. Even then it showed a 30% increase over the fracture toughness of conventional composite. Further improvement in both strength and fracture toughness is expected with decrease in constituent layer thickness.

More advanced structures in nature are essentially three dimensional. Dr. Ko has developed in his laboratory excellent capabilities of fabricating 3D composites. He described the braiding technique for the fabrication of 3D composites and the relationship of the fiber orientation with their mechanical properties. He demonstrated that the 3D composites exhibited much greater energy absorption than the laminates. Hence they are excellent candidates for impact resistant structures.

At the end of each session there was a general discussion of issues and research opportunities. Also during the workshop three subcommittees were established with the task of formulating some recommendation for future research in the light of the work presented by various speakers. The short reports submitted by each subcommittee are given in Appendix I. In the following some of the important conclusions and recommendations are summarized.

1. Characterization of the structure property relationships in biosystems: Elucidation of the hierarchical structure, architecture, and design principles involved for various functions in selected biosystems is an important area expected to yield exciting new concepts of materials design and engineering. In addition to the mechanical behavior, these studies should be expanded to include optical, electrical, thermal, transport, and acoustic properties.
2. Biomineralization: Understanding the mechanisms of biomineralization and the behavior of biological tissues containing inorganic contents, is needed to identify techniques for remodelling, repair and developing adaptive structures. These studies offer opportunities to meet needs of the DOD for repair of damage of biosystems, as well as civilian applications in health industry.
3. Biological systems in unusual environments: A number of unique biological systems have evolved that are capable of operating in unusual environments, such as extremely low and high temperatures, high pressures, electrical and magnetic fields, low/high gravity and a variety of chemical conditions. The structure and mechanisms of operation of such systems are unique, and must be explored.

4. Design of artificial materials: The object of mimicking biological materials with synthetic systems is duplication or enhancement of the performance of the natural material. This area includes prosthetics, for which some of the important areas of studies include developing special materials including composites, adhesives, coatings, and sensors.
5. Smart Materials: Biological systems are considered "smart", as they carry within them templates necessary to synthesize their constituent parts and assemble them in a manner that the system continues to perform its functions. Biostructures are also capable of remodelling in response to the alteration of the environments, and can repair some types of damage inflicted upon them. This ability to locally or globally change properties and response is of great interest. Similarly within biological constituents, there are several types of molecular structures, such as proteins, which have intrinsic capability of sensing, response and control. Study of such materials can lead to design concepts for the synthesis of novel "smart" materials and systems.
6. In view of the importance of the areas of future research as indicated above, the participants of the workshop, unanimously recommended that a follow up workshop should be held after about two years, to review the advances made in this exciting field. ARO is expected to sponsor that workshop in 1991.

BIO-STRUCTURES AS COMPOSITE MATERIALS SYSTEMS

Program

MONDAY, OCTOBER 23, 1989

8:30 a.m. Registration, Room 13 - Crawford Bldg.

9:15 a.m. Welcome - L. Katz, Dean of Engineering
E. Baer, Chairman
I. Ahmad, ARO

Session I: **CONNECTIVE TISSUES,**
J. Blackwell, Moderator, CWRU

9:30 a.m. **MULTIDIMENSIONAL COLLAGEN SYSTEMS,**
S. Wainwright, Duke University

10:15 a.m. **HIERARCHICAL STRUCTURE OF TENDON,**
E. Baer, CWRU

11:00 a.m. Break

11:15 a.m. **HIERARCHICAL STRUCTURE AND FUNCTION OF CORNEA,**
R. Farrell, JHU, APL

12:00 p.m. **DISCUSSION OF SESSION I**

12:30 p.m. Lunch

Session II: **CONNECTIVE TISSUE,**
L. Katz, Moderator, CWRU

1:30 p.m. **DEFORMATION AND FRACTURE BEHAVIOR OF BONE,**
W. Bonfield, Queen Mary College; University of London

2:15 p.m. **ORIGIN OF STRESS GENERATED ELECTRICAL SIGNALS IN BONE,**
W. Williams, CWRU

3:00 p.m. Break

3:15 p.m. **HIERARCHICAL STRUCTURE OF INTERVERTEBRAL DISC,**
A. Hiltner, CWRU

4:00 p.m. **STRUCTURE FUNCTION RELATIONSHIPS IN THE AORTIC VALVE,**
M. Thubrikar, University of Virginia

4:45 p.m. **DISCUSSION OF SESSION II**

TUESDAY, OCTOBER 24, 1989

Session III: IMPACT RESISTANT STRUCTURES,
G. Mayer, Moderator, IDA

9:00 a.m. **IMPACT RESISTANCE OF INVERTEBRATE MINERALIZED TISSUES,**
J. Currey, University of York

9:45 a.m. **IMPACT MANAGEMENT OF SKULL AND OTHER BONE,**
J. McElhaney, Duke University

10:30 a.m. Break

10:45 a.m. **MECHANICAL PROPERTIES AND ENERGY ABSORPTION IN NATURAL CELLULAR MATERIALS,**
L. Gibson, MIT

11:30 a.m. **DISCUSSION OF SESSION III**

12:00 p.m. Lunch

Session IV: SELF-ASSEMBLY OF HIERARCHICAL STRUCTURES,
L. Klein, Moderator, CWRU

1:30 p.m. **SELF-ASSEMBLY IN VIVO OF FIBROUS PROTEINS,**
A. Veis, Northwestern University

2:15 p.m. **COLLAGEN SELF-ASSEMBLY AND RECONSTITUTION OF ANALOGS,**
F. Silver, Rutgers University

3:00 p.m. Break

3:15 p.m. **COLLAGEN FIBRIL ASSEMBLY BY A NUCLEATION GROWTH MODEL,**
D. Wallace, Collagen Corporation

4:00 p.m. **DISCUSSION OF SESSION IV**

4:30 p.m. **SHORT PRESENTATIONS**

6:30 p.m. **DINNER AT THE GWINN ESTATE**

8:30 p.m. **QUO VADIS - NATIONAL SCIENCE AND TECHNOLOGY POLICY,**
A. Bement, TRW

WEDNESDAY, OCTOBER 25, 1989

Session V: **FROM BIOLOGICAL TO SYNTHETIC COMPOSITES.**
L. Nicolais, Moderator, University of Naples

9:00 a.m. **MODELS OF THE STRESS ADAPTATION OF BONE TISSUE,**
S. Cowin, CUNY

9:45 a.m. **ANISOTROPIC COMPOSITES FOR SOFT AND HARD TISSUE REPLACEMENTS,**
J. Kardos, Washington University

10:30 a.m. Break

10:45 a.m. **PROCESSING AND PROPERTIES OF NATURAL CERAMIC POLYMER COMPOSITES,**
I. Aksay, University of Washington

11:30 a.m. **IMPACT BEHAVIOR OF 3-D COMPOSITES,**
F. Ko, Drexel University

12:15 p.m. **DISCUSSION OF SESSION V**

12:45 p.m. Lunch

Session VI: **WORKSHOP CONCLUSIONS "BIO-STRUCTURES AS COMPOSITE MATERIALS SYSTEMS."**
E. Baer & I. Ahmad - Moderators

1:45 p.m. **GROUP DISCUSSIONS TO IDENTIFY ISSUES AND OPPORTUNITIES FOR FUTURE RESEARCH**

Multidimensional Collagen Systems

Stephen A.Wainwright
Zoology Department
Duke University
Durham, North Carolina 27706

ABSTRACT

Some ligaments are virtually 1-dimensional; some membranes and skin are 2-dimensional; and arteries, intervertebral discs, worms, seastars, squid, sponges, and whales are 3-dimensional. All are collagen-based structural systems. 1-dimensional collagen molecules are found in particular arrays in membranes that are often formed into hollow, pressurized cylinders. The linking, orientation, spacing, length and diameter of the collagen fibrils determine the properties of the membrane and the cylinder. All collagen systems are composites. Soft collagenous tissues in vertebrates contain highly hydrated glycosaminoglycans (GAG) in an ionic fluid. Since material properties are always a reflection of the distribution of charge densities in the material, the aqueous GAG environment lends itself to the possible physiological or engineering control and variation of properties in situ. Examples will be presented of locomotor systems that use fibrillar collagen to a wide variety of structural and functional ends, including natural "smart materials" that perceive environmental signals, compute the information, and respond by changing their properties. From the study of animal locomotion, we see that the study of the material is often best approached by studying the system from which it comes.

References

Wainwright, S.A., W.D. Biggs, J.D. Currey, J.M. Gosline. 1976. Mechanical Design in Organisms, Princeton University Press, Princeton, NJ.
Wainwright, S.A., 1988. Axis and Circumference. Harvard University Press. Cambridge, MA.

Figures 1 through 10 added for amplification of the lecture.

Fig. 1. Collagen systems provide the reaction, containment, and framework for muscle in animals. Because muscle is constant volume, its forceful contraction causes equally forceful orthogonal expansion. The graph shows the length/ diameter relationships of a constant volume cylinder. A muscular organ, like the tongue, can be modeled as a cylinder such as B. A slight decrease in diameter due to contraction of transverse muscles would cause the tongue to greatly increase its length (C). This is, in fact, the way you stick out your tongue. Collagen wrappings must either allow or constrain such forceful changes in shape: they are brilliantly designed to do so.

Fig. 2. Cylindrical bodies of animals, arteries, guts, and intervertebral joints are pressurized from inside and they are wrapped by helically wound collagen fabrics. The figure shows how helically wound high modulus fibers such as collagen change their winding angles with change in shape of the cylinder. The volume of the open cylinder shown here approaches zero as the fiber winding angle approaches 0° or 90°, and maximum volume occurs when the fibers wrap at an angle of 54° 44' to the long axis of the cylinder. In constant volume cylinders, as fiber angle changes with shape away from 55°, internal hydrostatic pressure rises and is available to do elastic work in returning the body to prestressed shape when the muscle relaxes. This works in nematode worms.

Fig. 3. The cause of anisotropy in skin and other membranes in animal bodies is the fabric of collagen fibers in the membrane. The figure shows that a single set of parallel fibers gives the membrane a high modulus parallel to the fibers (A) and a low modulus normal to the fibers (B). Most membranes have at least two directions of oriented fibers that give the membranes a J-shape fress-strain curve (C). This means these membranes are stretchy at low strains but stiff at higher strains. Among other things, this is a mechanism of a safety factor for animals.

Fig. 4. Low power polarized light micrograph of an oblique section through the skin of a shark showing 3 of the 40+ layers of collagen fibers. Fiber diameter is 60 $\pm$12 μm. Fibers within each layer are parallel. Where swimming muscles pull on the skin over most of the body, fiber winding angle is about 60°.

Fig. 5. Biaxial stress-strain curves for shark skin, where skin is stressed a set amount in the circumferential (hoop) direction and then pulled in the longitudinal direction. Lower curve: hoop stress is set at the value represented by the shark's internal pressure during slow swimming. Ciné films tell us that the skin stretches and contracts ±10% during slow swimming. The stiffness of the skin over that strain range is very low. Upper curve: hoop stress is set higher at the value created by 4x higher internal pressure as the shark swims rapidly. Skin strains are now ±15%. The stiffness of the skin has increased by a factor of 13. Message: fiber array allows dramatic changes of skin properties that are involved in the transmission of muscle forces in locomotion.

Fig. 6. Photo of a longitudinal slice through the swimming muscle of a shark. Approximately life size. Each muscle cell extends from one collagen septum to the next. Splits in the tissue show muscle cell orientation and length. Muscle contraction for swimming starts at the head end, to the left, and sweeps backward, to the right. When all muscles in a conical segment contract, they apply a distributed load to the next collagen septum, stiffening it and causing it to transmit forces in the directions of its collagen fibers. Most of the force directed in this way goes to the skin that transmits the force to the tail.

Fig. 7. Whale blubber. Low power polarized light micrograph of a section normal to the body surface. Fibers oriented up and down are radially oriented in the whale. Fibers oriented left to right lie in tangential planes on the whale. Nonfibrous volume is filled with fat in fat cells.

Fig. 8. Whale blubber, same magnification as Fig. 7, but this section is tangential to the whale. By comparing the two micrographs, one can see that the tangential collagen fibers are not round but are lath-shaped, and they are in two interwoven sets that are wound helically around the whale. Whale blubber is 40-50% collagen by volume. Note that even though this sample is cut away from the whale and all stresses present in the animal are released, there is no indication of crimping: collagen fibers in all three directions are straight, i.e., under tension. Whale blubber is a very rubberlike, elastic solid that probably stores and usefully releases elastic energy during swimming. Photos and research by Dr. Lisa Orton in my lab.

Fig. 9. The base of a sea urchin spine where it touches the shell of the urchin at a ball and socket joint that allows the ring of muscle (shown in longitudinal section) to point the spine in any direction. Collagen fibers comprising the ligament underlying the muscle are in parallel with the muscle - not in series as our ligaments are. The ligament is called a "catch connective tissue" because it may be

extensible to allow the spine to be moved, or it may be stiff, holding the spine forcefuly in one posture. This change in property from stretchy to stiff is reversible and totally under the nervous control of the animal. There is a ganglion of neurons on each such ligament, and axonal processes from the ganglion penetrate throughout the ligament and are filled with large vesicles of differently staining material. Isolated catch connective tissue shows that stiffness varies with the concentration of divalent cations in the ambient fluid. This is a genuine "smart material". While we know that human articular cartilage has the same dependence on divalent cations for its stiffness, there is no evidence *yet* that we control the mechanical properties of any tissue in the body via neural or hormonal mechanisms. In future, we may control these properties medically.

Fig. 10. Every collagenous tissue in all animal bodies is accompanied by glycoproteins such as those diagrammed here. A protein core is the central attachment for many polysaccharide chains that carry readily ionized negative side groups. These repel each other forcefully and make the whole molecule look like a 3-D bottle brush, rather than the 2-D featherlike shapes shown here. The degree to which the molecule swells forcefully varies with the ionic concentration of the ambient aqueous medium. While collagen is certainly the major mechanism of integrity for animal bodies, these long-unloved molecules are responsible for the elastic and visco-elastic properties of all our soft tissues.

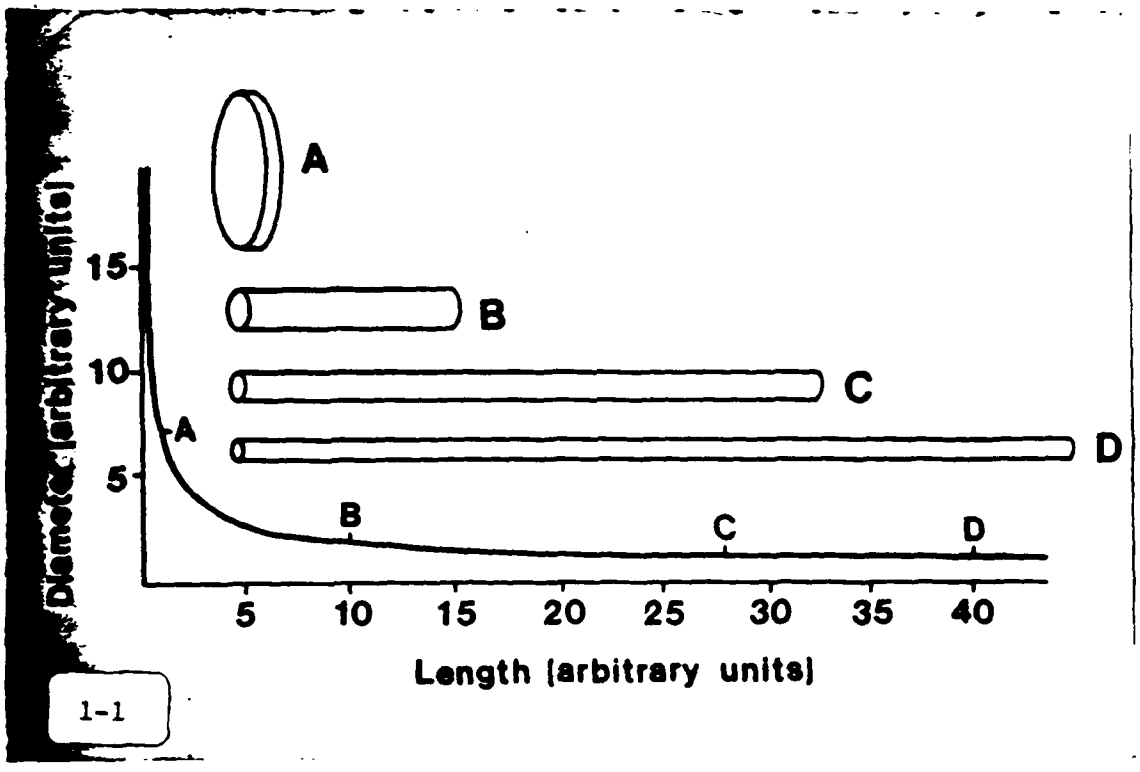
A
B
C
D
15
10
5
A
B
C
D
5
10
15
20
25
30
35
40
Length (arbitrary units)
1-1

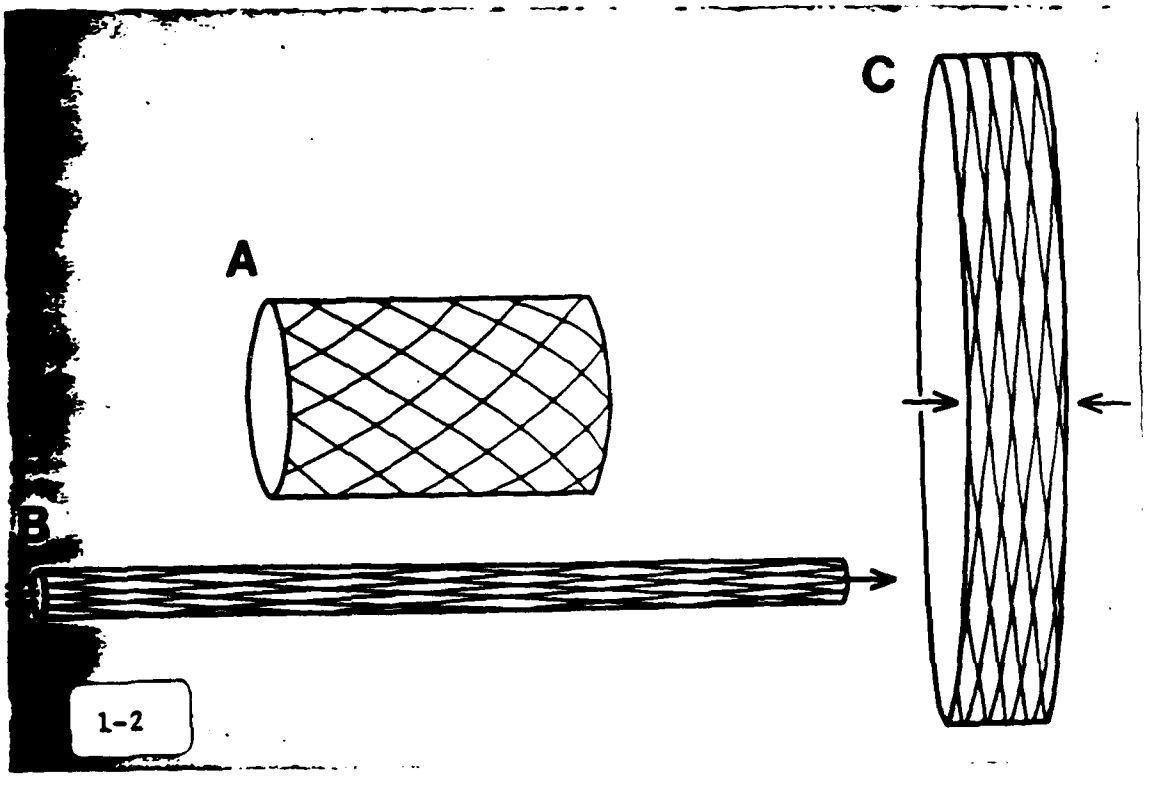
C
A
B
1-2

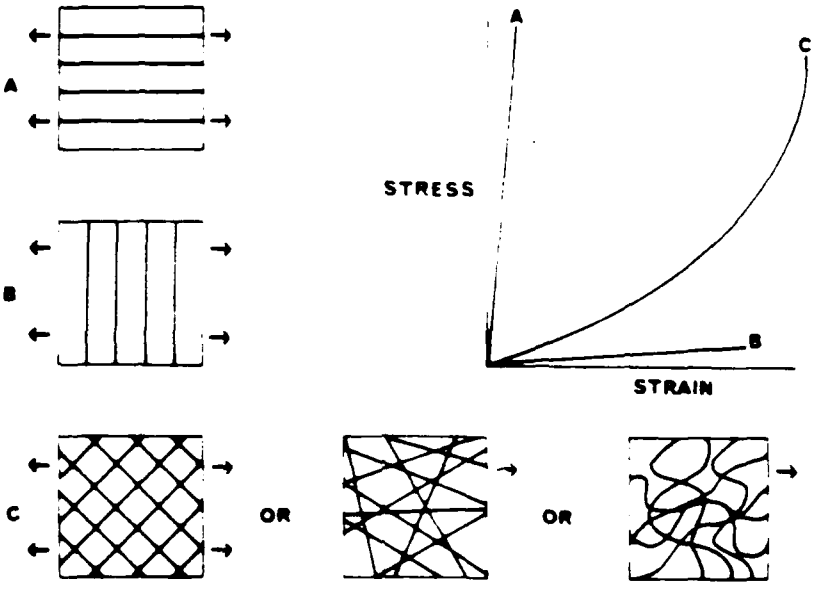

1-3

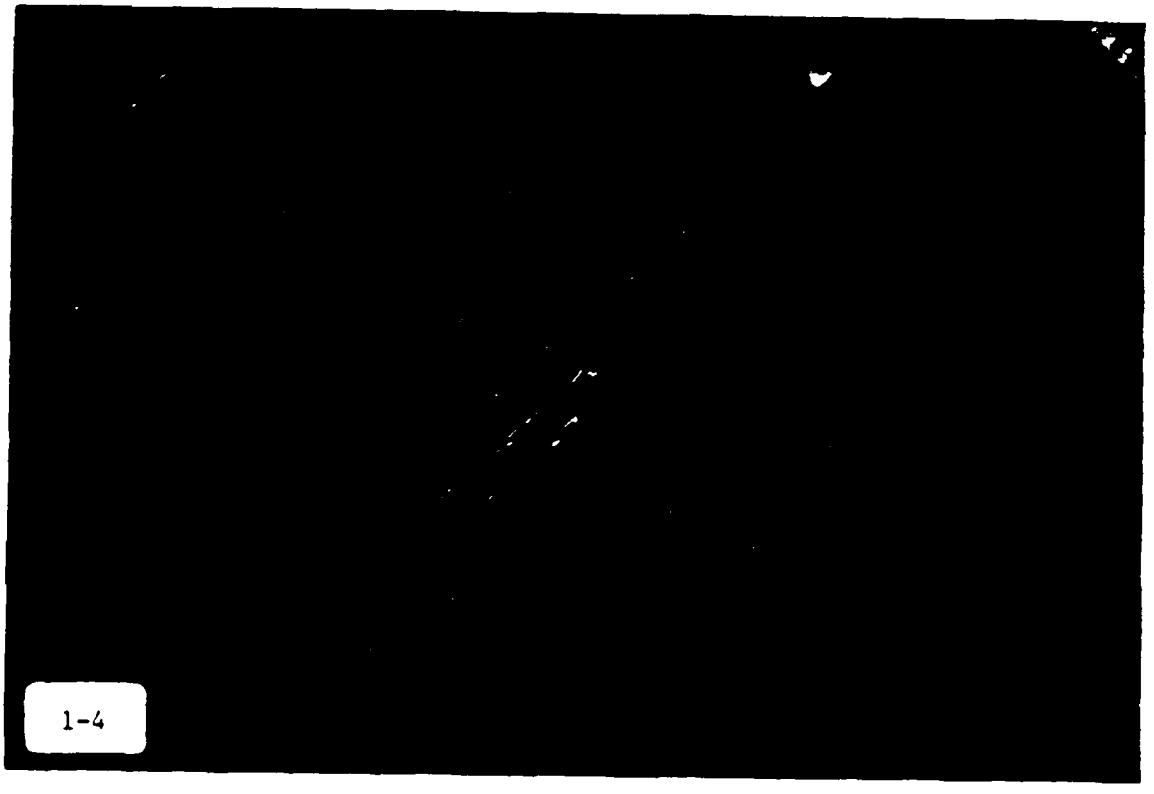

FIG. 3

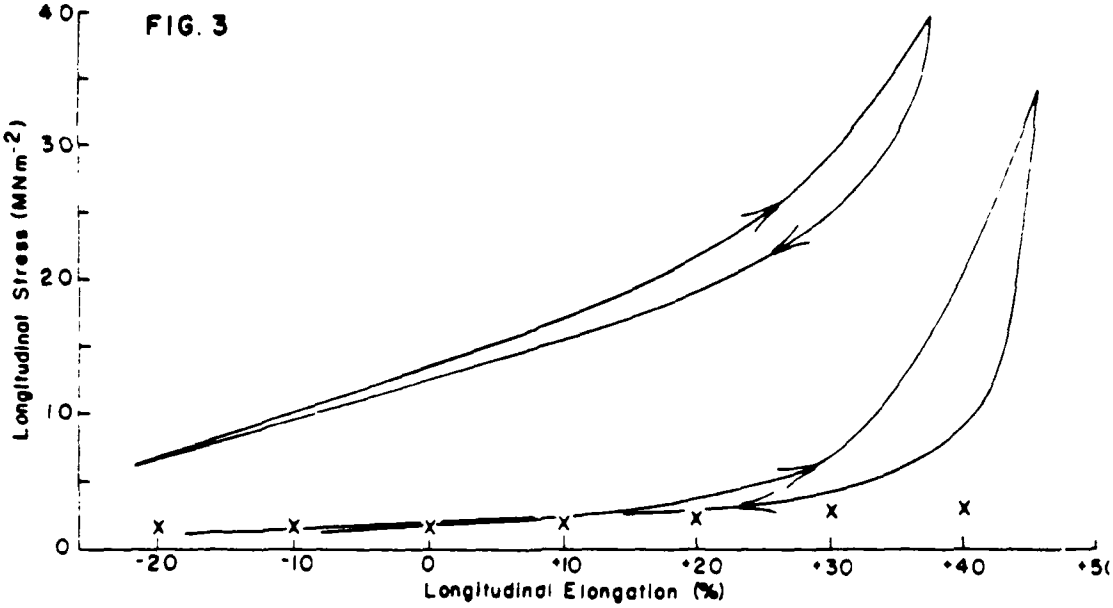
40
30
20
10
0
Longitudinal Stress (MNm-2)
-20
-10
0
+10
+20
+30
+40
Longitudinal Elongation (%)

1-5

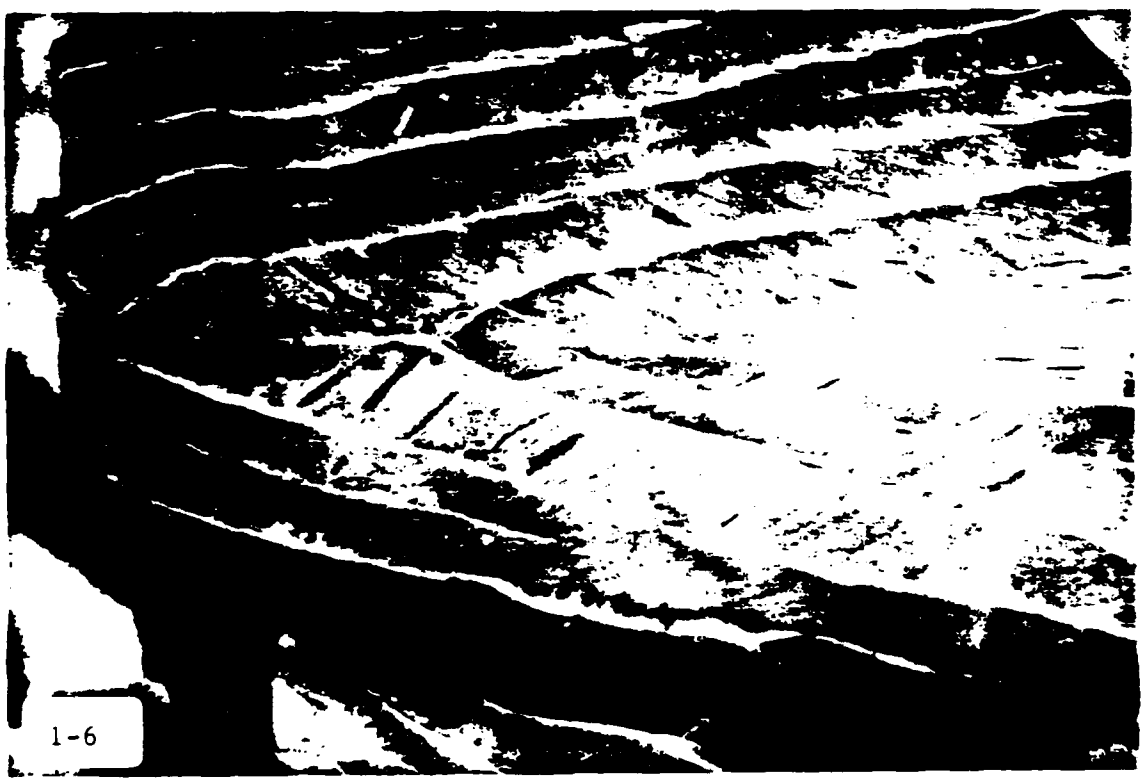

1-6

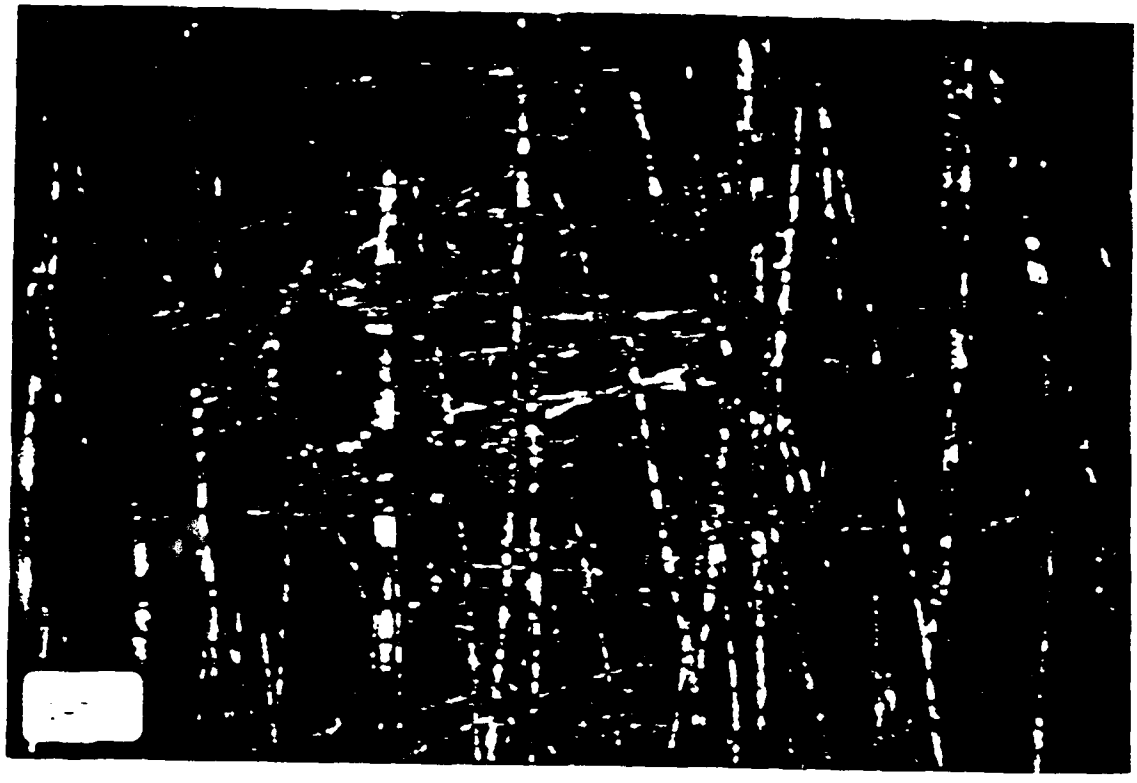

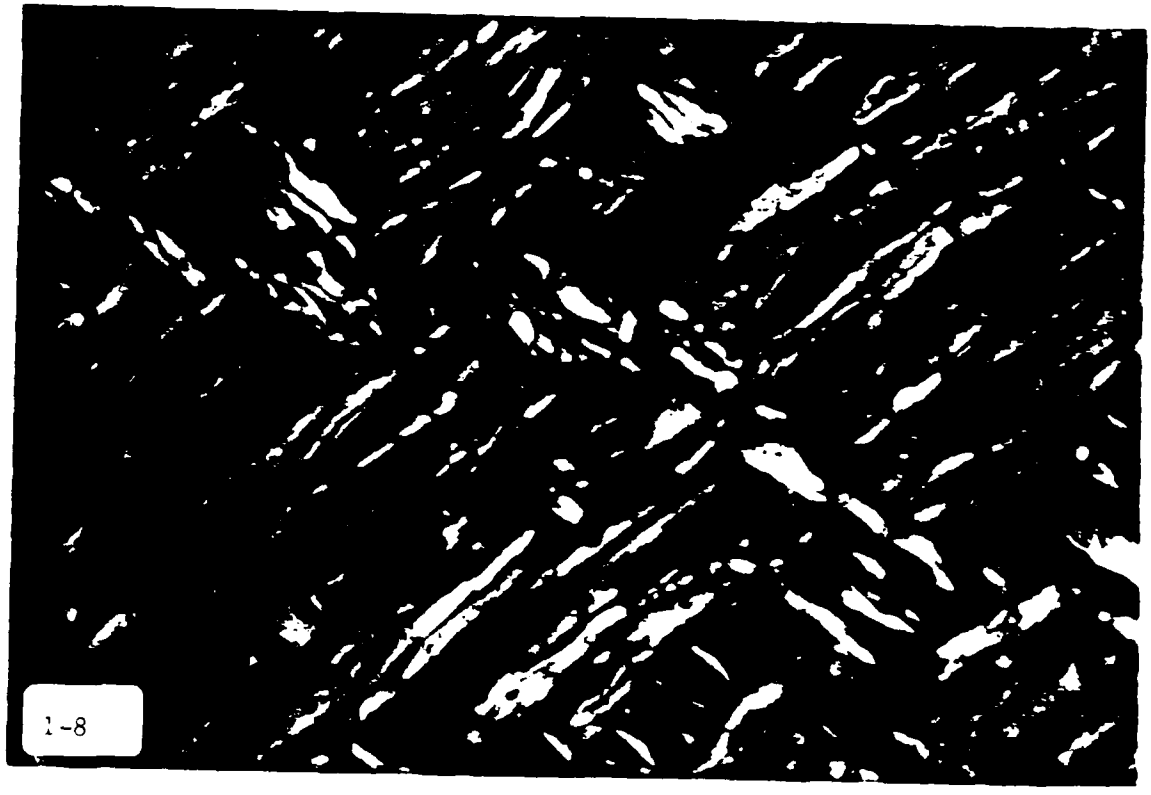
1-8

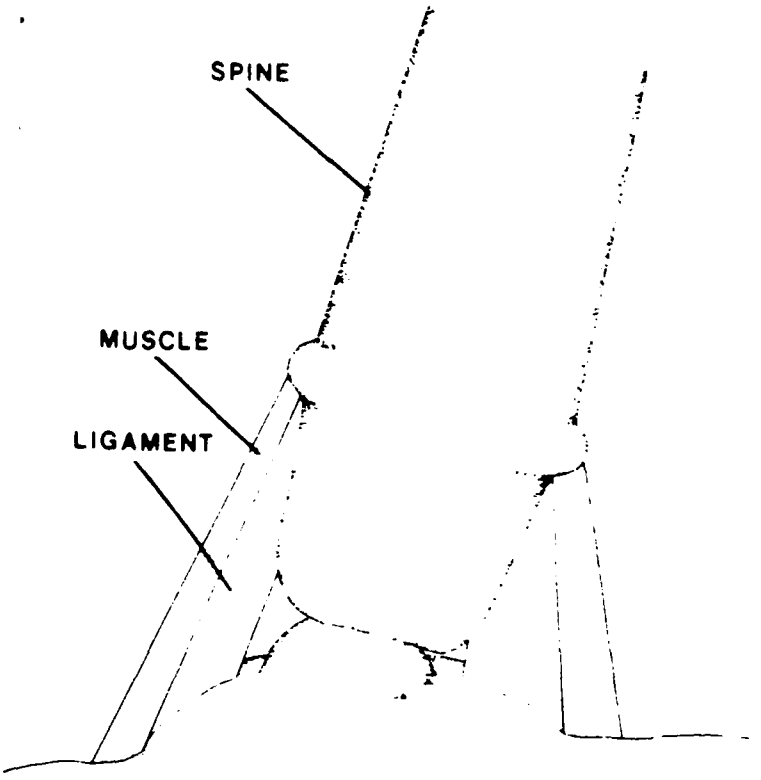
SPINE
MUSCLE
LIGAMENT

1-9

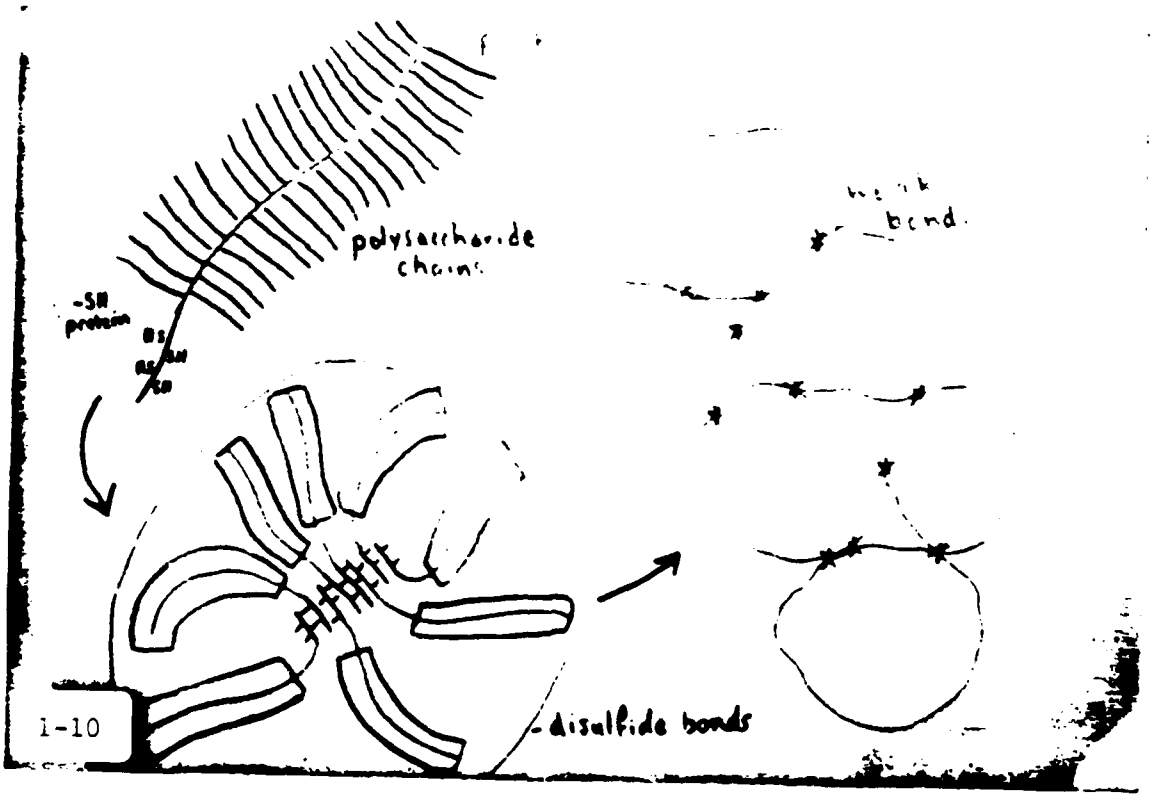
polysaccharide chains
-SH protein
weak bond
-disulfide bonds

1-10

HIERARCHICAL STRUCTURE OF THE TENDON

Eric Baer
Center for Applied Polymer Research
and Dept. of Macromolecular Science
Case Western Reserve University
Cleveland, Ohio 44106

The hierarchical structure of the tendon is described in Figure 1.[1] At its most basic level, chains of amino acids 290 nm in length form the triple helical tropocollagen molecule. Five tropocollagen molecules are staggered horizontally, overlapping by one quarter of their molecular length to form a microfibril 3.6 nm in diameter. Microfibrils are packed in a tetragonal lattice to form subfibrils about 30 nm in diameter.[2] These subfibrils are then assembled into the collagen fibril, the basic unit of connective tissue. These fibrils vary in diameter from 50 to 500 nm depending upon the tissue type and age of the animal. The fibrils are surrounded by an amorphous gel-like matrix of proteoglycan molecules and water. This matrix forms an efficient network that connects and maintains the fibrillar architecture. Collagen fibrils are arranged in parallel and oriented along the longitudinal axis of the tendon.[3] The fibrils are characterized by a planar crimped waveform with sharply defined crimp angles. (Figure 2)[4] The fibrils associate into fascicles with a triangular cross-section 150 to 300 um in diameter.[3] Within fascicles, fibrils are crimped in register. Fascicles are found packed two or three together in the rat tail tendon.

The hierarchical structure of tendon is designed to accommodate uniaxial tensile loads. The stress-strain curve of the tendon is characterized by four distinct regions. (Figure 3)[5] The toe region of increasing modulus corresponds to gradual straightening of the waveform in the collagen fibrils. (Figure 4) Most physiological strains fall within this non-linear region. A linear elastic region follows which represents reversible extension of the collagen. Yield region I is characterized by irreversible elongation and damage by a shear-slip mechanism between microfibrils. The crimp waveform does not appear following a recovery period. The damage mechanism in Yield region II is characterized by slippage of tropocollagen units within microfibrils and by permanent dissociation between microfibrils by shear/slip. This cooperative interaction between discrete levels of the hierarchical structure enable it to absorb enormous amounts of damage prior to failure.

References:

1. Kastelic, J., Galeski, A., and Baer, E., "The multicomposite structure of tendon", Conn. Tiss. Res., 6, 11, 1978.
2. Baer, E., Gathercole, L., and Keller, A.,"", Proc. Colston Conf., 189, 1974.
3. Niven, H., Baer, E., and Hiltner, A., "Organization of collagen fibers in rat tail tendon at the optical microscope level", Collagen Rel. Res., 2, 131, 1982.
4. Diamant, J., Keller, A., Baer, E., Litt, M., and Arridge, R.G.C., "Collagen: ultrastructure and its relation to mechanical properties as a function of ageing", Proc. R. Soc. Lond., B180, 293, 1972.
5. Kastelic, J. and Baer, E., "Deformation in tendon collagen", Soc. Exp. Biol. Symp. XXXIV, 197, 1980.

Figure Captions

Fig. 1 Hierarchical structure of the tendon showing discrete levels of organization. Abbreviations: DSC, differential scanning calorimetry; EM, electron microscopy; SEM, scanning electron microscopy; OM, optical microscopy.

Fig. 2 Optical micrograph of rat tail tendon fascicle showing (a) uniaxially oriented textures and, at higher magnification, (b) the planar crimped waveform between cross polarizers.

Fig. 3 Stress-strain behavior of rat tail tendon in toe, linear, and yield regions as a function of age. Neutral saline; strain rate of 8 %/min

Fig. 4 Partially dissected tendon with wavy morphology in different stage of extension.

TENDON HIERARCHY

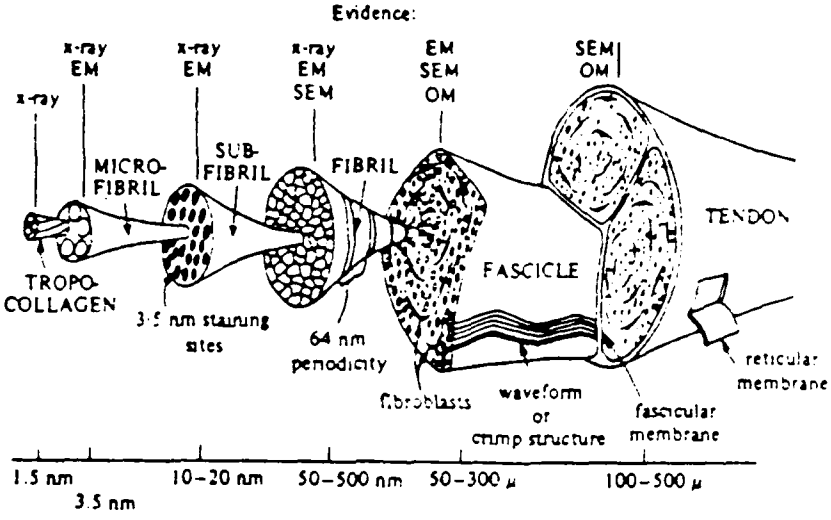

2-1

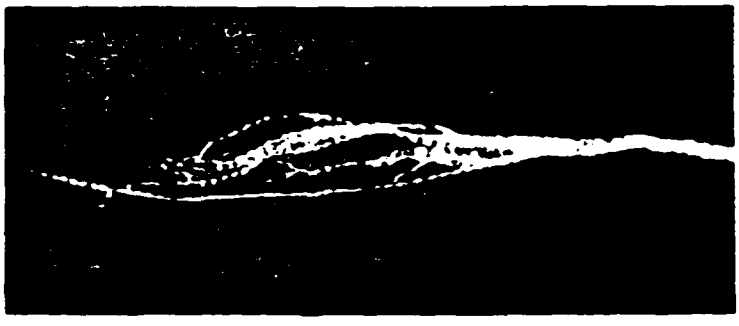

a

b

2-2

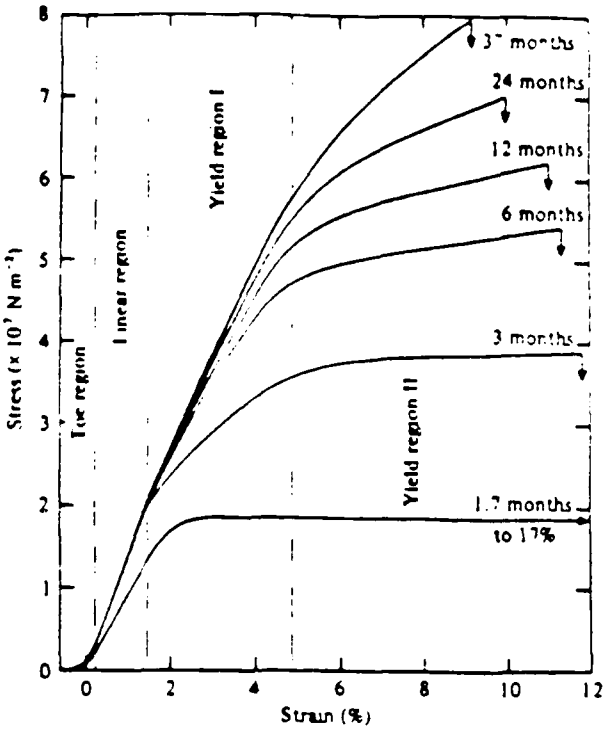
Stress (x 10³ N m⁻²)
Strain (%)
Toe region
Linear region
Yield region I
Yield region II
24 months
12 months
6 months
3 months
to 17%

2-3

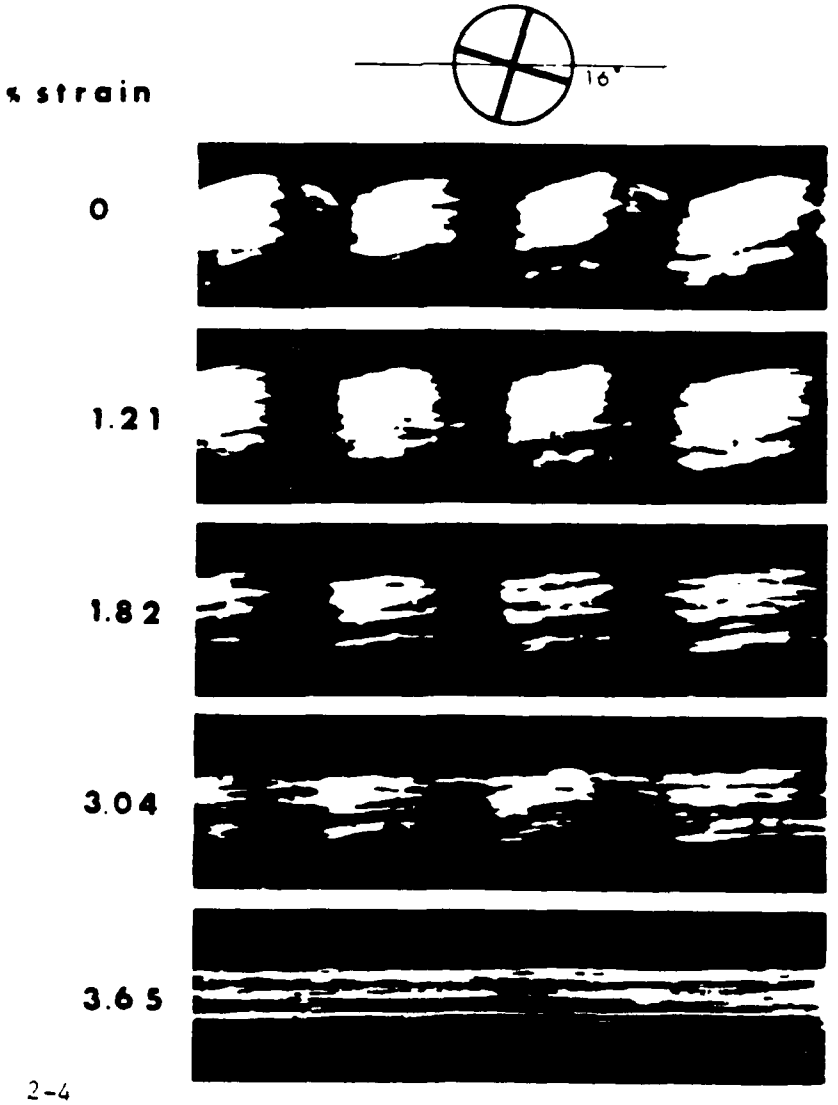
% strain
16°
0
1.21
1.82
3.04
3.65

2-4

Figures 5 through 11 added for amplification of the lecture.

Fig. 5 Histological cross-section of the basic tendon unit, the fascicle, showing the characteristic triangular shape.

Fig. 6 Electron micrograph of the collagen fibril. The characteristic 64 nm banding pattern is visible. Fibrils have been stretched to straighten the crimp waveform.

Fig. 7 Stress-strain behavior of the tendon as a function of water content.

Fig. 8 Enlarged view of the toe region of the stress-strain curve showing the increase in the length of the toe with age.

Fig. 9 Hierarchical structure of the intestine.

Fig. 10 Polarized light micrograph of salted rat intestine. Longitudinal direction is horizontal. Magnification is 160x. (top) Unstretched. (bottom) Stretched.

Fig. 11 Stress-strain behavior of salted bovine intestine for specimens cut at the indicated angle to the longitudinal direction.

2-5

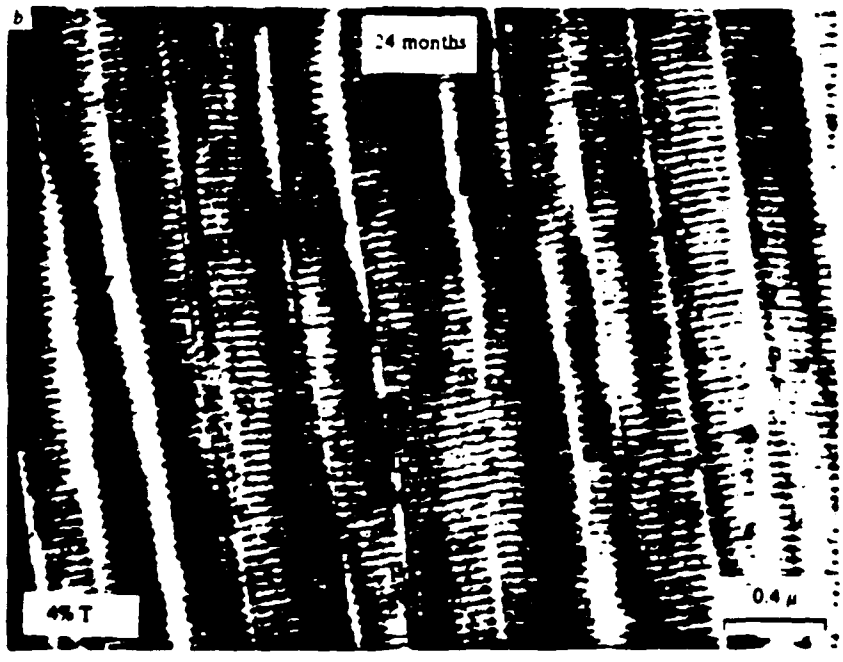

2-6

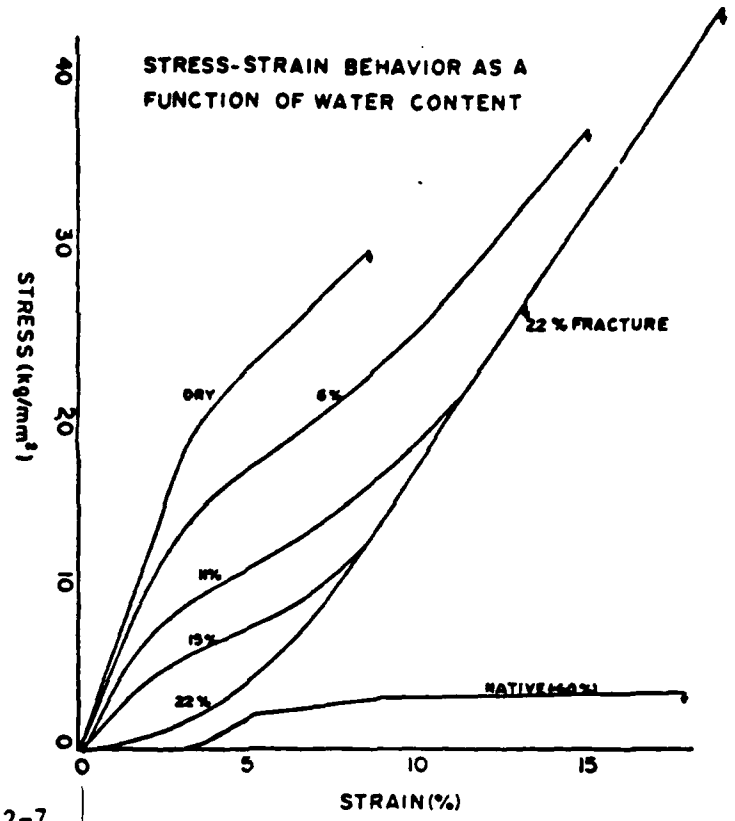
STRESS-STRAIN BEHAVIOR AS A
FUNCTION OF WATER CONTENT
STRESS (kg/mm²)
STRAIN (%)
0
10
20
30
40
0
5
10
15
DRY
6%
11%
13%
22%
22 % FRACTURE
NATIVE (40%)

2-7

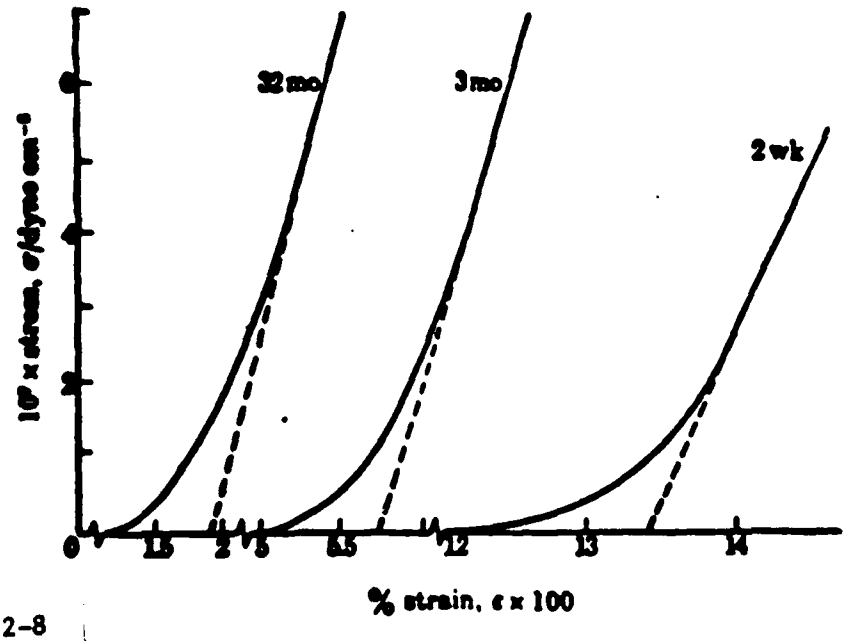
32 mo
3 mo
2 wk
0
1.5
2
5
8.5
12
13
14
% strain, ε x 100

2-8

Collagen Hierarchy of Intestine

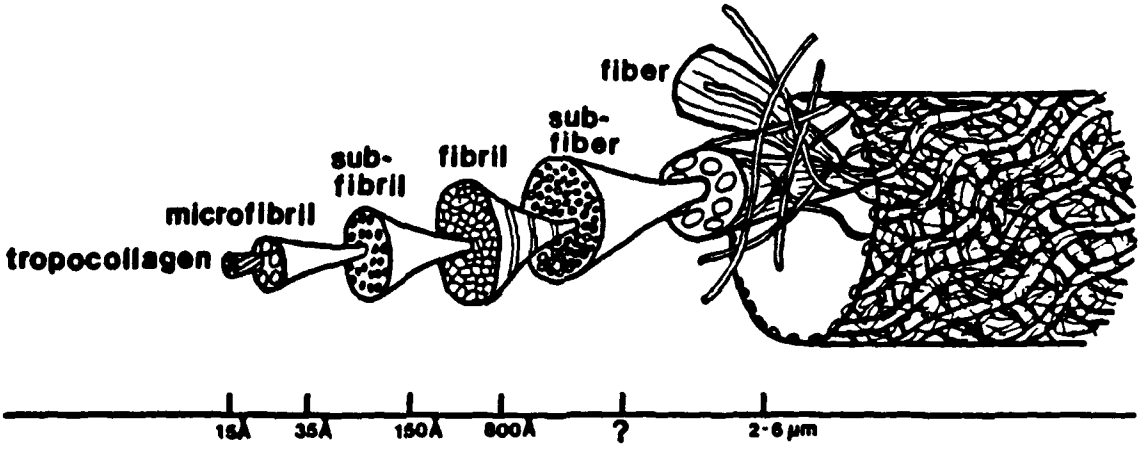

2-9

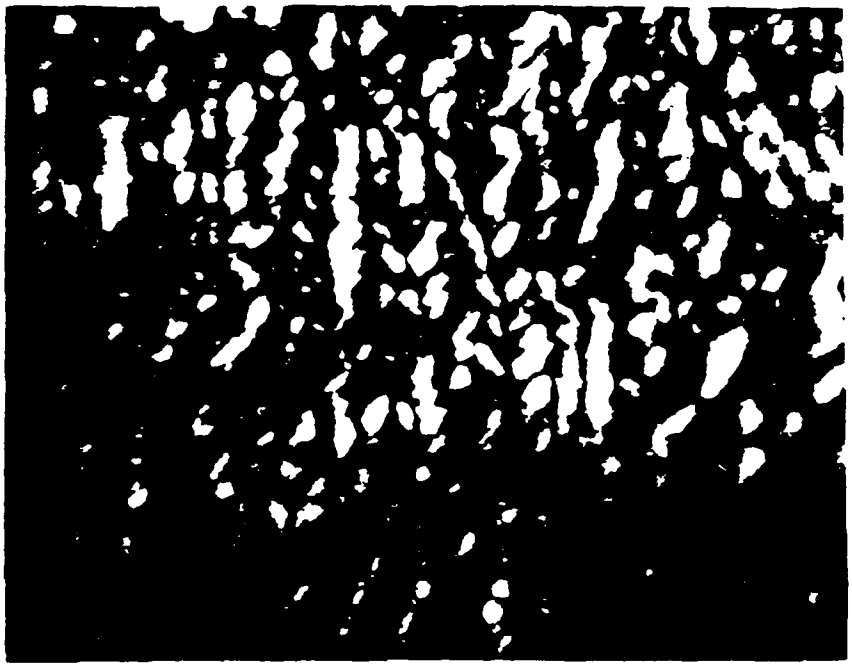

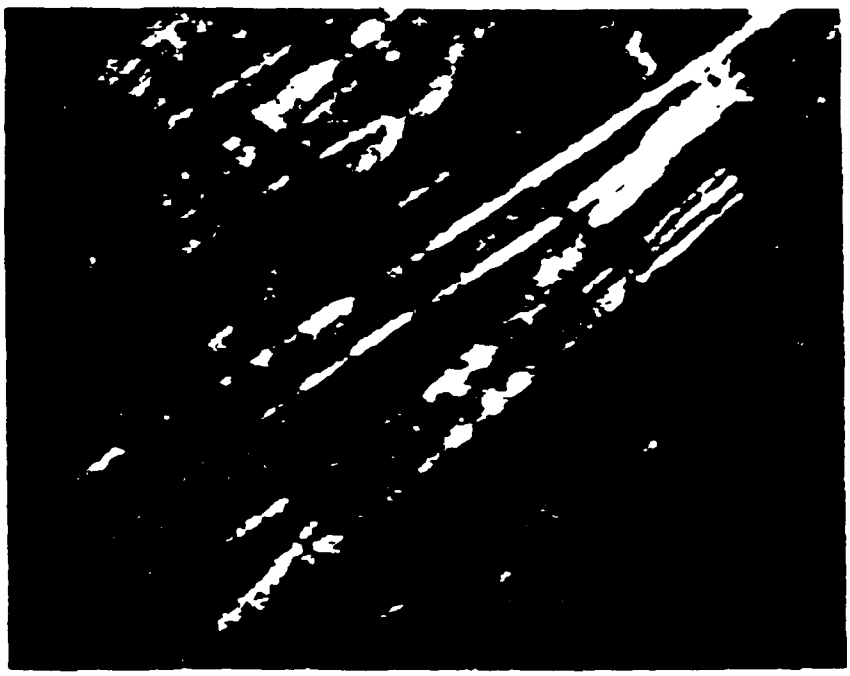

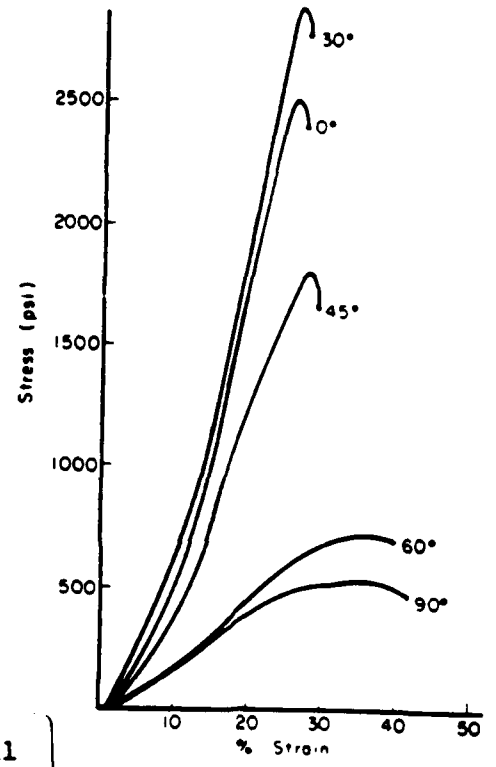
30°
0°
45°
60°
90°
2500
2000
1500
1000
500
Stress (psi)
10
20
30
40
50
% Strain

2-11

HIERARCHICAL STRUCTURE AND FUNCTION OF THE CORNEA†

R. A. Farrell
Milton S. Eisenhower Research Center
The Johns Hopkins University
Applied Physics Laboratory
Johns Hopkins Road
Laurel, MD 20707

The most distinguishing characteristic of the cornea is its clarity or transparency, which is essential to its primary function of being the window in the front of the eye wall through which we see the outside world. In addition, about 75 percent of the refractive power of the eye occurs at the curved air-cornea interface. Figure 1 shows the approximately spherical surface of the central cornea protruding in front of the pupil, or opening, in the pigmented iris. The intraocular pressure produces the corneal curvature and also protects the photosensitive elements of the retina from trauma. The vascularized regions depicted in Fig. 1 include the opaque white scleral region of the eye wall, the choroid, and the retina. These regions are indicated in the schematic of Fig. 2, which also shows the ocular lens that provides the fine focusing of the image onto the fovea. This region of the retina has the highest density of photosensitive elements and also contains the cones which give us color perception.

The microscopic structure of the cornea is depicted in Fig. 3, which shows a cross-section cut through its thickness. The cellular layers at the outer and inner surfaces are called, respectively, the epithelium and endothelium, and they help regulate the flow of fluids across the cornea. This flow is of vital importance since it carries nutrients from the clear fluids of the anterior chamber to nourish the avascular cornea. These layers are attached to the stroma via membraneous layers, Basement and Descemet's membrane. The stroma is a connective tissue layer that is composed of collagen fibrils embedded in a

†Work supported in part by NIH, the Navy and the Army.

glycoprotein ground substance. The stroma itself is a layered structure composed of approximately 200 lamellae, each about 2-3 μm thick. The collagen fibril axes are parallel to the cornea's surfaces and extend entirely across it; i.e., from limbus to limbus. The axes of the fibrils within a given lamellae are parallel to one another, while those in adjacent lamellae make large angles with respect to one another. In some species, including man, there is a thin collagenous layer in the front of the stroma that is composed of fibrils whose orientations appear to be random. There is also a network of cells, called keratocytes, that are located between the lamellae. These cells send out long processes and can communicate with one another.

Figure 4 is an electron micrograph of a cut through the cornea that shows the constituent collagen fibrils in cross-section. The fibrils have been stained dark. They are uniformly about 25 nm in diameter and their nearest neighbor center-to-center spacing is about 60 nm. This electron micrograph is from a central region. It might be noted that the fibrils in the periphery (near the limbus) are somewhat larger and appear to merge with the large fibrils of the opaque white sclera. The diameters of the scleral fibrils are several times larger than those of the cornea and have a wide range of values. Detailed descriptions of the structure of various elements of the eye can be found in various books, e.g. Ref. 1.

Physicists, chemists, physiologists and various other ophthalmic researchers have been fascinated by the properties of the transparent yet rugged cornea of the eye. Among the topics of interest, we will concentrate on the relationship of transparency to the fibrillar ultrastructure,[2,3,4,5] the use of light scattering measurements to probe structure,[6,7,8] and some work by others showing the contributions of various layers to the elastic properties of the cornea.[9]

References

1. Hogan MJ, Alvarado JA, and Weddell, JE. Histology of the human eye. Philadelphia: Saunders, 1971.
2. Maurice DM. The structure and transparency of the corneal stroma. J Physiol (London), 1957; 136:263-286.
3. Hart RW, Farrell RA. Light scattering in the cornea. J Opt Soc Am. 1969; 59:766-774.
4. Benedek GB. The theory of transparency of the eye. Appl Opt. 1971; 10:459-473.
5. Twersky V. Transparency of pair-related, random distributions of small scatterers, with applications to the cornea. J Opt Soc Am. 1975; 65:524-530.
6. Bettelheim FA, Magrill R. Small angle light scattering patterns of corneas of different species. Invest Ophthalmol. 1977; 16:236-240.
7. Chang EP, Keedy DA, Chein JCW. Ultrastructure of rabbit corneal stroma: mapping of optical and morphological anisotropies. Biochim Biophys Acta. 1974; 343:615-626.
8. McCally RL, Farrell RA. Structural implications of small-angle light scattering from cornea. Exp Eye Res. 1982; 34:99-111.
9. Freund DE, McCally RL, Farrell RA. Effects of fibril orientations on light scattering in the cornea. J Opt Soc Am A. 1986; 3:1970-1982.
10. Jue B, Maurice DM. The mechanical properties of the rabbit and human cornea. J. Biomechanics, 1986; 19:847-853.
11. Maurice DM. The cornea and sclera. In: Davson H, ed. The eye (3rd ed.). Orlando: Academic Press, 1984: Vol. 1b, pp. 1-158.

Figure Captions

Fig. 1 Pictorial representation of the eye.

Fig. 2 Schematic of the eye.

Fig. 3 Microscopic structure of the cornea.

Fig. 4 Electron micrograph of a stromal lamella.

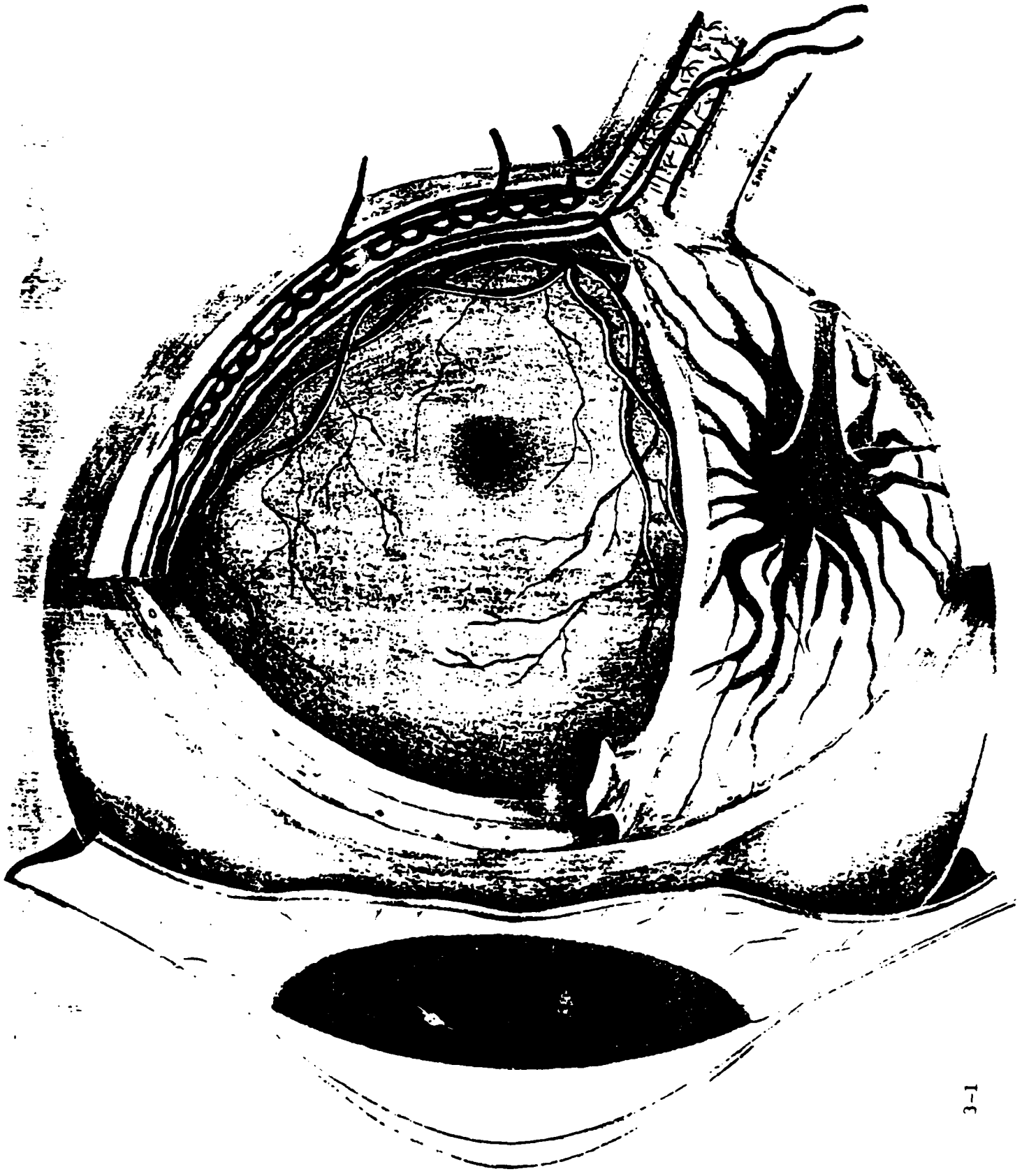

3-1

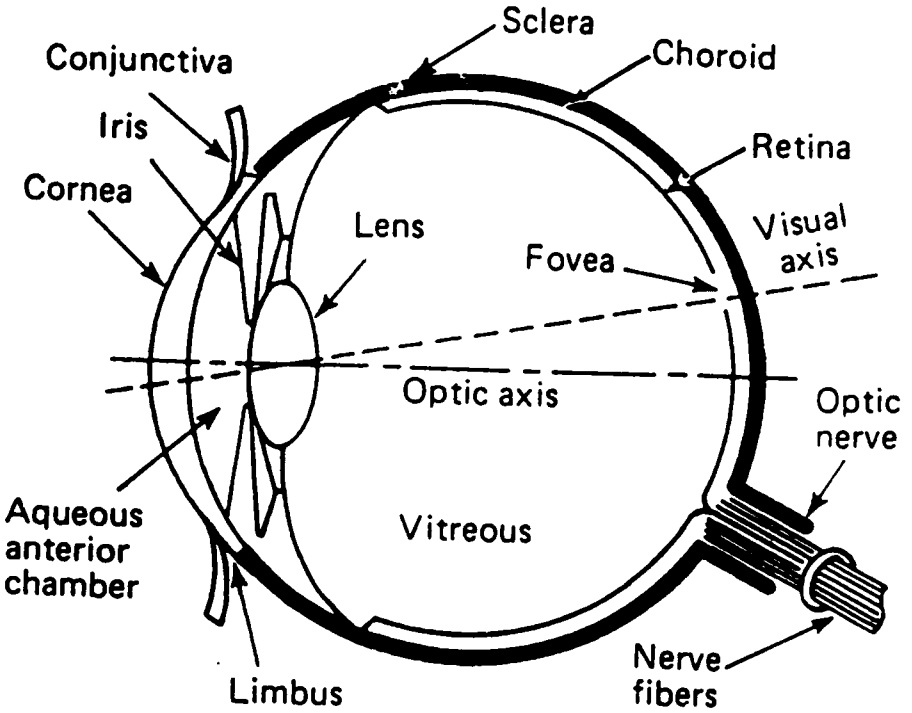
Sclera
Conjunctiva
Choroid
Iris
Retina
Cornea
Lens
Visual axis
Fovea
Optic axis
Optic nerve
Aqueous anterior chamber
Vitreous
Limbus
Nerve fibers

3-2

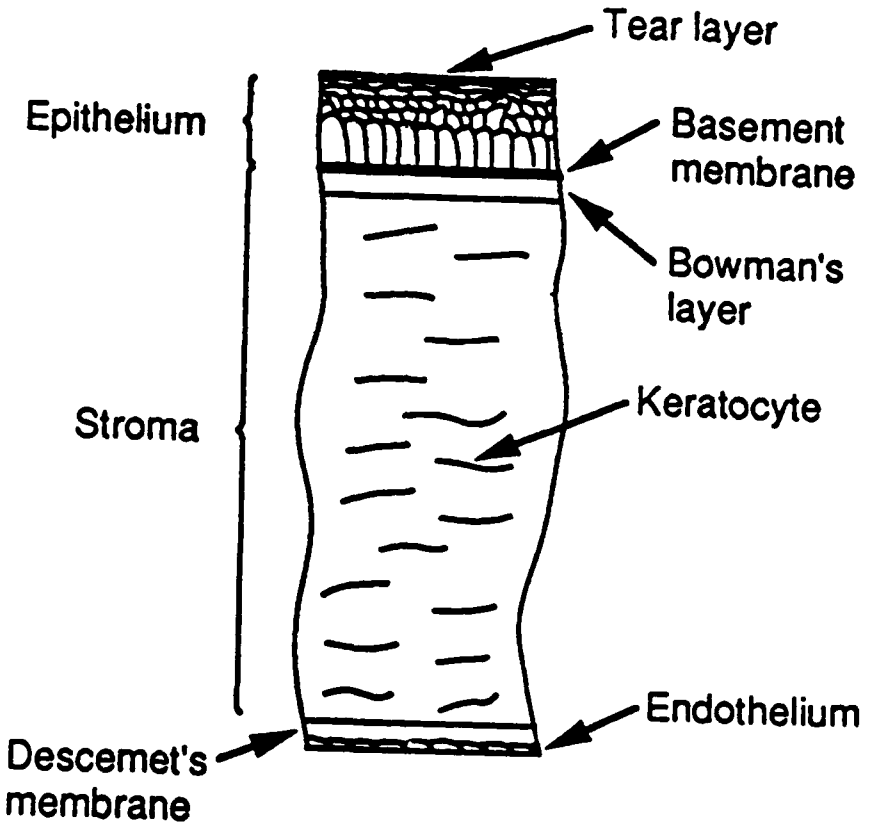
Tear layer
Epithelium
Basement membrane
Bowman's layer
Stroma
Keratocyte
Endothelium
Descemet's membrane

3-3

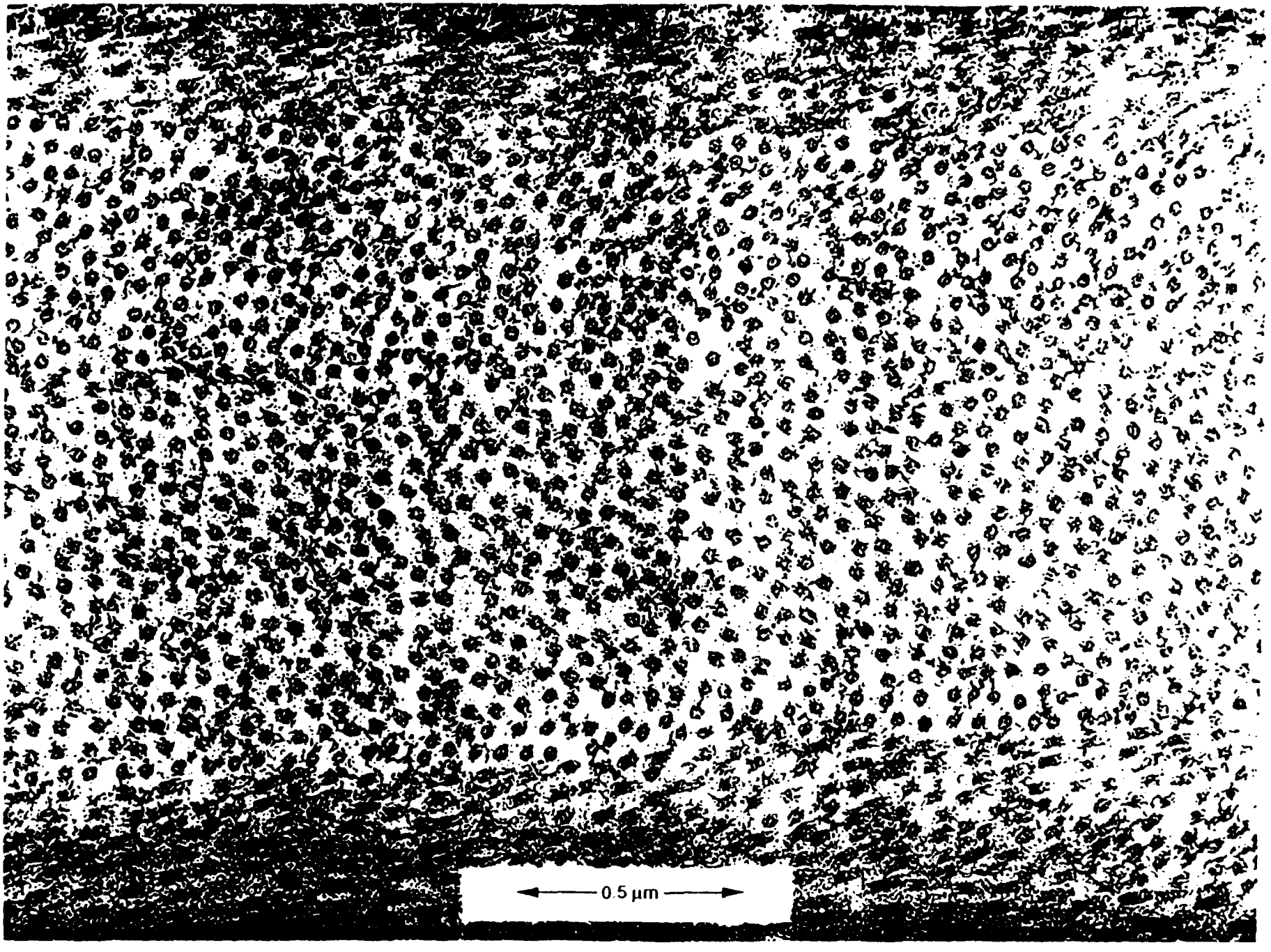
0.5 µm

Figures 4 through 18 added for amplification of the lecture

Fig. 5 **Top.** Schematic showing the cornea as the transparent window in the front of the eye wall which helps focus images onto the photosensitive elements of the retina. **Left.** Light micrograph showing the cornea is composed of cellular layers that cover the inner and outer surfaces of the connective tissue layers, Bowman's, stroma and Descemet's. **Right.** Electron micrograph of a portion of a cut through the thickness of the stroma showing several lamellae. The lamellae are composed of collagen fibrils embedded in a mucoprotein ground substance.

Fig. 6 A low magnification electron micrograph of a full thickness cut through the cornea. The preparative procedures are described in Cox, Farrell, Hart and Langham [J Physiol. 210, 601-616 (1970)]. It should be noted that the transcorneal pressure was not maintained during fixation, and there is a quasi-periodic waviness in the stromal lamellae, which is not seen when the pressure is maintained.

Fig. 7 Comparison of the structure of the opaque white sclera (left) with that of the transparent cornea (right) at similar magnifications. The fibrils are stained dark and are much larger in sclera than in cornea. It can also be seen that the fibril axes, which are parallel to the corneal surface, are parallel to one another in a given lamella and make large angles with respect to one another in adjacent lamellae.

Fig. 8 Histogram of fibril radii measured in central cornea from rabbit, showing the fibrils are uniformly of diameter ~310 nm.

Fig. 9 Steps involved in characterizing the spatial distribution of fibrils depicted in the electron micrograph of normal rabbit cornea shown in the upper left. The two-dimensional conditional probability distribution function on the upper right is obtained by: 1) choosing a centrally located fibril axis as a reference center; 2) placing a dot at the location of the other fibril axes relative to this center; and 3) repeating this process using other reference centers. The radial distribution function at the bottom gives the probability density of finding a fibril axis located at a distance from a reference center. It is obtained by drawing concentric rings about the origin in the two-dimensional distribution, counting the number of centers in a given ring, and dividing by the (unconditional) average number of fibrils one would expect to find in the area of the ring. Hart and Farrell [J. Opt. Soc. Am. 59, 766-774 (1969)] showed that the spatial ordering characterized by the measured radial distribution function is sufficient to yield the interference effects needed to explain the transparency of normal corneas.

Fig. 10 A piece of excised cornea placed between two fritted glass disks and immersed in saline imbibes solution and swells in its thickness direction. The external pressure needed to maintain the cornea at a given thickness is called the swelling pressure. Hart and Farrell [Bull. Math. Biophys. 33, 165-186 (1971)] used a modified polyelectrolyte gel theory to show that attaching the mucoproteins to the collagen fibrils could explain the observed variation of swelling pressure with thickness.

Fig. 11 When the cornea swells (slowly), it begins to lose its transparency due to increased light scattering. Farrell, McCally and Tatham [J. Physiol. 233, 589-612 (1973)] measured the fraction of light transmitted undeviated through corneas having various degrees of swelling as a function of light wavelength.

Fig. 12 Electron micrographs of swollen corneas reveal the presence of voids called "lakes" in the distribution of fibrils. Benedek [Appl. Opt. 10, 459-473 (1971)] suggested that lakes are responsible for the increased light scattering.

Fig. 13 The scattering measurements of Farrell, McCally and Tatham [J. Physiol. 233, 589-612, 1973)] showed that the total scattering cross-section for normal thickness corneas has a $1/\lambda^3$ dependence and a $(\lambda^{-3} + b\lambda^{-2})$ dependence for swollen corneas, with b increasing with the degree of swelling. They showed that these results are consistent with the structures in the electron micrographs (fixed tissue).

Fig. 14 Variations in the transmission of linearly polarized light through the cornea as the crossed analyzer and polarizer are rotated in tandem. The signal at the minimum transmission orientation is two orders of magnitude larger than the "leakage" present when the cornea is removed. The large changes on rotation mean that the orientation of the lamellae (fibril axes) in the central cornea is not random, rather, there is a preferred orientation direction (or two at right angles) superimposed on a random background [McCally and Farrell, Exp. Eye Res. 34, 99-113 (1982)].

Fig. 15 Small angle light scattering (SALS) patterns from rabbit cornea in the crossed configuration at various transcorneal pressures. The pattern essentially vanishes at pressures greater than the normal intraocular pressure of 18 mm Hg. The intensity maximum in the lobes occurs at a scattering angle of 2°.

Fig. 16 Electron micrograph prepared with (bottom) and without (top) transcorneal pressure. The spatial period of the waviness and its disappearance with pressure suggest that the wavy lamellae are responsible for the SALS patterns in Fig. 11.

Fig. 17 Schematic [from Hogan, Alvarado and Weddell, Histology of the Human Eye, W. B. Saunders Co., Philadelphia, 1971] showing the stromal lamellae with a network of flat cells between them. The cells act like little mirrors at specular angles, so these conditions must be avoided if one wishes to probe fibrillar structures. The orientation of the lamellae are crucial for understanding angular light scattering such as the SALS above and the existence of a universal curve of scattering versus effective wave number ($k \sin(\theta_s/2)$ with $k = 2\pi/\lambda$ and θ_s = scattering angle; see [Freund, McCally and Farrell, J. Opt. Soc. Am. A 3, 1970-1982 (1986)].

Fig. 18 Suggested low pressure stress-strain relationship of the intact cornea (broken line) in relation to that of its component layers, for the rabbit and human [from Jue and Maurice, J. Biomech. 10, 849-853 (1986)]. The stroma and Descemet's membrane undergo identical strains as the tissue stretches, so that the stress in the intact cornea is the sum of that in the two layers. The difference between the species can be explained on the basis of the relative initial strain in the layers.

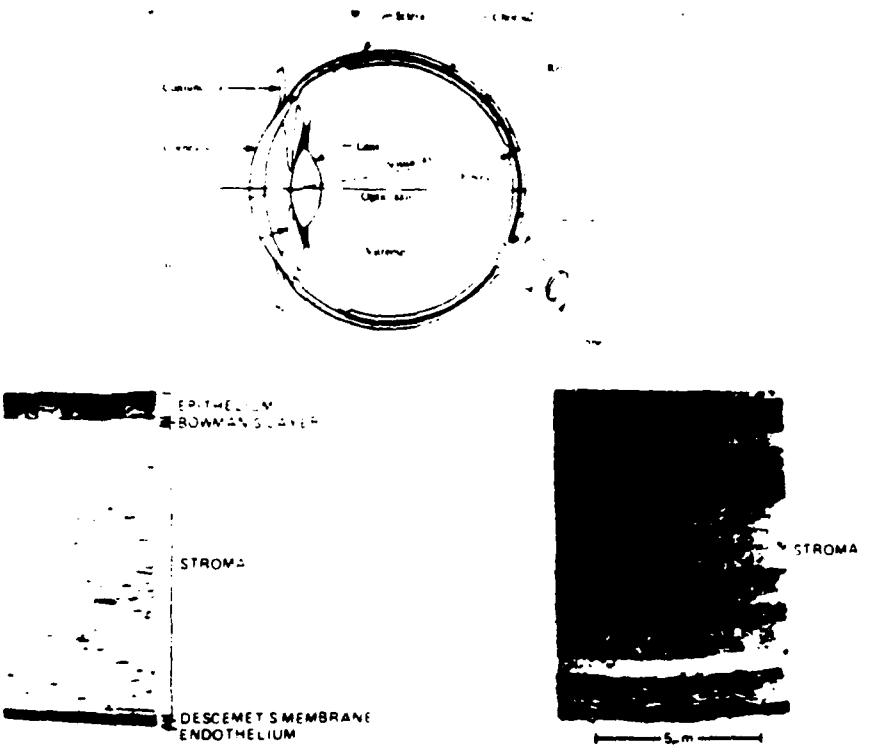

3-5

3-6

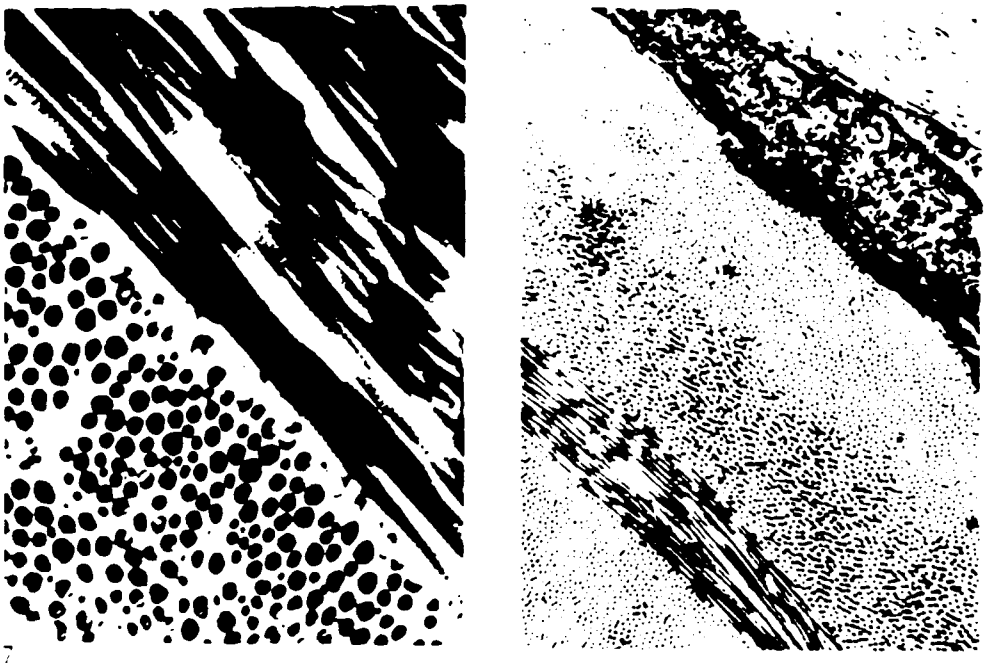

3-7

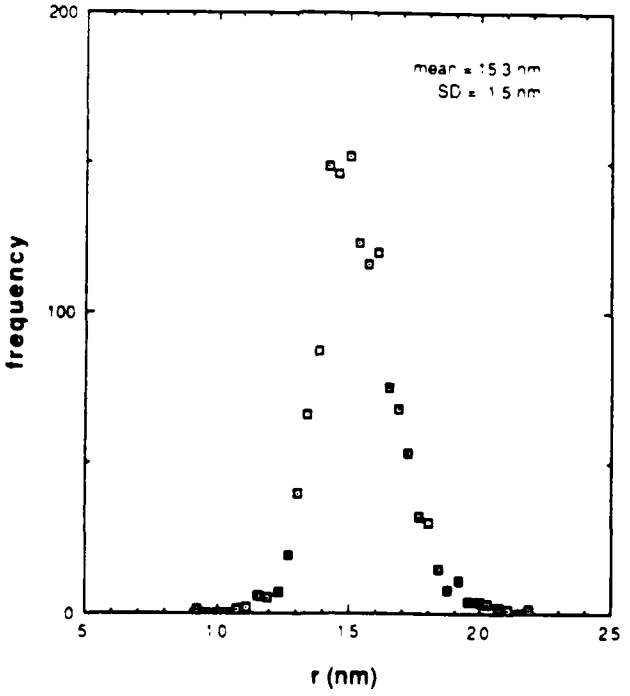

3-8

2-DIM DISTRIBUTION FUNCTION

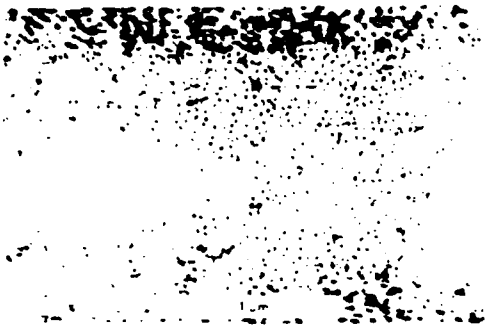

RADIAL DISTRIBUTION FUNCTION

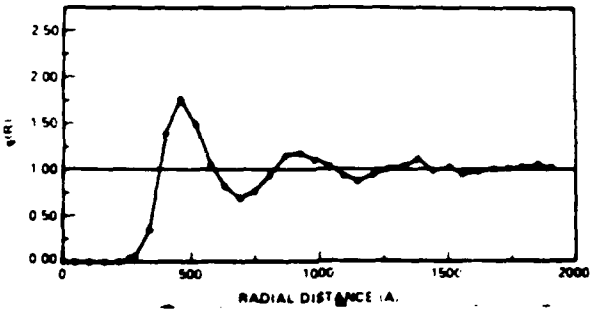

3-9

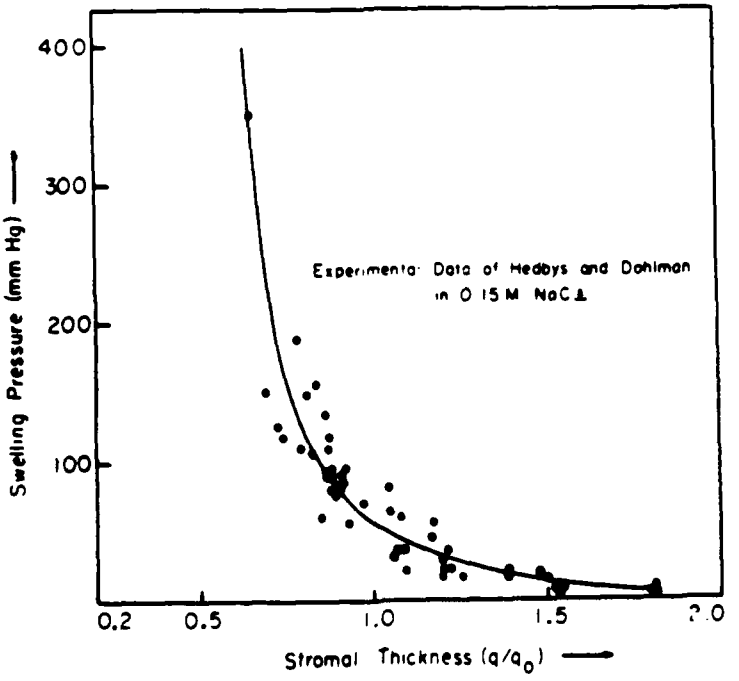

3-10

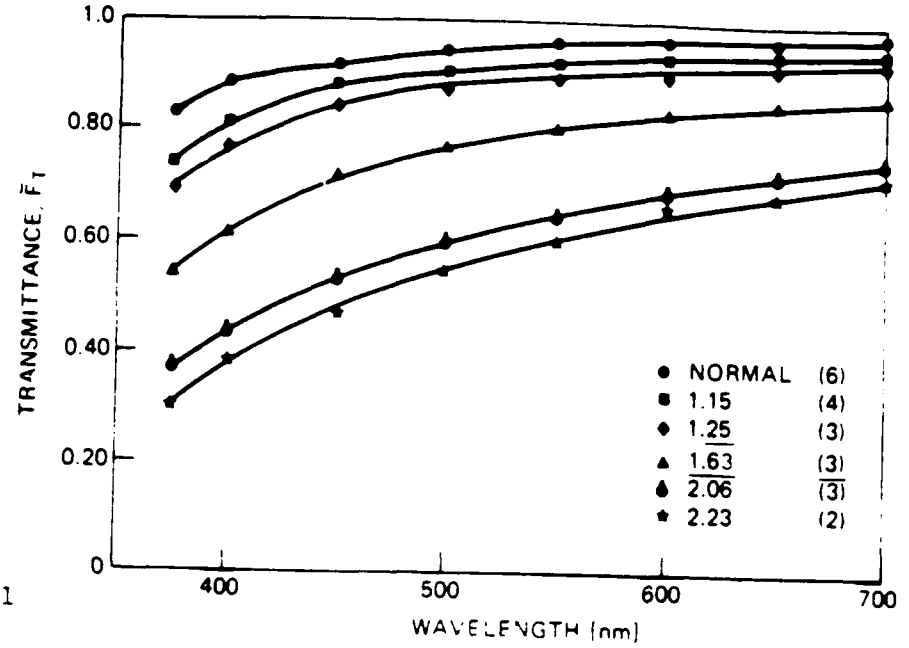

3-11

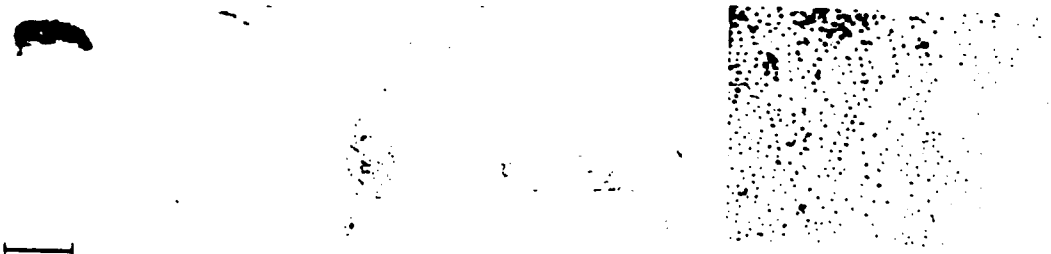

5000A

(a) Normal rabbit cornea. Fibrils are distributed with radial symmetry. No "lakes" or inhomogeneities are present.

5000A

(b) Rabbit cornea swollen 1 25X initial thickness Small "lakes" are evident

5000A

(c) Rabbit cornea swollen 1.9X initial thickness. Lakes are larger.

3-12

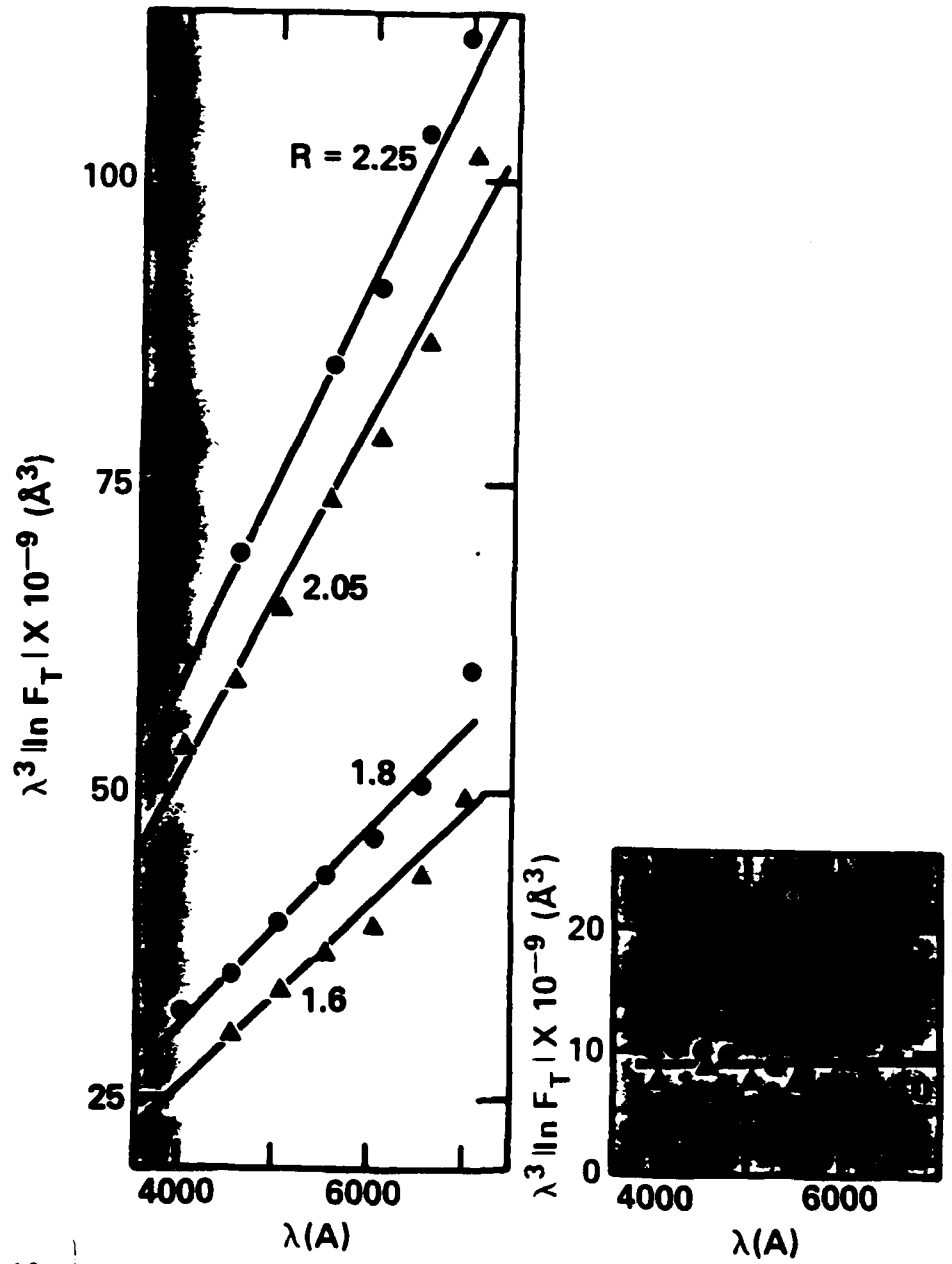
R = 2.25
2.05
1.8
1.6
100
75
50
25
4000
6000
λ(A)
$\lambda^3 |\ln F_T| \times 10^{-9}$ (Å^3)
20
10
0
4000
6000
λ(A)
$\lambda^3 |\ln F_T| \times 10^{-9}$ (Å^3)

3-13

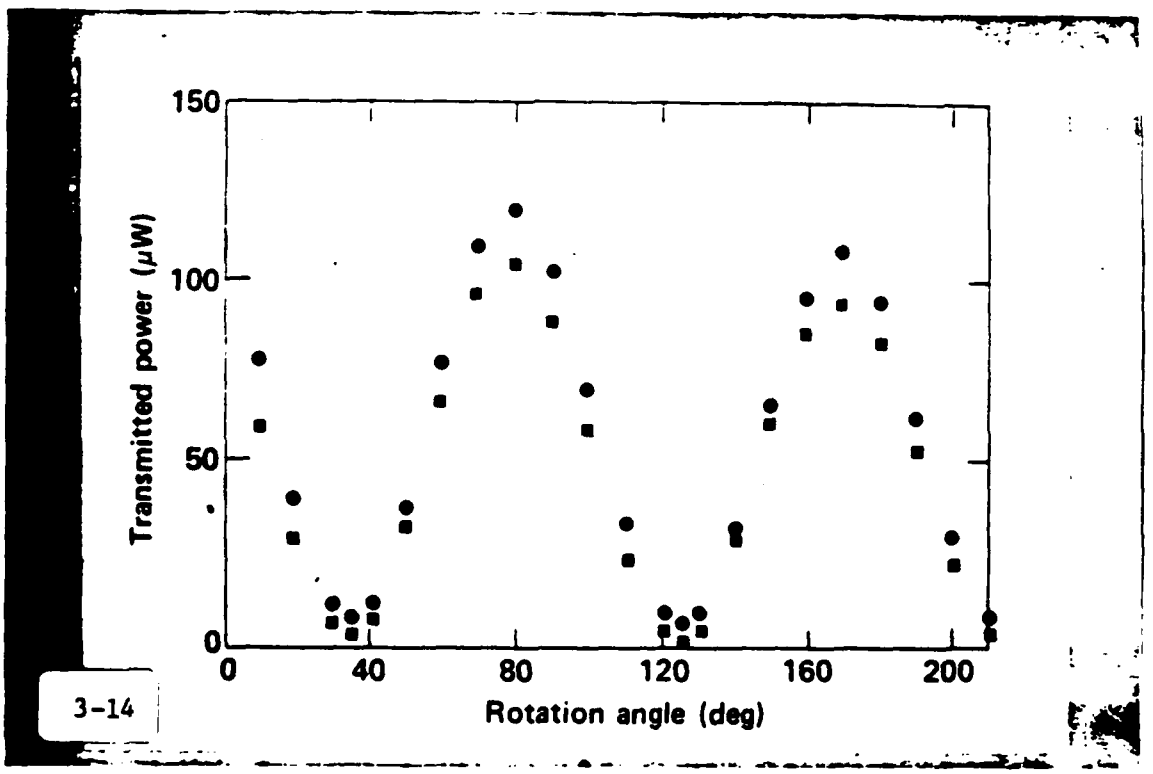
150
100
50
0
Transmitted power (μW)
0
40
80
120
160
200
Rotation angle (deg)
3-14

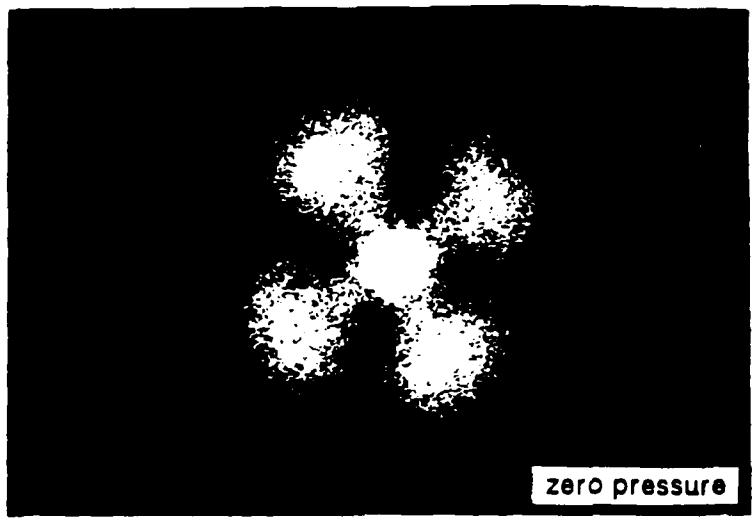

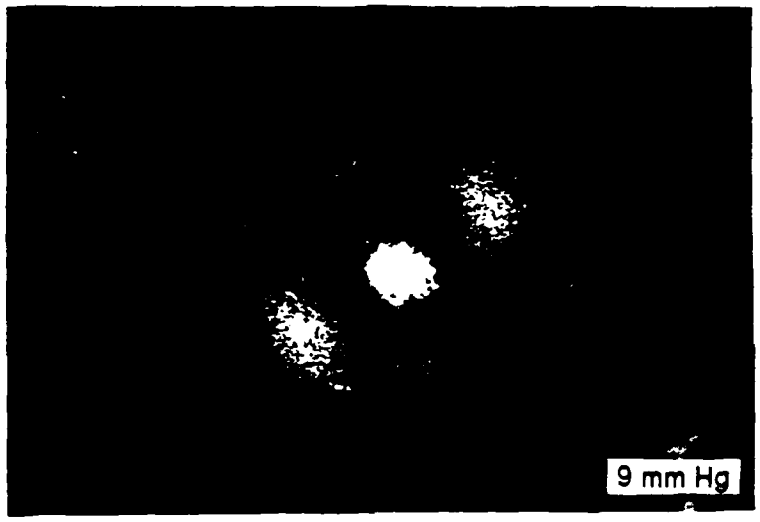

3-15

3-16

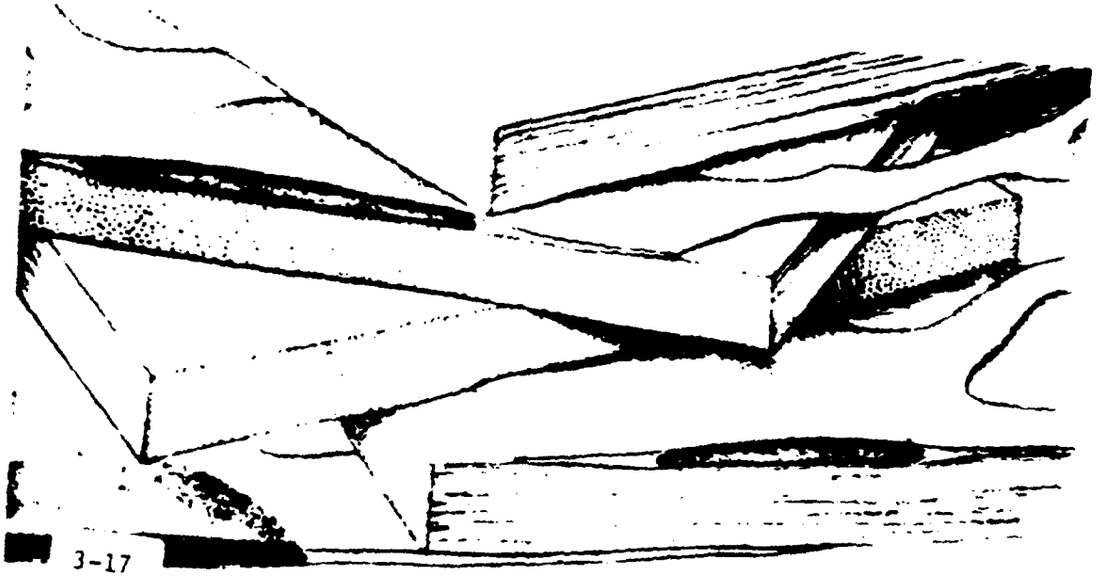

3-17

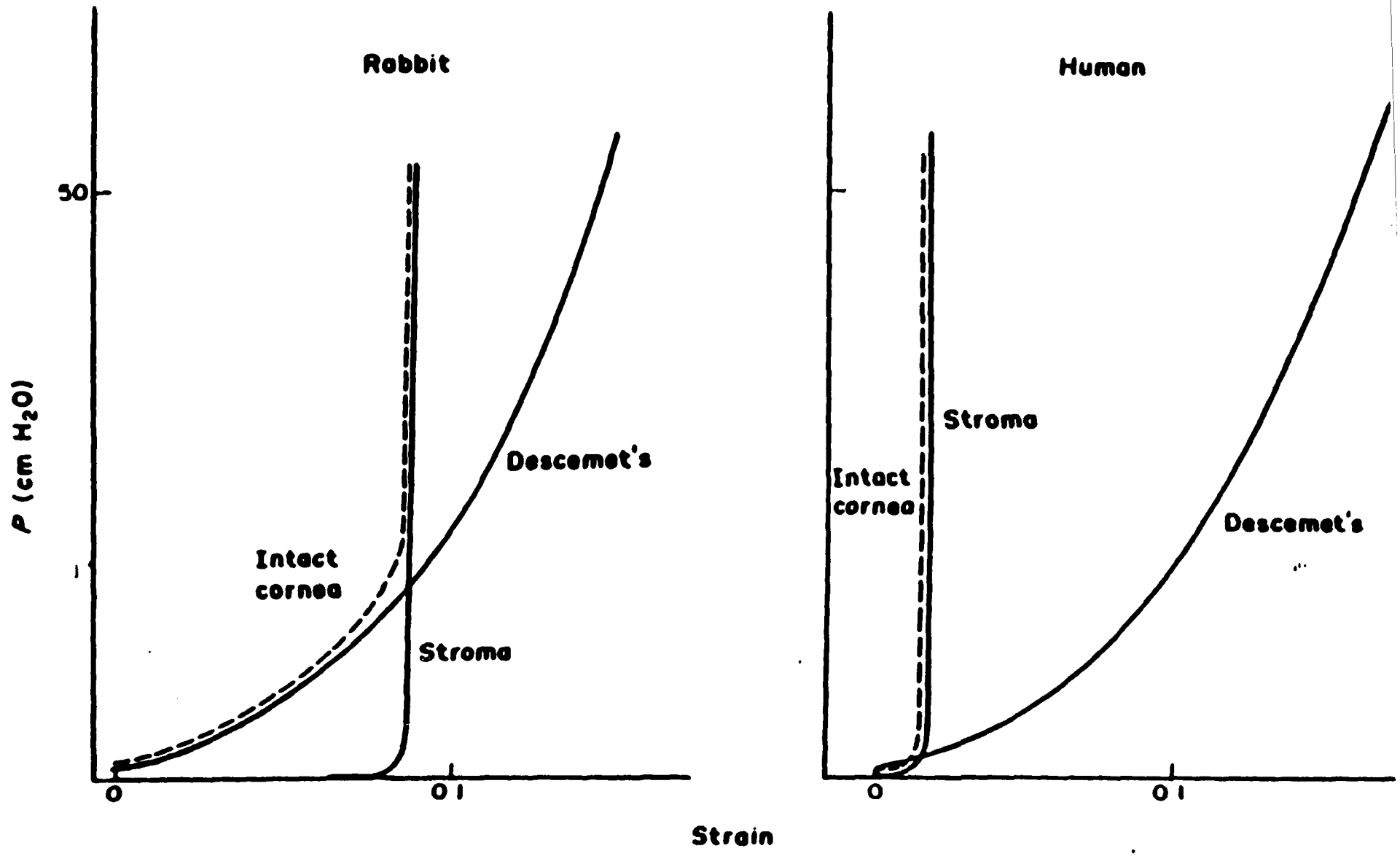

3-18 Suggested low pressure stress–strain relationship of the intact cornea (broken line) in relation to that of its component layers, for the rabbit and human. The stroma and Descemet's membrane undergo identical strains as the tissue stretches, so that the stress in the intact cornea is the sum of that in the two layers. The difference between the species can be explained on the basis of the relative initial strain in the layers.

DEFORMATION AND FRACTURE BEHAVIOUR OF BONE

W. Bonfield,
Department of Materials,
Queen Mary & Westfield College,
(University of London),
Mile End Road,
London, E1 4NS,
UK.

Cortical bone has a structural organisation which is complex at the macroscopic level, but displays progressive order with increasing levels of magnification. At the nm level of resolution, cortical bone has been well characterised as a hydroxyapatite reinforced collagen composite, with recent lattice imaging studies additionally defining the presence of imperfections in hydroxyapatite single crystals. The combination of hydroxyapatite and collagen produces anisotropic elastic deformation, together with an associated small, but significant, anelastic (viscoelastic) component of deformation, which is seen in hysteretic strain rate dependent load-unload behaviour for human cortical bone across a spectrum of ages. As the strain to fracture of cortical bone is limited, fracture is conditioned either by the presence of variable intrinsic crack initiaters or of random introduced surface defects. It has been demonstrated that a fracture mechanics approach can be applied to fracture in cortical bone to give values of the fracture toughness as defined by both the plane strain critical stress intensity factor (K_{IC}) and the plain strain critical strain energy release rate (G_{IC}) for specimens with a characterised starter crack. These fracture toughness values depend sensitively on the velocity of the propagating crack, with a transition from controlled to catastrophic fracture above a critical velocity, and are orientation dependent. The establishment of a quantitative measure of the deformation and fracture behaviour of cortical bone has been a major precursor in the recent innovation of synthetic bone-analogue materials.

References

(1) Deformation and fracture of bone,

W. Bonfield and C.H. Li,

J. Appl. Phys., 37, 869 (1966).

(2) Anisotropy of non-elastic flow in bone,

W. Bonfield and C.H. Li,

J. Appl. Phys., 38, 2450 (1967).

(3) Anelastic deformation and the friction stress of bone,

W. Bonfield and P. O'Connor,

J. Mater. Sci., 13, 1329 (1978).

(4) Advances in the fracture mechanics of cortical bone,

W. Bonfield,

J. Biomechanics, 20, 1071 (1987).

(5) Composites for bone replacement,

W. Bonfield,

J. Biomed. Eng., 10, 522 (1988).

Figures 1 through 10 added for amplification of the lecture.

Fig. 1. Variation of mechanical behavior with hydroxyapatite volume fraction in a synthetic bone replacement composite.

Fig. 2. A synthetic hydroxyapatile-polyethylene composite developed for bone replacement.

Fig. 3. Osteon pullout in bone fracture. (20μm marker)

Fig. 4. Model of bone anisotropy.

Fig. 5. Measured deformation behavior of critical bone.

Fig. 6. Model of deformation of bone.

Fig. 7. Lattice imaging of {100} planes in hydroxyapatite crystal in situ in bone using high resolution transmission electron microscopy. (Spacing = 0.82 nm).

Fig. 8. Hydroxyapatite crystals and collagen fibres in a cortical bone lamella using transmission electron microscopy.

Fig. 9. Optical microscope view of transverse and longitudinal sections of bone in a support bone.

Fig. 10. Macroscopic schematic view of cortical bone and cancellous bone.

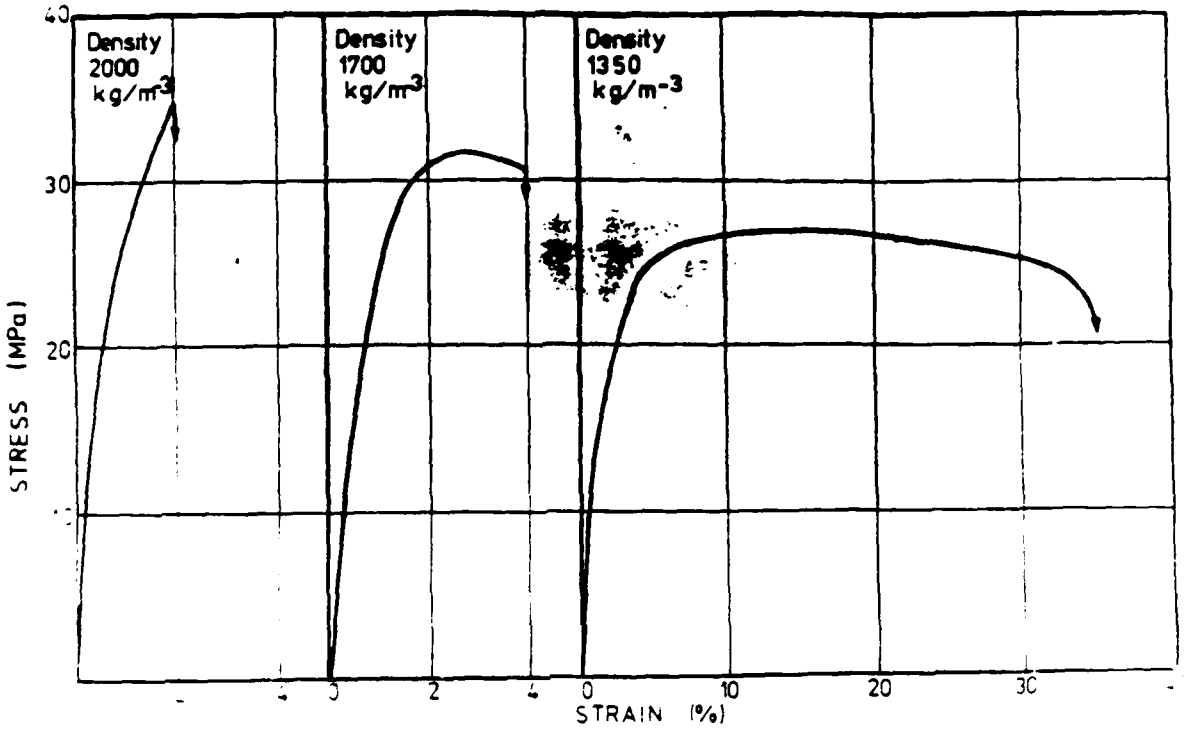
Density
2000
kg/m-3
Density
1700
kg/m-3
Density
1350
kg/m-3
40
30
20
STRESS (MPa)
2
4
0
10
20
30
STRAIN (%)

4-1

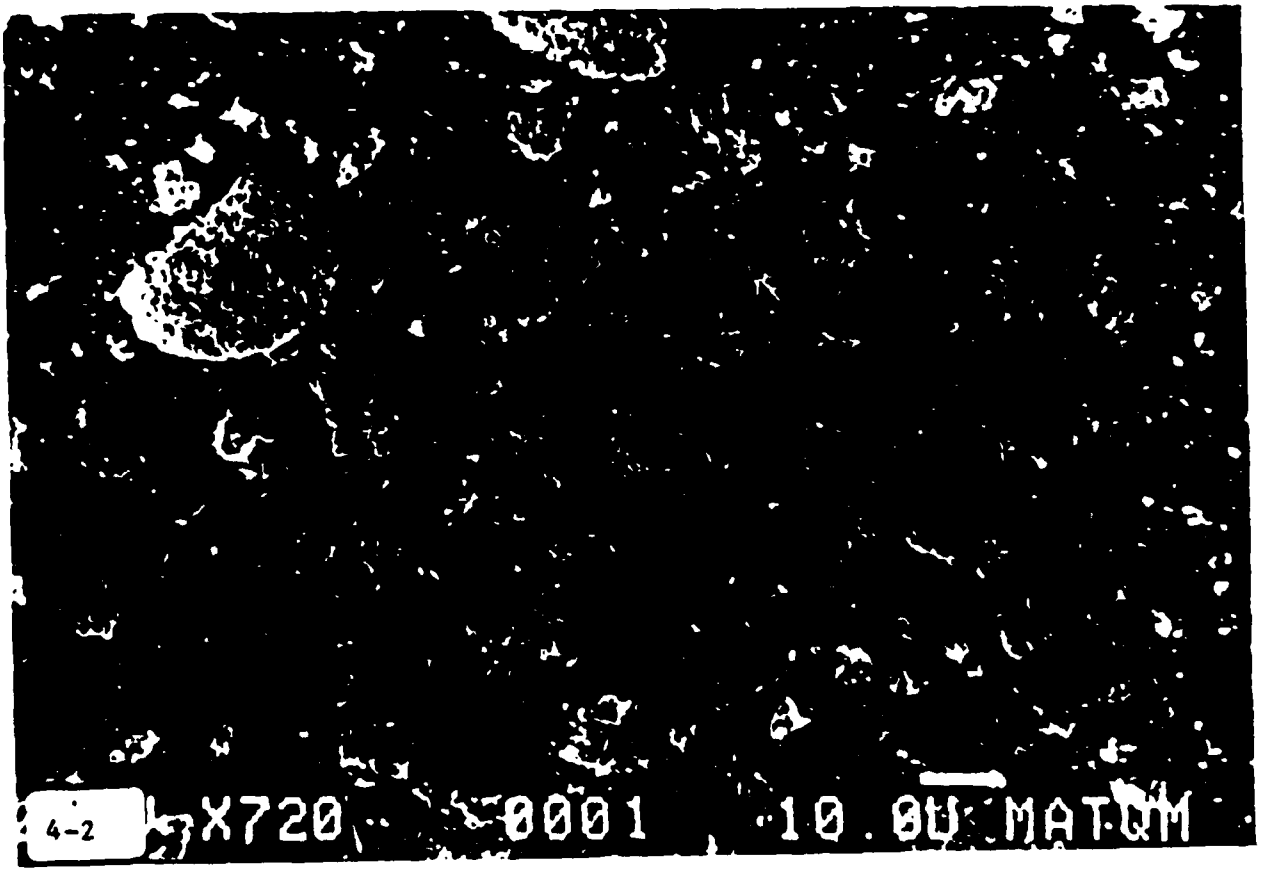
X720 0001 10.0U MATQM

4-2

4-3

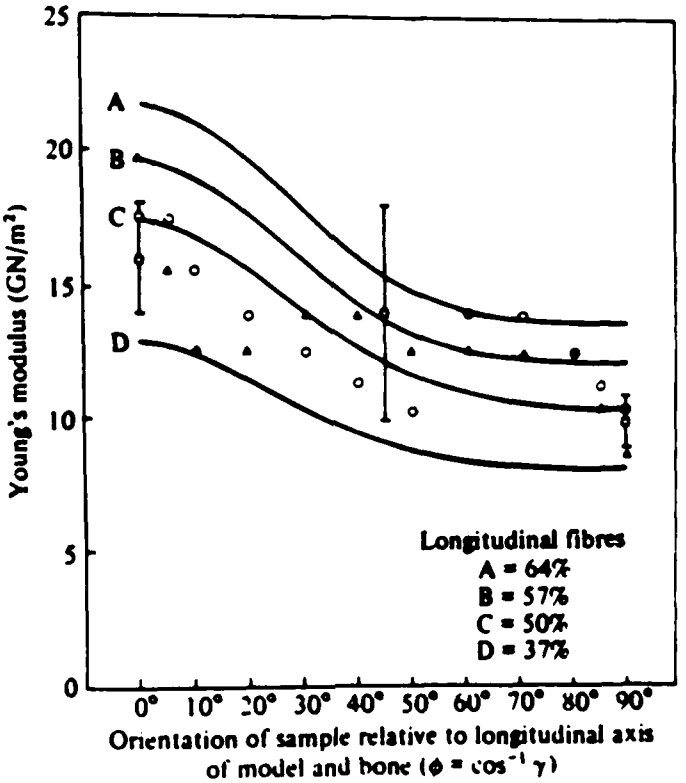
25
20
15
10
5
0
A
B
C
D
Young's modulus (GN/m²)
Longitudinal fibres
A = 64%
B = 57%
C = 50%
D = 37%
0° 10° 20° 30° 40° 50° 60° 70° 80° 90°
Orientation of sample relative to longitudinal axis
of model and bone (ϕ = cos⁻¹ γ)

4-4

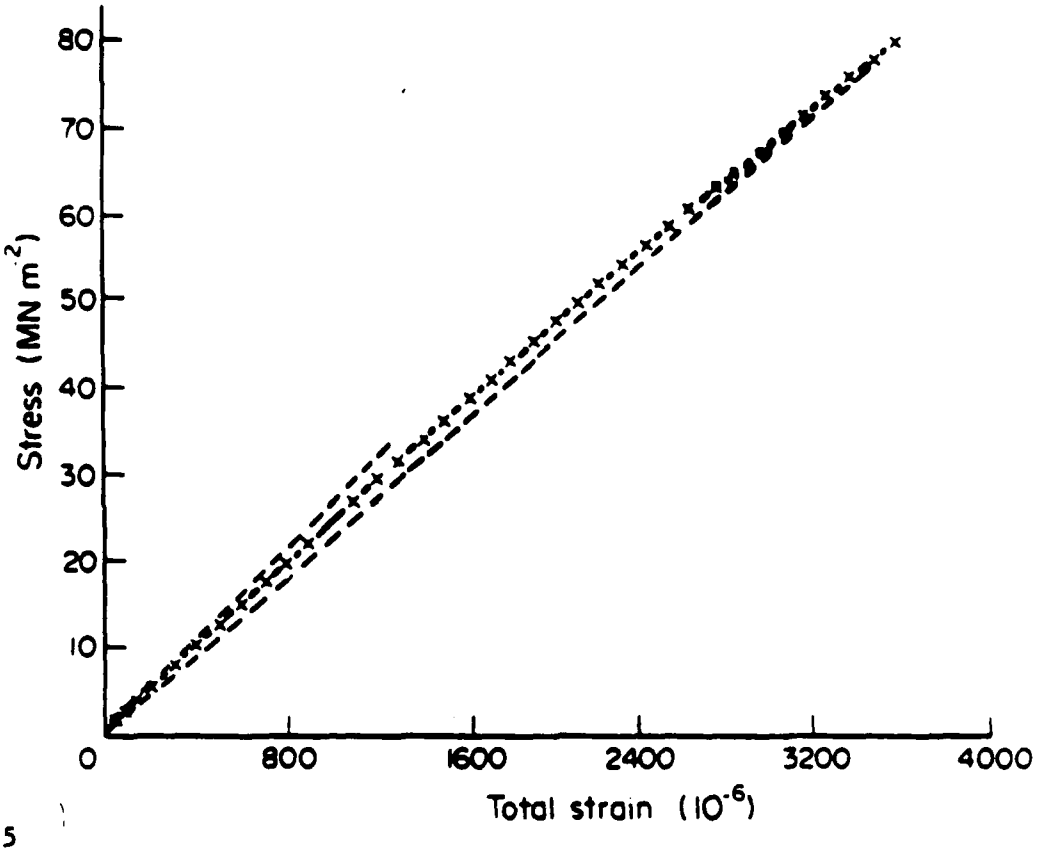
80
70
60
50
40
30
20
10
0
800
1600
2400
3200
4000
Stress (MN m^{-2})
Total strain (10^{-6})

4-5

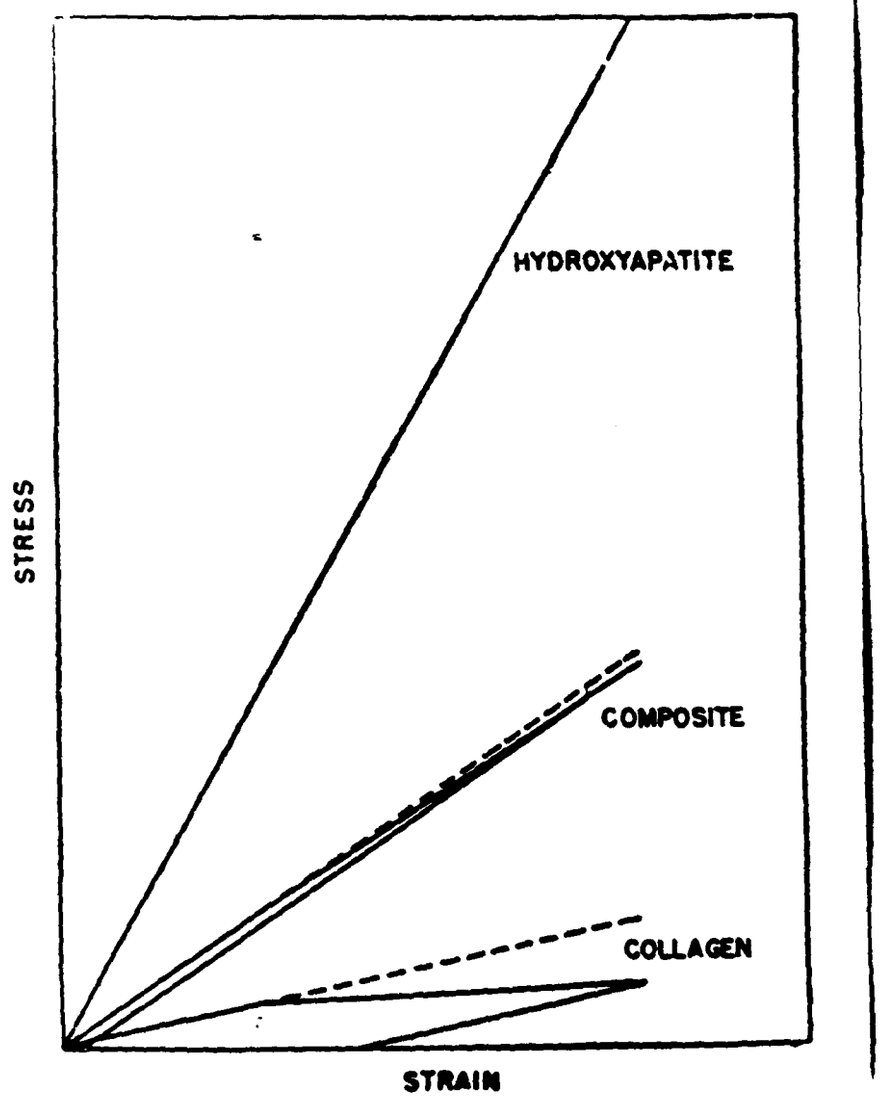

4-6

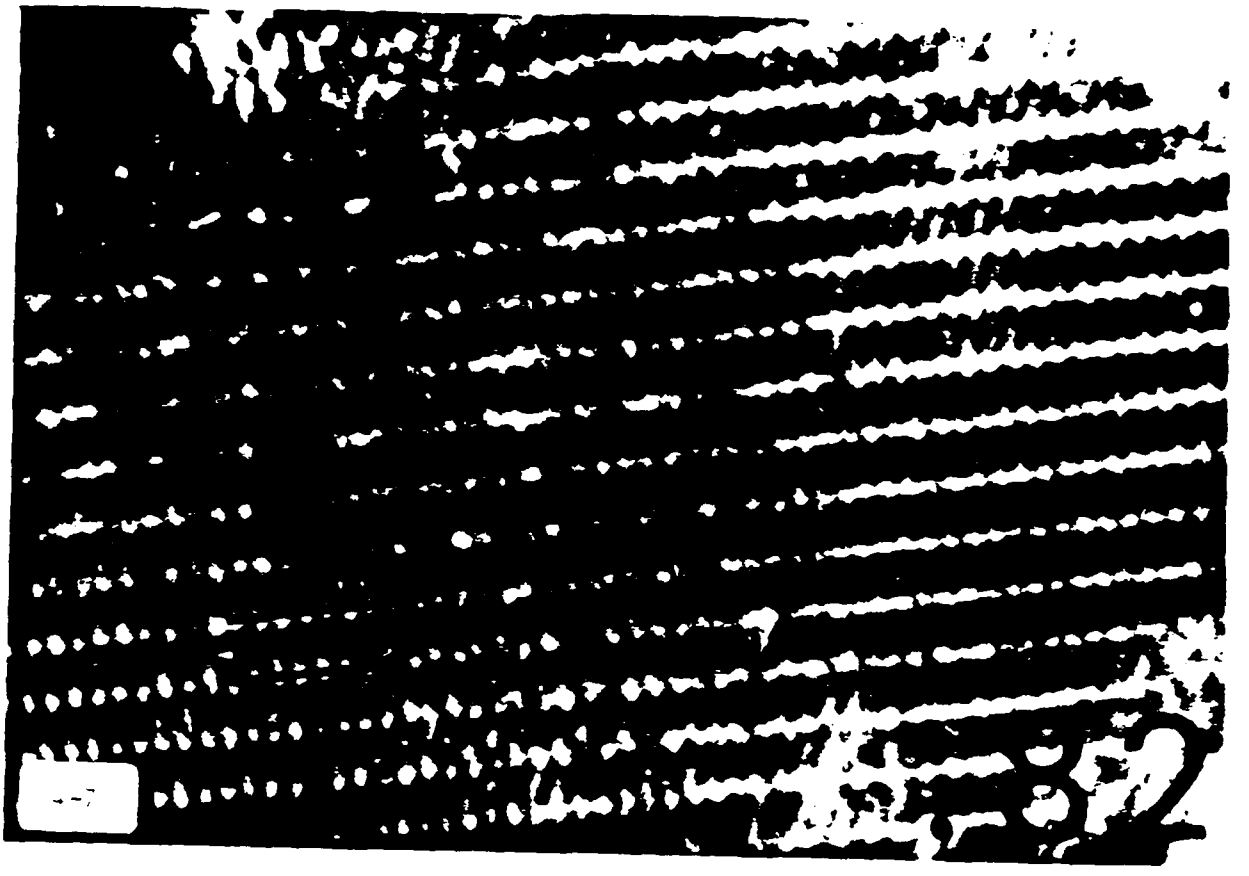

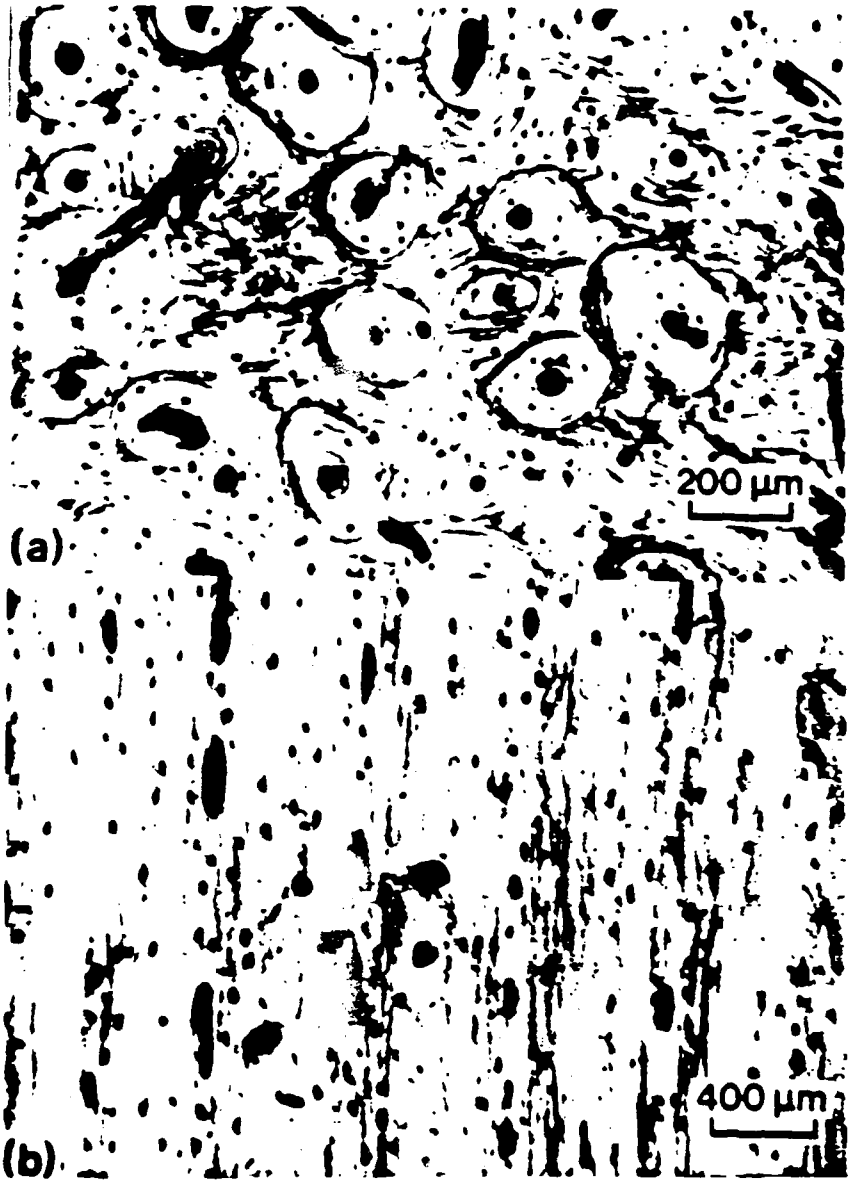

4-9

4-10

ORIGIN OF STRESS-GENERATED ELECTRICAL SIGNALS IN BONE AND TENDON

Wendell S. Williams

Department of Materials Science and Engineering
Case Western Reserve University
Cleveland, Ohio 44106, USA

The ability of certain biological tissues--e.g., bone and tendon--to respond to a mechanical stress by producing an electrial voltage has been recognized for only thirty years. Yet, this property is inherent in the structure of the tissue and therefore universal to all vertebrates. Ironically enough, this capacity for electro-mechanical transduction in biological tissues does not depend on biological activity but is believed by many investigators to have a biological function in the development, maintenance and repair of the tissues by influencing cellular activity. The purpose of the present paper, however, is to review the evidence that identifies two well known phenomena from inorganic science--piezoelectricity and the streaming potential--as the mechanisms responsible, respectively, for stress-generated potentials in dry and wet biological tissues.

At the discovery of stress-generated potentials in bone by Fukada and Yasuda in 1957 and in a similar period by Bassett and Becker, the effect was called a piezoelectric response, after the familiar property of mineral crystals such as quartz. However, it was appreciated that the piezoelectric response of bone must be associated not with the mineral phase of bone--hydroxyapatite--but with the collagen or other organic phase, as tendon, containing no mineral, exhibits the same piezoelectric response.

Although bone and tendon specimens in uniaxial loading appeared to give reasonable matrices of piezoelectric coefficients and display both the direct and converse effects expected of piezoelectric materials, Williams and Breger found it impossible to rationalize their experimental findings on bone subjected to non-uniform stress with the classical third-rank tensor theory of piezoelectricity. A resolution of the issue was proposed by Johnson, Gross and Williams, who assumed a spatial variation in the piezoelectric coefficients of bone, corresponding to local variations in the texture of the tissue, and whose resulting theoretical model matched the experimental findings for dry bone.

However, living bone is obviously not dry but immersed in an ionic fluid. The influence of this conducting medium was at first thought merely to alter the wave form of the piezoelectric signal, but experiments by Anderson and Eriksson, by Johnson, Chakkalakal, Harper and Katz, by Gross and Williams and by Pienkowski and Pollack implicated a second mechanism--the streaming potential. This effect results from forced flow of a conducting liquid through a porous medium which either donates charge of one sign to the liquid or traps charge from it. Streaming was demonstrated in bone by Gross and

without mechanically straining it and detected a potential difference across the specimen. The theoretical dependence on solution conductivity and viscosity expected for the streaming effect was also demonstrated, confirming the identification of mechanism. With beam samples of bone soaked in the same solutions and subjected to cantilever bending, Gross and Williams found the same dependence of the signal on solution parameters, indicating that the streaming mechanism is primarily responsible for the stress generated potential signal in wet bone.

1. E. Fukada and I. Yasuda, J. Phys. Soc. Jap. 12, 1158 (1957).

2. C. A. L. Bassett and R. O. Becker, Science 137, 1063 (1962).

3. W. S. Williams and L. Breger, J. Biomechanics 8, 1 (1975).

4. M. W. Johnson, W. S. Williams and D. Gross, J. Biomech. 13, 565 (1980).

5. J. C. Anderson and C. eriksson, Nature 227, 491 (1970).

6. M. W. Johnson, D. A. Chakkalakal, R. A. Harper and J. L. Katz, J. Biomech. 13, 437 (1980).

7. D. Gross and W. S. Williams, J. Biolmech. 15, 277 (1982).

8. D. Pienkowski and S. R. Pollack, J. Orthop. Res. 1, 30 (1983).

Figures 1 through 3 added for amplification of the lecture.

Fig. 1 Voltage generated by cantilever bending of dried beam made of specimen of bovine tibia with electrodes placed opposite each other on tension and compression surfaces. The voltage is proportional to the applied load with little scatter of data points. However, if the electrodes are moved to new positions, the resulting line will be quite different, indicating inhomogeneity of the tissue. If the electrodes are held fixed and the point of application of load varied, a linear relation between signal and this spacing results. This result is not predicted by the simple theory of piezoelectricity applied to a homogeneous solid.

Fig. 2 The linear relation between voltage and distance between electrodes and point of application of force mentioned in the preceding figure is displayed for dry bone and for two model materials--a piezoelectric "bimorph," and a radially poled PZT cylinder. The theoretical model developed interprets the results in terms of a spatially varying piezoelectric modulus in the bone, as in the model materials. Also shown is a similar linear relation for wet bone, for which a different mechanism for the stress-generated potentials is recognized--the streaming potential.

Fig. 3 Although most of the experiments on streaming in bone have been done in vitro, there is evidence for the effect in vivo, as there must be if the effect is to be biologically significant. A correlation between pulsatile flow of blood and what is considered to be a streaming signal was found by Otter and Cochran.

Generation of Streaming Potential by Pulse in Bone

(M. Otter and G.V.B. Cochran
Helen Hayes Hospital
West Haverstraw, NY)

SCHEMATIC

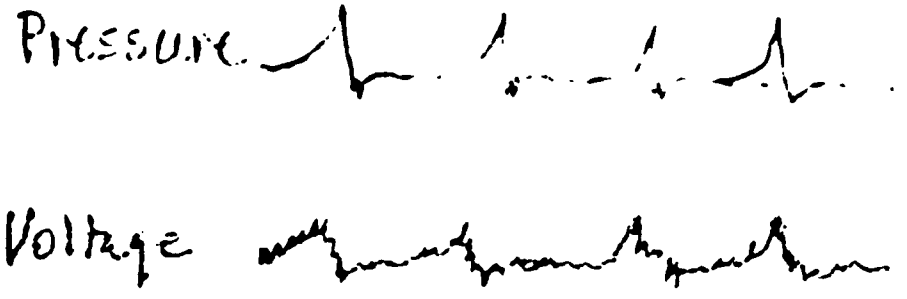

Dry Bone

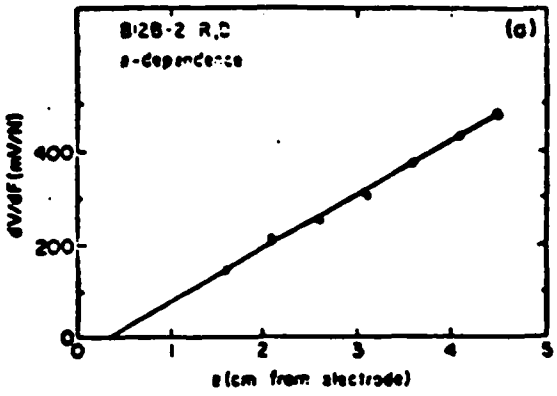

Wet Bone

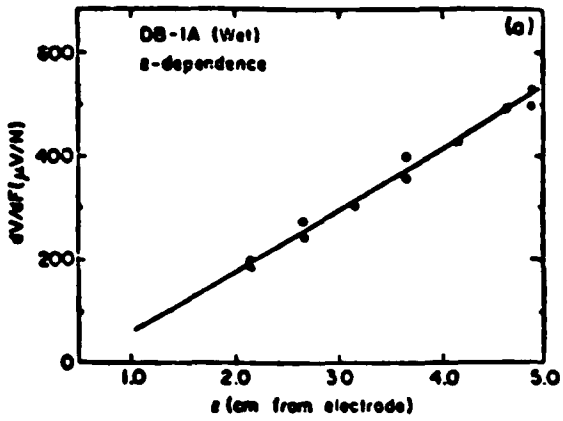

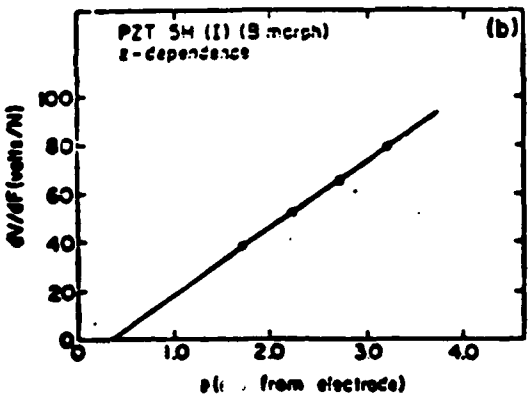

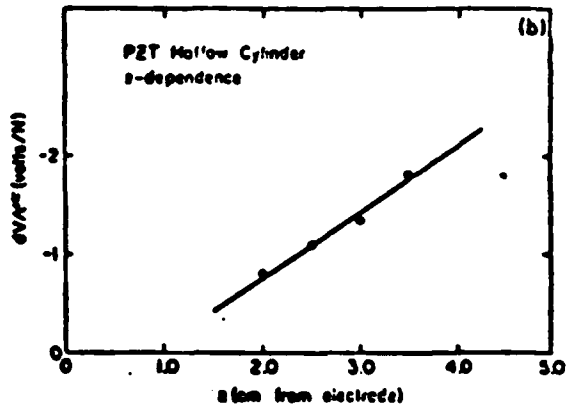

Bimorph

Poled Cylinder

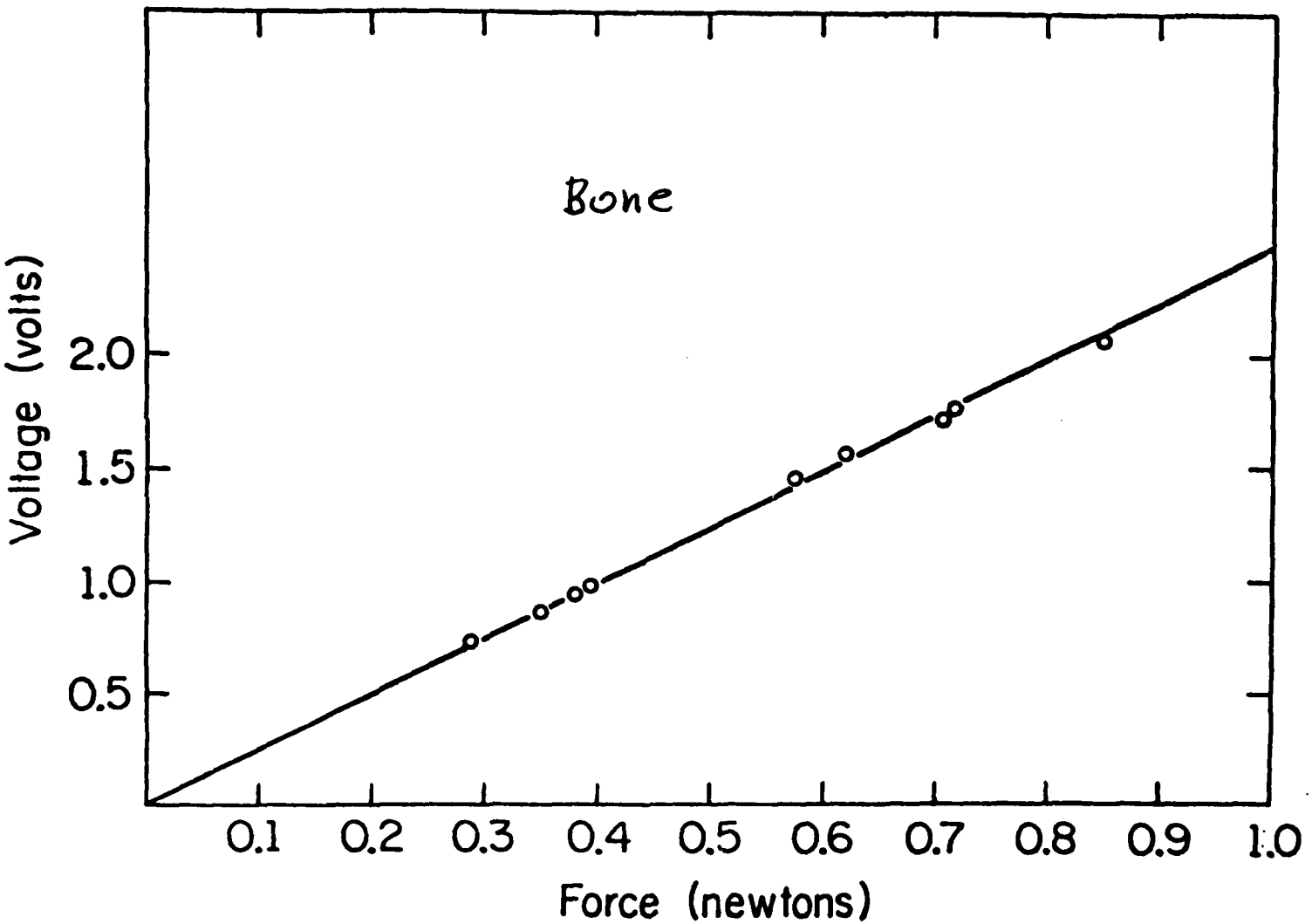
Bone
Voltage (volts)
2.0
1.5
1.0
0.5
0.1
0.2
0.3
0.4
0.5
0.6
0.7
0.8
0.9
1.0
Force (newtons)

5-3

HIERARCHICAL STRUCTURE OF THE INTERVERTEBRAL DISC

Anne Hiltner
Center for Applied Polymer Research
and Dept. of Macromolecular Science
Case Western Reserve University
Cleveland, Ohio 44106

The hierarchical organization of collagen fibrils in the intervertebral disc is characterized by structural gradients. In the annulus fibrosus, the thickness of lamellae increases abruptly 2 mm inward from the edge of the disc, dividing the annulus into peripheral and transitional regions. Lamellae in the lateral and posterior annulus have a broad distribution of lamellar thicknesses. In alternate lamellae, fibrils are inclined with respect to the vertical axis of the spine in a layup structure. From the edge of the disc inward to the nucleus, this interlamellar angle decreases from 62 to 45 degrees. Within lamellae, collagen fibrils exhibit a planar crimped morphology. (Figure 1) The plane of the waveform is inclined with respect to the spinal axis by the interlamellar angle. From the edge of the disc inward, the crimp angle increases from 20 to 45 degrees and the crimp period decreases from 26 to 20 um. A hierarchical model of the disc is presented that incorporates these morphological gradients. (Figure 2)[1]

Mechanical testing in load-deflection, stress relaxation, and creep modes reveals the response at each level of the hierarchy to compression. The stress-strain curve of the disc in compression contains toe, linear elastic, and yield regions similar to other collagenous tissues in tension. (Figure 3) This demonstrates that while the disc is loaded in compression, the fibrils of the annulus are loaded in tension.[2]

The role water transport plays in determining the mechanical properties of the disc is also established. During constant compressive strain stress relaxation experiments, the volume of the disc decreases with time by an amount equal to the macroscopic strain. (Figure 4)[3] A model is developed which hypothesizes that the relaxation and creep response is due to flow of water out of the disc as the result of the pressure gradient across the cartilage endplates caused by an externally applied stress. (Figure 5) The model considers cases with strain- and time- and strain-dependent pressure gradients, both of which fit the observed creep response of the disc. (Figure 6) These cases are analogous to the 3- and 4-parameter viscoelastic models, but contain elements which have a physical significance.[3]

References:

1. Cassidy, J.J., Hiltner, A., and Baer, E., "Hierarchical structure of the intervertebral disc", Conn. Tiss. Res., 23: 75-88, 1989.
2. Cassidy, J.J., Hiltner, A., and Baer, E., "The response of the hierarchical structure of the intervertebral disc to uniaxial compression", submitted to Materials in Medicine.
3. Cassidy, J.J., Silverstein, M., Hiltner, A., and Baer, E., "An analytical model of the creep mechanism in the intervertebral Disc ", submitted to Materials in Medicine.

Figure Captions

Fig. 1 Crimped collagen fibers within a single lamella stained with sirius red and viewed in crossed polarized light.

a. +24 degree rotation
b. 0 degree
c. -20 degree rotation

Fig. 2 Hierarchical model of the intervertebral disc showing lamellar structure, fiber orientation, and crimp morphology in the annulus fibrosus.

Fig. 3 Stress-strain curve of intervertebral disc in compression showing toe, linear, and yield regions.

Fig. 4 Decrease in disc volume with time as calculated from bulge measurements during stress relaxation.

Fig. 5 Creep model of the intervertebral disc.

Fig. 6 Creep data for a typical specimen plotted according to Case II, strain-dependent pressure gradient, and Case III, time- and strain-dependent pressure gradient.

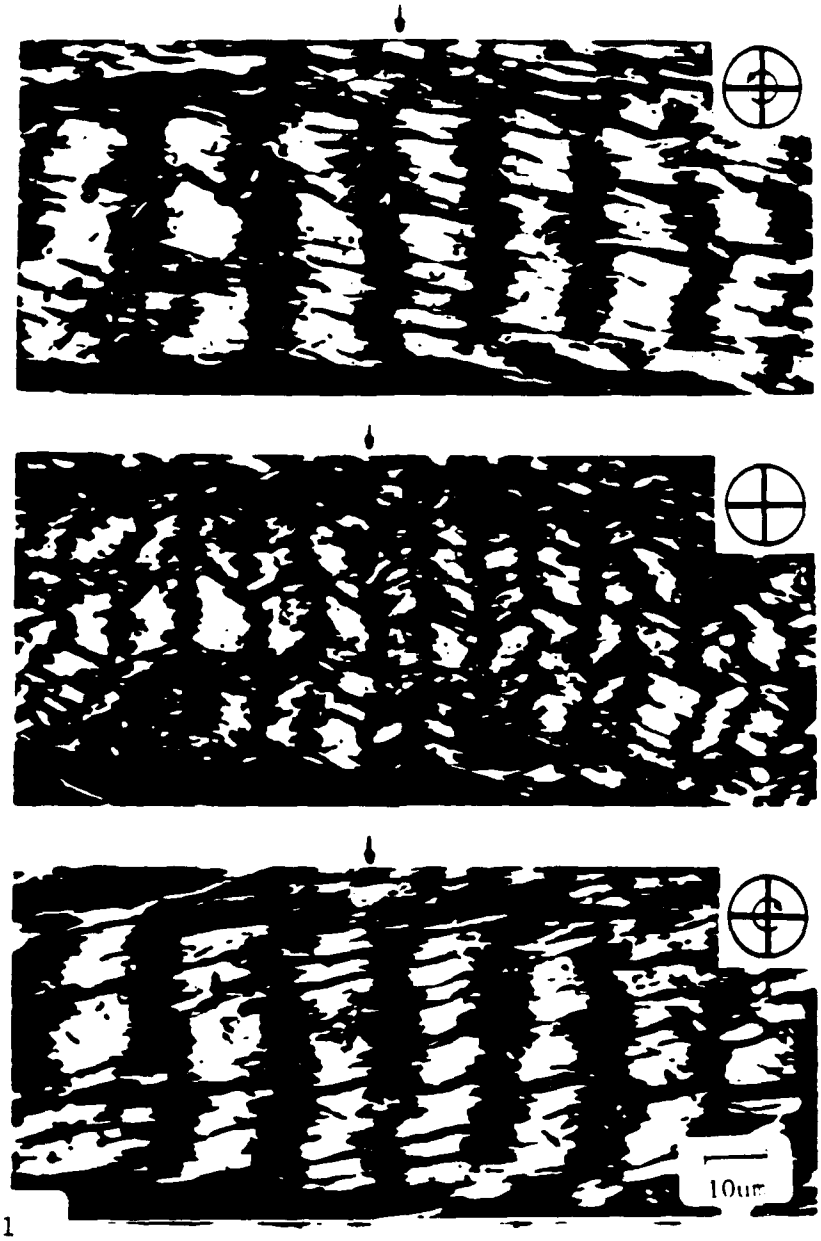

6-1

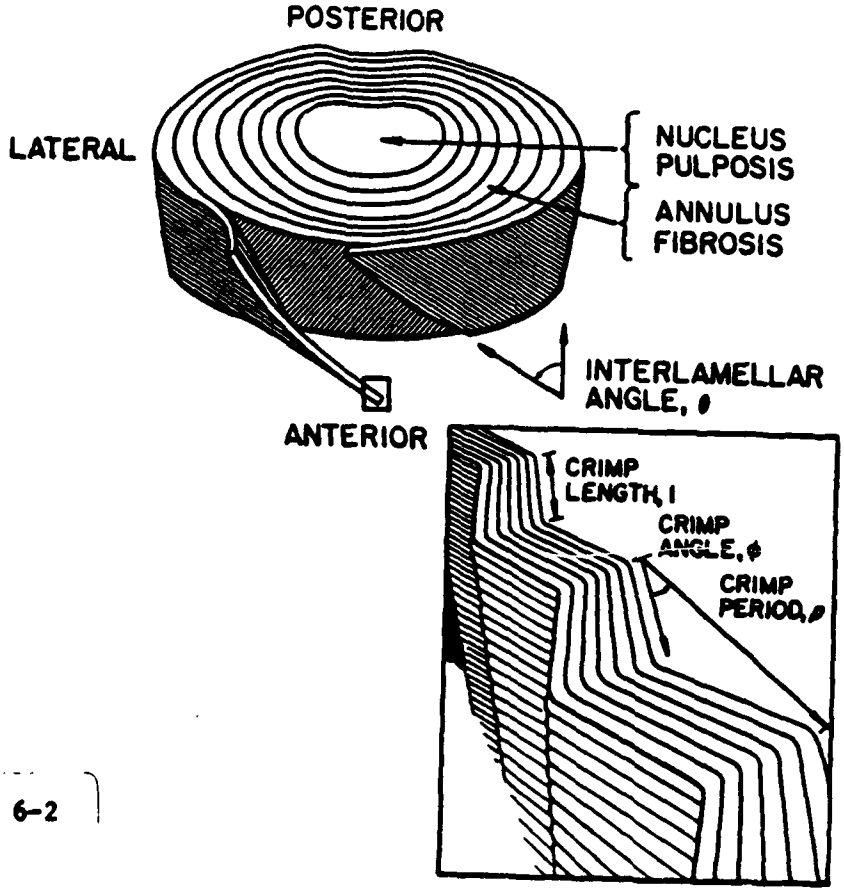
POSTERIOR
LATERAL
NUCLEUS PULPOSIS
ANNULUS FIBROSIS
INTERLAMELLAR ANGLE, θ
ANTERIOR
CRIMP LENGTH, l
CRIMP ANGLE, ϕ
CRIMP PERIOD, p

6-2

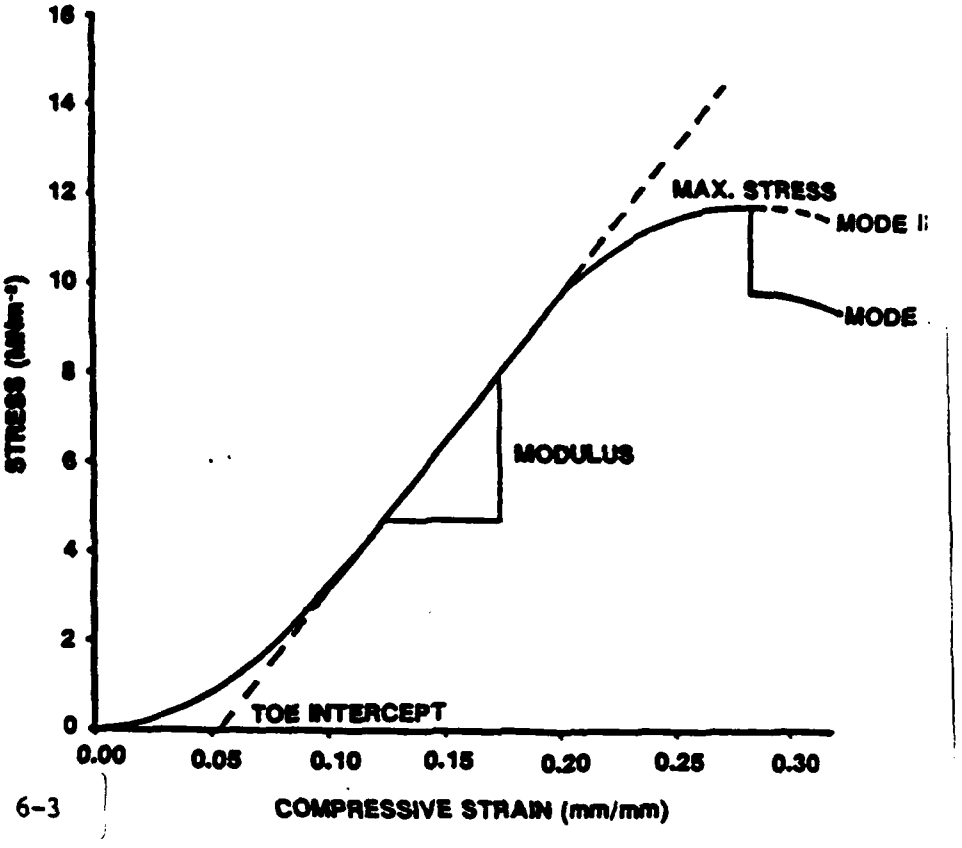
STRESS (MNm⁻²)
16
14
12
10
8
6
4
2
0
MAX. STRESS
MODE I
MODE
MODULUS
TOE INTERCEPT
0.00
0.05
0.10
0.15
0.20
0.25
0.30
COMPRESSIVE STRAIN (mm/mm)

6-3

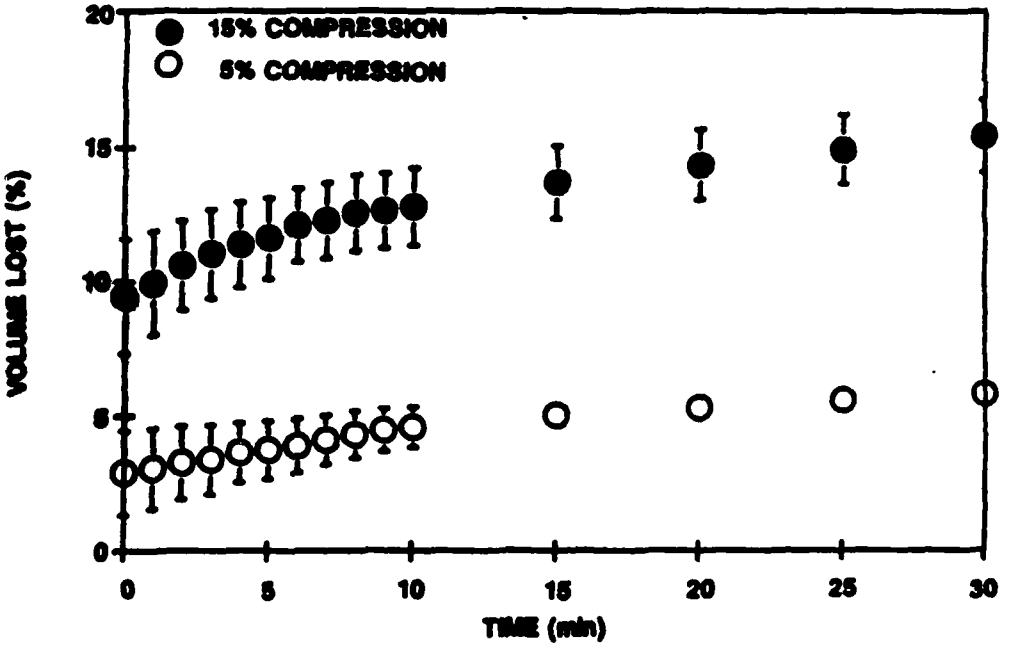
15% COMPRESSION
5% COMPRESSION
VOLUME LOST (%)
20
15
10
5
0
0
5
10
15
20
25
30
TIME (min)

6-4

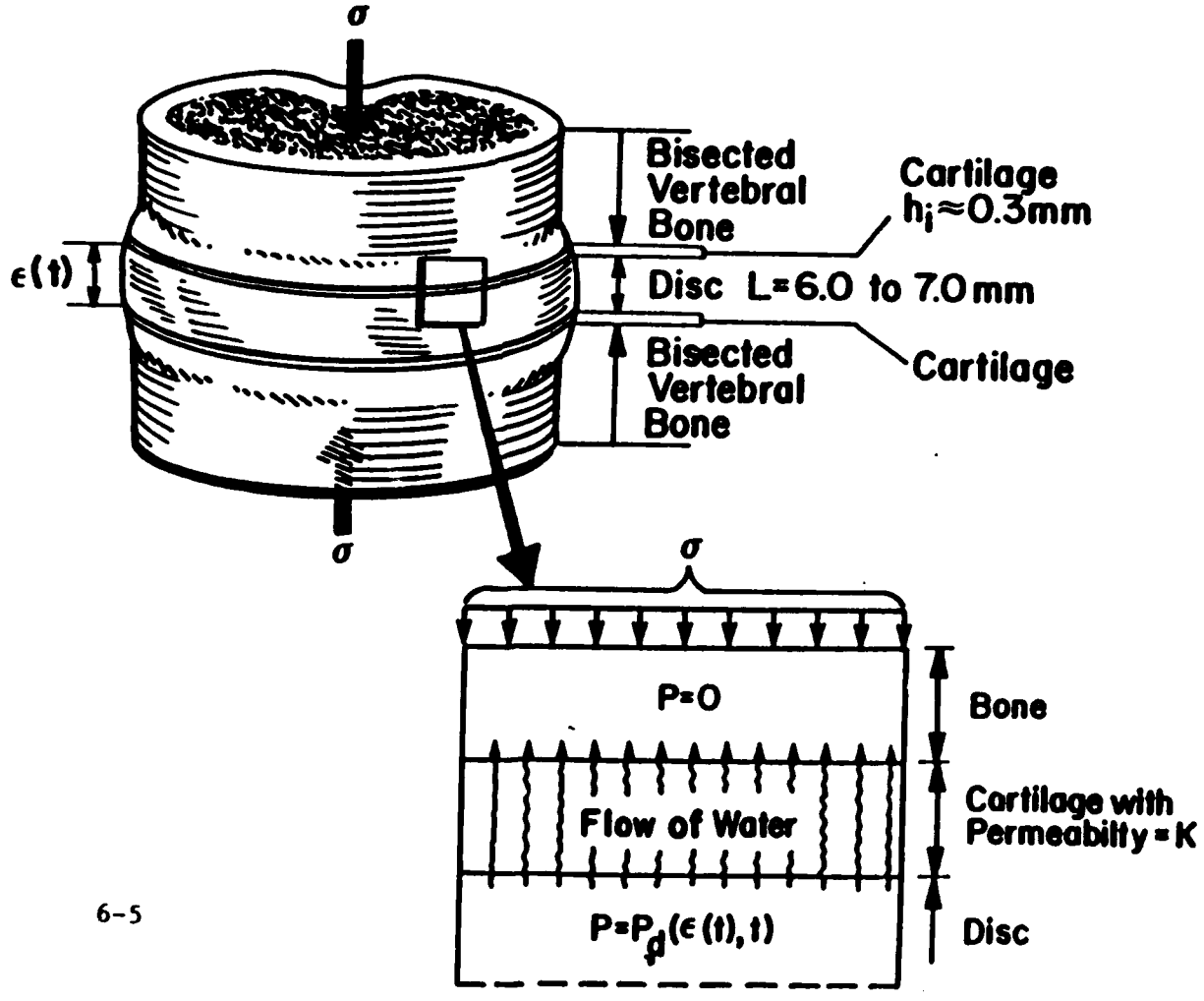
σ
Bisected Vertebral Bone
Cartilage $h_i \approx 0.3$mm
$\epsilon(t)$
Disc L=6.0 to 7.0mm
Cartilage
Bisected Vertebral Bone
σ
σ
P=0
Bone
Flow of Water
Cartilage with Permeability = K
$P=P_d(\epsilon(t),t)$
Disc

CREEP RESPONSE OF THE DISC

7 MNm^{-2}: EXPERIMENTAL DATA, CASE II AND III MODELS

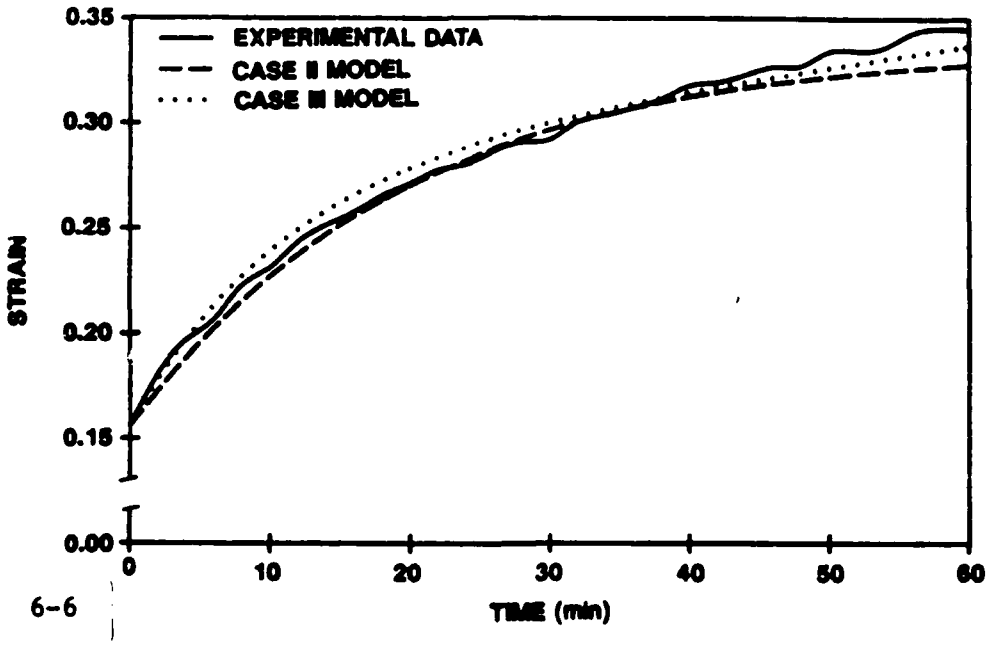

6-6

Figures 7 through 11 added for amplification of the lecture.

Fig. 7 Compressive modulus vs. location in the spinal column. The loading rate is 5 mm/min. The bars indicate the standard deviation.

Fig. 8 Compressive modulus vs. strain rate.

Fig. 9 Master relaxation curve of normalized stress vs. time.

Fig. 10 Water content of the disc vs. compressive strain.

Fig. 11 Three cases of the creep model.

a. Case I: Constant pressure gradient.
b. Case II: Strain-dependent pressure gradient.
c. Case III: Time- and strain-dependent pressure gradient.

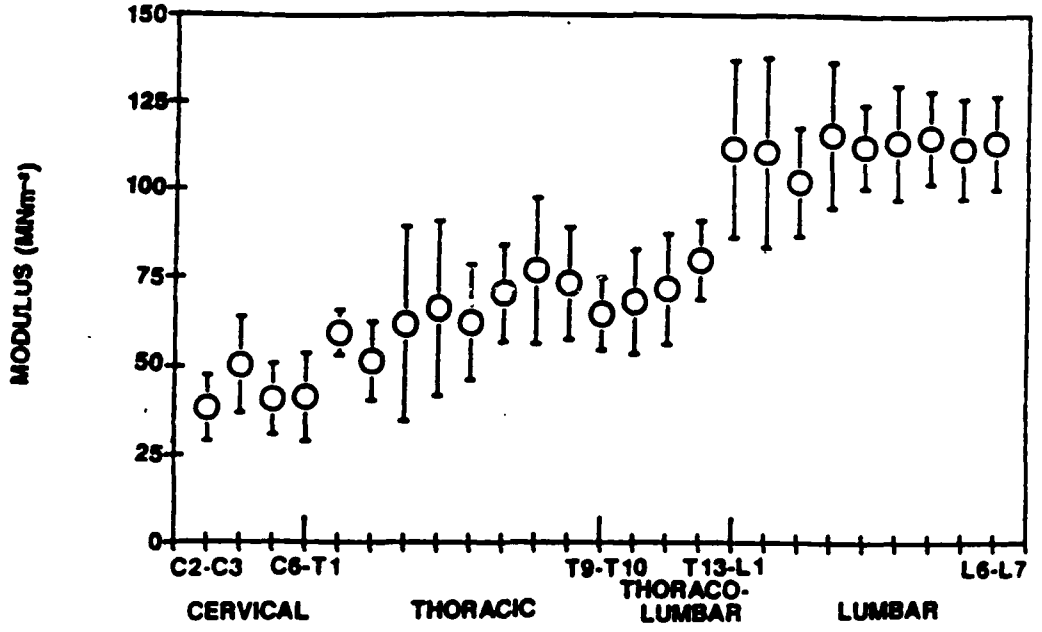
MODULUS (MNm⁻¹)
150
125
100
75
50
25
0
C2-C3
C6-T1
T9-T10
T13-L1
L6-L7
CERVICAL
THORACIC
THORACO-LUMBAR
LUMBAR
LOCATION IN SPINAL COLUMN

6-7

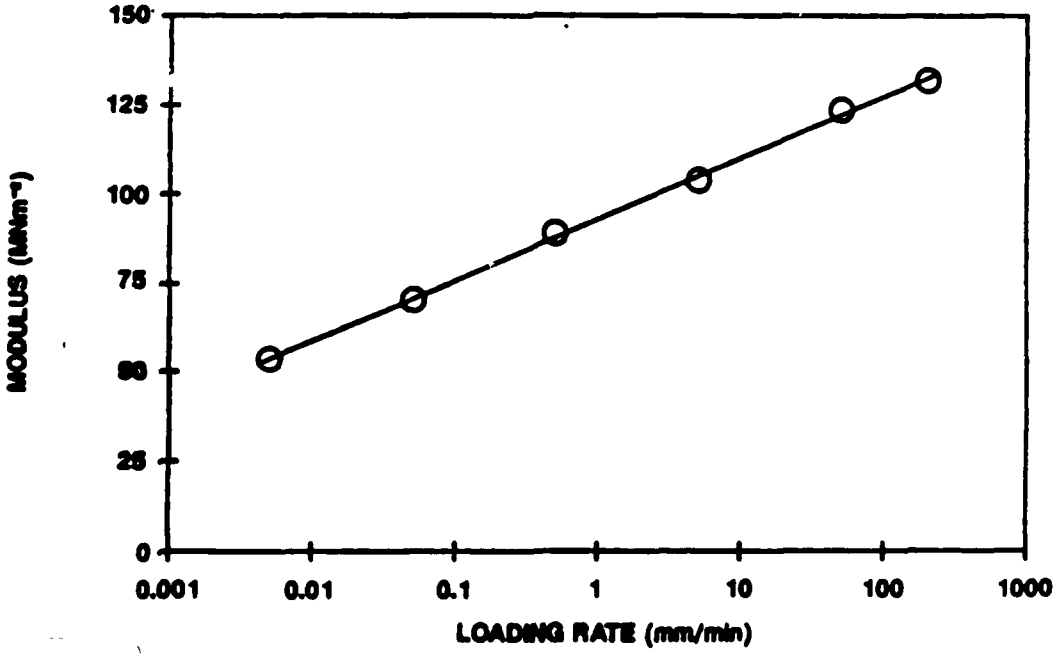
MODULUS (MNm⁻¹)
150
125
100
75
50
25
0
0.001
0.01
0.1
1
10
100
1000
LOADING RATE (mm/min)

6-8

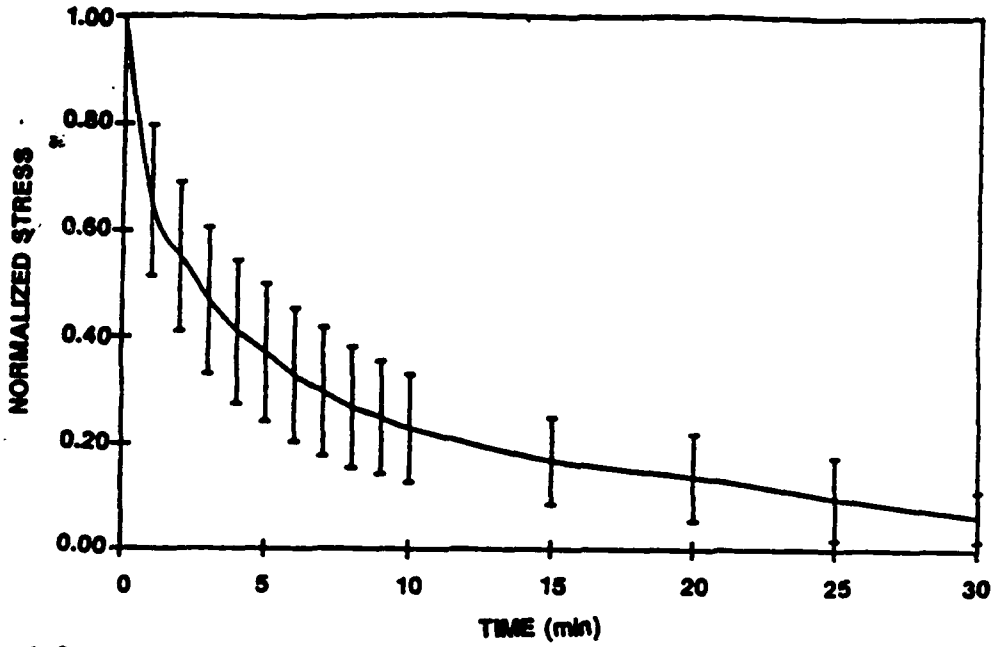
NORMALIZED STRESS
1.00
0.80
0.60
0.40
0.20
0.00
0
5
10
15
20
25
30
TIME (min)

6-9

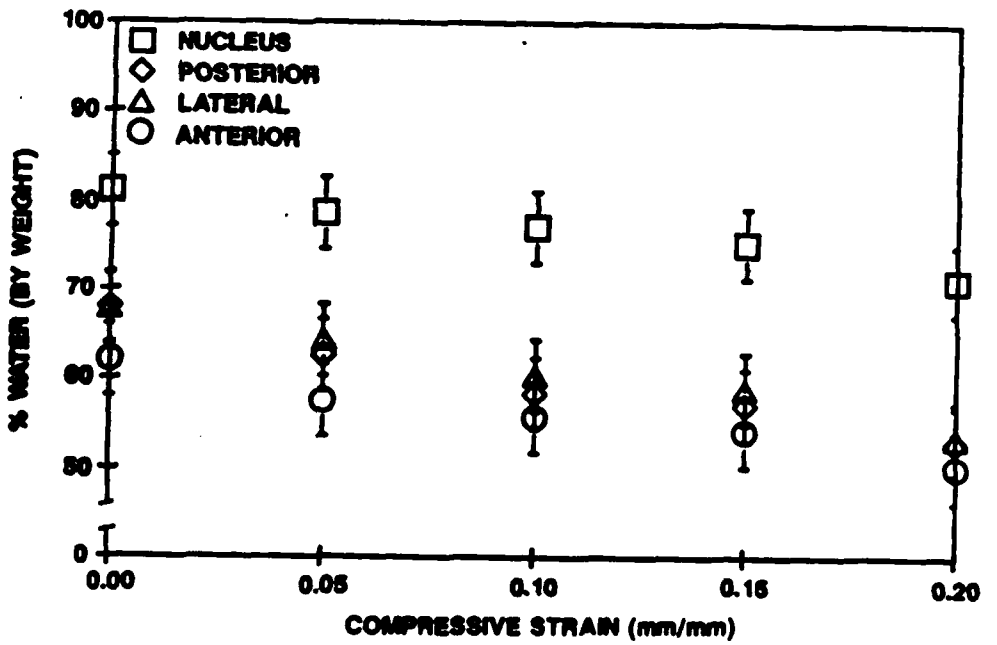
NUCLEUS
POSTERIOR
LATERAL
ANTERIOR
% WATER (BY WEIGHT)
100
90
80
70
60
50
0
0.00
0.05
0.10
0.15
0.20
COMPRESSIVE STRAIN (mm/mm)

6-10

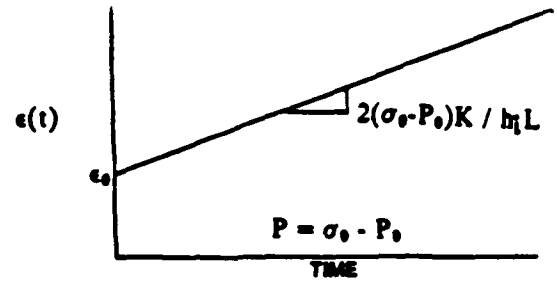

CASE I: CONSTANT PRESSURE GRADIENT

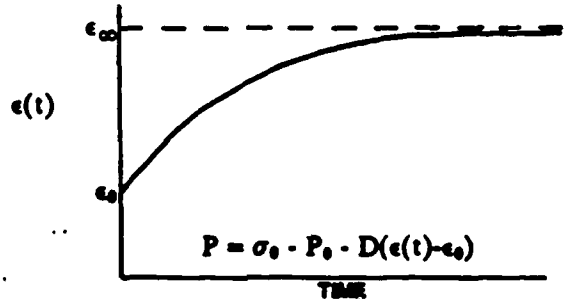

CASE II: STRAIN DEPENDENT PRESSURE GRADIENT

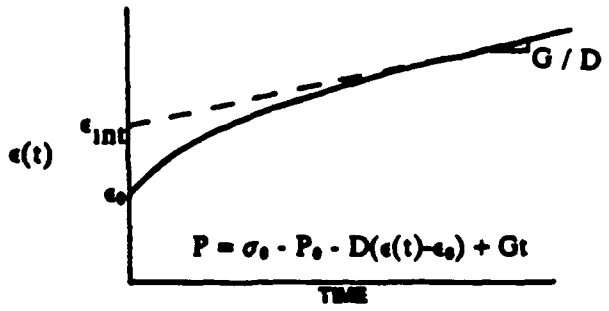

CASE III: STRAIN AND TIME DEPENDENT PRESSURE GRADIENT

6-11

STRUCTURE FUNCTION RELATIONSHIPS IN THE AORTIC VALVE

Mano Thubrikar

Department of Surgery
University of Virginia
Charlottesville, VA 22908

The aortic valve opens and closes for about 103,000 times a day. In the process it undergoes pressure loading and unloading, reversal of curvature, and a large amount of flexion for several billion cycles (fig. 1). We investigated its structure and function, to understand the reasons for its longevity. Substitute cardiac valves under the same conditions, break down much sooner. The aortic valve consists of three sinuses and three leaflets (fig. 2). The sinus wall is composed primarily of collagen, elastin, and smooth muscle cells. Consequently, the sinuses can expand and contract. The leaflets are thin sheets of connective tissue with dense collagen cords running parallel in the circumferential direction. This alignment of collagen makes the leaflet anisotropic. In systole, the leaflets move rapidly to a fully open position, then move gradually towards valve closure, and then move rapidly towards complete closure (fig. 3). The valve orifice is circular in early systole and gradually changes towards triangular in late systole. The valve commissures move outward during systole and inward during diastole. The bases of the leaflets move inward during systole and outward during diastole. The initial valve opening occurs without the forward blood flow, and because of the outward movement of the commissures. The

leaflet is longer in diastole and shorter in systole. The circumferentially oriented collagen cords influence the change in leaflet length. Study of pathologic aortic valves indicated that bileaflet and unileaflet valves become diseased more frequently than do trileaflet valves (fig. 4). Many diseased valves show degenerative calcification along the lines of leaflet flexion. The deviation from the normal design predisposes the aortic valves to the disease processes. The principles for the ideal valve design were investigated. The criteria for the ideal valve were: minimum valve height, minimum leaflet flexion, a prescribed leaflet coaptation, and no leaflet folds. The design parameters which satisfied these criteria were found to be similar to those of the aortic valve in several mammalian species. In conclusion, structure, material properties, and design are uniquely suited to impart efficiency and longevity to the aortic valve.

Figure Captions

1. The aortic valve showing one leaflet in both the open and closed positions.

2. Cross-section of the aortic valve through regions near base of noncoronary leaflet (smallest in figure). Three leaflets (L), three sinuses (S), and three commissural regions (C) can be seen.

3. Leaflet motion (distance between the two leaflets), commissure perimeter (perimeter of an imaginary triangle formed by 3 commissures), and aortic pressure versus time.

4. Radiographs of the bicuspid aortic valves from 3 patients who had aortic stenosis. Calcific deposits (white) appear to occur in identifiable patterns.

THE AORTIC VALVE

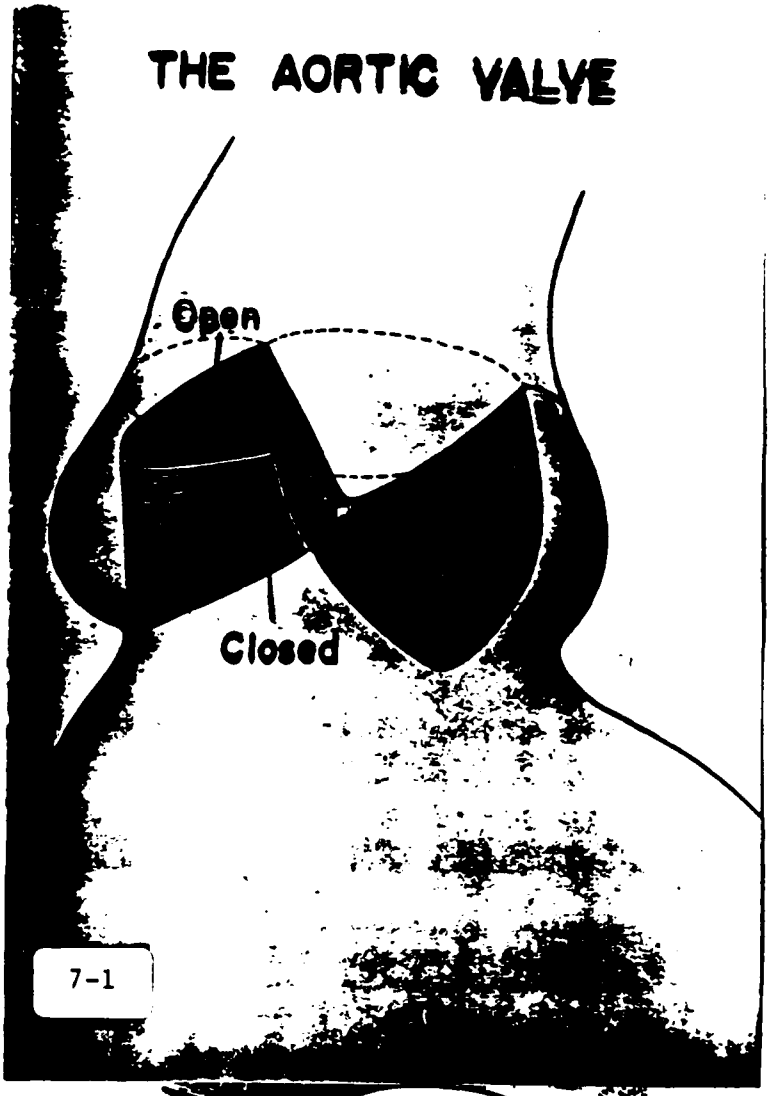

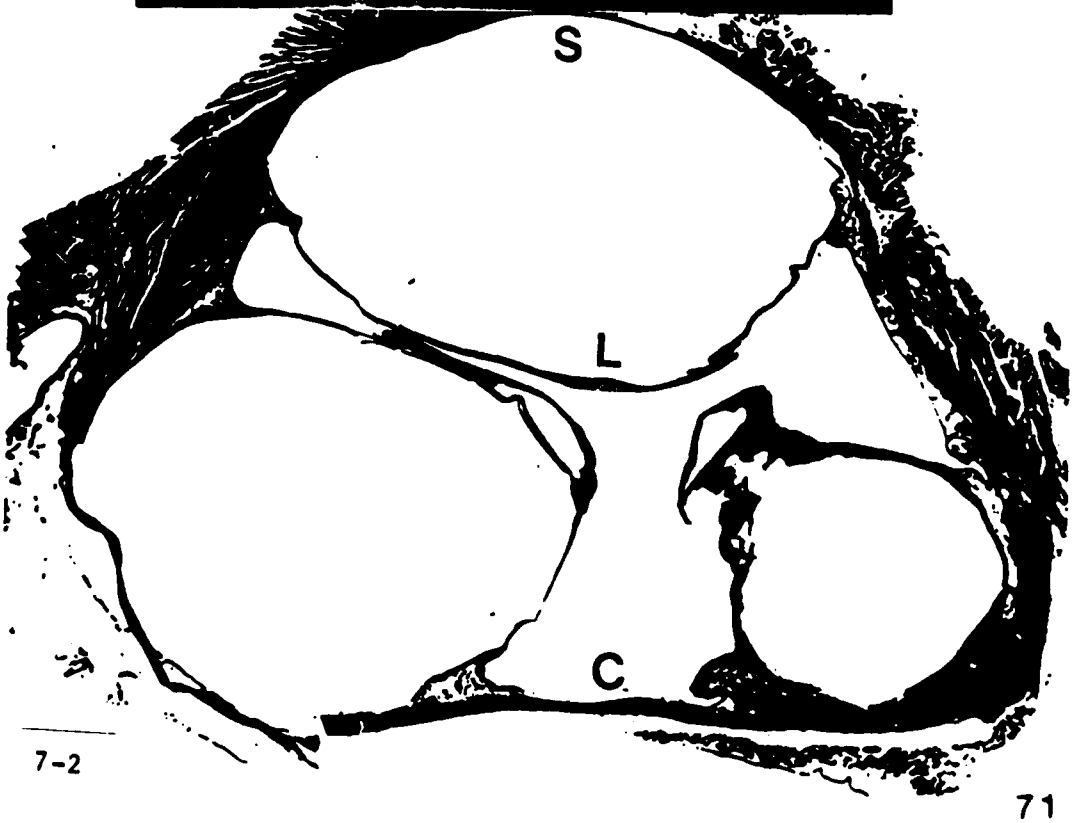

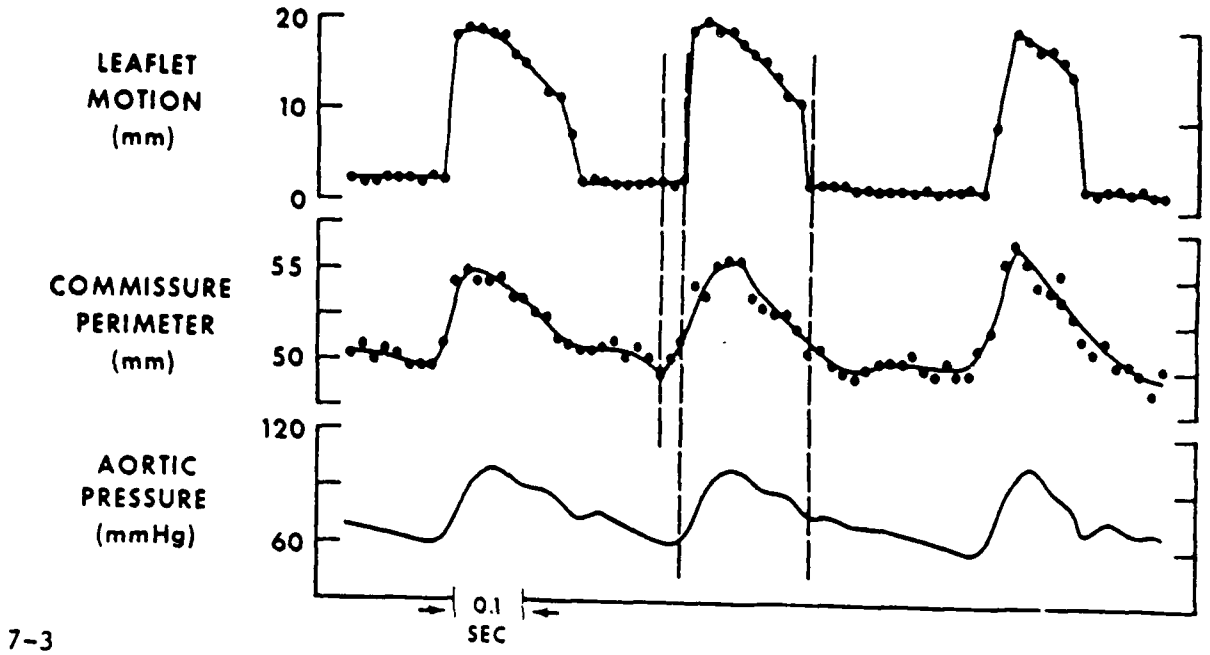
LEAFLET MOTION (mm)
20
10
0
COMMISSURE PERIMETER (mm)
55
50
AORTIC PRESSURE (mmHg)
120
60
0.1 SEC

7-3


63
4
2

7-4

Figures 5 through 10 added for amplification of the lecture.

Fig. 5 The closed aortic valve viewed from below. The three coapting leaflets of the valve, the aorta above, and the ventricular myocardium along with aorto-ventricular membrane below are seen. Only the load-bearing portion of the leaflet is visible.

Fig. 6 A direct view of a single leaflet. The nodule of Arantius at the center of the free edge appears unusually prominent in this leaflet. The inferior margin of the lunules which is also the line of leaflet coaptation marks a separation between the coaptation surface above and the load-bearing surface below. The line of leaflet attachment to the aortic wall has a crescentic shape.

Fig. 7 The mechanism of opening of the aortic valve. When pressure in the left ventricle equals the pressure in the aorta, the commissures move outward (arrows) and carry the leaflets along with them to produce a stellate orifice.

Fig. 8 Left: Leaflet length vs. pressure across the leaflet in vivo. The circles represent measured leaflet length and measured pressure gradient in diastole. Vertical bars represent measured leaflet length and an assumed pressure gradient of 0-10 mm Hg in systole. Right: Increase in leaflet length vs. load on the leaflet in vitro. The stress-strain curve is nonlinear, indicating that the leaflet has a variable modulus.

Fig. 9 Typical plot of leaflet length versus pressure gradient across the leaflet in vivo in a single dog. The circles represent measured leaflet length and measured pressure gradient in diastole. The bars represent measured leaflet length and assumed pressure gradient of 0 to 10 mm Hg in systole. The lengths ℓ_0, ℓ, ℓ, and ℓ_2 correspond to the gradients of 0, 10, 60, and 200 mm Hg, respectively. ϵ_D and ϵ_S represent strains. The origin (12,0) is arbitrarily chosen.

Fig, 10 Schematic representation of the leaflet structure showing circumferentially oriented collagen cords as the dominant structural component. When the leaflet is pulled only radially, the collagen cords can separate and do not offer resistance to stretching. When the leaflet is pulled both radially and circumferentially, then tension in the collagen cords in the circumferential direction prevents them from separating.

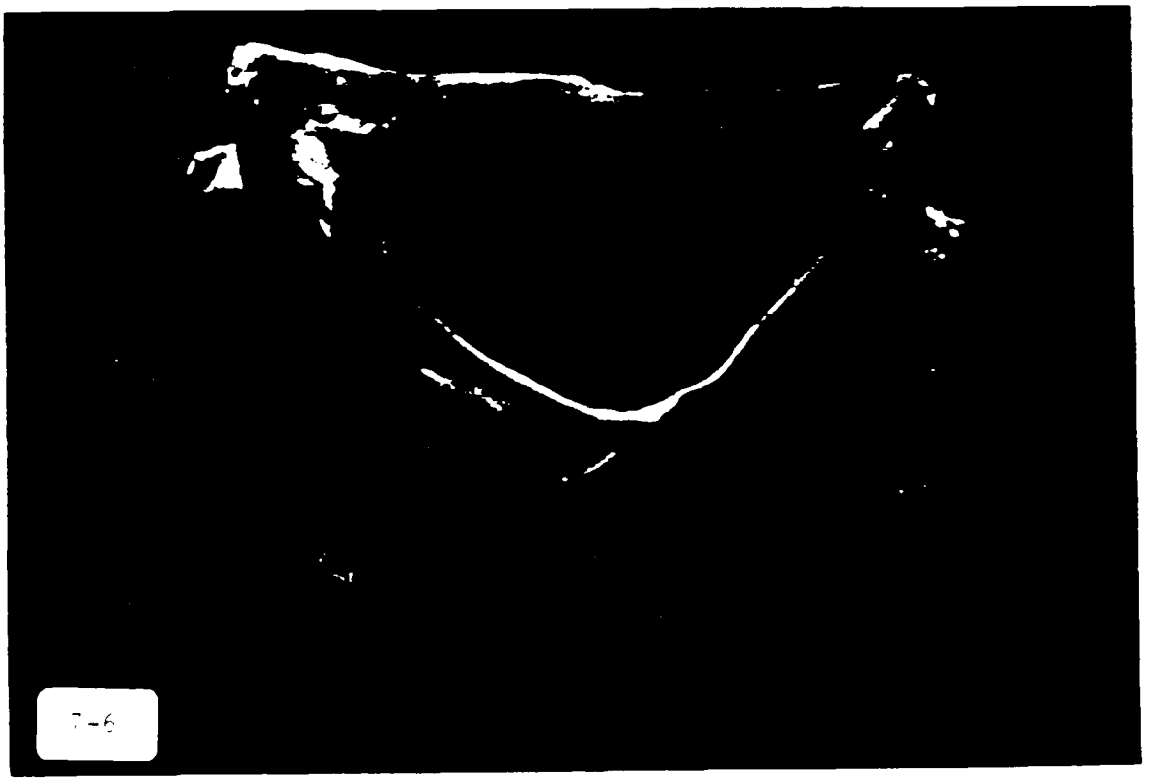

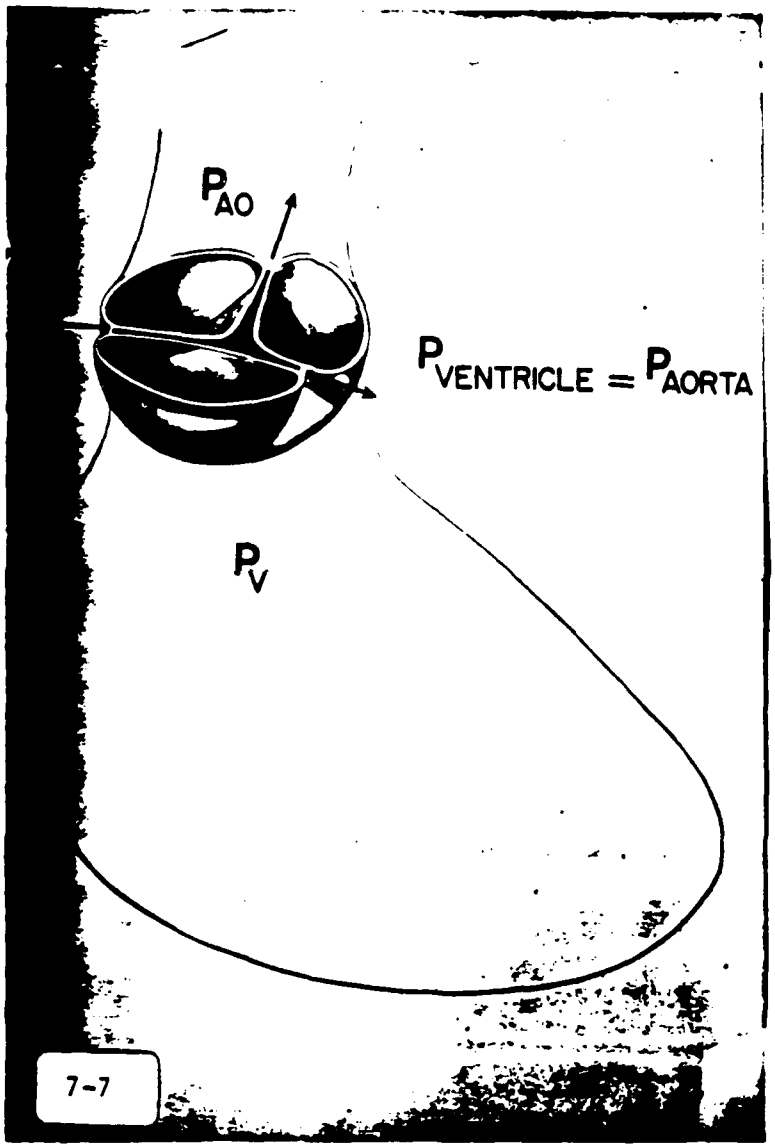
P_{AO}
$P_{VENTRICLE} = P_{AORTA}$
P_V
7-7

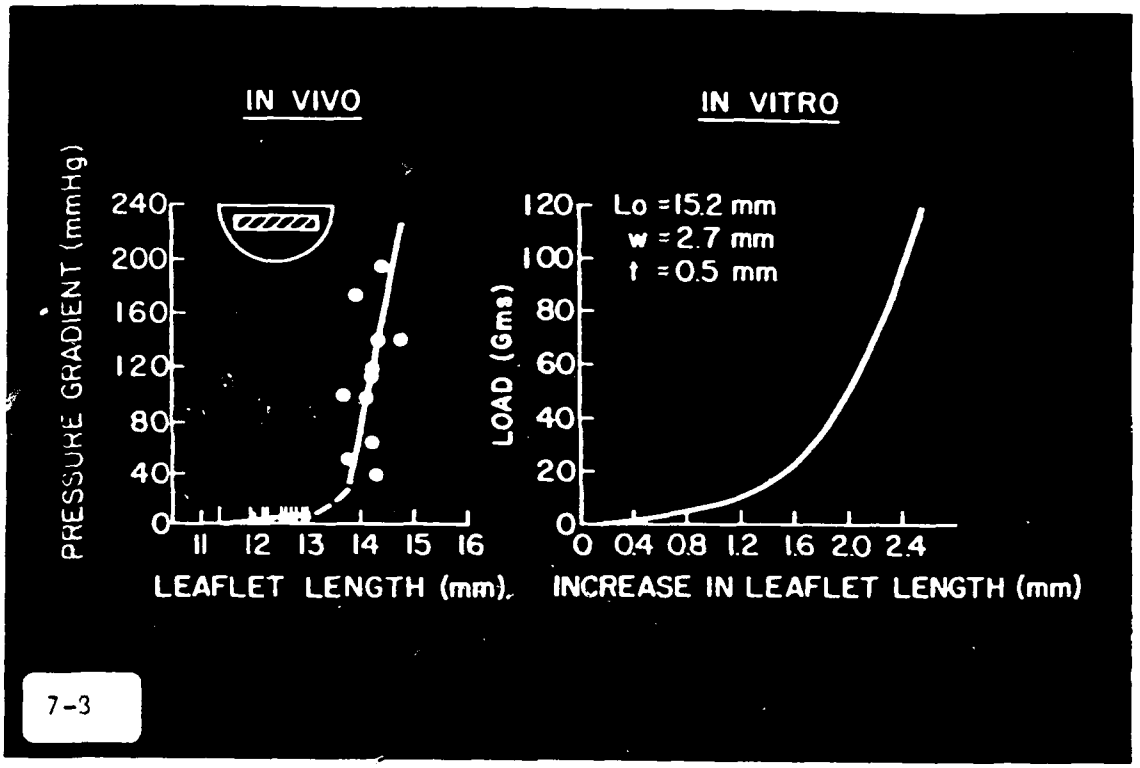
IN VIVO
IN VITRO
PRESSURE GRADIENT (mmHg)
240
200
160
120
80
40
0
11 12 13 14 15 16
LEAFLET LENGTH (mm)
120
100
80
60
40
20
0
LOAD (Gms)
Lo = 15.2 mm
w = 2.7 mm
t = 0.5 mm
0 0.4 0.8 1.2 1.6 2.0 2.4
INCREASE IN LEAFLET LENGTH (mm)
7-3

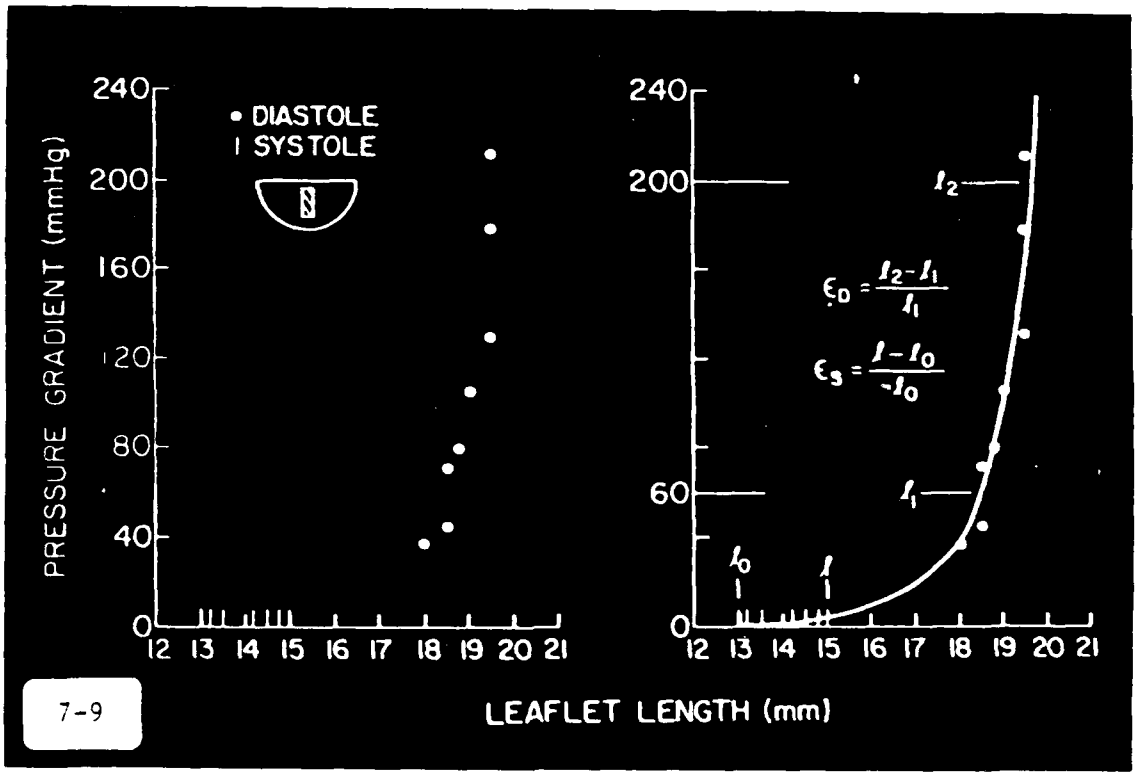
PRESSURE GRADIENT (mmHg)
240
200
160
120
80
40
0
• DIASTOLE
I SYSTOLE
12 13 14 15 16 17 18 19 20 21
240
200
60
0
l_2
$\epsilon_D = \frac{l_2 - l_1}{l_1}$
$\epsilon_S = \frac{l - l_0}{l_0}$
l_1
l_0
l
12 13 14 15 16 17 18 19 20 21
LEAFLET LENGTH (mm)
7-9

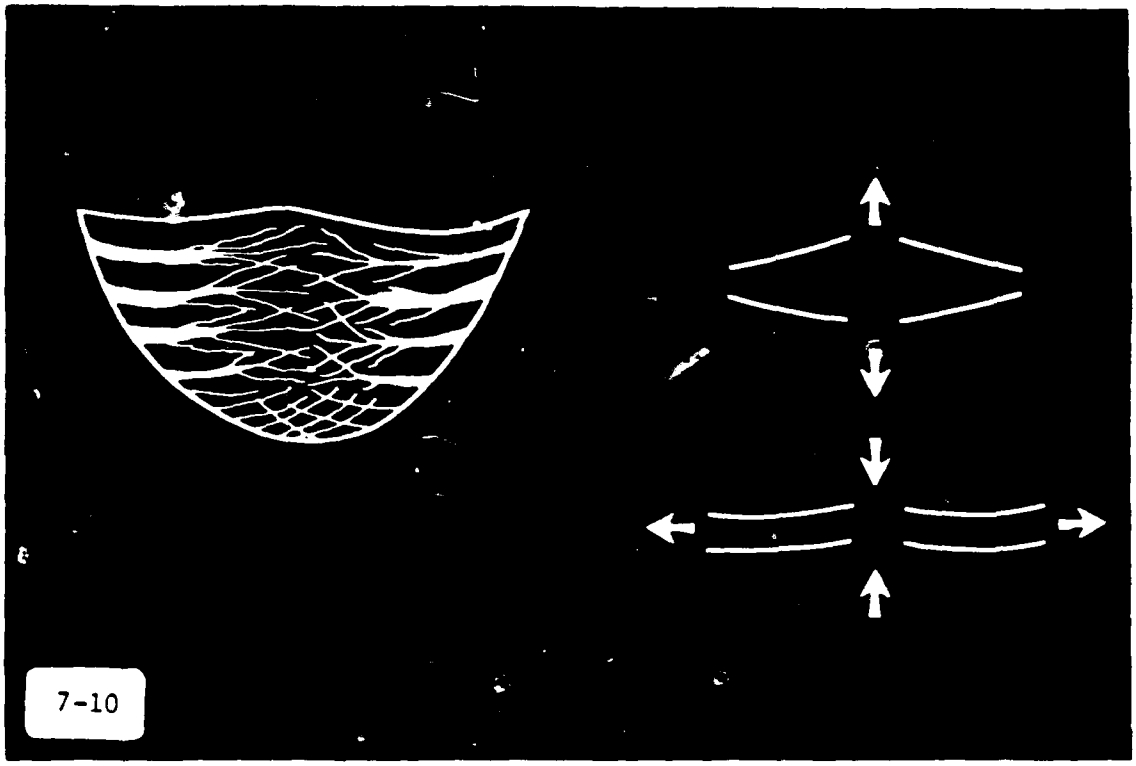
7-10

IMPACT RESISTANCE OF INVERTEBRATE MINERALIZED TISSUES

John Currey

Department of Biology
University of York
York YO1 5DD, UK

Invertebrate mineralized structures (mollusc shells, crab cuticles, sea urchin tests etc.) must be tough, rigid, or resilient, if they are not to be broken by impact.

Toughness Being highly mineralized (with calcium carbonate or calcium phosphate) makes it difficult to produce tough materials. Various molluscan shell types have been analyzed for their toughness, and a few for their impact resistance. The toughness is not in general high, although many ingenious mechanisms have been evolved to make crack travel difficult and energetically expensive.

Rigidity Some structures are relatively massive, and are made of a very stiff material. In any likely impact situation this results in the strain energy density in the material being low. Many mollusc shells, particularly large ones such as those of Tridacna, fall into this category. This is a doomed strategy, however, if the animal can be carried into the air and dropped onto a hard surface! The smashing limbs of the mantid shrimp Gonodactylus are extremely hard, with a glossy surface. Despite being brittle, they give nearly all their kinetic energy to the prey, and so are rarely damaged in service.

Resilience The tail shields of Gonodactylus, used in territorial fights with conspecifics, also have a brittle, highly mineralized outer layer. However, it is underlain by a thick compliant layer of cuticle. When hit by the smashing limb the large deformations induced do not produce large strains in the brittle layer, because it is so thin. This mode of absorbing impact is probably not common in mineralized tissues. Although some shells, such as that of the brachiopod Lingula, have the correct structure for resilience (alternating very thin layers of mineral and organic material) this is probably not its function, which is that of flexibility in burrowing.

High mineralization has the great advantage for invertebrates that mineral is cheap and organic material is expensive. High stiffness is easily obtained, high toughness only with difficulty. Impact avoidance, by a hidden way of life, or avoidance of high strains in impact, by high stiffness and massiveness, are the effective strategies most commonly found in nature.

Reference

Currey, J.D., 1989 Biomechanics of mineralized skeletons. In: Skeletal Biomaterialization: Patterns, processes and evolutionary trends, Edit J. Carter. American Geophysical Union, Washington D.C. pp 11-25

Currey, J.D., Nash, A. & Bonfield, W. 1982 Calcified cuticle in the stomatopod smashing limb. J. Materials Sci., 17, 1939-1944.

Jackson, A.P., Vincent, J.F.V. & Turner, R.M. 1988 The Mechanical Design of Nacre. Proc. Roy. Soc. B 415-440.

Figures 1 through 10 added for amplification of the lecture.

Fig. 1. Block diagrams of different types of molluscan shell materials.

Fig. 2. Scanning electron micrograph of prismatic structure of a cone shell.

Fig. 3. Scanning electron micrograph of a shadowed specimen of mother of pearl showing the organic material binding the "bricks" together.

Fig. 4. Stress-strain curves for four different skeletal materials loaded in tension.

Fig. 5. Impact strength, in joules per square meter, of unnotched specimens of prisms, nacre (mother of pearl) and crossed lamellar structures of mollusc shell.

Fig. 6. Comparison of similar structures in crossed lamellar structure of molluscs and in enamel. In both cases, there are "easy " and "difficult" ways for the crack to travel. The structures are arranged similarly so that a crack traveling in any direction will sooner or later move from an easy direction into a difficult direction. The lower pictures show the characteristic fracture pattern shown in shell and enamel. The four lower left hand blocks are the same mollusc specimen loaded to ever-increasing loads (shown by the numbers). All cracks started in the easy direction and were brought to a halt when moving into the difficult direction.

Fig. 7. Fracture surface of a crossed lamellar structure of a cone shell.

Fig. 8. Scanning electron micrograph of a fracture in a crossed lamellar structure running in the easy direction.

Fig. 9. Fracture surface of mother of pearl. Production of this highly irregular fracture surface absorbs a very large amount of energy.

Fig. 10. Relationships between microhardness and P/Ca ratio at various points in the hammer of the gonodactyloid shrimp. Note the log scale.

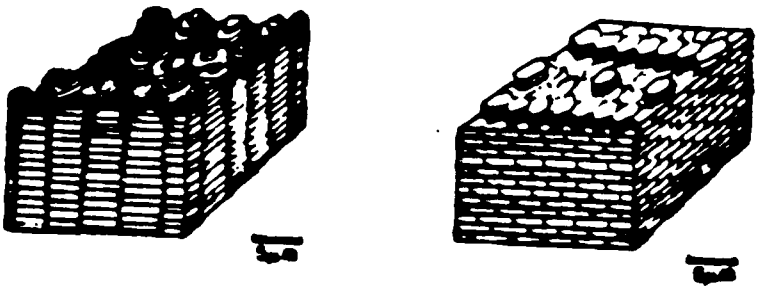

NACRE

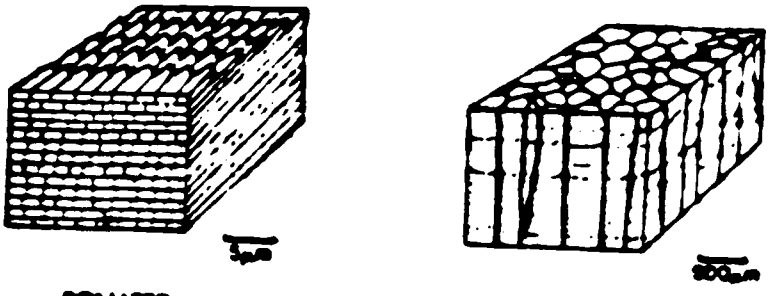

FOLIATED

PRISMS

CROSSED-LAMELLAR

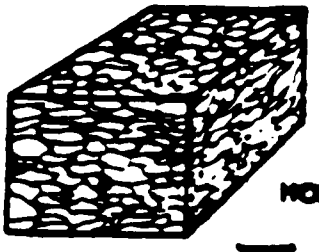

HOMOGENEOUS


8-3

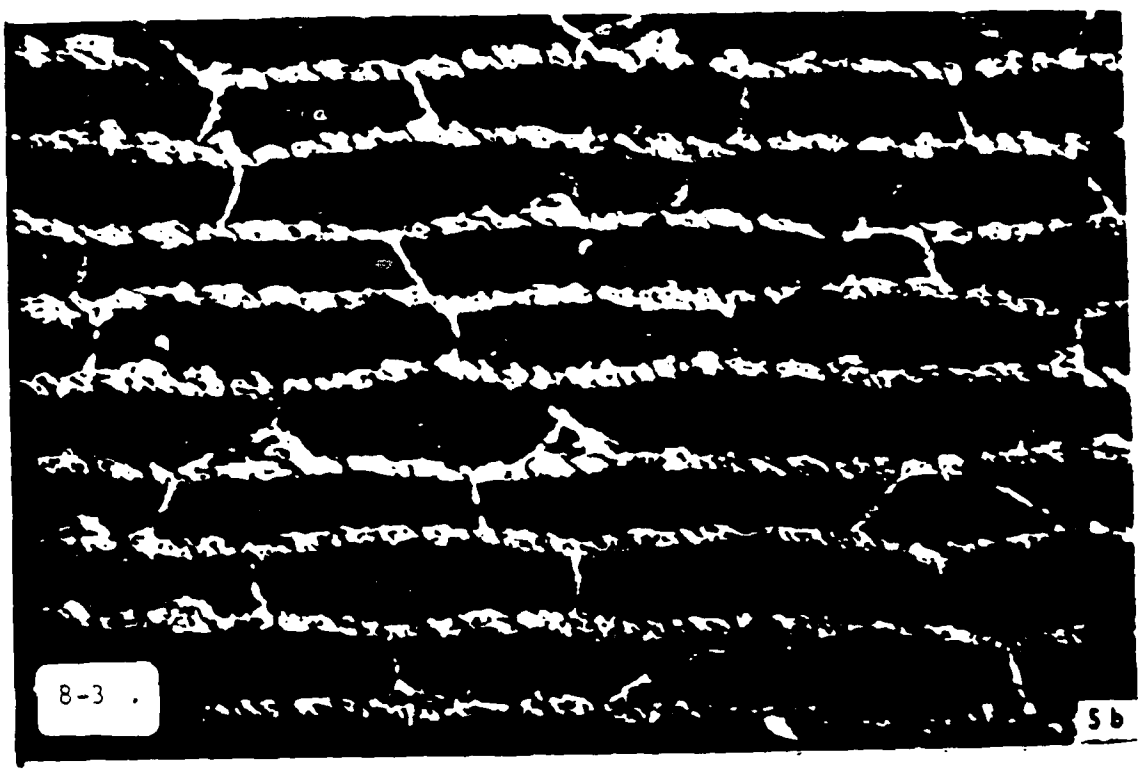
8-3
5b

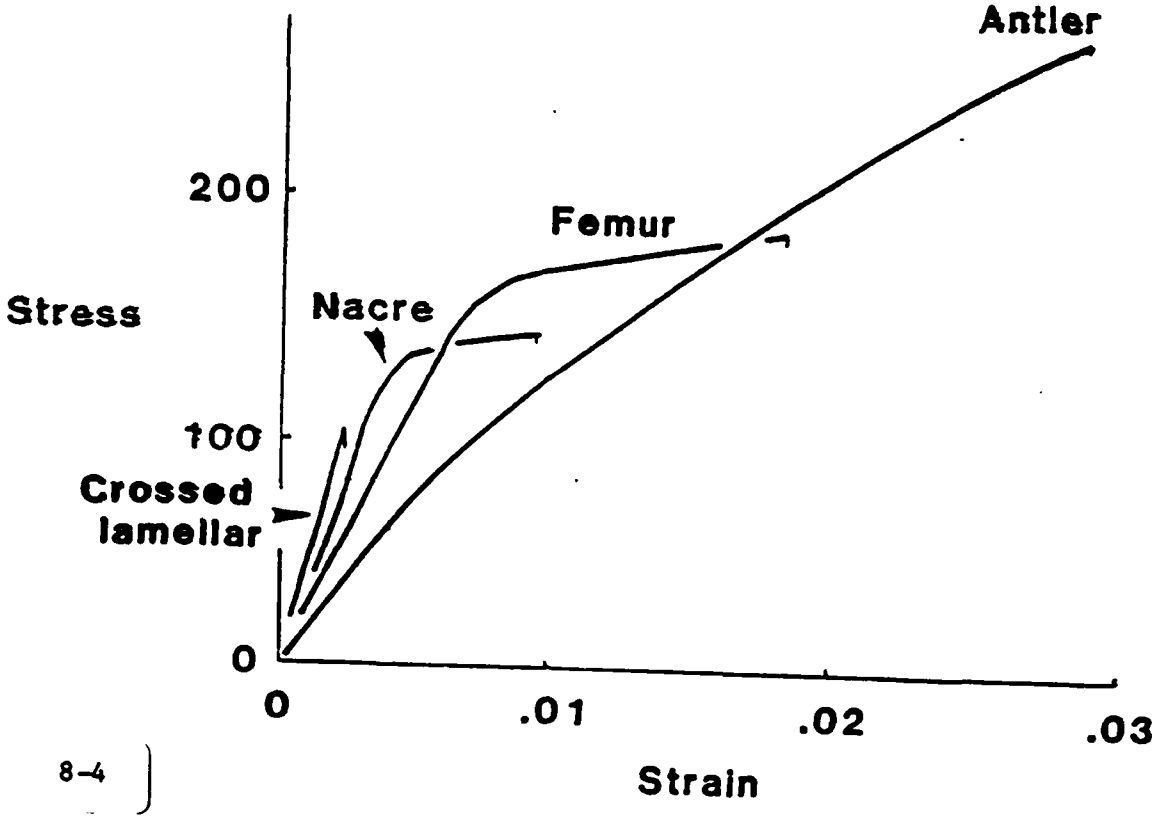

8-4

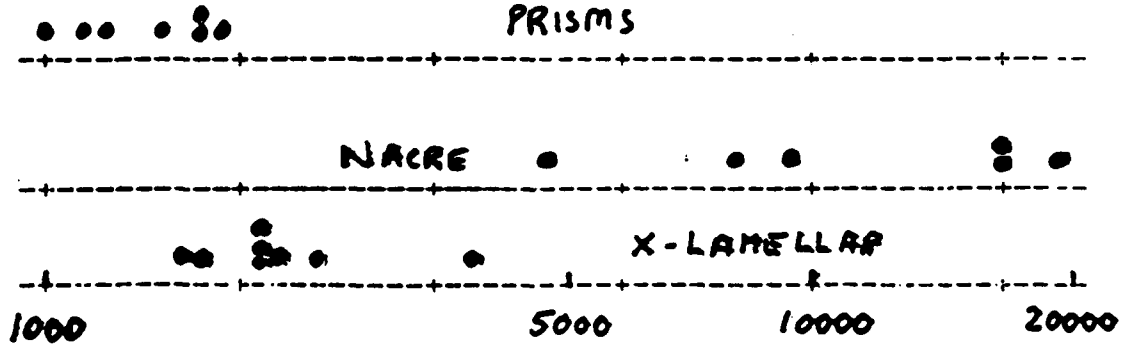

8-5

IMPACT STRENGTH $J\,m^{-2}$

SHELL

TOOTH

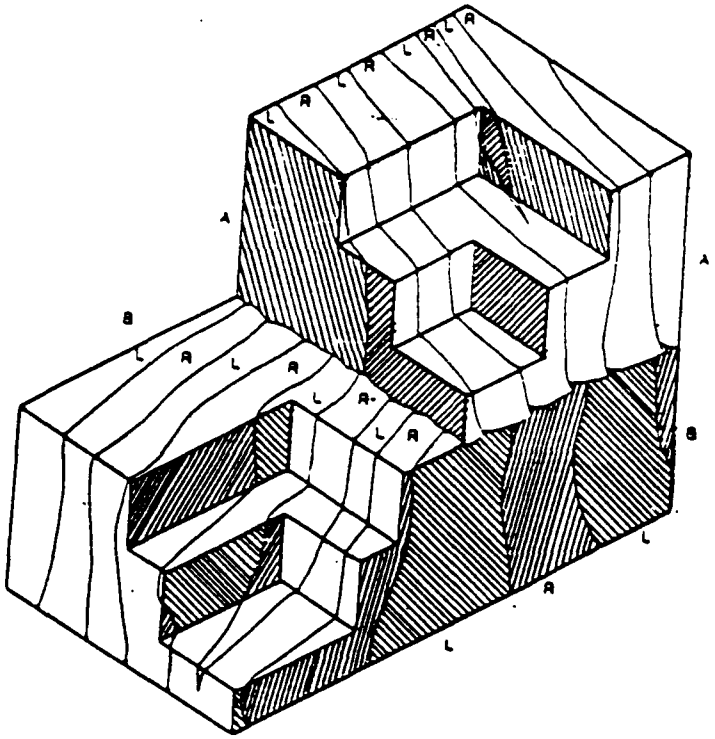

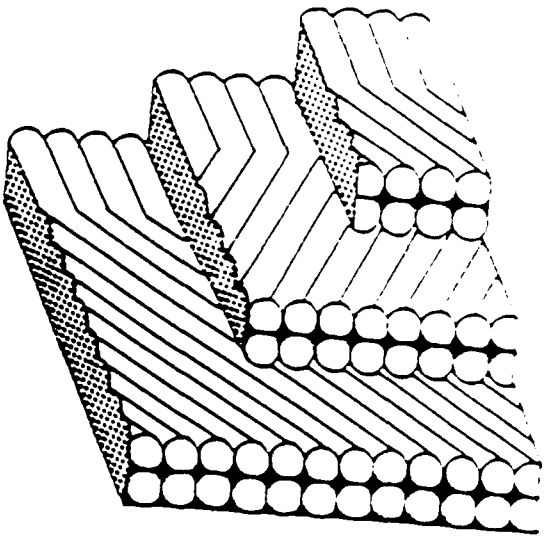

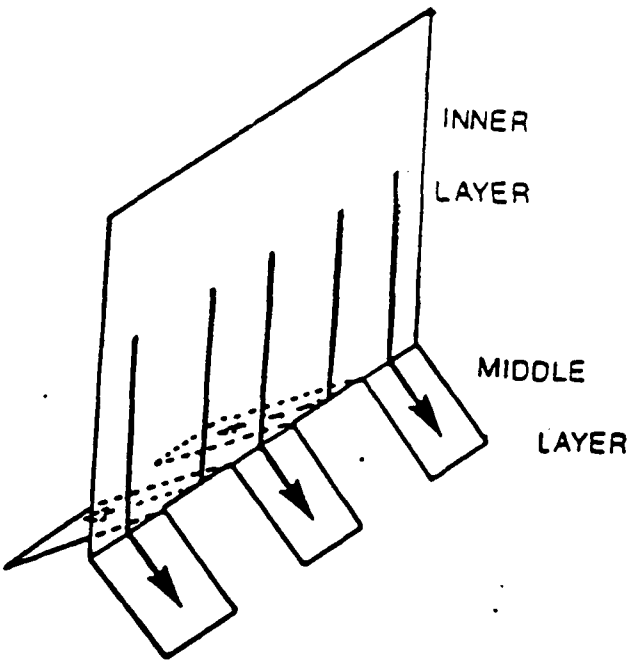

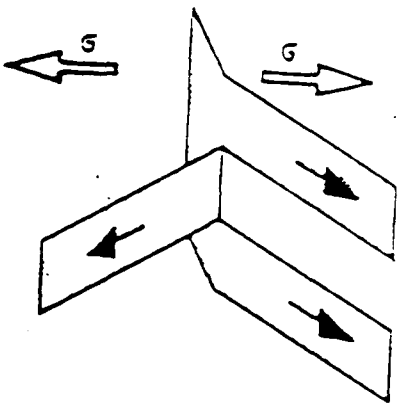

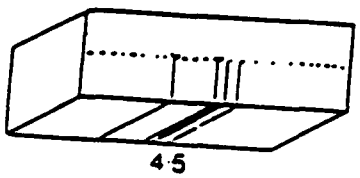

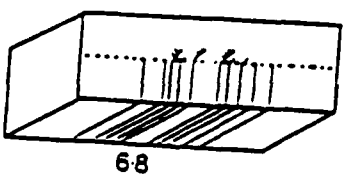

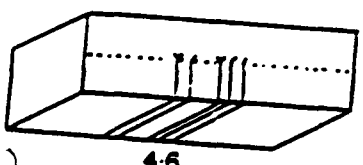

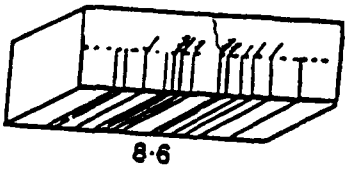

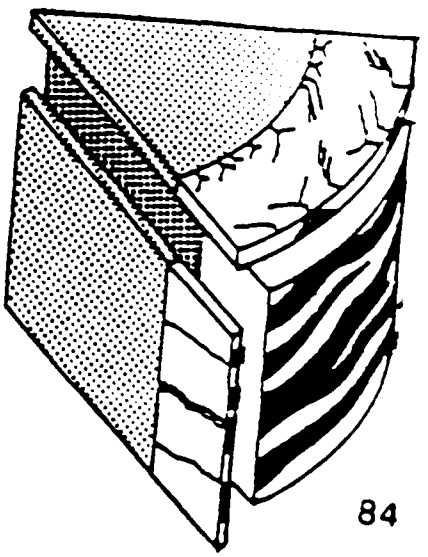


8-7


8-8


8-9

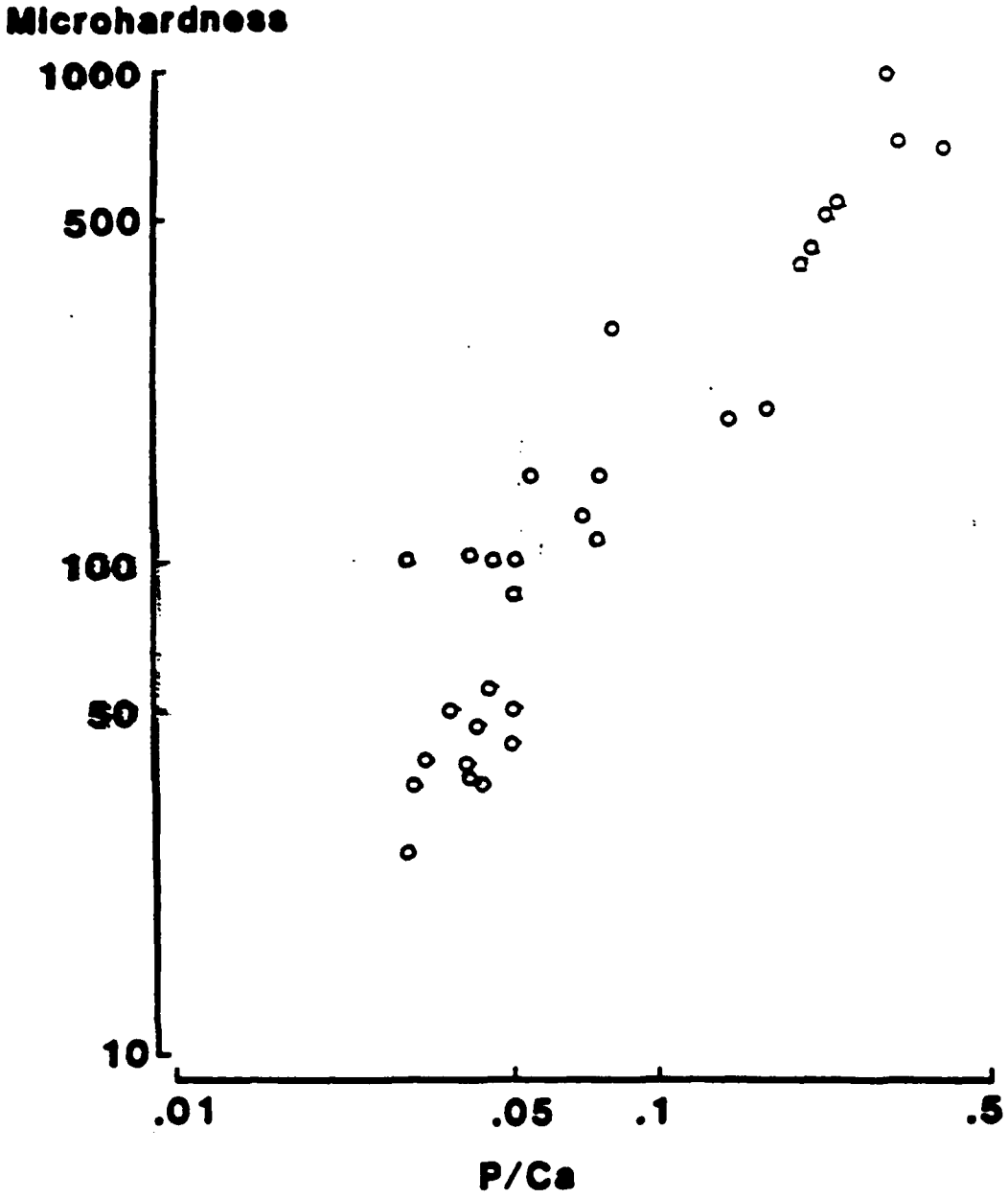

Relationship between microhardness and P/Ca ratio at various points in the gonodactyloid hammer. Note the log scale.

IMPACT MANAGEMENT OF SKULL AND OTHER BONE

by James McElhaney

Biomedical Engineering Department
Duke University
Durham, North Carolina 27706

From a biomechanical viewpoint the boney skeleton has a variety of functions. It provides a stiff framework of joints and levers so that the contraction of the muscles can produce precise, repeatable motions. It provides a scaffold in which the softer organs can be attached so that they can maintain their configuration and resist the effects of gravity and it provides protection to these soft organs from impact and other external forces. The scalp and skull offer significant protection to the brain, the rib cage protects the heart and lungs, and the vertebrae protect the spinal cord. The long bones have bulbous ends to support the large areas of articular cartilage required to resist the repetitive impact forces associated with limb actions.

In addition to these structural requirements there is a most important demand for the lightest weight possible. Bone has therefore developed a most intricate and fascinating mechanism to adjust and organize its internal structure to compensate for changes in load and function always aiming at the lightest weight necessary.

The head is an excellent example of a light weight, energy managing design. The scalp serves to distribute the force over the skull and reduce stress concentrations and local pressure variations in impact situations. The skull bones are composed of an inner and outer table of compact bone separated by a core of cancellous bone (diploe). Compact bone surrounds and reinforces the sutures. Due to the sandwich structure of the skull bones, it is well suited to dissipate energy in an impact through crushing of the diploe. This sandwich structure has different directional properties. It is much stiffer and stronger in the tangential directions than the radial directions.

Statistical correlations of the properties have been made with density, and a model that summarises this result has been developed based on porosity. Even though the pores are fluid filled the cancellous bone is much less rate sensitive than compact bone. The material properties of compact bone and cancellous bone in the small, i.e. hardness, density and local compressive strength are not significantly different. The amount and distribution of the trabecular however is quite variable and, therefore, the structured responses, in particular the energy absorption, gross stiffness and damping characteristics which are strongly dependent on structure vary greatly from section to section.

Figure Captions

Fig. 1. The knee joint

Fig. 2. Photoelastic analysis of compressive strains in simulated skull sections.

Fig. 3. Section through human parietal bone.

Fig. 4. Stress-strain curves for human bone in compression.

Fig. 5. Normalized radial modulus versus porosity for human cranial bone in compression.

Fig. 6. Porous block model for cancellous bone.

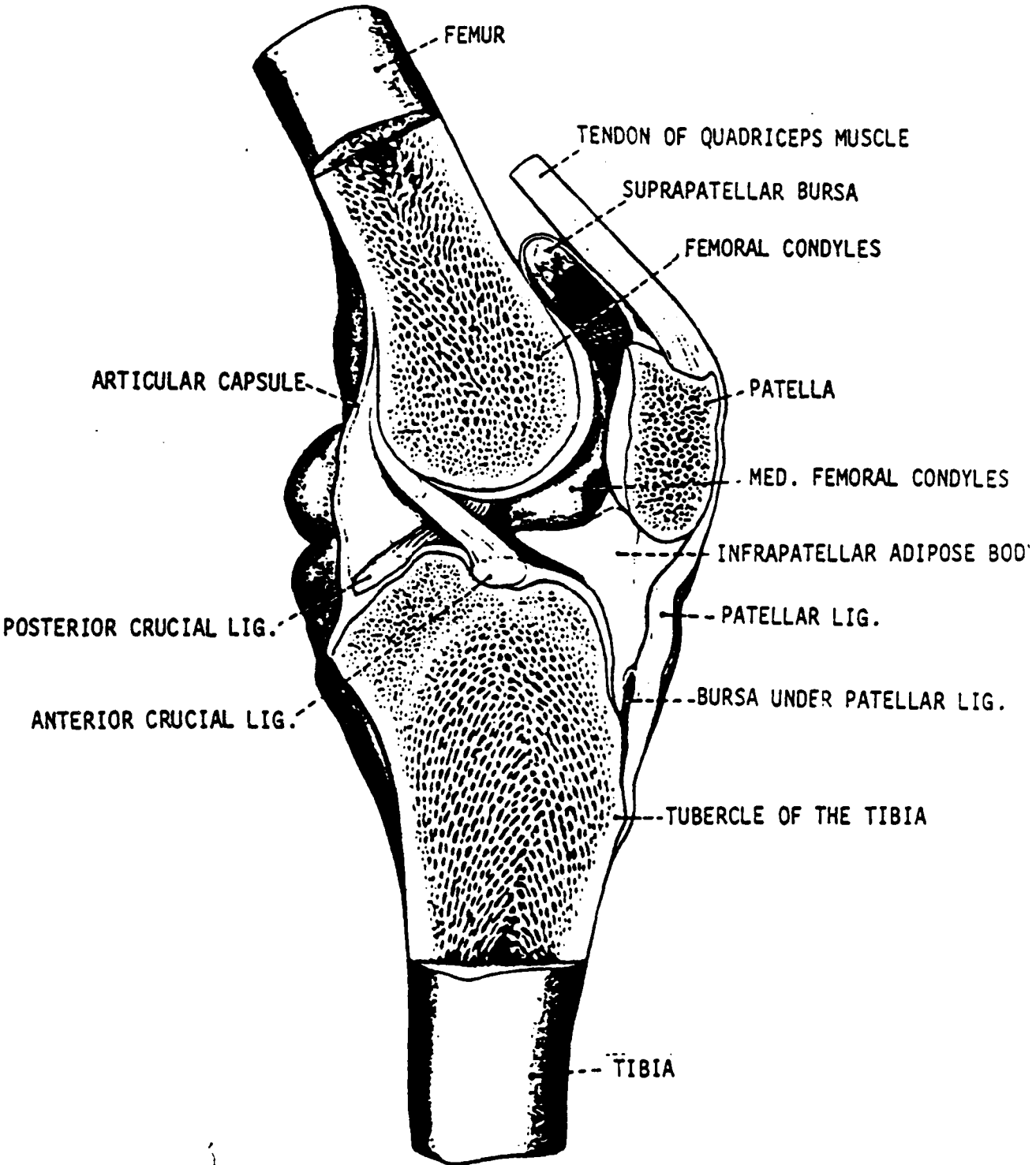
FEMUR
TENDON OF QUADRICEPS MUSCLE
SUPRAPATELLAR BURSA
FEMORAL CONDYLES
ARTICULAR CAPSULE
PATELLA
MED. FEMORAL CONDYLES
INFRAPATELLAR ADIPOSE BOD
POSTERIOR CRUCIAL LIG.
PATELLAR LIG.
ANTERIOR CRUCIAL LIG.
BURSA UNDER PATELLAR LIG.
TUBERCLE OF THE TIBIA
TIBIA

9-1

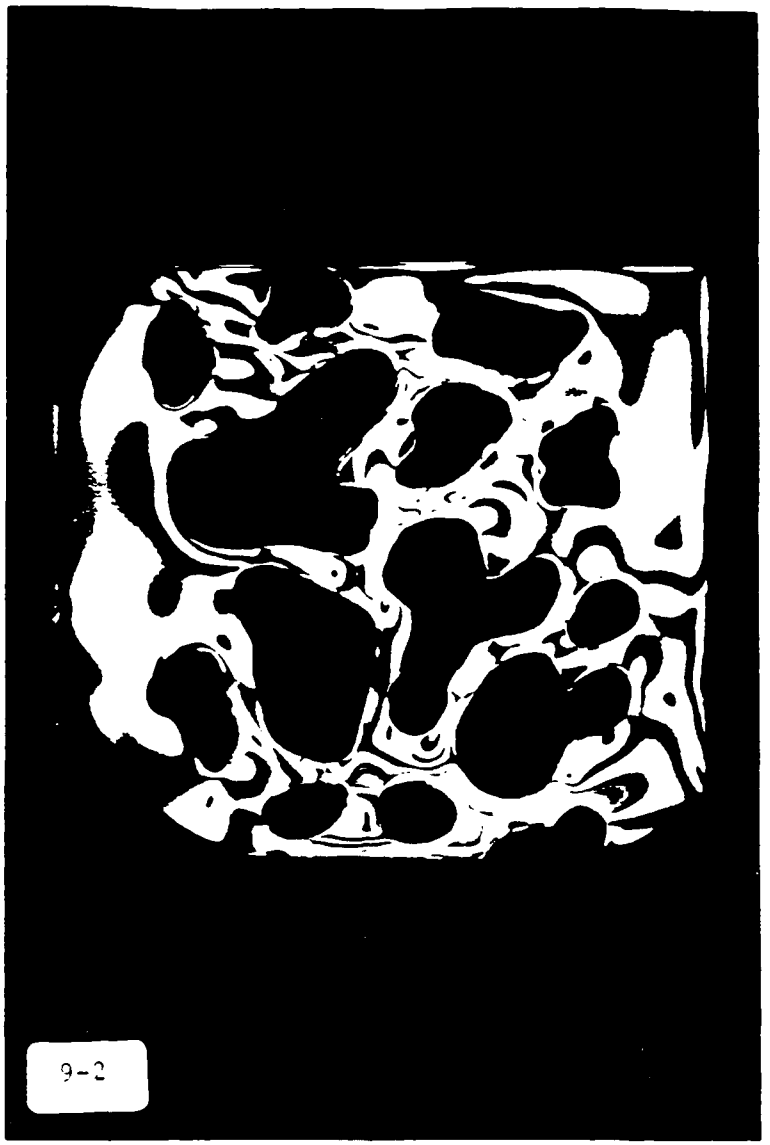
9-2

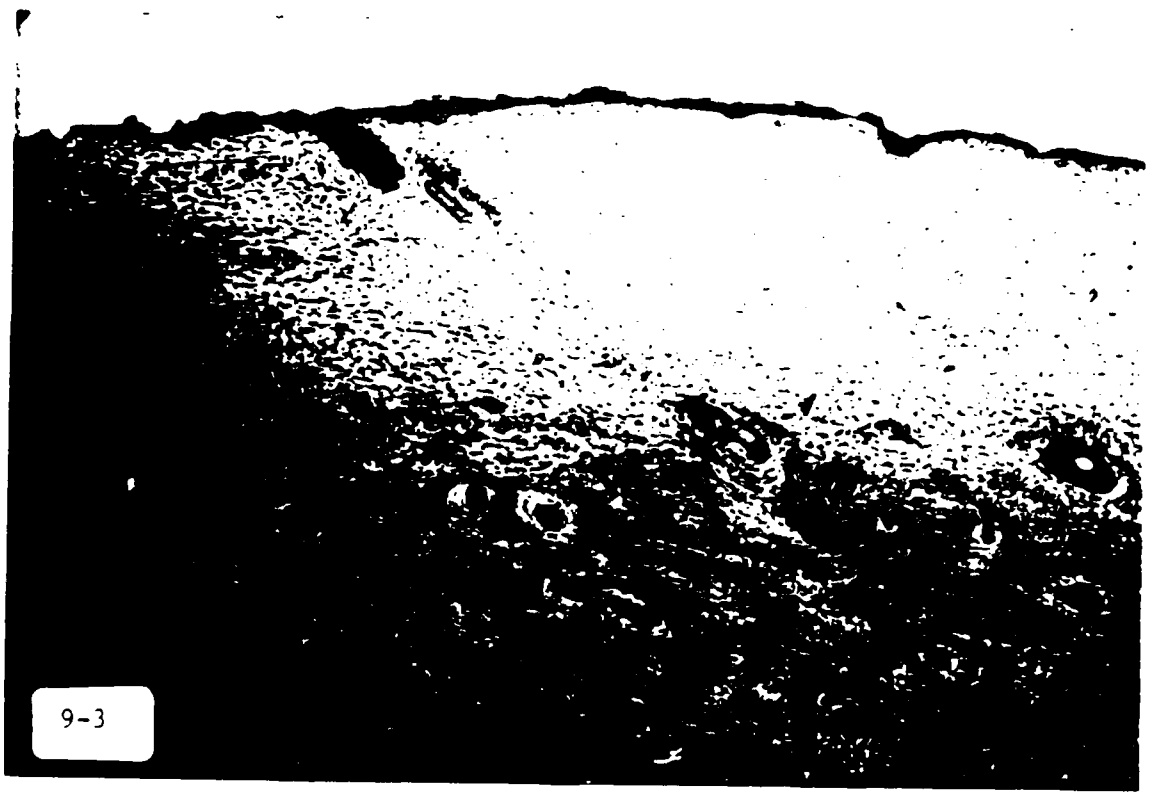
9-3

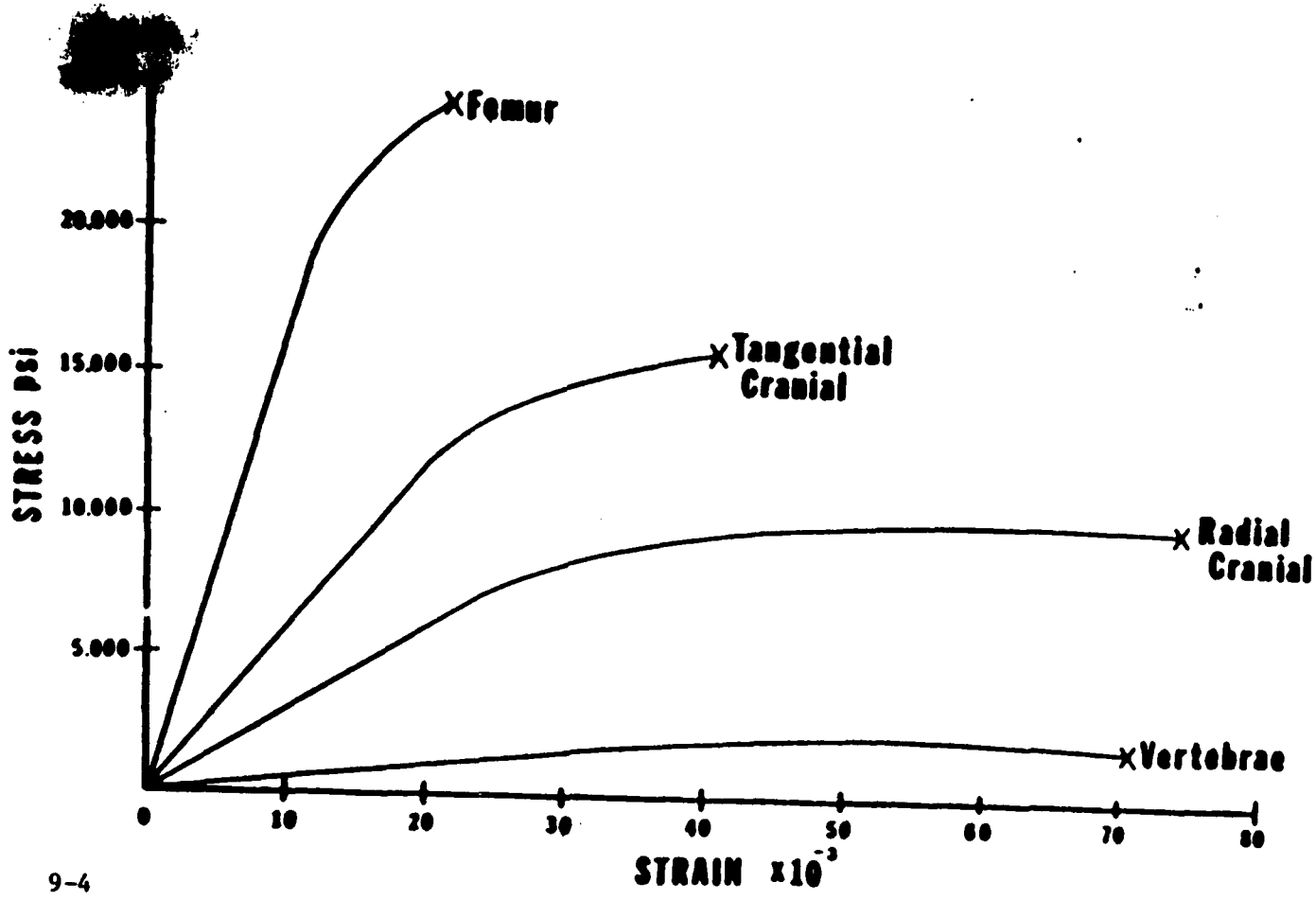
Femur
Tangential Cranial
Radial Cranial
Vertebrae
STRESS Psi
20,000
15,000
10,000
5,000
0
10
20
30
40
50
60
70
80
STRAIN x10⁻³

9-4

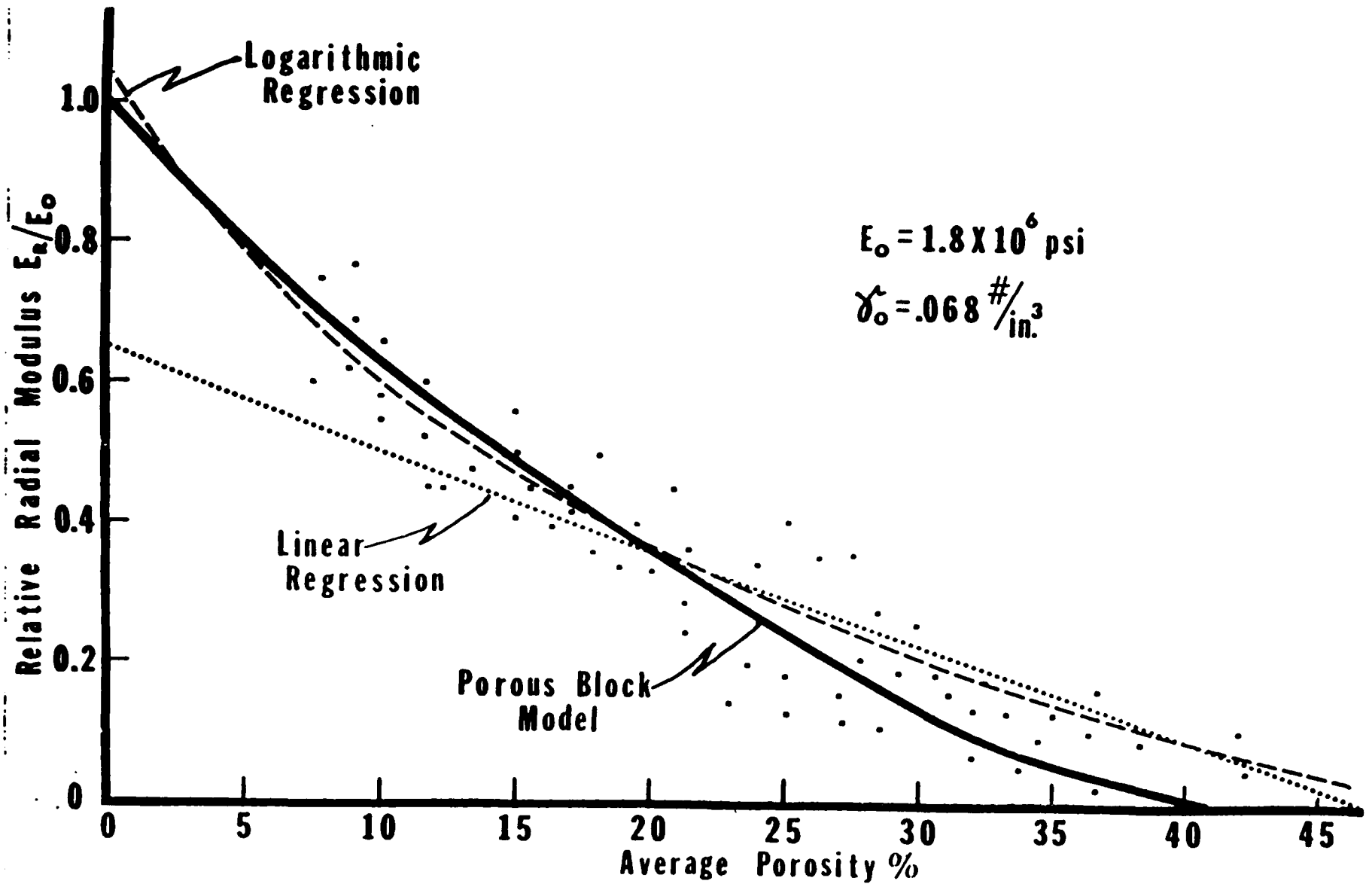
Logarithmic Regression
Linear Regression
Porous Block Model
$E_o = 1.8 \times 10^6$ psi
$\gamma_o = .068\ ^{\#}/_{in.^3}$
Relative Radial Modulus E_R/E_o
1.0
0.8
0.6
0.4
0.2
0
0
5
10
15
20
25
30
35
40
45
Average Porosity %

9-5

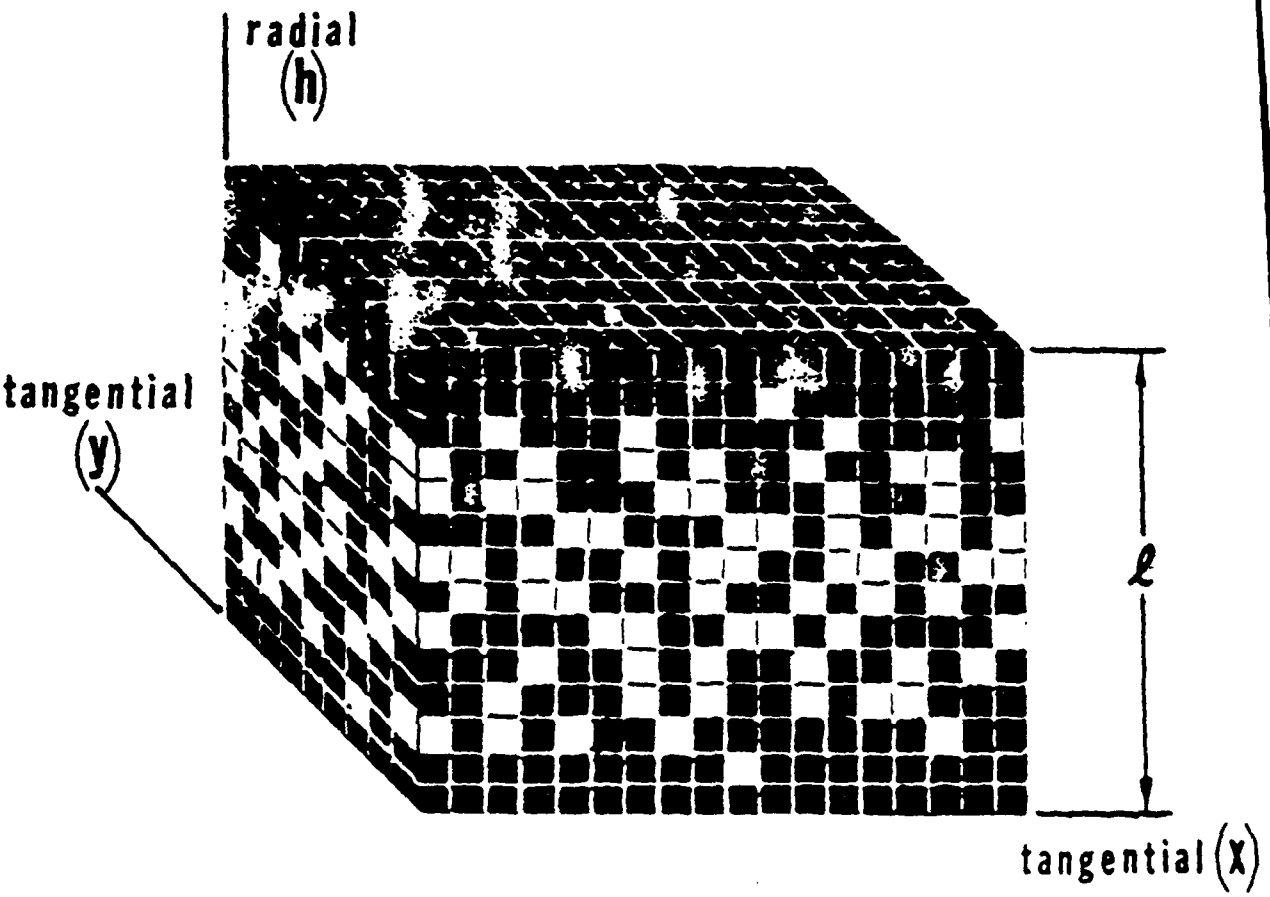
radial
(h)
tangential
(y)
ℓ
tangential (x)

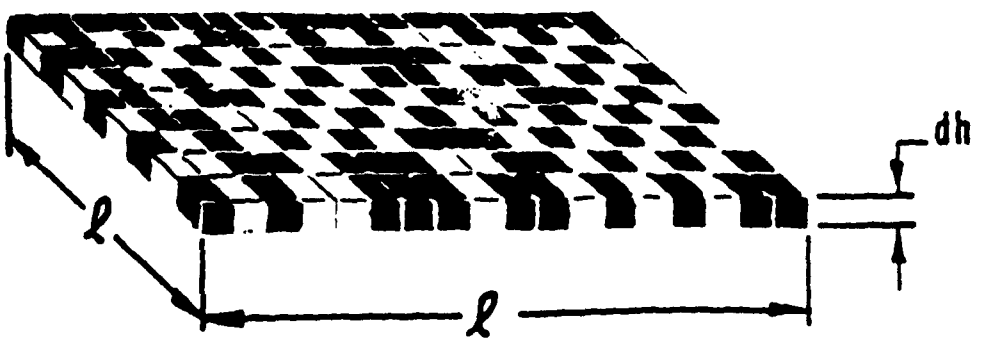
dh
ℓ
ℓ

Figures 7 through 11 added for amplification of the lecture.

Fig. 7. Detailed cross-section of the layers adjacent to the skull.

Fig. 8. Sections through human and primate (Macoca mulatta) parietal bones.

Fig. 9. Section through human femur.

Fig. 10. Comparison of femoral trabeculae and stress trajectories.

Fig. 11. Strength versus porosity for human cranial bone in compression.

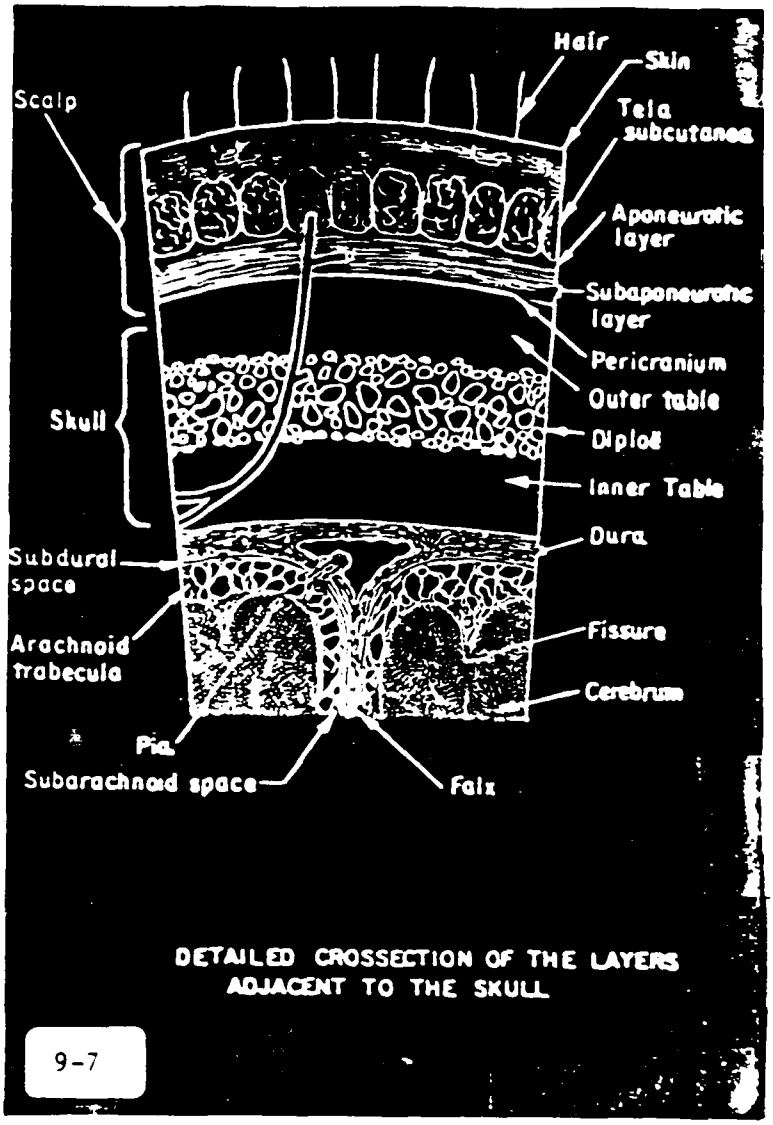

DETAILED CROSSECTION OF THE LAYERS ADJACENT TO THE SKULL

9-7

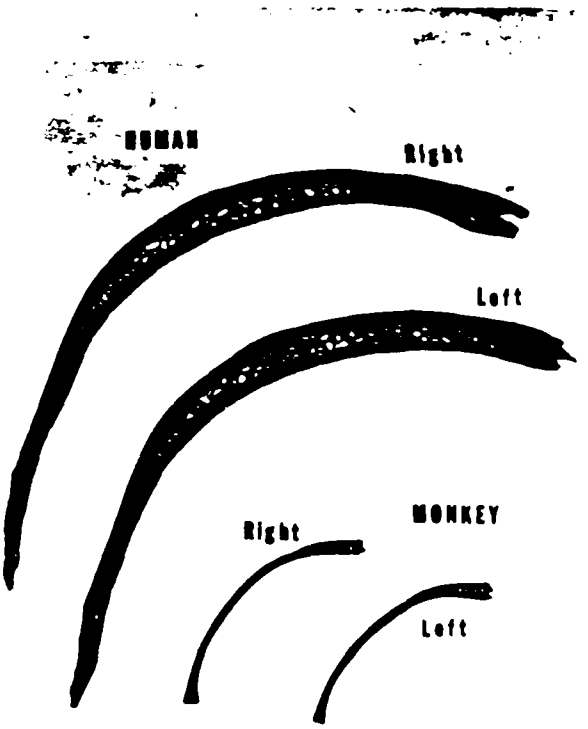

SECTIONS THRU HUMAN AND PRIMATE (Macaca mulatta) PARIETAL BONES.

figure 3

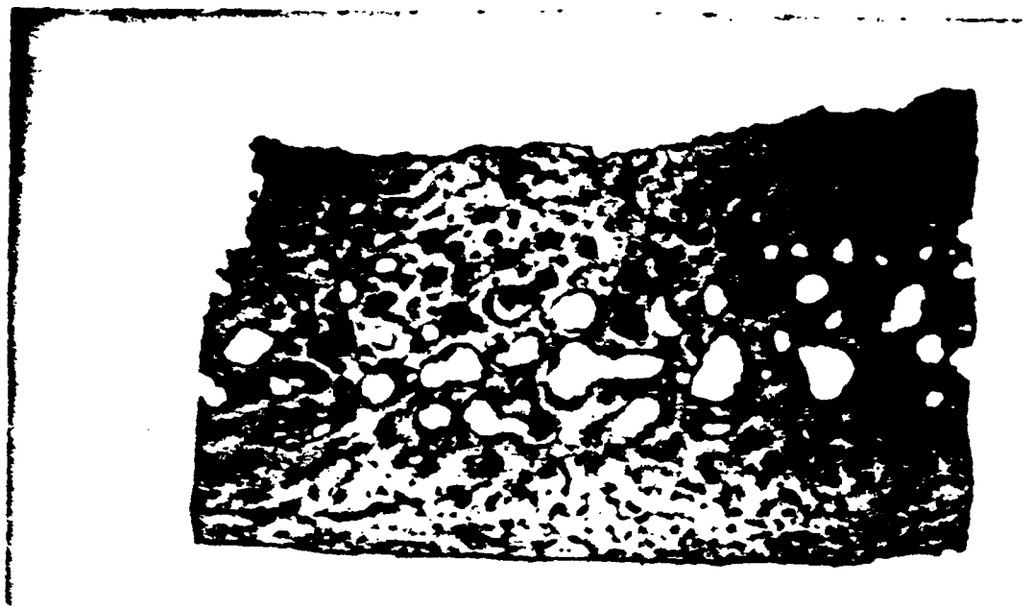

9-9

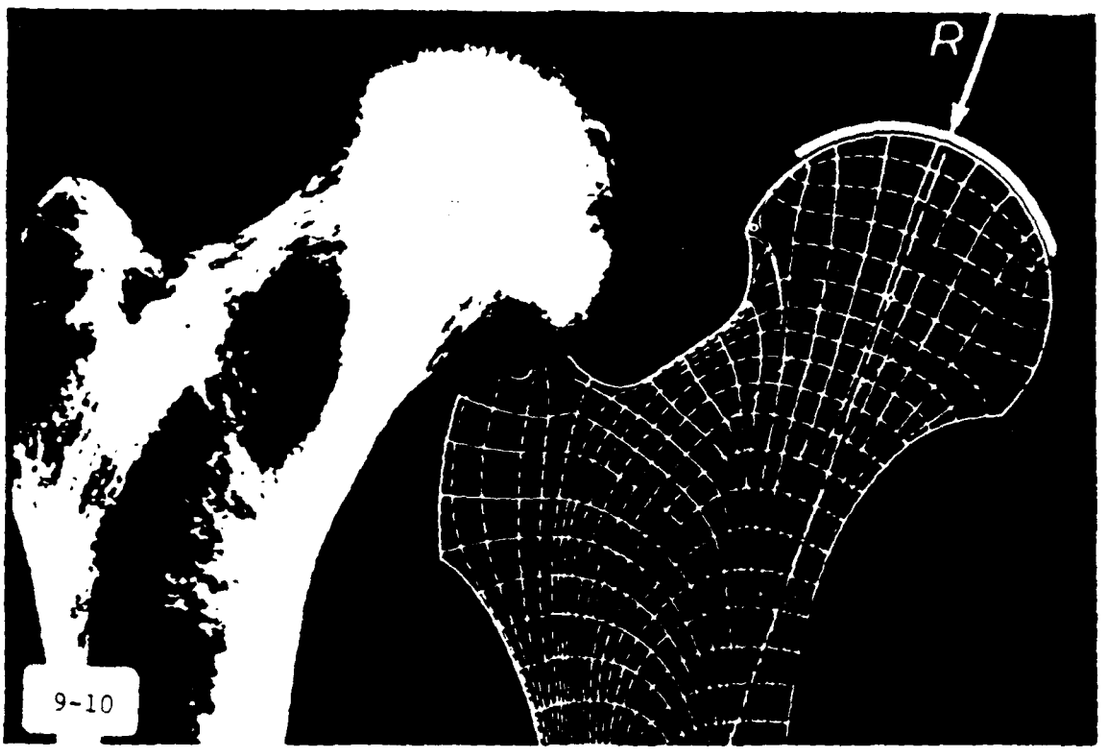

9-10

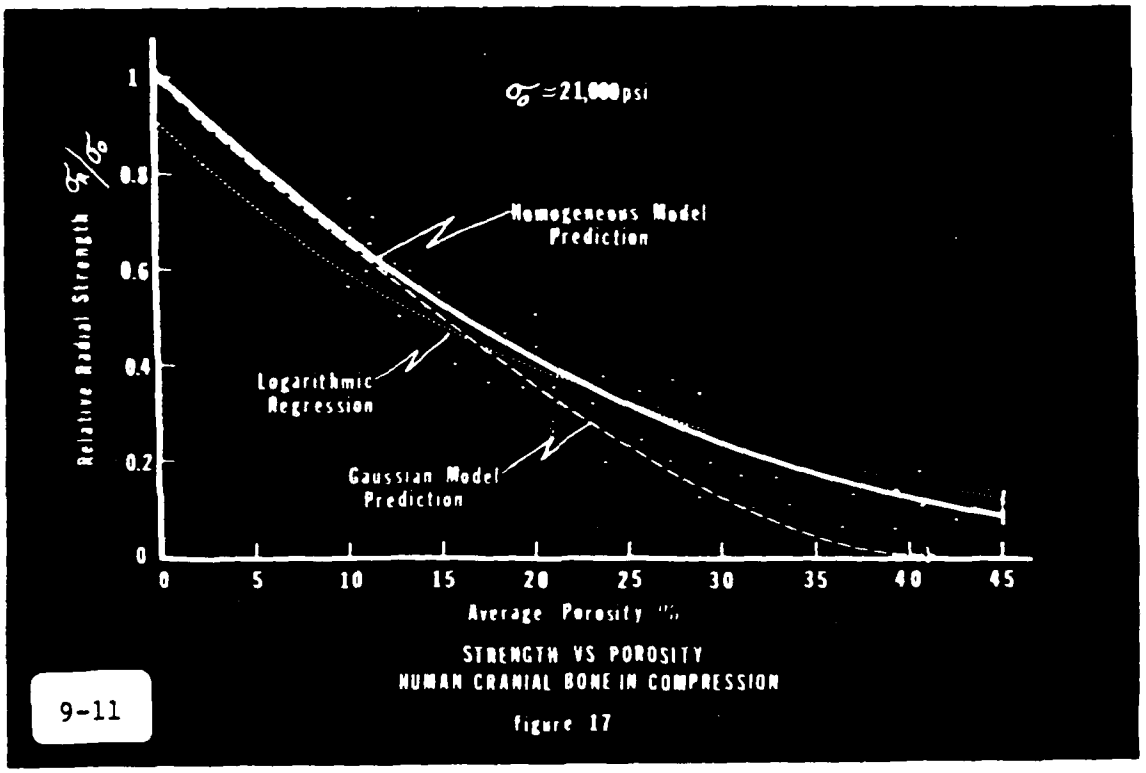

STRENGTH VS POROSITY
HUMAN CRANIAL BONE IN COMPRESSION

9-11

figure 17

"Mechanical Properties and Energy Absorption in Natural Cellular Materials"

L.J. Gibson
Department of Civil Engineering
Massachusetts Institute of Technology
Cambridge, MA 02139

Many materials have a cellular structure. Natural ones include cork, wood, and cancellous bone. Recently, man has made his own cellular materials in the form of honeycombs or foams. There are striking similarities in the mechanical behaviour of these diverse materials as a result of their cellular structure. Their compressive stress-strain curves, for instance, all have the same shape: a linear elastic regime is followed by a stress plateau which terminates in a final, sharp increase in stress at large strains (Fig. 1). The mechanical properties of cellular solids can be understood by identifying and analyzing the mechanisms by which the cells deform and fail. In this presentation, models for the mechanical properties of honeycombs are first reviewed and then used to describe wood. Next models for the behaviour of foams are applied to cancellous bone. And finally, the models are used to develop energy absorpton diagrams for both foams and natural cellular materials.

The in-plane moduli of honeycombs are governed by *bending* of the cell walls; an analysis of the mechanics shows that they are proportional to the *cube* of the relative density of the honeycomb. The out-of-plane moduli, on the other hand, are governed by *uniaxial extension or compression* of the cell walls and are simply *linearly* related to the relative density. At a crude level, the cells of wood are somewhat like the hexagonal cells of a honeycomb; as Fig. 2a indicates this simple model describes the data for the Young's moduli of woods fairly well. Similar ideas can be applied to the compressive strength; they indicate that the in-plane plastic

strength is related to the square of the relative density while the out-of-plane strength is linearly related to the relative density. Data are compared with the models in Fig. 2b.

The linear elastic behaviour of open-cell foams is governed by bending of the cell walls; dimensional arguments indicate that, as a result, their Young's moduli of are proportional to the square of their relative density. At sufficiently high loads, the cells begin to collapse by elastic buckling, plastic yielding or brittle crushing, giving rise to the stress plateau of the stress-strain curve of Fig. 1. Dimensional arguments can again be used to analyze each failure mechanism: the relevant results here are that the stress plateau for elastic buckling of open-cell foams is proportional to the relative density squared while that for plastic yielding is proportional to the relative density raised to the 3/2 power.

Because cancellous bone grows in response to the loads on it, the orientation of its trabeculae varies: in locations where the stresses are highly oriented in one plane, the trabeculae assume a parallel plate structure while in locations where the stresses are roughly equal in all directions, the cells are roughly equiaxed. The parallel plate structure behaves somewhat like a honeycomb: loading across the plates induces bending in the cell walls while loading along the plates induces uniaxial extension or compression. The equiaxed structure behaves somewhat like a foam. The Young's moduli of cancellous bone, when plotted on a log-log scale against relative density, are then expected to lie between lines of slope 1 and 3. The compressive strength is expected to lie between lines of slope 1 and 2. The models are compared with data in Fig. 3.

Energy absorption diagrams, which plot the energy absorbed per unit volume of material against the peak stress generated in an impact, can be produced from compressive stress-strain curves for cellular solids as is illustrated in Fig. 4.

Theoretical energy absorption diagrams for both natural and man-made cellular solids can be developed using models for the Young's modulus and compressive strength, such as those described above.

Reference: Gibson, L.J. and Ashby, M.F. (1988) Cellular Solids: Structure and Properties, Pergamon.

Fig. 1. A schematic stress strain curve for a typical cellular solid.

Fig. 2. Data for (a) the elastic moduli and (b) the compressive strength of woods. The results of the simple models are represented by the solid lines.

Fig. 3. Data for (a) the elastic moduli and (b) the compressive strength of cancellous bone. The results of the simple models are represented by the solid lines.

Fig. 4. The construction of an energy absorption diagram for a cellular solid.

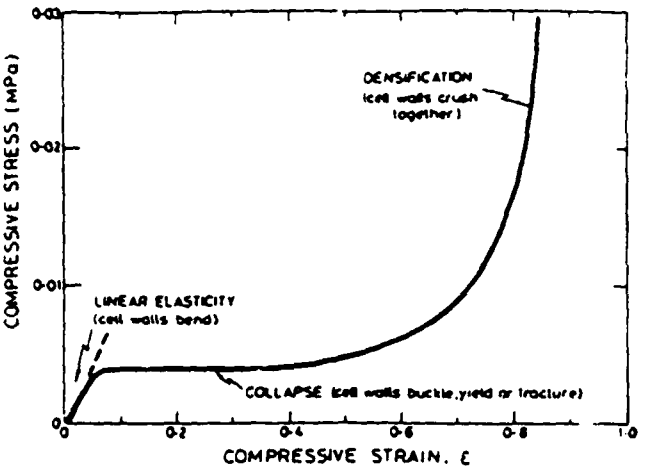

10-1 . A schematic stress strain curve for a typical cellular solid.

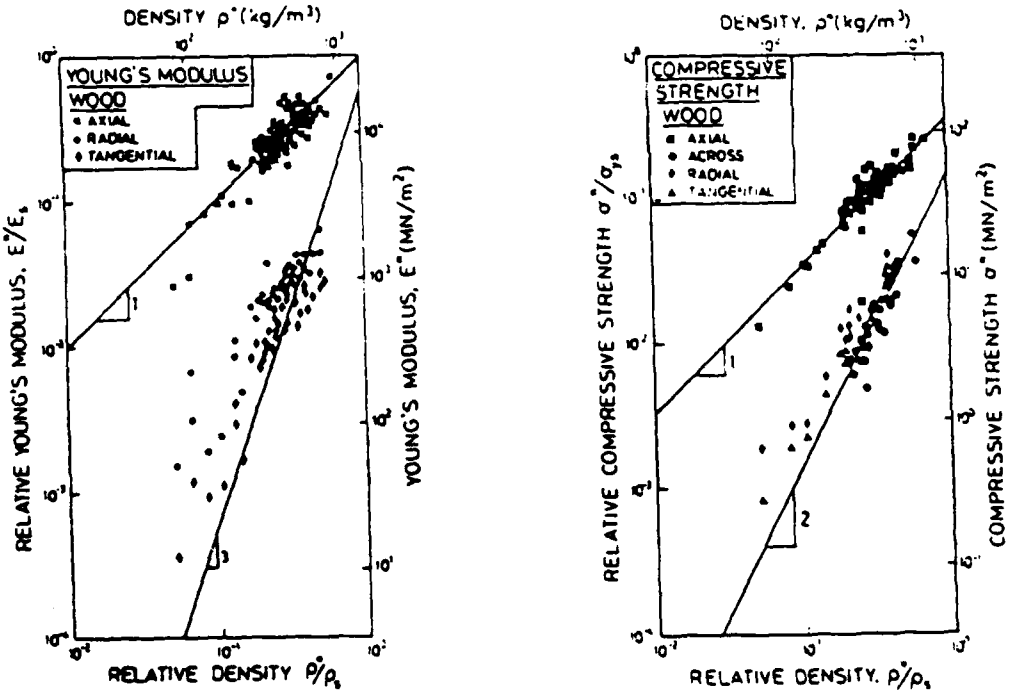

10-2 . Data for (a) the elastic moduli and (b) the compressive strength of woods. The results of the simple models are represented by the solid lines.

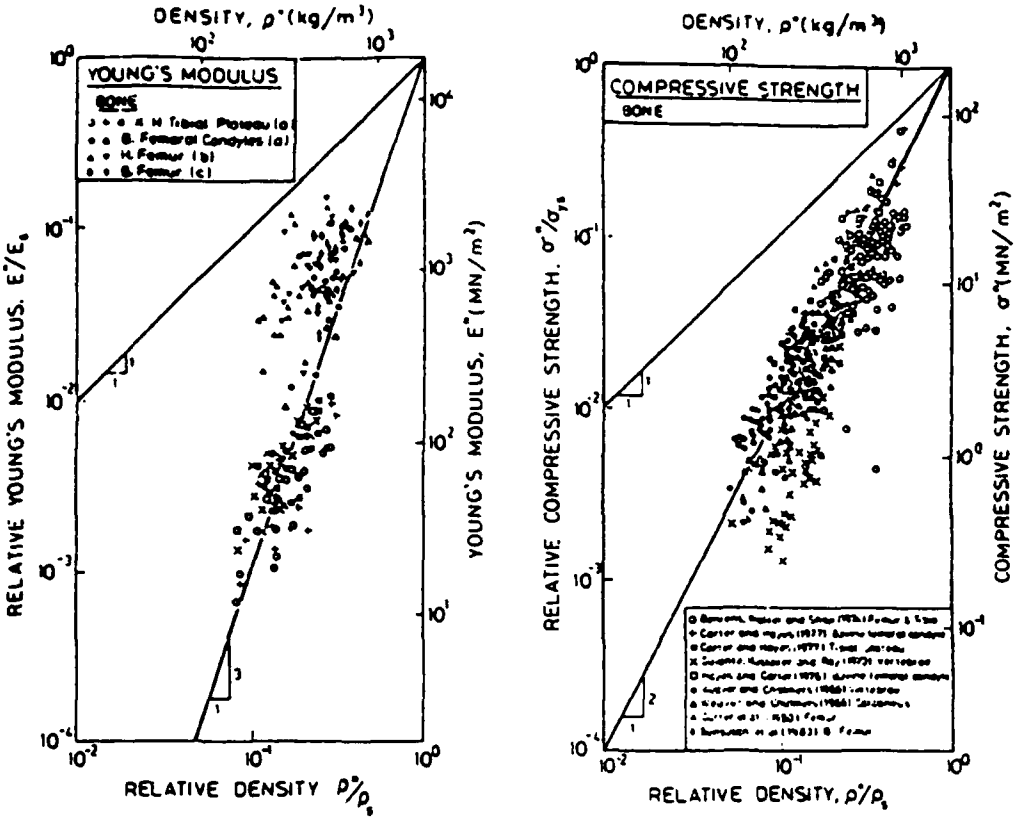

10-3 . Data for (a) the elastic moduli and (b) the compressive strength of cancellous bone. The results of the simple models are represented by the solid lines.

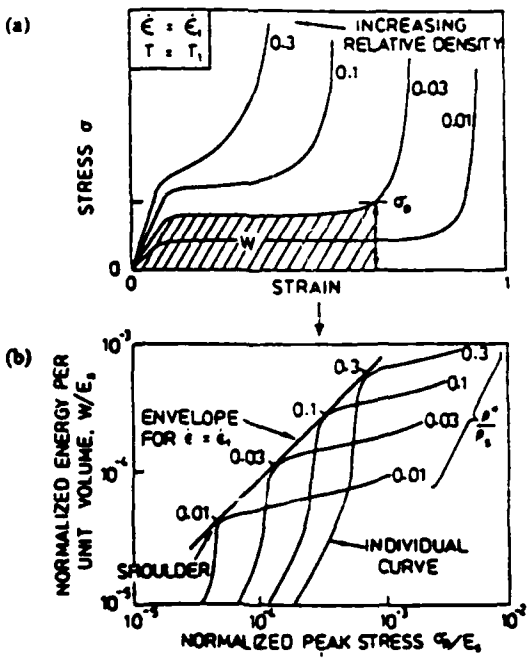

10-4 . The construction of an energy absorption diagram for a cellular solid.

Figures 5 through 12 added for amplification of the lecture.

The figures are taken from the book that I have written with Prof. Ashby of Cambridge University (Cellular Solids: Structure and Properties, Pergamon Press, 1988) and are copyright L.J. Gibson and M.F. Ashby, 1988; please acknowledge this in your report.

Fig. 5. The range of properties obtained by foaming a material, in comparison with those for fully dense solids. The properties can be exploited in engineering design: the low density is taken advantage of in low weight structural sandwich panels; the low conductivity in thermal insulation; the low Young's modulus in cushioning; and the low compressive strength (and high strain before densification) in energy absorption devices.

Fig. 6. (a) Stress-strain curves for an elastic solid and a foam made from the same solid, showing the energy per unit volume absorbed at a peak stress, σ_p. (b) Energy absorbed per unit volume against peak stress generated by an impact for both foams and the solid from which the foams are made. The foams always absorb more energy than the solid for a given maximum peak stress. Both axes are normalized by the solid modulus.

Fig. 7. Micrographs showing three orthogonal sections of balsa wood.

Fig. 8. Compressive stress strain curve for balsa loaded in the tangential direction, showing cell deformation by cell wall bending and cell collapse by the formation of plastic hinges within the bent cell walls.

Fig. 9. Compressive stress-strain curve for balsa loaded in the axial direction, showing cell deformation by uniaxial compression of the cell walls and cell collapse by end cap fracture.

Fig. 10. Scanning electron micrograph of cancellous bone taken from the femoral head, showing a low density, open-cell, rod-like cellular structure.

Fig. 11. Scanning electron micrograph of cancellous bone taken from the femoral condyle, showing an intermediate density, stress-oriented, parallel plate structure with rods normal to the plates.

Fig. 12. Compressive stress-strain curves for several relative densities of wet cancellous bone (after Hayes, W.C. and Carter, D.R. (1976) *J. Biomed. Mat. Res.* Symposium, 7, 537.)

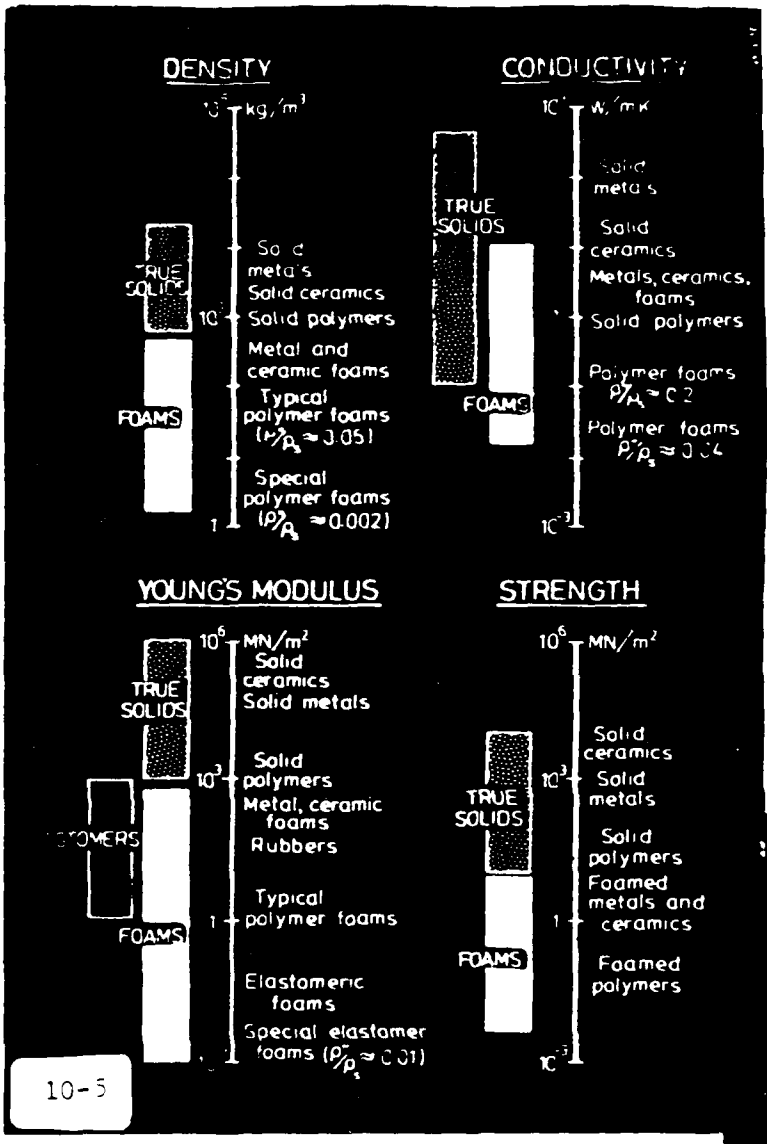
DENSITY
kg/m³
TRUE SOLIDS
FOAMS
Solid metals
Solid ceramics
Solid polymers
Metal and ceramic foams
Typical polymer foams
Special polymer foams
CONDUCTIVITY
W/m K
TRUE SOLIDS
FOAMS
Solid metals
Solid ceramics
Metals, ceramics, foams
Solid polymers
Polymer foams
Polymer foams
YOUNG'S MODULUS
MN/m²
TRUE SOLIDS
FOAMS
Solid ceramics
Solid metals
Solid polymers
Metal, ceramic foams
Rubbers
Typical polymer foams
Elastomeric foams
Special elastomer foams
STRENGTH
MN/m²
TRUE SOLIDS
FOAMS
Solid ceramics
Solid metals
Solid polymers
Foamed metals and ceramics
Foamed polymers
10-5

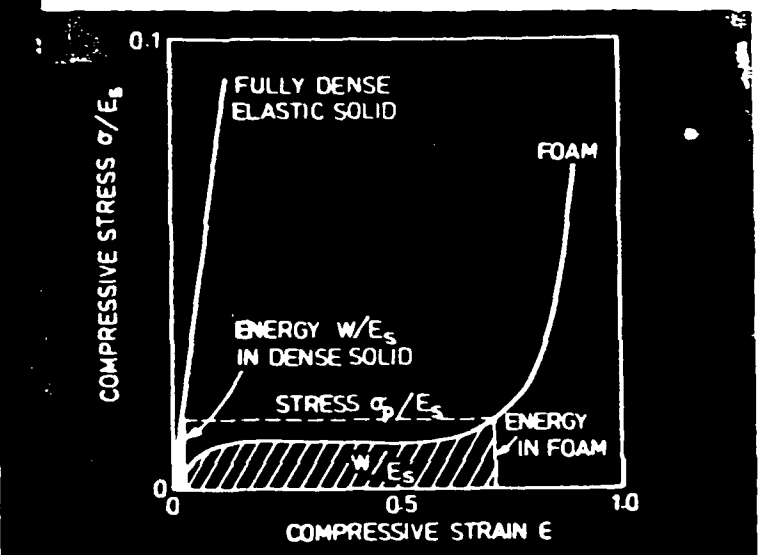
FULLY DENSE ELASTIC SOLID
FOAM
ENERGY W/Es IN DENSE SOLID
STRESS σp/Es
ENERGY IN FOAM
W/Es
COMPRESSIVE STRESS σ/Es
COMPRESSIVE STRAIN ε
0.1
0
0.5
1.0

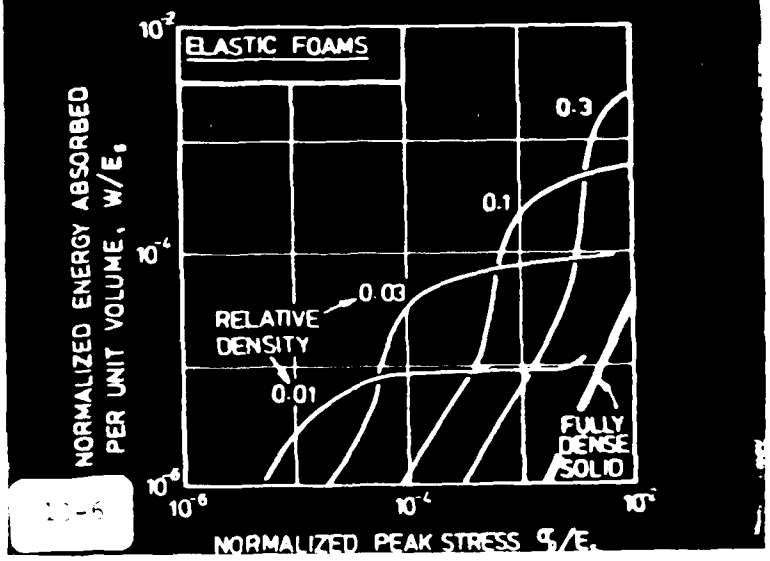
ELASTIC FOAMS
NORMALIZED ENERGY ABSORBED PER UNIT VOLUME, W/Es
NORMALIZED PEAK STRESS σp/Es
RELATIVE DENSITY
0.3
0.1
0.03
0.01
FULLY DENSE SOLID

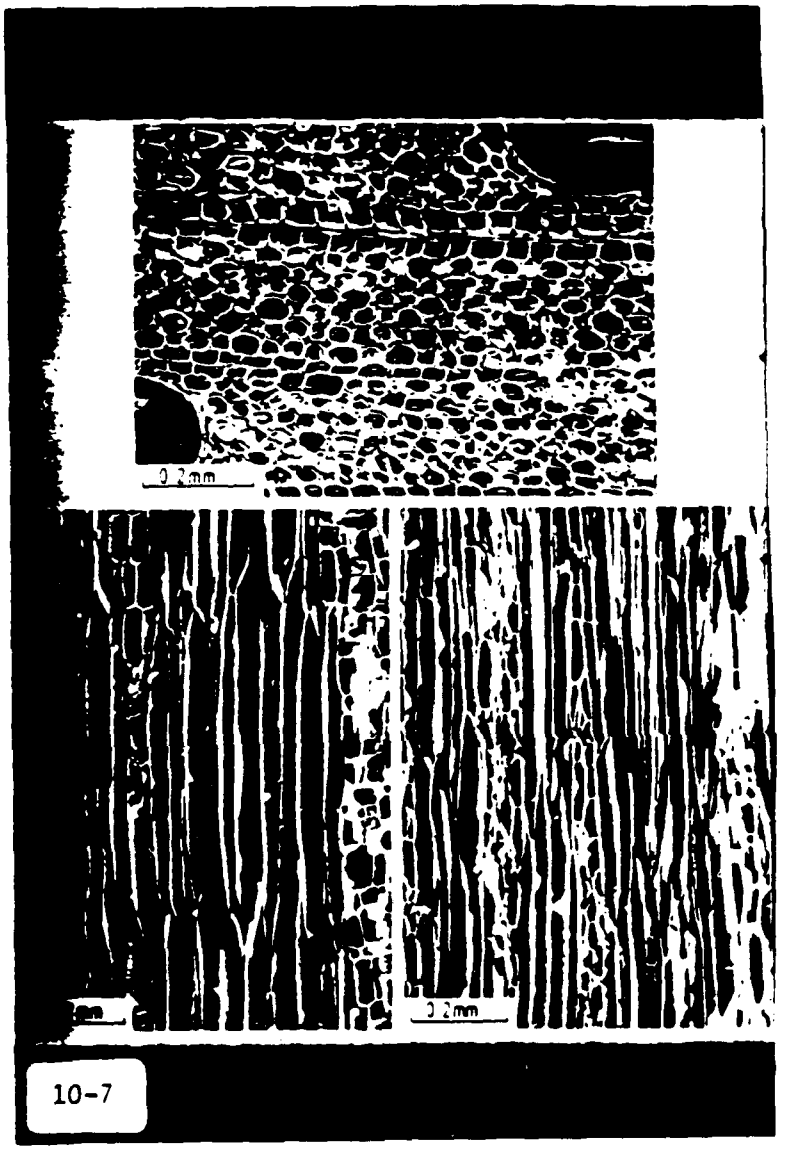

10-7

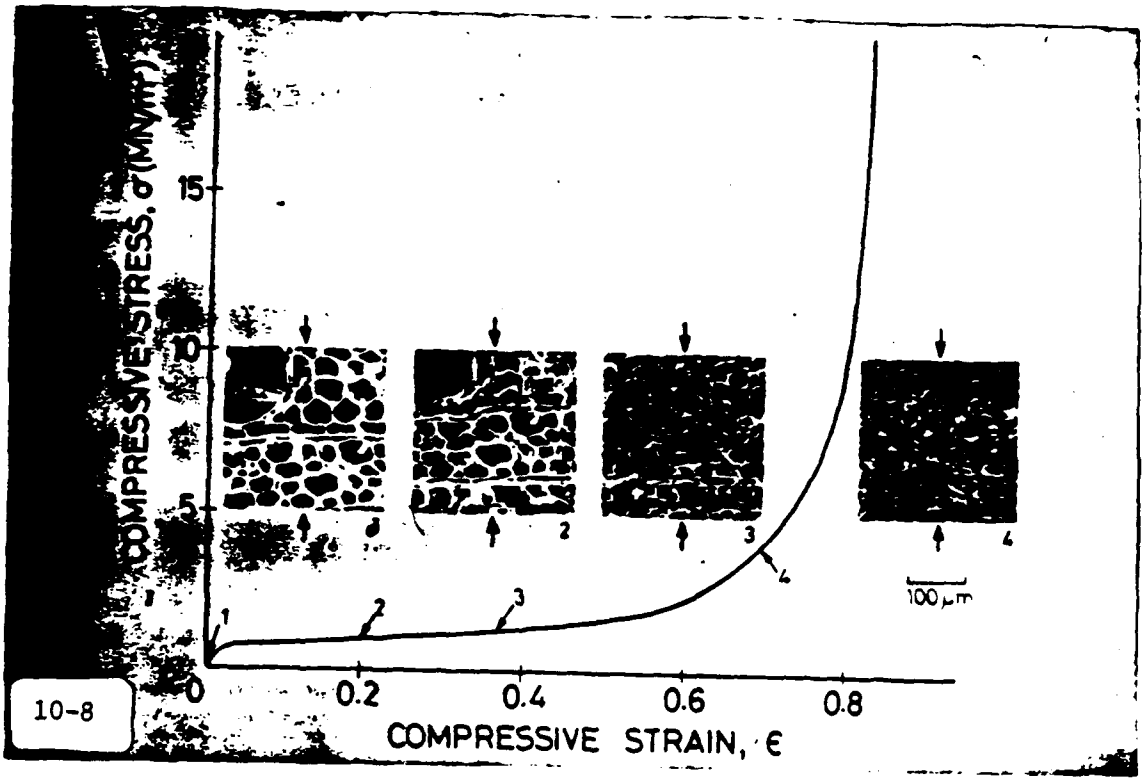
COMPRESSIVE STRESS, σ (MN/m²)
15
10
5
0
0.2
0.4
0.6
0.8
COMPRESSIVE STRAIN, ϵ
1
2
3
4
100 μm

10-8

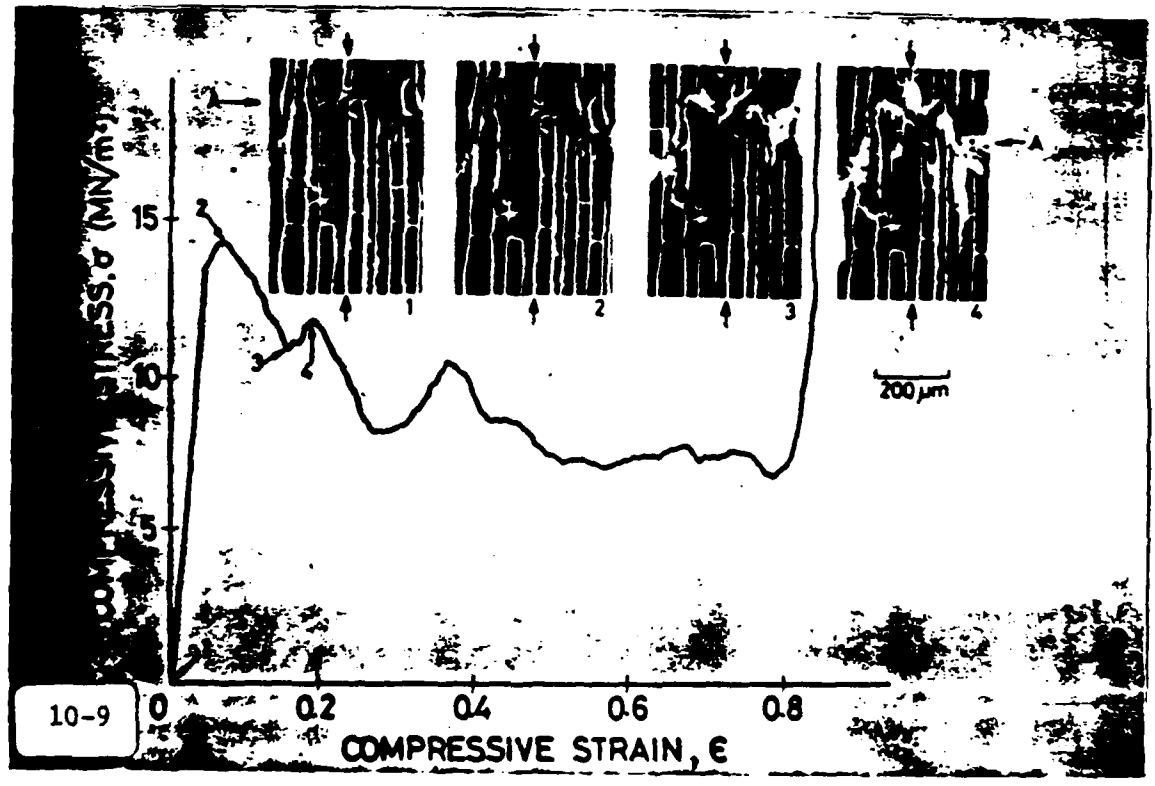
15
10
5
0
0.2
0.4
0.6
0.8
COMPRESSIVE STRAIN, ϵ
1
2
3
4
A
200 μm

10-9

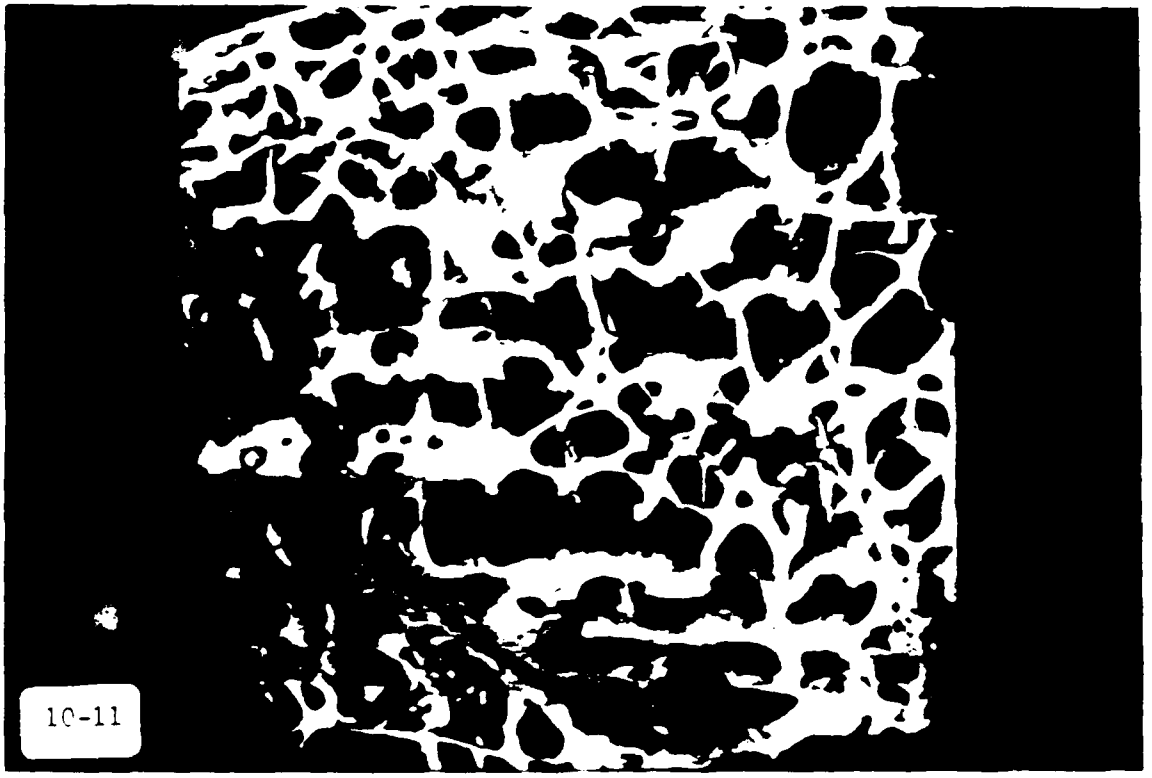
10-11

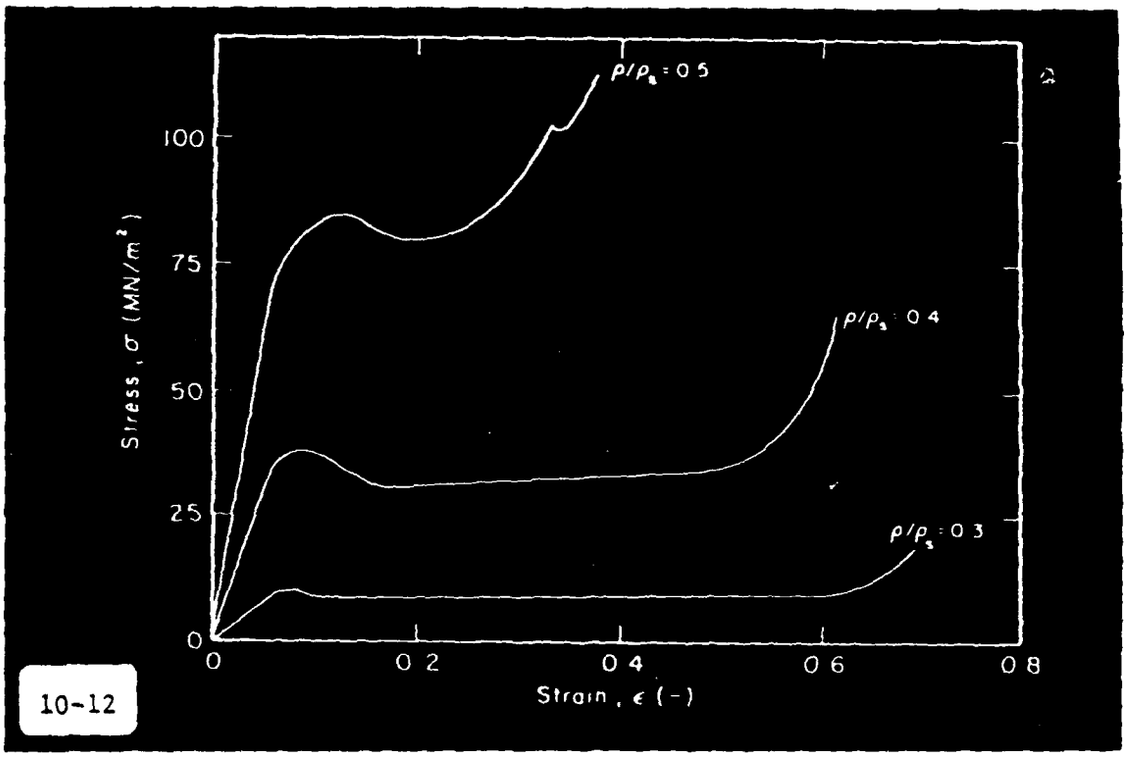
ρ/ρs = 0.5
ρ/ρs = 0.4
ρ/ρs = 0.3
100
75
50
25
0
0
0.2
0.4
0.6
0.8
Stress, σ (MN/m²)
Strain, ε (-)
10-12

THE SELF-ASSEMBLY OF FIBROUS PROTEINS. CONCEPTUAL DIFFERENCES BETWEEN IN VITRO AND IN VIVO ASSEMBLY PROCESSES

Arthur Veis
Division of Oral Biology
Department of Basic Sciences
Northwestern University
Chicago, IL 60611

Most of what we know concerning the assembly of proteins into fibrous structures has been gained from studies of the assembly of the fibers in vitro beginning from solutions of monomers. There are very profound differences between the in vitro and in vivo situations. In particular, the potential organizing effects of the cells which produce the proteins cannot be easily reproduced. Nevertheless, distinct modes of assembly can be expected for different types of monomer.

The intracellular assembly of actin filaments from the globular actin molecules represents one extreme. In this case, monomers are activated by binding to ATP. The activated monomers, under appropriate conditions of pH, ionic strength and divalent cation concentration, aggregate and grow into filaments, hydrolyzing the ATP to ADP in the process. A key feature is the bifunctionality of the polymerization. In vitro filament growth is linear and monomers can add to either end of the filament. There is a critical concentration of monomer, and both ends of the filament are in dynamic equilibrium. The ends grow at a rate independent of the filament length. Perturbation of the local conditions leads to rapid depolymerization. In vivo it is likely that free monomer does not exist, the actin is bound to another protein. Further, in vivo depolymerization appears to go to oligomer rather than monomer.

The extracellular assembly of collagen fibrils represents the other extreme case. The molecule is produced and secreted in precursor form, with amino and carboxyl propeptides. Normal fibril assembly is contingent upon cleavage of these propeptides. Assembly of the resultant collagen, in vitro, depends upon very specific interactions between collagen monomers which register the molecules so that they have the correct orientation within filaments. These same constraints, that is focused interactions assuring correct axial packing, must also operate in vivo. Collagen filaments grow in diameter either by the addition of monomers, or by the side-by-side in-register aggregation of filaments. The in vivo and in vitro axial registration mechanisms are probably mediated in the same way in both situations. However, the fibril diameter regulation is probably controlled more by cellular patterns of secretion in vivo, whereas in vitro fibril diameters are dependent on the mechanisms and rates of removal of the propeptides, as well as on the specific solvent ionic strength and pH, which modulate intermolecular interactions as well as telopeptide structures.
Work on these problems has been supported by NIH, Grant AR 013921.

Figures 1 through 6 added for amplification of the lecture.

Fig. 1 Electron micrograph of Type I Procollagen Segment-Long-Spacing (SLS) precipitates. In these structures the molecules are triple-helical through the major central section but contain the intact amino and carboxyl propeptide extensions. Micrograph courtesy of Dr. Jerome Gross.

Fig. 2 Electron micrograph of rotary shadowed monomeric rat skin collagen. In this case the molecules are without the end-propeptide regions. This slide demonstrates the intrinsic flexibility of the triple helical region. Acid-soluble monomeric collagen is usually referred to as a rigid rod. Clearly, the rigidity does not prevent molecular flexing.

Fig. 3 The proposed mechanism of type I collagen in vitro fibril formation as driven by pH and temperature changes. From A.Veis and K.Payne. In "Collagen, Vol 1. Biochemistry. M. Nimni, ed. CRC Press, Boca Raton, Fl. pp 113-138, 1988.

Fig. 4 , Fig. 5 Two models suggesting that the most flexible regions of the collagen molecule must become "stiffened" during intermolecular association to form the 4-D staggered native collagen fiber structure. These models suggest that the flexible regions have a key role in the intermolecular interaction leading to molecular registration within the fibril.

Fig. 6 A detailed mechanism for interaction of the amino telopeptide of the α1(I) chain with the 4-D staggered section of helical region of an α1(I) chain on an adjacent molecule. A. The initial interaction of the collagen helix receptor site (top) and the telopeptide in ß-sheet conformation (bottom). B. Formation of the aldehyde on Lys 9^{N} causes a rearrangement of the ionic interactions and minimizes the repulsion between similarly charged Lys 9^{N} and Hyl^{930}. C. Schiffs Base formation stabilizes the interaction. From Helseth, D.L., Lechner, J.H. and Veis, A. Bioplymers 18:3005-3014 (1979).

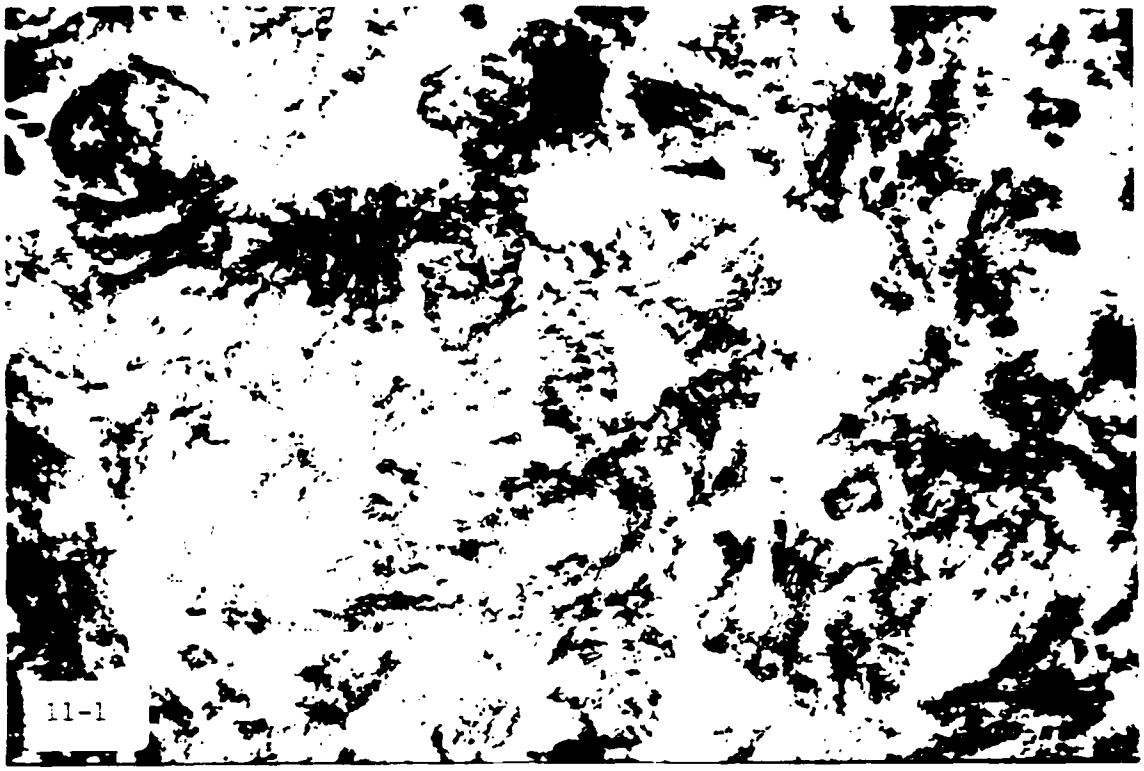
11-1

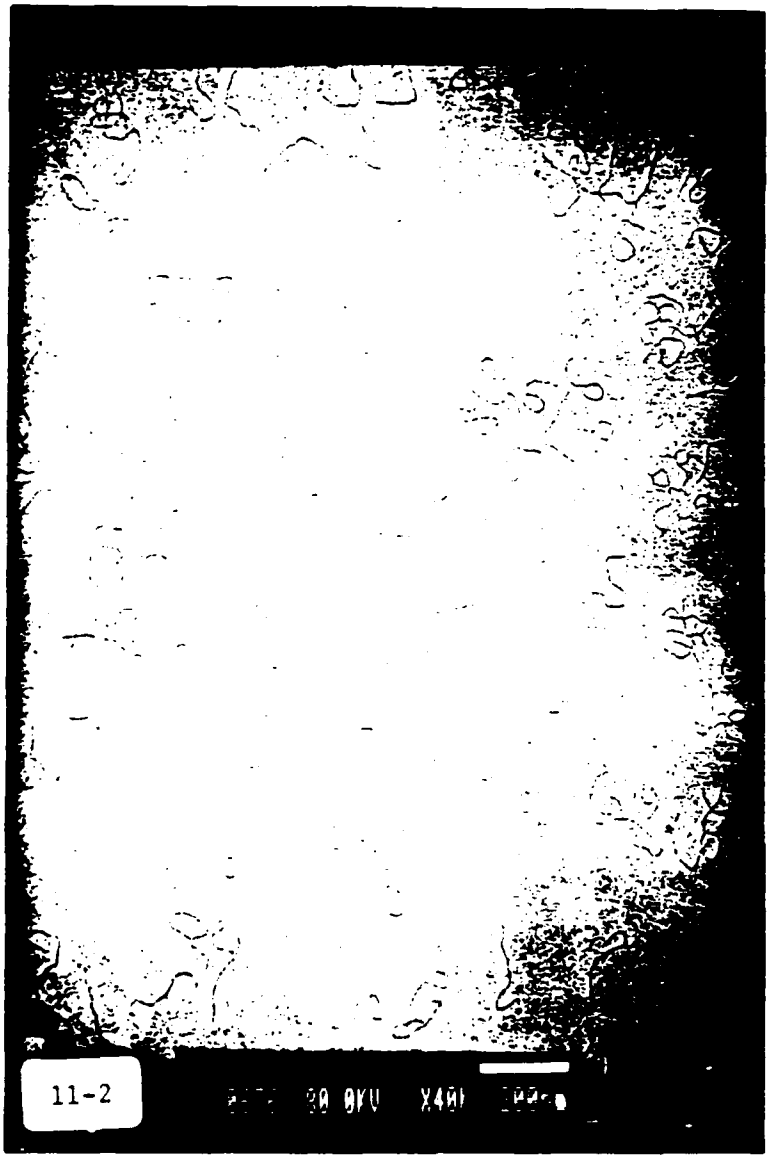
11-2

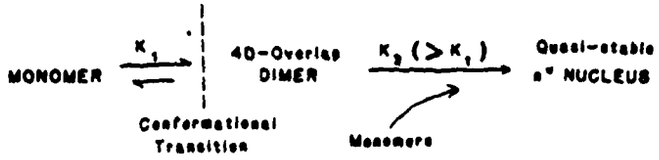

LAG-PHASE

EARLY GROWTH PHASE

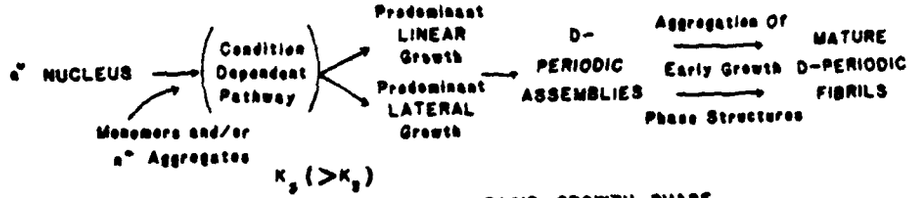

EARLY GROWTH PHASE (cont'd)

RAPID GROWTH PHASE

11-3

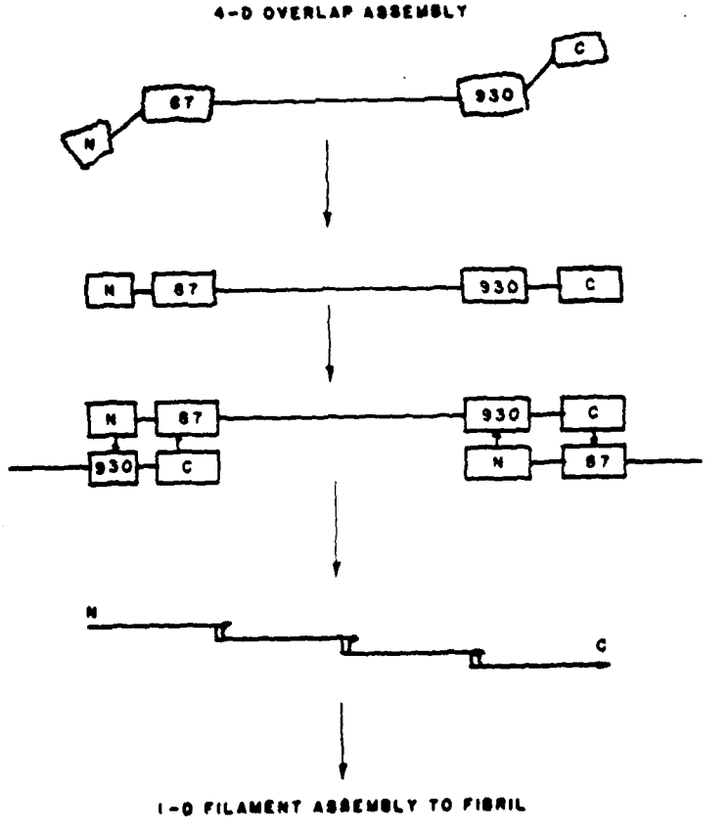

11-4

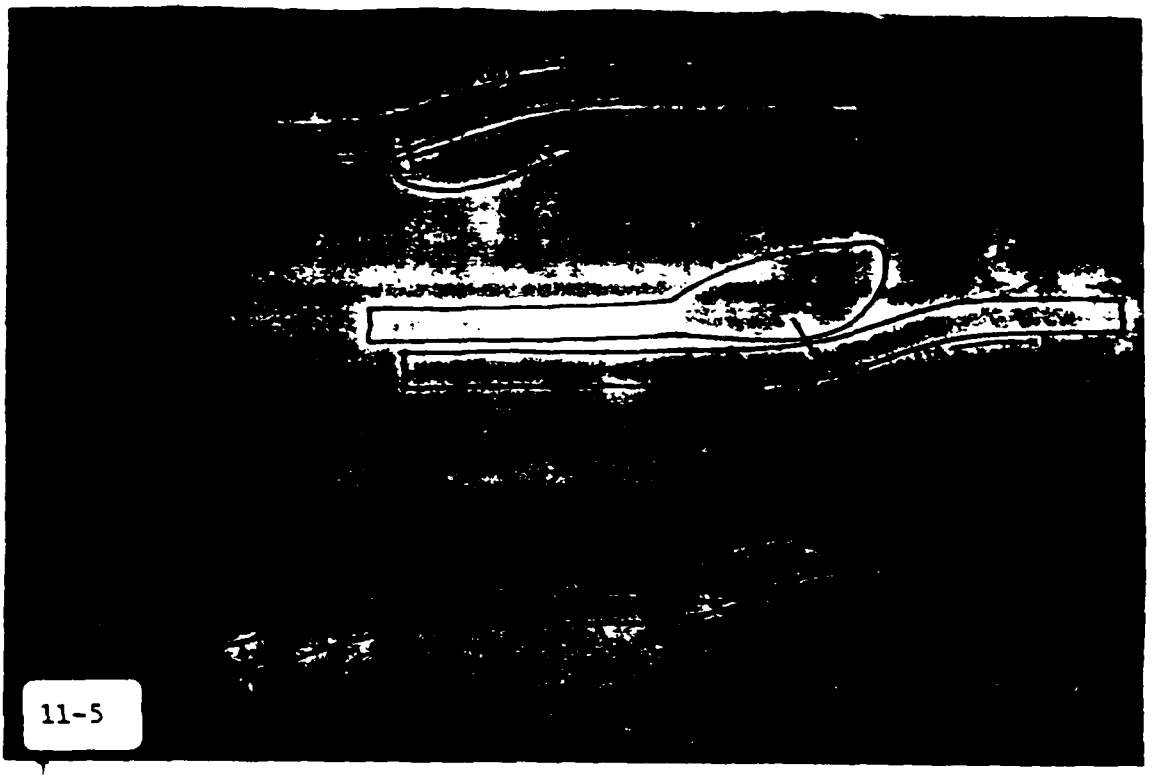

11-5

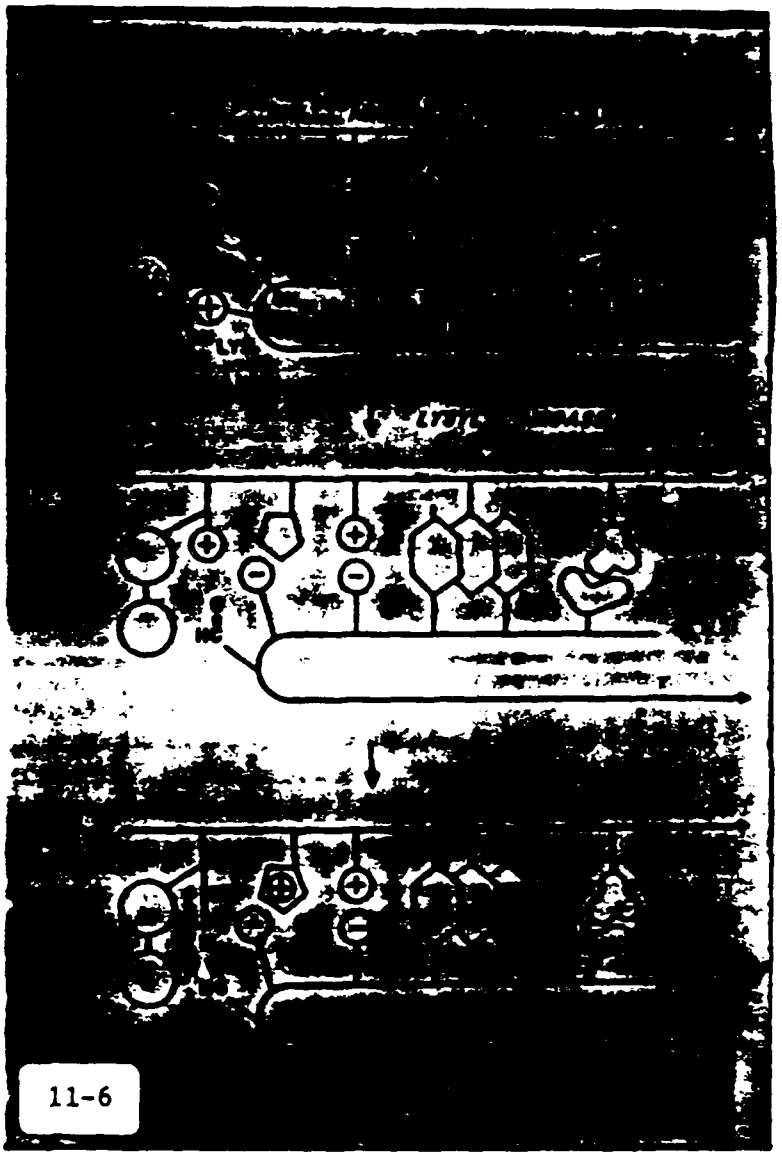

11-6

Self-Assembly and Reconstitution of Tissue Analogs

Frederick H. Silver, Y. Pedro Kato, David L. Christiansen and Arthur J. Wasserman, Biomaterials Center, Department of Pathology, UMDNJ-Robert Wood Johnson Medical School, Piscataway, NJ 08854.

Collagen is used in the medical device industry as a hemostat, for augmentation of soft tissue, and as a coating for vascular and other prostheses (1). In addition to these uses, recent advances in the growth of mammalian cells on collagenous substrates has led to the concept of engineering tissues and even functional organs by seeding with the appropriate cell lines a reconsituted analog of the normal connective tissue.

In this paper we present results of recent studies conducted in our laboratories describing the reconstitution of type I collagen into prosthetic tendons, nerve conduit materials, and dura mater. Our experience to date indicates that tendon (Figure 1), nerve (Figures 2 and 3) and dura (Figure 4) can be regenerated in animal models using collagenous materials with the appropriate geometry.

Insoluble type I collagen from bovine hide was purified and reconstituted into fibers about 50 μm in diameter which were either formed into a tow containing 250 parallel fibers (coated with a collagen dispersion) to be used as a tendon prosthesis, or packed into a silicone tube (0.2 mm in diameter) for a nerve prosthesis. Collagen dispersions were air dried at room temperature to form a membrane 100 μm in thickness for dura mater replacement.

Implantation of collagen prostheses into rabbit Achilles tendon and skull, and into rat sciatic nerve was used to evaluate the tissue response in animal models. Results of tendon studies suggest that within 10 weeks neotendon is observed in the presence of a collagen fiber prosthesis and that the ultimate tensile strength of this tissue is above that of an autograft control (2). In the case of peripheral nerve, by 6 weeks post-implantation increased numbers of myelinated and unmyelinated axons are observed when the prosthesis contains collagen fibers. After approximately 2 months a reconstituted collagenous dural substitute is replaced by new connective tissue in the presence of limited inflammatory and fibrotic complications (3).

Results of animal studies suggest that reconstituted collagenous

tendon, nerve and dural prostheses are rapidly replaced with functional connective tissue and based on these studies it may be possible to regenerate the structural and biochemical function of a wide variety of pathologic tissues using reconstituted collagenous matrices.

References

1. Silver, F.H. and Doillon, C.J., Biocompatibility: Interactions of Biological and Implantable Materials, Volume I, Polymers, VCH Publishers, New York, N.Y., chapter 1.

2. Goldstein, J.D. Tria, A.J., Zawadsky, J.P., Kato, Y.P., Christiansen, D., and Silver, F.H., Development of a Reconstituted Collagen Tendon Prosthesis: A Preliminary Implantation Study, J. Bone and Joint Surgery, in press September,1989.

3. Collins, R.L.L., Christiansen, D., Zazanis, G.A., and Silver, F.H., Use of Collagen Film as a Dural Substitute, submitted for publication.

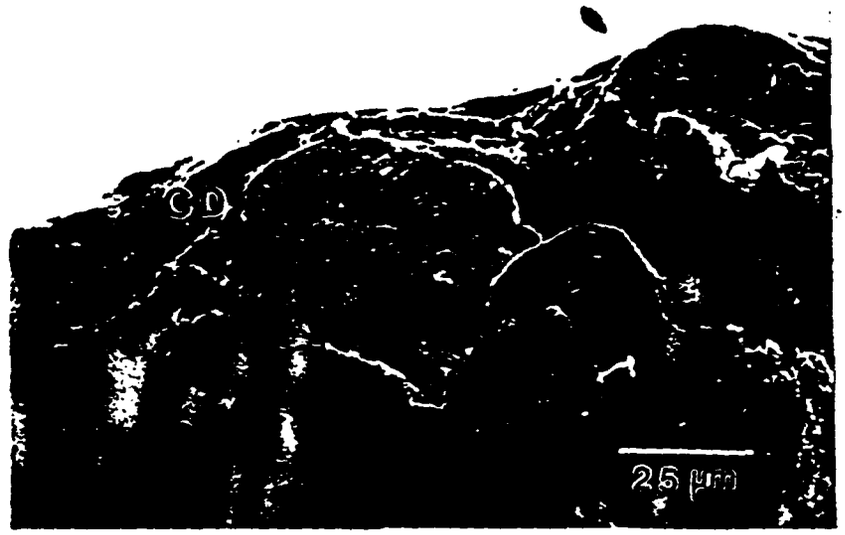

Figure 1. Scanning electron micrograph of reconstituted tendon prosthesis showing collagen fibers (CF) and collagen dispersion (CD) used to hold the fibers together.

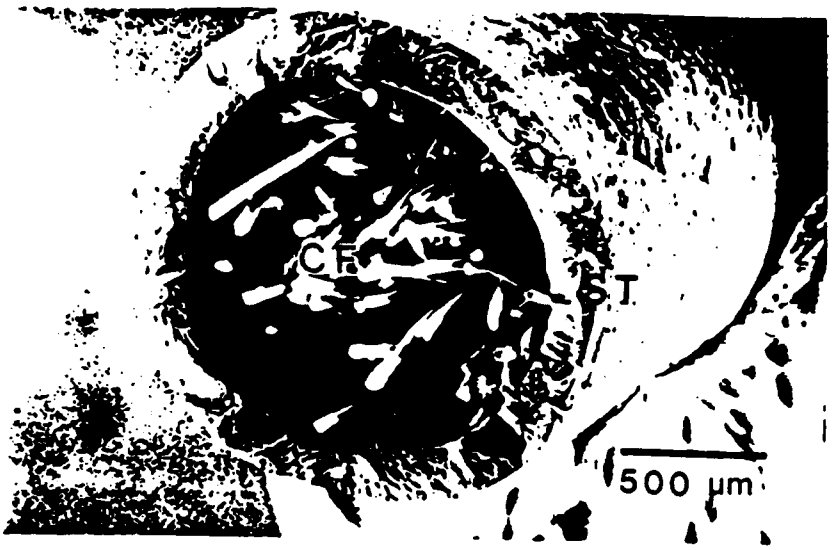

Figures 2. Scanning electron micrographs of reconstituted nerve prosthesis showing (top) individual reconstituted collagen fibrils (CF) and silicone tube (ST) and (bottom) individual nerve cell growing along a thin collagen fiber.

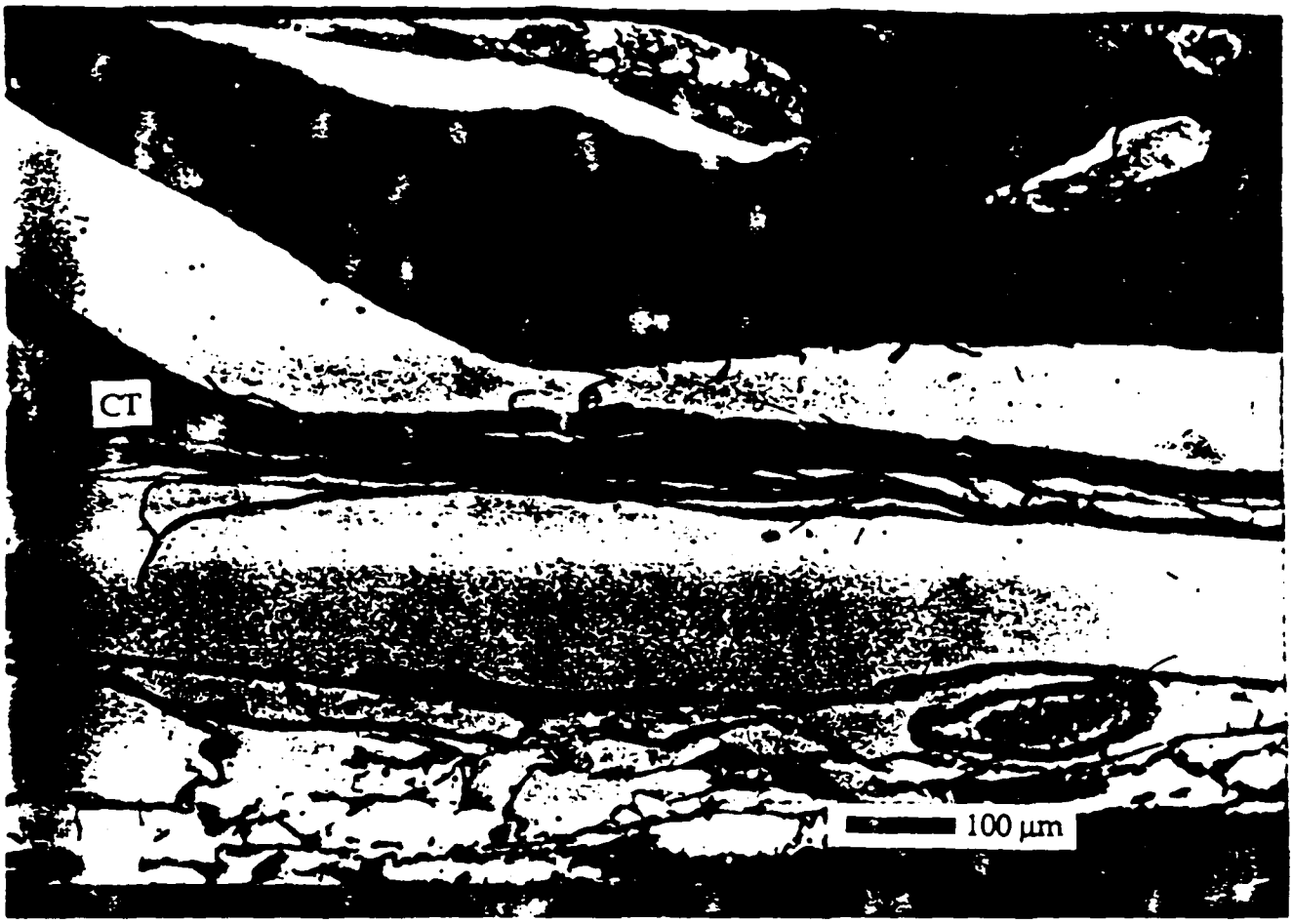

Figure 4. Light micrograph showing connective tissue (CT) replacing type I collagen membrane used as a dural replacement two months after implantation in rabbits. Densely stained tissue above connective tissue layer is the skull and that directly below it is pia mater.

Figures 5 through 11 added for amplification of the lecture.

Figures added for amplification of the lecture

Fig. 5 Polarized light micrographs of type I collagen fibres during self assembly. The morphology of type I collagen fibres formed during self assembly was observed using polarized light at 546 nm photographed at a magnification of 500x. Micrograph shows an apparent layered structure observed during the end of the growth phase. Only the mass of collagen within the fibres was observed to increase during the growth phase and not the fibre birefringence retardation or diameter.

Fig. 6 Collagen fibre morphology showing variation in the orientation of the collagen fibrils.

Fig. 7 Electron micrograph showing the substructure of collagen fibrils.

Fig. 8 Electron micrograph showing proteoglycan molecules attached to the D bands of collagen fibrils.

Fig. 9 Stress-strain curves of collagen fibrils. Typical stress-strain curves of control collagen fibrils (◇) and fibres extruded into fibre formation buffer containing CS-PG from scars (□) or containing high density PG from articular cartilage (PG1-PG) (△). Measurements were made in uniaxial tension at room temperature and a strain rate of 10 %/min.

Fig. 10 Typical stress-strain curves obtained at a strain rate of 50 %/min for collagen fibres cross-linked: (a) for 3 d using the dehydrothermal technique and for 1 d in cyanide vapour (DHT3+C1); (b) for 2 d in glutaraldehyde vapour (Glut 2); and (c) for 4 d in glutaraldehyde vapour (Glut 4). For comparison, the curve for rat tail tendon fibres in shown (d).

Fig. 11 Ultimate tensile strength versus proteoglycan type. Plot of tensile strength obtained from uniaxial tensile measurements similar to those shown in Figure 12-5 for collagen fibre control and fibre containing CS-PG from scars and high density PG from articular cartilage (PG1-PG). Error bars represent standard deviations of the mean.

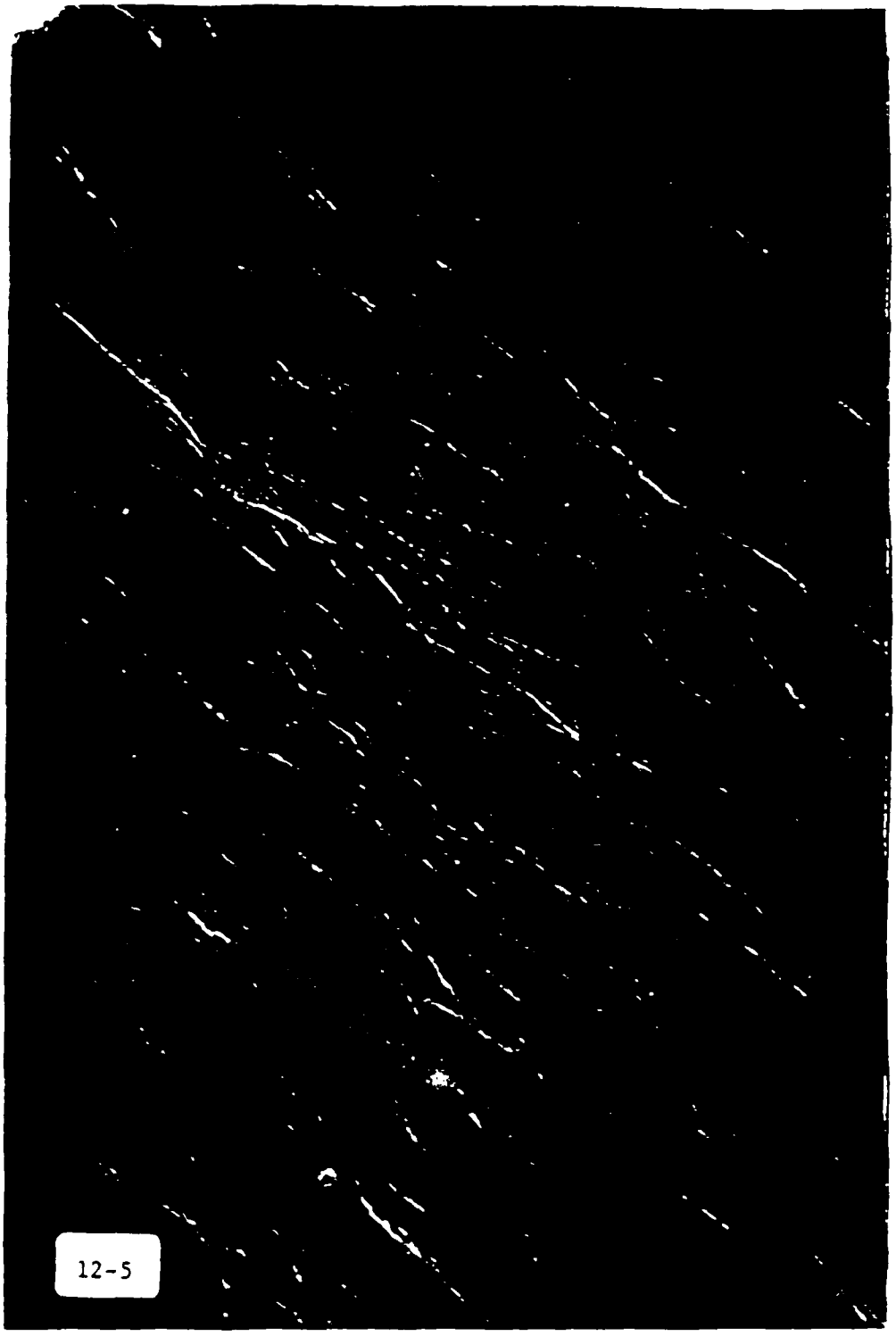
12-5

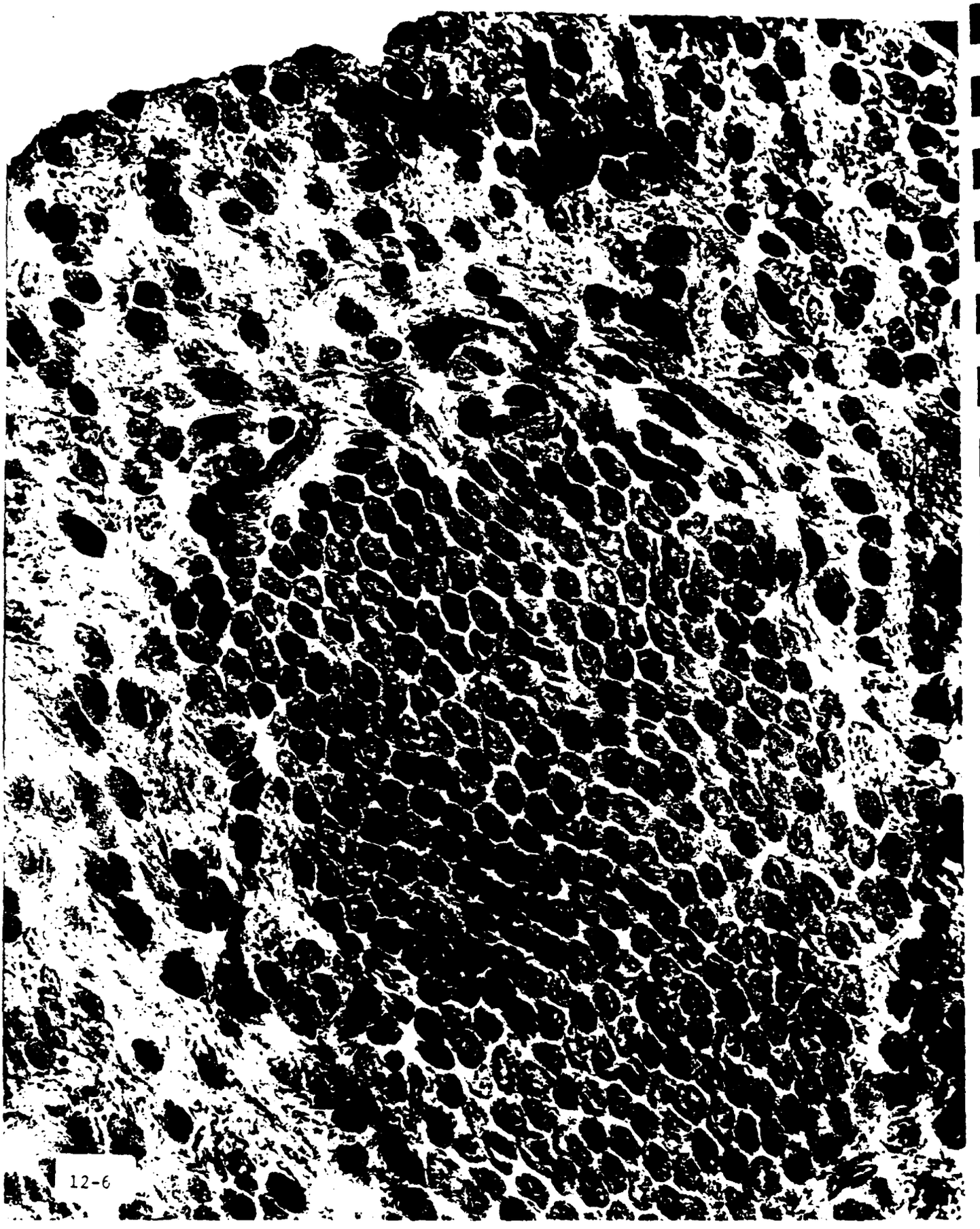

12-6

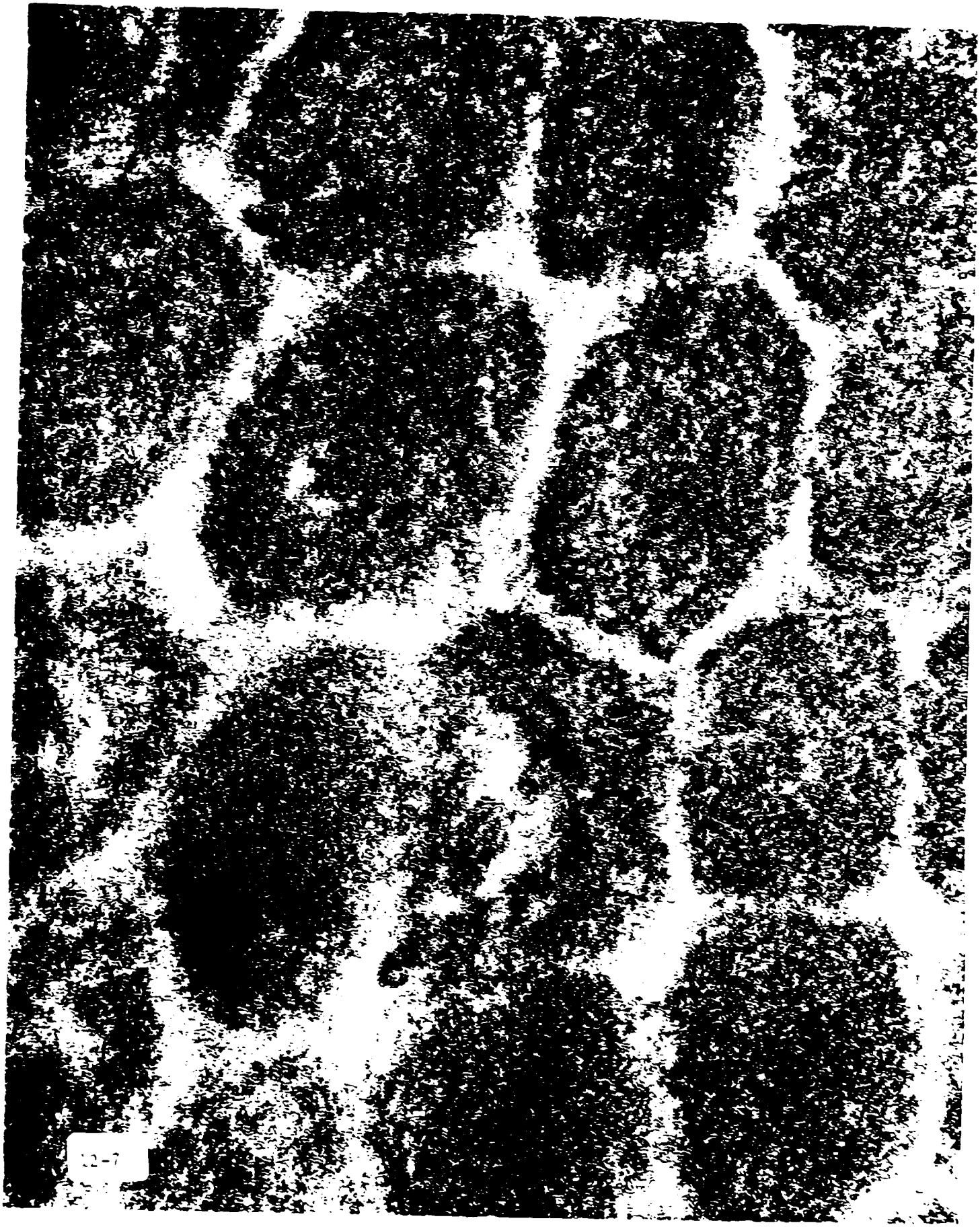


12-8

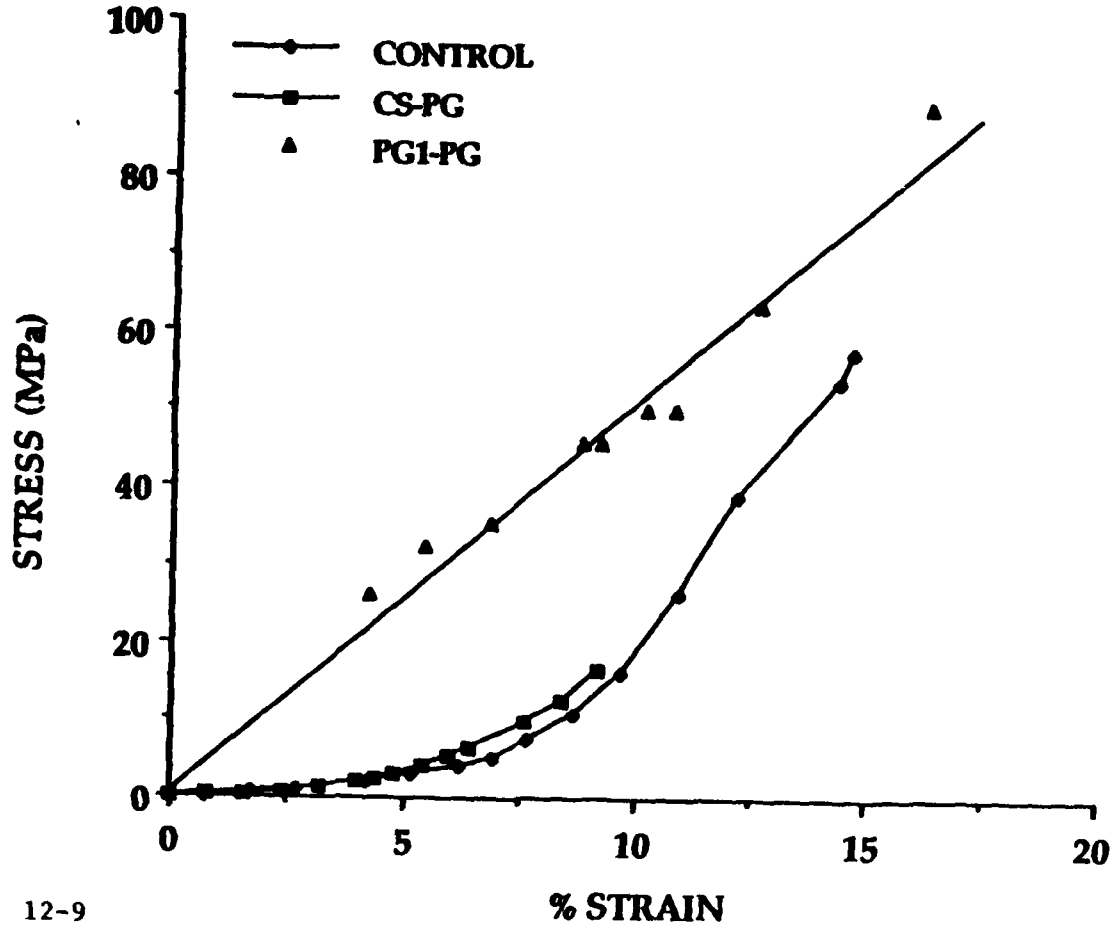
CONTROL
CS-PG
PG1-PG
STRESS (MPa)
100
80
60
40
20
0
0
5
10
15
20
% STRAIN

12-9

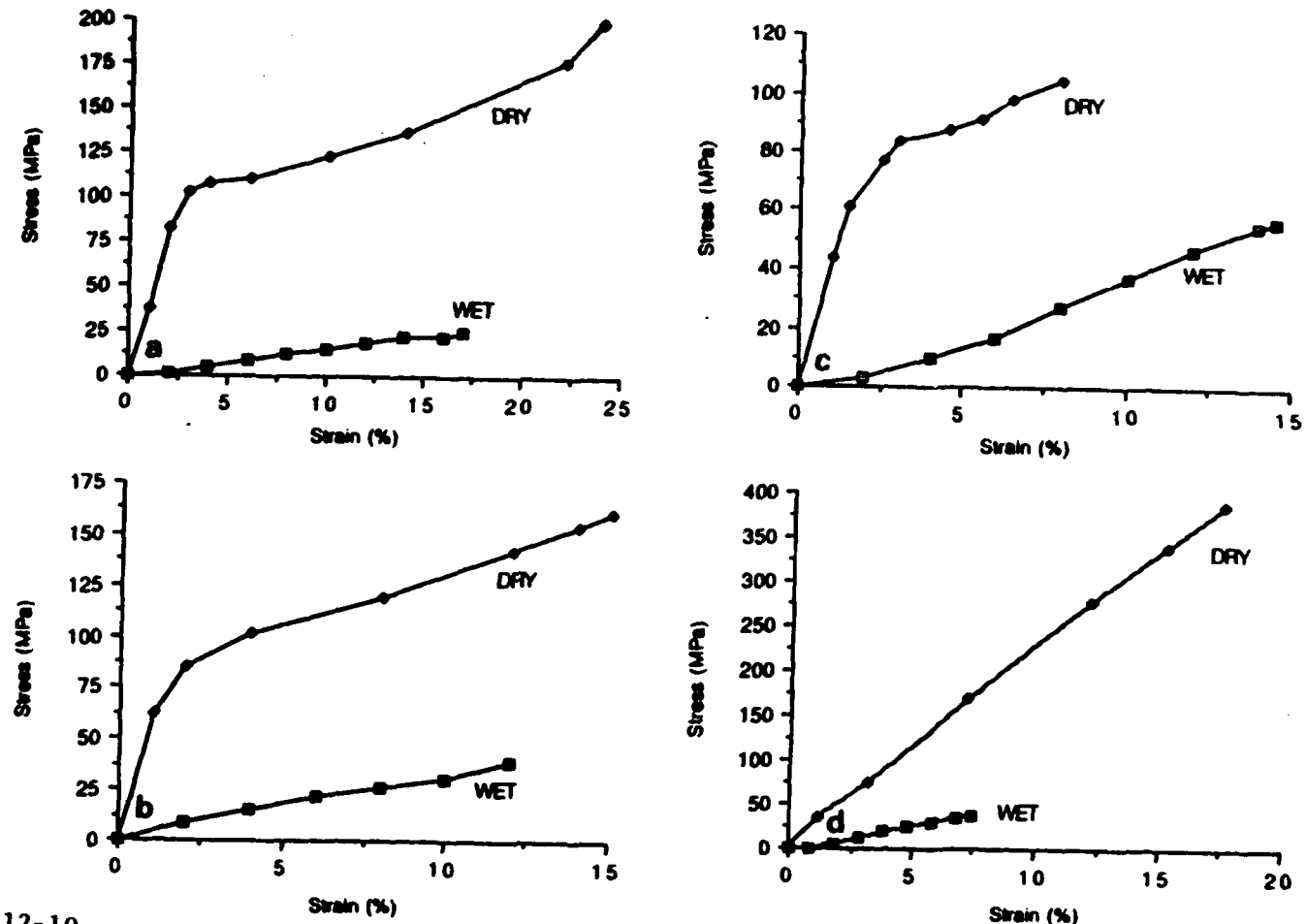

12-10

Typical tensile stress-strain curves obtained at a strain rate of 50%/min for collagen fibres cross-linked: (a) for 3 d using the dehydrothermal technique and for 1 d in cyanamide vapour (DHT3 + C1); (b) for 2 d in glutaraldehyde vapour (Glut 2); and (c) for 4 d in glutaraldehyde vapour (Glut 4). For comparison, the curve for rat tail tendon fibres is shown (d).

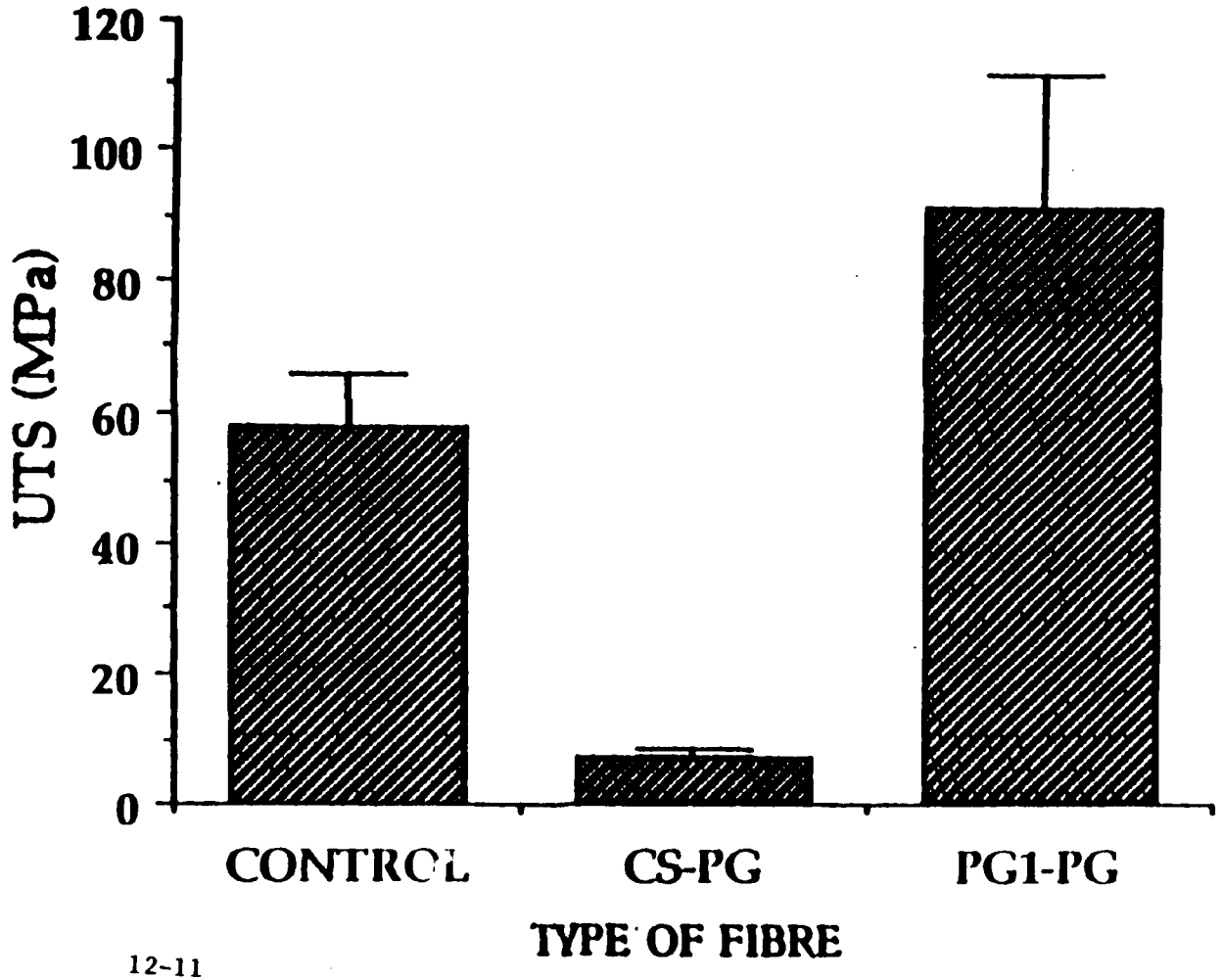

12-11

COLLAGEN FIBRIL ASSEMBLY BY A NUCLEATION-GROWTH MODEL

Donald Wallace
Celtrix Laboratories
Collagen Corporation
Palo Alto, CA 94303

A quantitative model has been developed for fibril assembly of Type I collagen. The phase equilibria between collagen and aqueous solvent were determined using an expression of Flory [1] for rigid, rod-like polymers. The collagen rod was modelled as a rod of axial ratio 200 (This ratio may also be considered as a segment length, x). The Flory expression also contained χ, the polymer-solvent interaction term, which is a measure of the energy change per polymer segment on transferring a polymeric solute molecule from pure solute (fibril phase) to infinitely dilute solution. χ was calculated based on the approximation that local (per segment) stabilization of fibrils was due to hydrophobic and electrostatic forces only. When fitted at one point to experimental solubilities, the Flory expression could describe the experimental solubility-temperature curve for intact and pepsin-treated collagen. The free energy of fibril formation could also be derived from these equations, and when applied to a nucleation-growth mechanism yielded 1) a curve for the extent of collagen precipitated as a function of time, and 2) curves for half-time (t 1/2) of fibril assembly *versus* temperature (T), ionic strength (I), pH, collagen concentration, and fibril diameter [2,3].

The above model was incomplete in that it did not explicitly describe the effects of the extra-helical peptides of Type I collagen. The current contribution addresses the phase equilibria and assembly kinetics of rod-like sequences to which short tails are appended. Such species are simulations of the collagen helix and extra-helical peptides (Fig. 1). The thermodynamics of such semi-rigid molecules have been described by Matheson and Flory [4]. Using this theory, phase diagrams for three solute species (x = 203, 201, and 200) were calculated (Fig. 2). These phase diagrams permitted the association of χ with T or I, as described [2,3]. Fig. 3 presents the dependence of solubility on I for a rigid solute species with two appended tails. Figs. 4 and 5 compare the solubility of three types of solute species as a function of temperature. The solubility data for Figs. 3, 4 and 5 were obtained by fitting X at a single experimental point for intact, pepsin-digested, and pronase-digested collagen. From the three χ values at the respective fit points (χa, χb, and χc, Figs. 3 and 4), χ could be resolved into the following components: $\chi 1 = 1.58$, $\chi 2 = 0.107$, and $\chi 3 = 4.80$, in which $\chi 1$ represents the solvent-polymer energy for an extra-helical segment of length 1; $\chi 2$, that for the helical segment of length 200; and $\chi 3$, for a second extra-helical segment of length 2 (Table 1). These χ factors could be associated with the N-terminal extra-helical, helical, and C-terminal extra-helical regions of Type I collagen, respectively. It was then possible to interpret these three χ values in terms of plausible numbers of energetic interactions involved in stabilizing the collagen fibril. Finally, since the solubility *versus* T curves for this modified theory were nearly identical to those observed previously [2,3], the theoretical kinetics of assembly were found

to fit experimental kinetic results. (Figs. 6,7 and 8 present such results for intact collagen).

References.
1. Flory, P.J. (1956) Proc. Roy. Soc. Lond. A234, 73-89.
2. Wallace, D.G. (1985) Biopolymers 24, 1705-1720.
3. Wallace, D.G., accepted for publication, Biopolymers.
4. Matheson, R.R., and Flory, P.J. (1981) Macromolecules 14, 954-960.
5. Cooper, A. (1970) Biochem. J. 118, 355-365.
6. Helseth, D.L., and Veis, A. (1981) J. Biol. Chem. 256, 7118-7128.
7. Wallace, D.G. and Thompson, A. (1983) Biopolymers 22, 1793-1811.
8. Kadler, K.E., Hojima, Y., and Prockop, D.J. (1988) J. Biol. Chem. 263, 10517-10523.
9. Williams, B.R., Gelman, R.A., Poppke, D.C., and Piez, K.A. (1978) J. Biol. Chem. 253, 6578-6585.

Legend to Table 1.

Title: Local Interaction Energies (χ) Associated with Three Sequences of the Collagen Molecule

a
1) $\chi = \chi_1(x1/x) + \chi_2(x2/x) + \chi_3(x3/x)$; where x1 = 1 is the segment length of the N-terminal extra-helical sequence, x2 = 200, that for the central helical sequence, and x3 =2, that for the C-terminal extra-helical sequence. The values of χ were obtained by solving three simultaneous equations similar to 1) containing χ_a, χ_b, χ_c, as given in the legend to Fig. 4.

b
Local energies calculated per segment at T = 302 K, I = 0.2, pH = 7.3, using $\chi_i = \Delta f_i/RT$.

c
Local energies per sequence = energy/segment times sequence length; e.g., -64 times 200 = -12,400 cal/mole for the total central sequence.

d
Hydrophobic and electrostatic energies of interaction per hydrophobic amino acid side chain or per charged amino acid side chain computed as in [2,3].

Figure legends.

Fig. 1. Schematic representation of a semi-rigid chain of total length x = 203 containing 3 rigid segments connected by non-dimensional flexible connections.

Fig. 2. Phase diagram for binary systems consisting of solvent and three species or solute: a) a single rod-like sequence with

axial ratio x = 200 with no appended tails, ——— ; b) a sequence of total length 201 segments, containing 1 rigid 200 segment sequence and a second rigid sequence of length 1, ····· ; and c) a sequence of total length 203 segments: 1 of length 1, 1 of length 200, and a third of length 2, —·— . Solute species a simulates a pronase-digested collagen molecule; species b, pepsin-digested collagen; and species c, intact collagen. In the diagram, the curves for isotropic solutions are on the left and those for ordered phases (i.e., fibrillar phases) are on the right. The biphasic region is between the two curves. A complete diagram is shown only for solute species a and includes the "stem" or "chimney" which extends to negative χ values. Curves for solute species were calculated using equations 1) through 5) of [2],or equivalently, equations 9), 15) -18), and 21), 22) of [1]. Curves for solute species b and c were calculated from equations 17), 23), and 24) of [4].

Fig. 3. Dependence of equilibrium solubility of intact Type I collagen on ionic strength. The phase equilibria were for an aqueous solvent containing mono-valent salt ions and a 3-segment solute species c; T =299 K, pH = 7.3. Curve calculated from equations of [3] and [4], with Zd = 0.45, b = 0.301, and Zs = 0, and other parameters as given in Table 1 of [3]. Parameters for the computation were set with the aid of a single experimental point [5]; solubility of intact collagen = 9.3 µg/ml at T =302 K, I = 0.2, pH =7.3, corresponding to χ = 0.161.

Fig. 4. Equilibrium solubility of Type I collagen as a function of protease treatment over a range of temperature. Solubility curves were calculated for species a, ———, species b, ·····, and species c, — — —,as described in Fig. 2. For species a, the single experimental fit point was taken as 433 µg/ml at T = 302, I =.02, and pH = 7.3, corresponding to χa = 0.107; approximate experimental data for pronase-digested collagen from [6]; ◌ . For species b, simulating pepsin-digested collagen, the solubility fit point was 98 µg/ml at T = 302 K, I =0.2, pH = 7.3 [7], corresponding to χb = 0.131; experimental points from [7]; ● . For species c simulating intact collagen, the fit point was as in Fig. 3, χc = .162, and experimental points from [5]; ○ ,[8]; □ .

Fig. 5. Equilibrium solubility of Type I collagen over a range of temperature. Data for species c as in Fig. 4, re-plotted on a different solubility scale (to show fit of curve to experiment).

Fig. 6. Kinetics of fibril assembly for intact collagen (species c) as a function of temperature. t1/2 of fibril assembly computed from equation 19) of [3] (or equation 3) of [7]); the free energy of fibril assembly computed from the phase diagram in Fig. 3 for species c. Fitting parameters (as described in [2,3]) were Zd = 0.54, b = 0.307, nf = 21, f(v2) = 3.56, and σ_s =0.043 ergs/cm^2. Experimental data from [9].

Fig. 7. Kinetics of fibril assembly for species c as a function of pH, computed as in Fig. 6, with assignments of discrete

charged groups as in [3]; data from [9].

Fig. 8. Kinetics of fibril assembly for species c as a function of ionic strength. Computations and data as in Fig. 6.

COMPONENTS OF CHI [a]

SEQUENCE	CHI VALUE	ENERGY [b] PER SEGM. (CAL/MOL)	ENERGY [c] PER ROD (CAL/MOL)
1. N-TERMINAL EXTRA-HEL.	CHI1= 1.58	-948	-948
2. HELICAL	CHI2=0.107	-64	-12400
3. C-TERMINAL EXTRA-HEL.	CHI3=4.80	-2880	-5760
COMPOSITE	CHI =.161	-97	-19600

CHI1= $-\Delta f/ RT$ (at T=302 K)

Δf [d] (hydrophobic) = -296 cal/mol ; Δf [d] (elec.) = -200 -1600 cal/mol

CONCLUSION: A FEW LOCAL HYDROPHOBIC OR ELECTROSTATIC INTERACTIONS COULD ACCOUNT FOR EXTRA-HELICAL ENERGIES

Table I

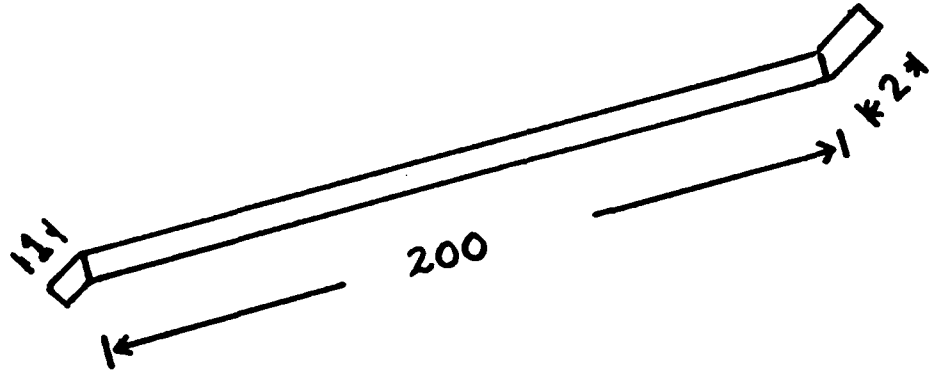
111
200
#21

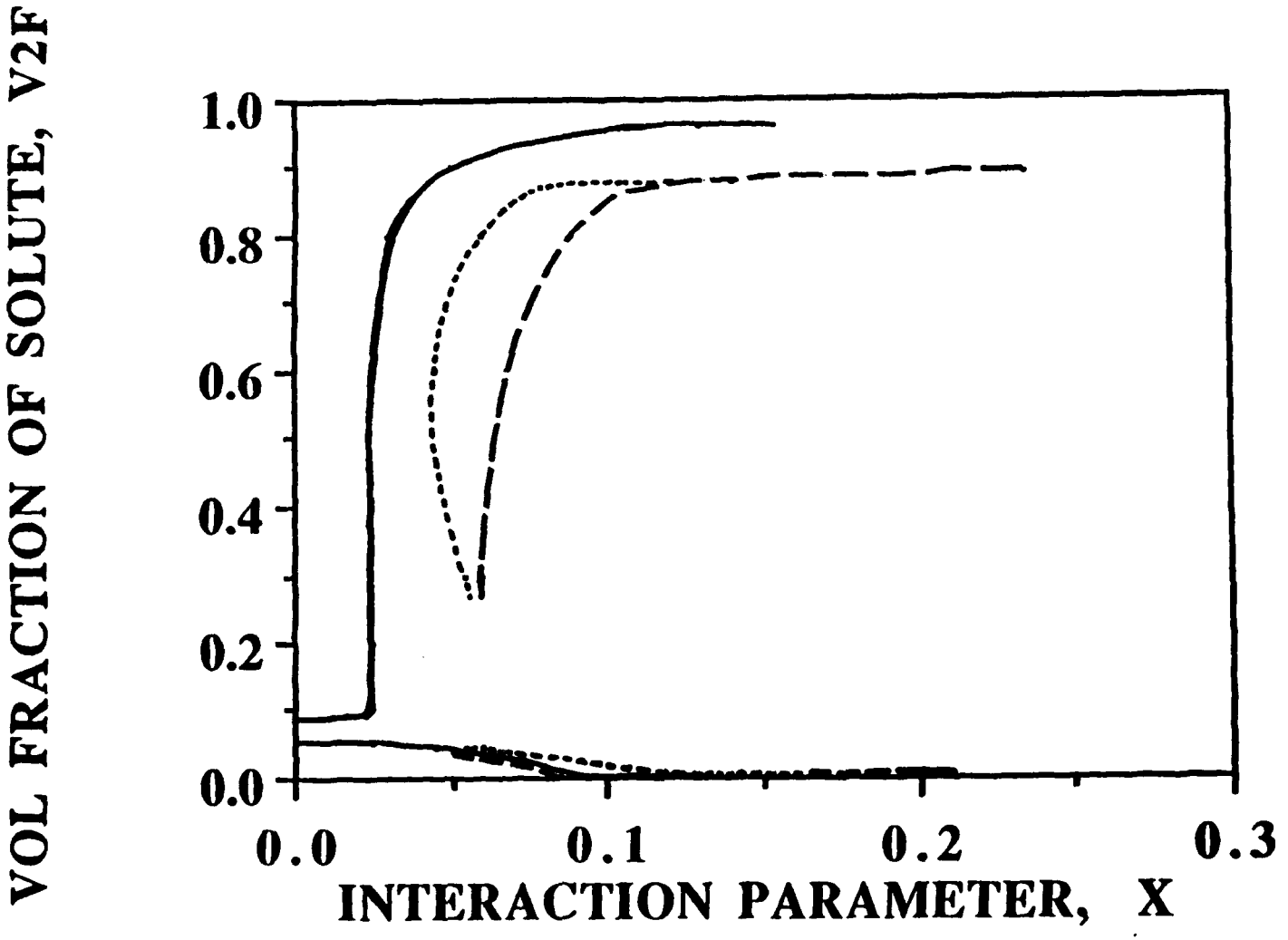
VOL FRACTION OF SOLUTE, V2F
1.0
0.8
0.6
0.4
0.2
0.0
0.0
0.1
0.2
0.3
INTERACTION PARAMETER, X

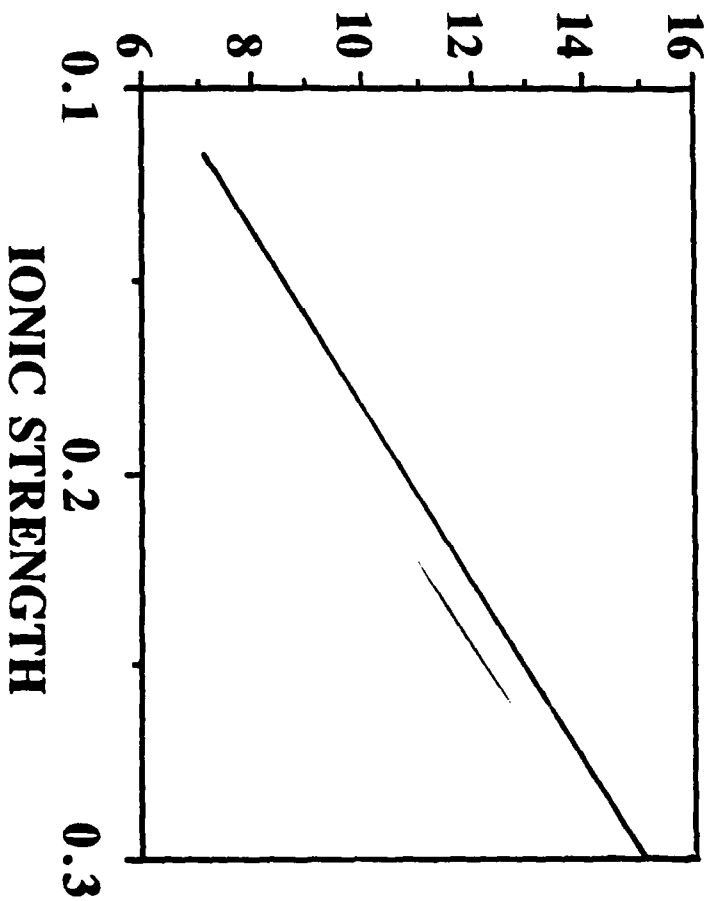
EQUILIBR. SOL. (UG/ML)
6
8
10
12
14
16
0.1
0.2
0.3
IONIC STRENGTH

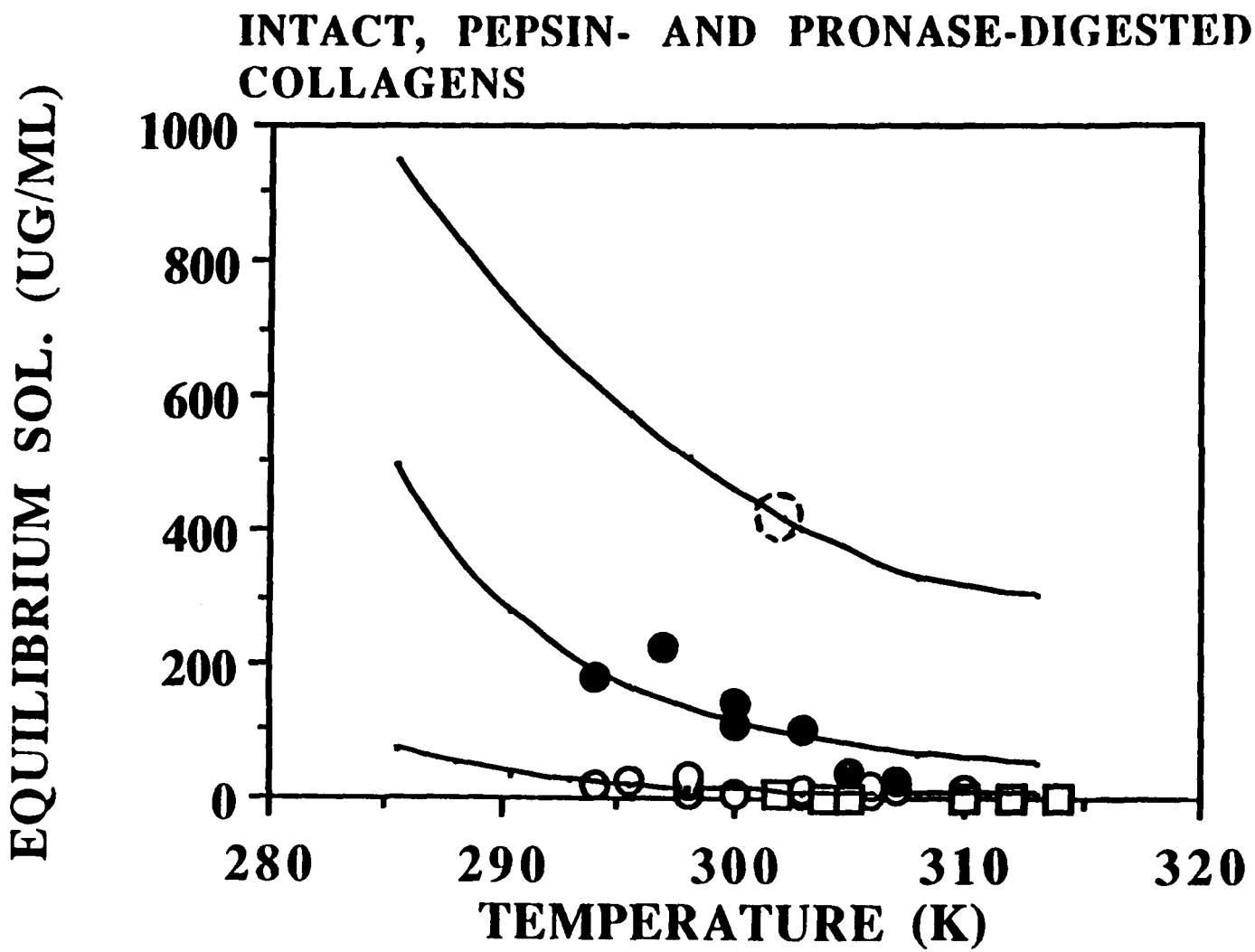
INTACT, PEPSIN- AND PRONASE-DIGESTED COLLAGENS
EQUILIBRIUM SOL. (UG/ML)
1000
800
600
400
200
0
280
290
300
310
320
TEMPERATURE (K)

INTACT COLLAGEN
EQUILIBRIUM SOL. (UG/ML)
80
60
40
20
0
280
290
300
310
320
TEMPERATURE (K)

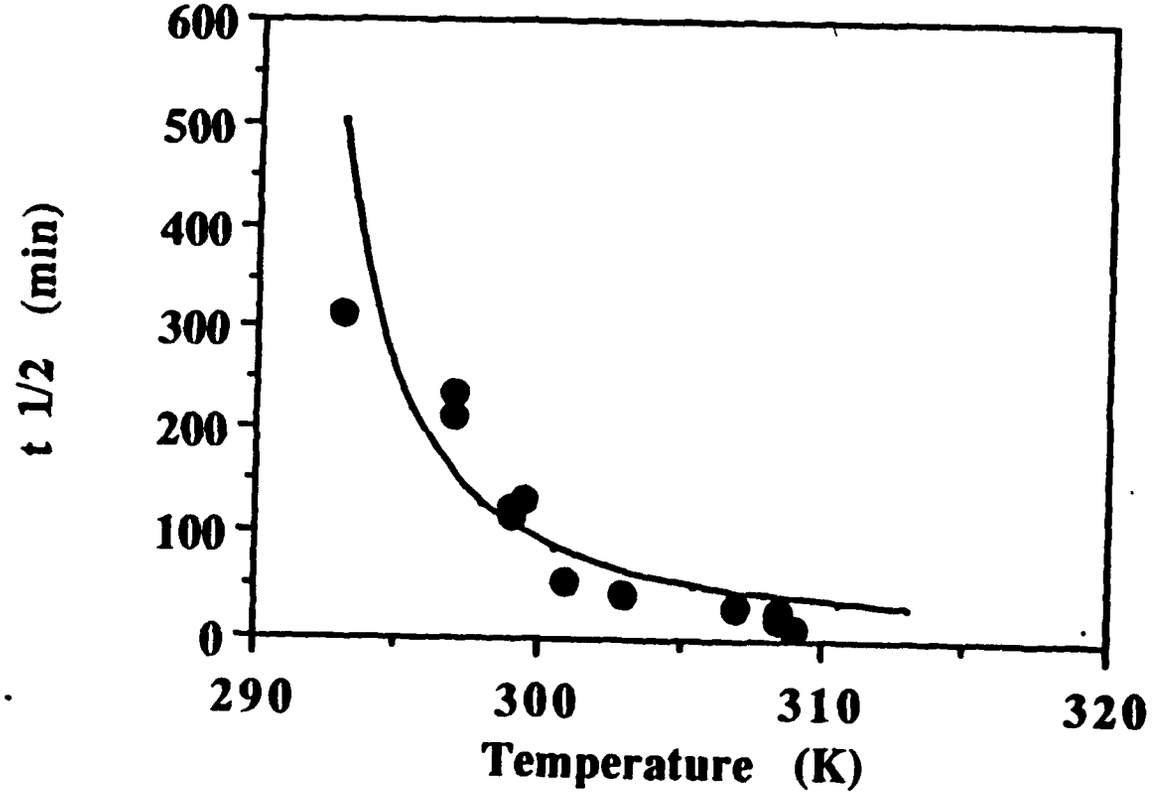
600
500
400
300
200
100
0
t 1/2 (min)
290
300
310
320
Temperature (K)

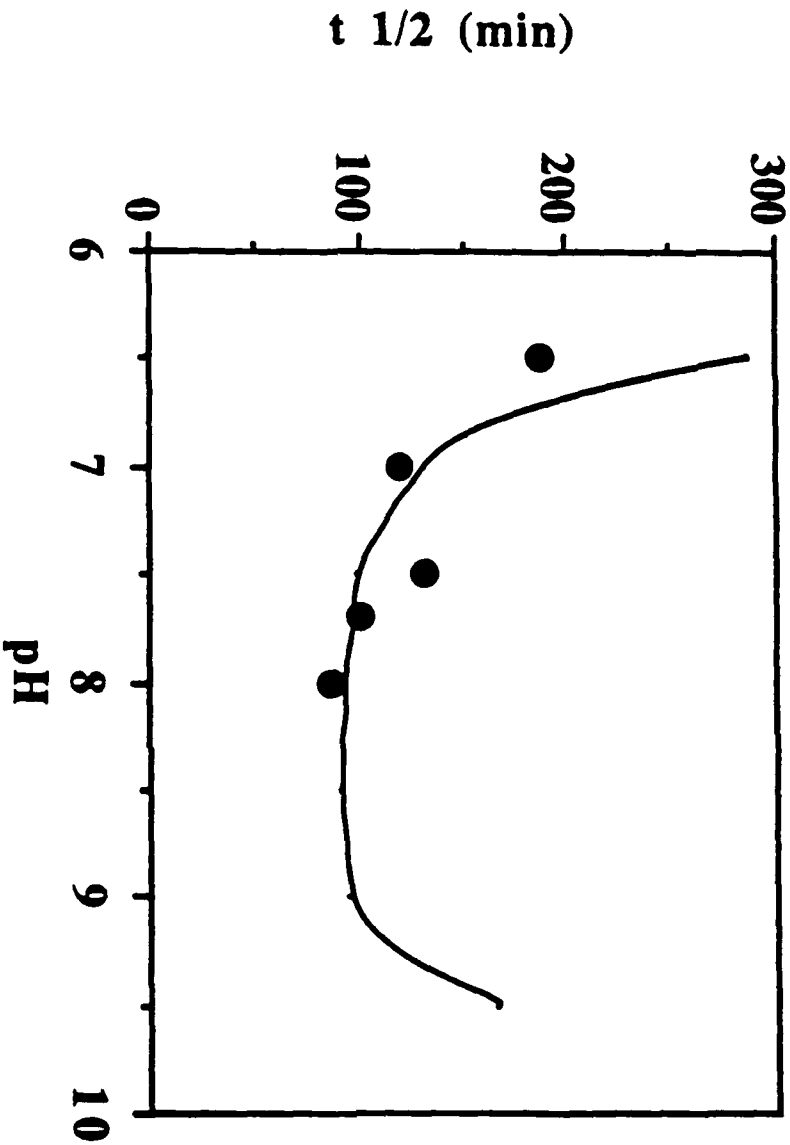
t 1/2 (min)
0
100
200
300
pH
6
7
8
9
10

13-8

BIOENGINEERED MATERIALS RELATED TO BIOMINERALIZATION

David L. Kaplan
U. S. Army Natick Research, Development & Engineering Center
Natick, Massachusetts 01760-5020

Current in-house research programs relative to bioengineered fibrous proteins and polysaccharides, as well as biomineralization processes themselves, are discussed with respect to composite materials. Chitin/chitosan and fibrous proteins with beta-sheet conformations have been implicated as integral to the formation of biomineralized composites. Genetic control over the composition/structure of these macromolecules will permit manipulation of function, and may be important in furthering our understanding of the roles played by these structures in natural composites. Similarly, aspects of our work relative to mussel matrix proteins and monolayer mineralization experiments are also expected to provide insights into the natural mechanisms involved in these processes.

Chemical characterization of spider silk, including composition, sequencing, cloning and conformational energy calculations is in progress to better define structure function relationships with this fibrous protein. Chitosan has been produced directly from the fungus Mucor rouxii through fermentation controls, and current efforts are directed towards the characterization of two key biosynthetic enzymes, chitin synthetase and chitin deacetylase, prior to cloning. Genetic controls over polymer formation will provide well defined materials to use in biomineralization studies. Biomineralization studies are focused on the isolation and characterization of matrix proteins from the mussel and on stereochemical controls over crystallization in Langmuir-Blodgett monolayers.

THE COMPONENTS AND STRUCTURE OF INSECT EXOSKELETONS COMPARED TO MAN-MADE ADVANCED COMPOSITES

David P. Anderson

University of Dayton Research Institute
Dayton, Ohio 45469

The United States Air Force and its contractors have a large continuing effort to develop strong, stiff, and light-weight structures. Biologists in the past have examined the morphology of biological systems, but not with the goal of using that information to build man-made composites. The arrangement of components of the insect cuticle of the Bessbug beetle was chosen for our study because the cuticle serves as a structural component which has similar requirements to Air Force applications and resembles man-made composites.

Examination of the leg, pronotum, and elytra by SEM revealed procuticle structures with layers of chitin fibers held together with matrix material which also appears fibrous. The cross-section and sizes of the fibers vary with small circular fibers near the outer surface and larger elliptical fibers in the middle of the procuticle. The plys of the procuticle consist of single layers of fibers with the non-circular fibers packed in regular arrays with the long axis of the cross-section perpendicular to the ply plane. The procuticle of the elytra (wing covering) is split into an inner and outer section. The fibers of the inner section appear lath like with the long direction lying in the ply plane.

The orientation of the fiber layers was found to vary in a regular fashion. Each successive parallel layer's orientation is nearly perpendicular to the last layer's with the angle of every other layer gradually changing the same amount in the same direction to form a helicoid. Thus the orientations of the fibers layers are laid up in an unsymmetrical pattern of a double helicoid repeating in a regular manner. The orientations from the SEM have been confirmed with wide-angle x-ray diffraction. Epoxy/carbon composites with similar layups are currently undergoing mechanical evaluation in our labs.

Much of this paper was recently presented elsewhere:

R. Schiavone and S. Gunderson "The Components and Structure of Insect Exoskeletons Compared to Man-Made Advanced Composites," Proceedings of the American Society for Composites, 4th Technical Conference, Blacksburg, VA, 876, October 1989.

Figures 1 thrugh 10 added for amplification of the lecture.

Fig. 1 . Possible arthropod exoskeletons to examine. Beetles chosen mostly as a matter of convenience in terms of size and availability. Also, they were chosen because some of their functions require light weight in structural and protective applications (they fly too). Specifically the Bessbug.

Fig. 2 . Insect procuticle schematic: This is a natural complex composite structure including fibers and matrix with fibers of different sizes, shapes, and orientation.

Fig. 3 . Top SEM is from the Bessbug, the bottom from a man-made composite. Natural system has layers of fibers in various directions, both show fibers and matrix. Many people working only in man-made composites are struck by the similarities of the pictures of natural composites to pictures of man-made composites.

Fig. 4 . SEM of Bessbug elytra. Epicuticle at the top of the picture with small, round fibers of the procuticle next. The fibers getting larger and non-circular the farther one goes into the structure. Note also both the matrix and fibers appear to be made of fibrils.

Fig. 5 . Close-up SEM of Bessbug elytra. The regular placement of non-circular fibers can be seen. The fibers also appear to contain levels of structure not yet determined.

Fig. 6 . Fiber comparison: Both SEMs show the similarity between man-made and natural composites as the fibers have matrix material clinging on. Natural fibers are generally smaller with more variety in cross-sectional shape than is found in man-made composites.

Fig. 7 . Bessbug elytra SEMs. Fibers in top with round to rectangular (long axis vertical) cross-section and easily distinguished cross ply arrangement. The lower photo of the bottom half of the elytra shows lath like fibers (long axis horizontal).

Fig. 8 . Bessbug pronotum torn to reveal successive layers of fibers. The orientation of these layers were determined and found to exist in a double helicoid arrangement.

Fig. 9 . Helicoids in Bessbug: orientation of chitin layers, each successive layer nearly orthogonal to the previous layer but alternating layers gradually changing orientation in a regular manner. Insect uses unbalanced and unsymmetrical

Fig. 10. Comparison of natural and man-made composite joints and stiffeners. Natural systems integrate these components into their structure without interrupting the fibers such as drilling holes for rivets does in man-made composites.

SELECTED NATURAL COMPOSITE

ARTHROPOD EXOSKELETON

INSECTA → **BEETLES**

CRUSTACEA → LOBSTERS, CRABS

ARACHNIDS → SPIDERS

MYRIAPODA → MILLIPEDES, CENTIPEDES

REASONS FOR SELECTION

1. Fiber Reinforced Laminate
2. Used in Structural Applications
3. Ultra-Light Weight

15-1

MAJOR DIVISIONS OF THE PROCUTICLE

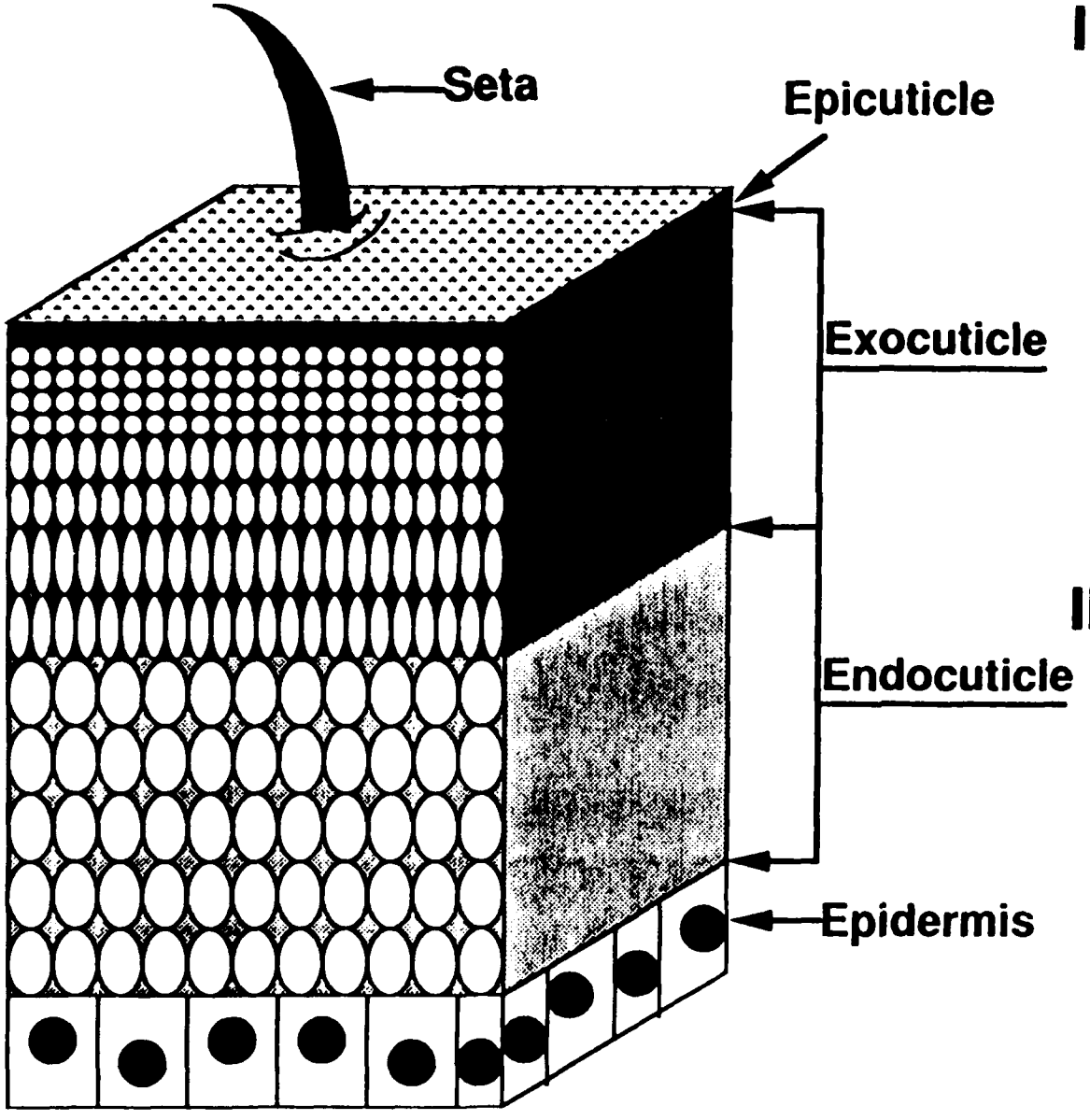

I. The Exocuticle

A. Protein matrix is crosslinked or sclerotized

B. Dark, stiff, brittle

C. Major contributor to strength and stiffness

II. The Endocuticle

A. Protein matrix is not crosslinked or unsclerotized

B. Softer, ductile

C. Major contributor to toughness and damping properties


FEEI OUHSI
0006 10KV X1,100 10Pm WD34


B-BUCEL
0019 10kV X1,600 10µm WD46
15-4


0010 10k X1,000 10µm WD36
15-5

FIBER COMPARISON

MAN-MADE

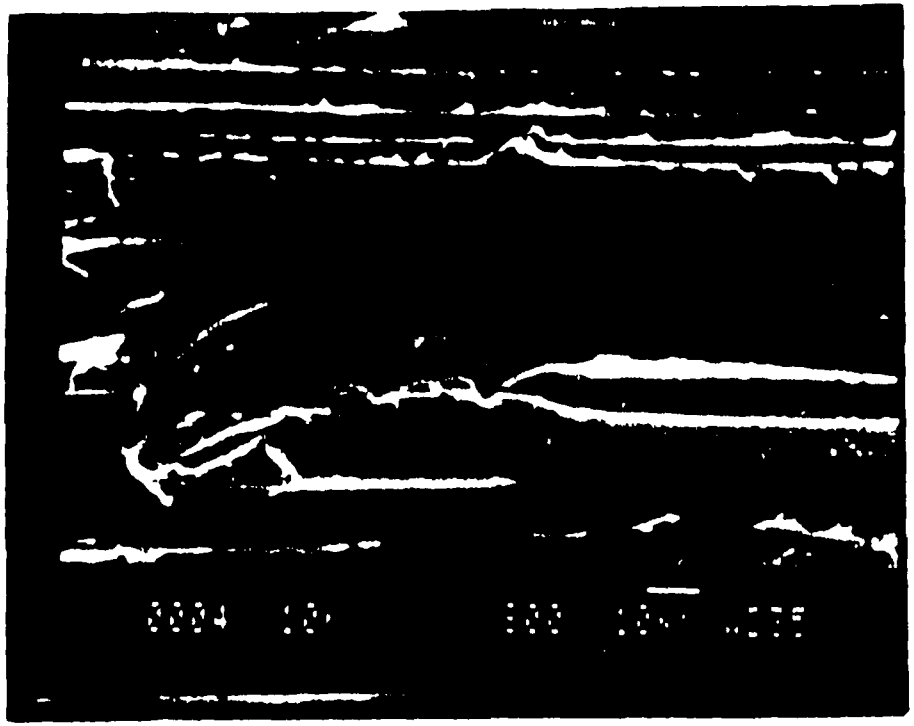

NATURAL

COMMON SHAPES

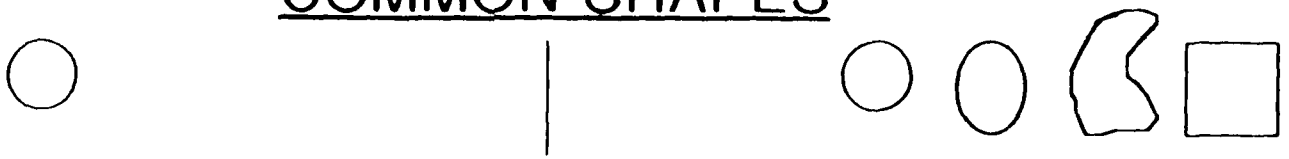

CROSS-SECTIONAL AREAS

MAN-MADE	NATURAL
19.6 um^2 -- 78.5 um^2	3.1 um^2 -- 19.6 um^2

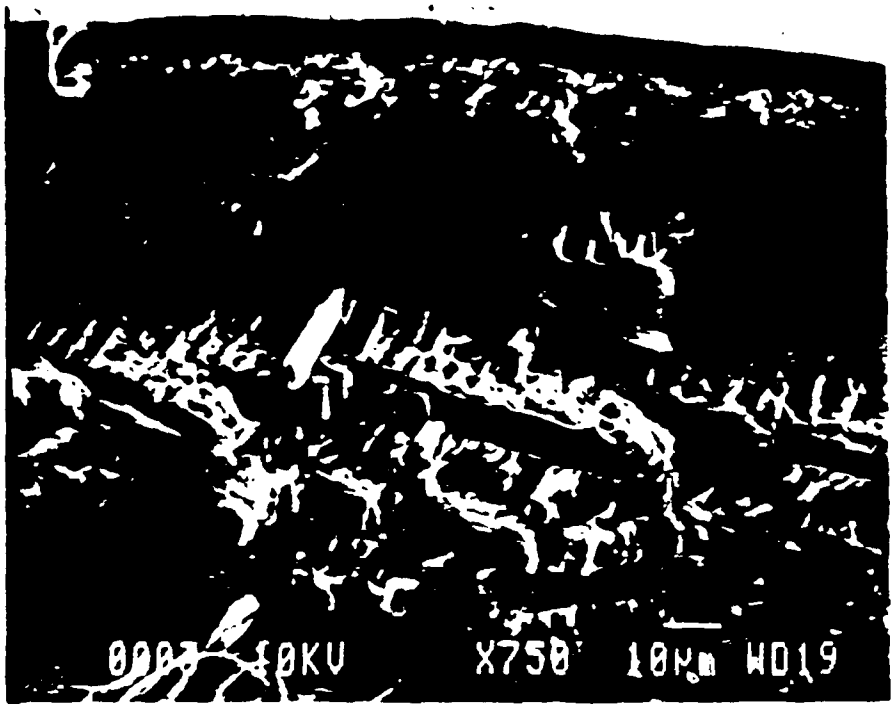
0004 10KV X750 10µm WD19

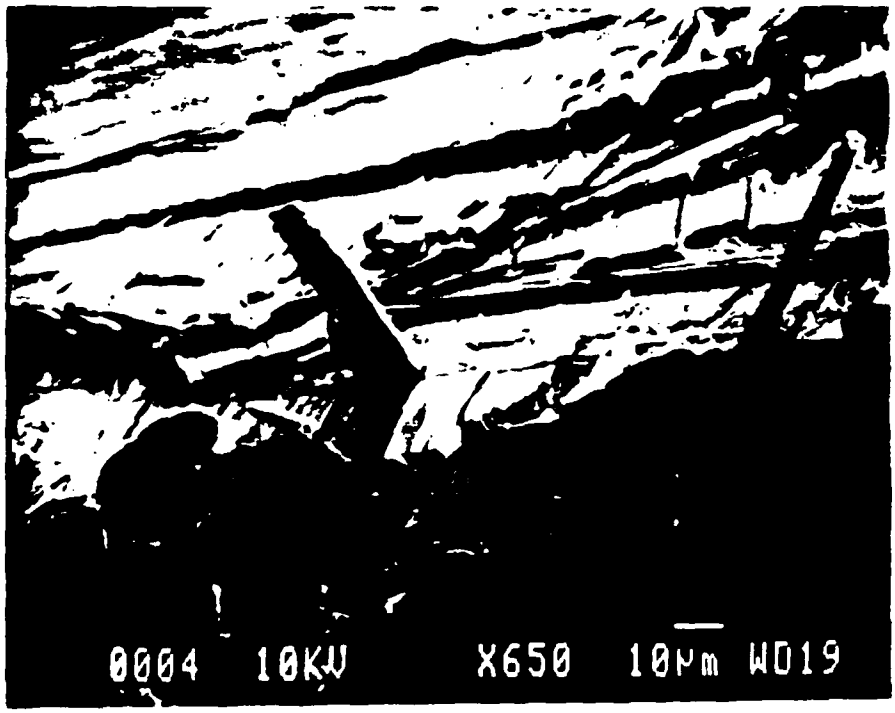
0004 10KV X650 10µm WD19

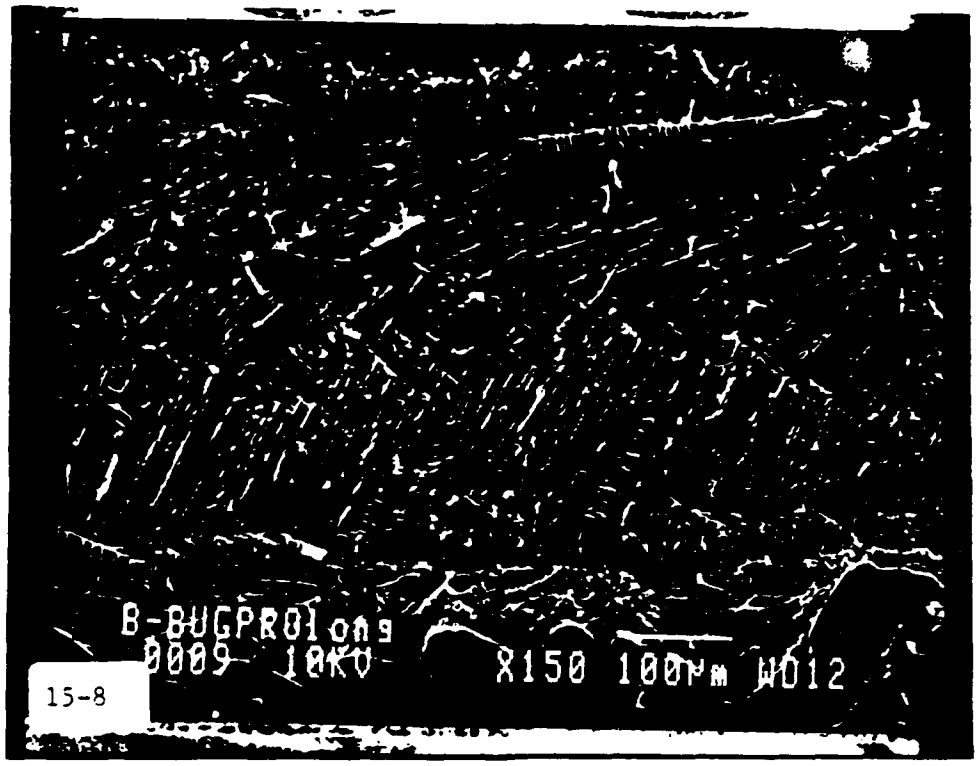
B-BUGPROIons
0009 10KV X150 100µm WD12
15-8

HELICOID ORIENTATION OBSERVED IN THE LEG, PRONOTUM, AND ELYTRA OF THE BESSBUG

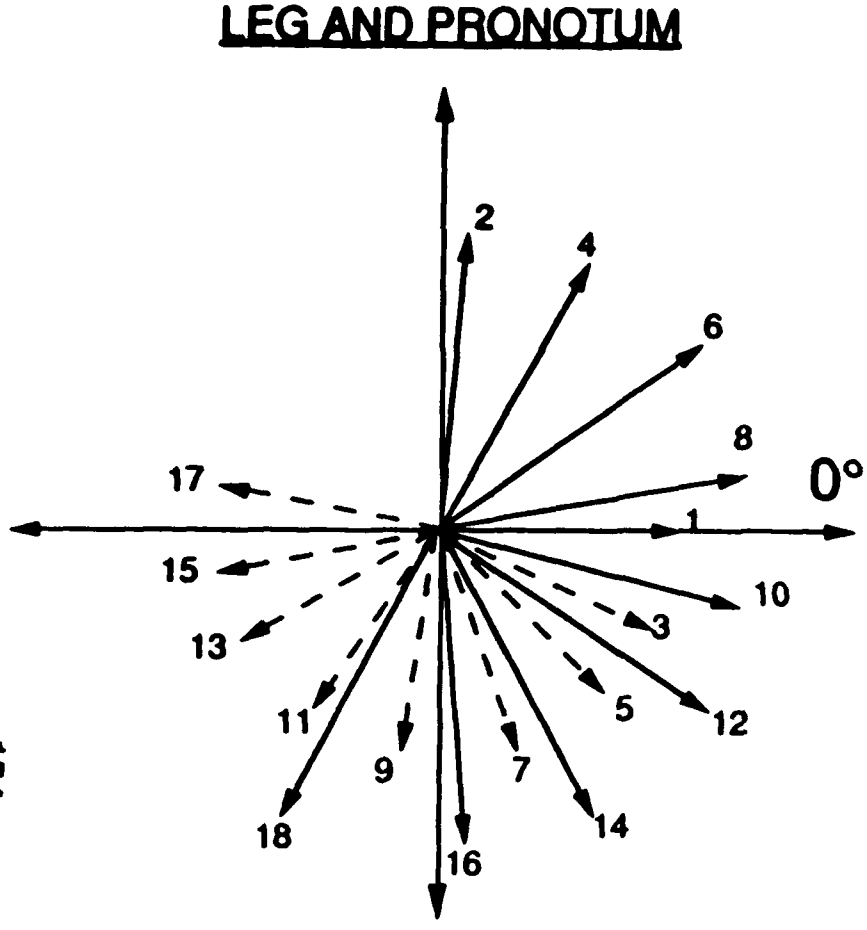

Average difference between alternating plies = 24°
Average difference between successive plies = 88°

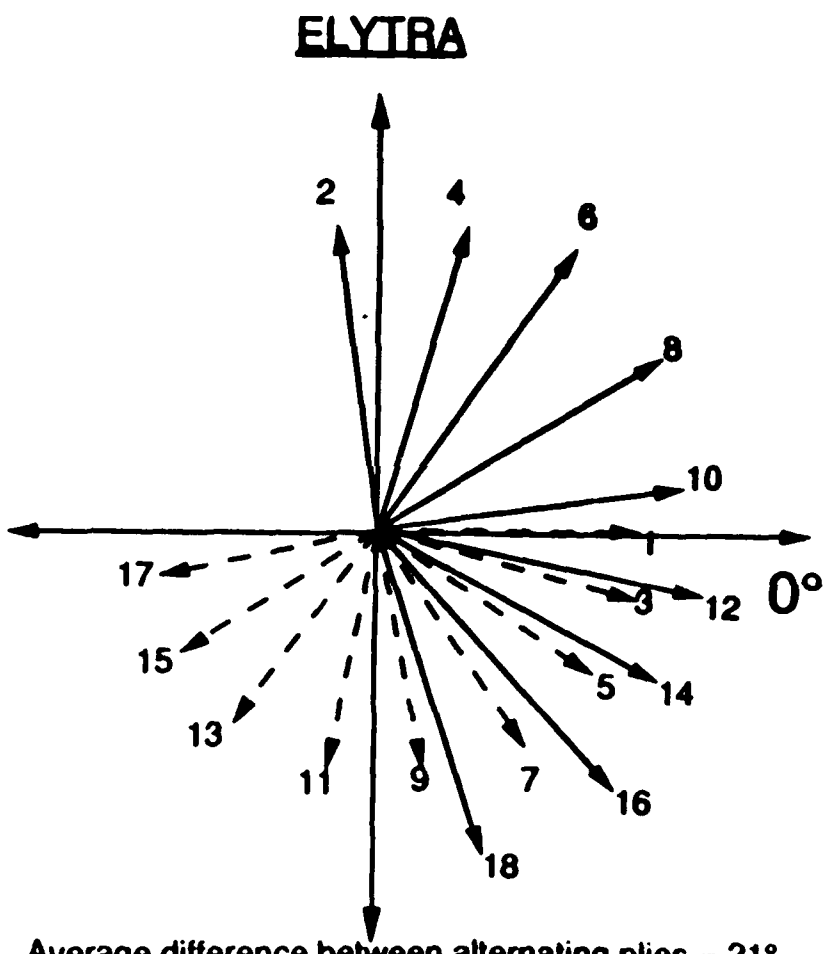

Average difference between alternating plies = 21°
Average difference between successive plies = 96°

JOINTS/STIFFENERS

NATURAL

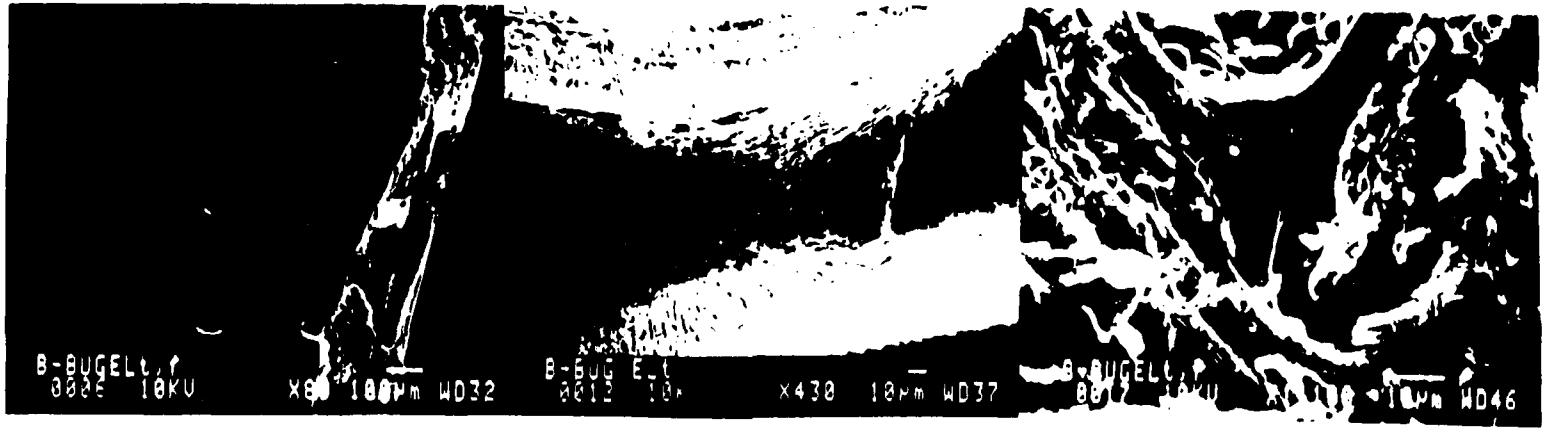

MAN-MADE

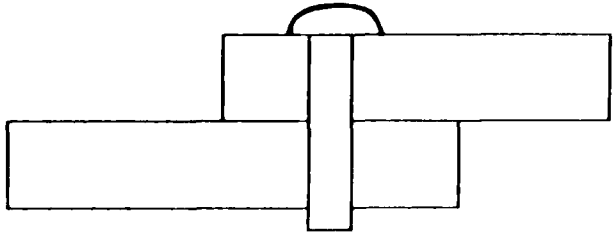

MECHANICAL FASTENERS

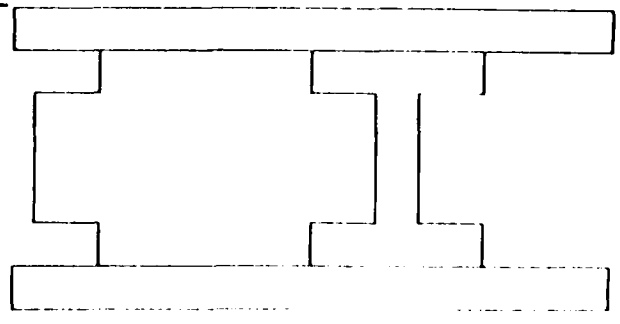

I BEAMS

Models of the Stress Adaptation of Bone Tissue

by
S. C. Cowin
Department of Mechanical Engineering
City College of the City University of New York
New York, N. Y. 10031

Many natural materials adjust to their environmentally applied mechanical loading by changing their material microstructure. Some materials, such as geological materials, do this passively by changing their density and/or their degree of anisotropy.[1] Living materials, such as plant and animal tissue, can actively change their density and/or their degree of anisotropy. Entire animal organs, bones, plants and trees can change their overall shape as well as their microstructure as an adaptation to mechanical loading.[2]

Functional adaptation is the term used to describe the ability of organisms to increase their capacity to accomplish their function with an increased demand and to decrease their capacity with lesser demand. Living bone is continually undergoing processes of growth, reinforcement and resorption which are collectively termed "remodeling". The remodeling processes in living bone are the mechanisms by which the bone adapts its overall structure to changes in its local environment. The time scale of the remodeling processes is on the order of months or years. Changes in life style which change the

loading environment, for example taking up jogging, have remodeling times on the order of many months.

Bone is a natural composite material[3] that is formed and resorbed at an internal or external bone surface. Surface remodeling refers to the resorption or deposition of the bone material on the external surface of the bone. Internal remodeling refers to the resorption or reinforcement of the bone tissue internally by changing the bulk density and internal trabecular structure of the tissue. In cancellous bone the trabeculae become more or less numerous, their thickness can vary, and their direction can change.

Two analytical models for the stress adaptation process are presented and illustrated. These are models for surface bone remodeling and internal bone remodeling. The model for surface remodeling[4] is applied to determine the overall size and shape changes in whole bones. The theory of internal remodeling[5,6] is applied to the load adaptation of trabecular architecture. These theories for surface and internal bone remodeling use a simple two constituent model for bone tissue. The bone matrix, that is to say the solid extra-cellular material and the bone cells, is modeled as a solid structure with interconnected pores, a porous solid. Since bone is adequately modeled as a linear anisotropic elastic solid, it is assumed that the bone matrix can be modeled as a porous anisotropic linear elastic solid. The extracellular fluid and blood are modeled as a single fluid. Thus the basic model of bone is a porous, anisotropic linear elastic solid perfused with a fluid. The chemical reactions which convert body fluids into solid porous bone matrix and vice-versa are mediated by the bone cells. The rate of remodeling depends on the strain is on the order of months.

The applications of these models of bone stress adaptation to the analysis and explanation of certain animal experiments will be described and illustrated

REFERENCES.

1. Cowin, S.C. in *Colloque International du CNRS No. 319* (eds. Boehler, J.P.) 3-28 (Compartement Plastique Des Solids Anisotropes, 1985).
2. D'Arcy Thompson, W. *On Growth and Form* (Cambridge University Press, Cambridge, 1942).
3. Cowin, S.C. *Bone Mechanics* (CRC Press, Boca Raton, FL, 1989).
4. Cowin, S.C., Hart, R.T., Balser. J.R. & Kohn, D.H. *J.Biomechanics* **18**, 665-684 (1985).
5. Cowin, S.C. & Hegedus, D.M. *J. of Elasticity* **6**, 313-325 (1976).
6. Cowin, S.C. *J. Biomechanical Engineering* **108**, 83-88 (1986).

Figures 1 through 6 added for amplification of the lecture.

1. Schematic diagram of the process of bone adaptation to applied environmental loading.(Adapted from Hart, R. T., Davy, D. T., and Heiple, K. G.., Calcif. Tissue Int., 36, S104, 1984: see also: Cowin, S. C. (editor), *Bone Mechanics*, CRC Press, Boca Raton, FL, 1989, page 264.)

2. An ulnar ostectomy experiment with mature sheep. Each illustration represents the bone cross sections in the sheep forelimb. **Top:** the contralateral control limb after 9 months showing the radius with the intact ulna. **Middle:** the experimental radius after 9 months showing marked asymmetric periosteal deposition. **Bottom:** the calculated remodeling. The solid lines represent the surface of the control bone and the dashed lines represent the predicted geometry at 9 months. The indicated length is 1 mm. (From Cowin, S. C., Hart, R. T., Balser, J. R., and Kohn, D. H., *J. Biomech.*, 18, 665, 1985: see also: Cowin, S. C. (editor), *Bone Mechanics*, CRC Press, Boca Raton, FL, 1989, page 295).

3. An illustration of cancellous bone from the porcine proximal tibia.

4. Test lines superimposed on a cancellous bone specimen. The test lines are oriented at the angle θ. The mean intercept length measured at this angle is denoted by $L(\theta)$. (From Cowin, S. C. (editor), *Bone Mechanics*, CRC Press, Boca Raton, FL, 1989, page 143).

5. The fabric ellipse is illustrated by superimposing it on the cancellous bone structure it represents. (From Cowin, S. C. (editor), *Bone Mechanics*, CRC Press, Boca Raton, FL, 1989, page 144).

6. The evolution of trabecular architecture in time. T^0, E^0 and H^0 represent the initial orientation of the axes of the stress ellipsoid,

the strain ellipsoid, and the fabric ellipsoid, respectively. T^*, E^* and H^* represent the final orientation of the axes of these three ellipsoids. When these kernel letters are without superscript they represent the orientation of the axes of the indicated ellipsoid at some intermediate time. **First panel:** the bone tissue is in remodeling equilibrium at $t = 0$ and the axes of the three ellipsoids are coincident. **Second panel:** a new environmental loading is applied to the bone tissue for all subsequent time. The new loading is represented by the axes of the new and final stress ellipsoid denoted by T^*. Since the material cannot change its structure instantaneously the axes of the fabric ellipsoid stay fixed in the position H^o. The axes of the strain ellipsoid adopt a new orientation instantaneously and begin to change their orientation as the orientation of the axes of the fabric ellipse H changes. The axes of the three ellipsoids must be either all coincident or all different; it is not possible for two to be coincident and the third one to be different. **Third panel:** the orientation of the axes of the stress ellipsoid remains fixed in the changing bone tissue, and the axes of the strain and fabric ellipsoid evolve in time to the fixed orientation of the axes of the stress ellipsoid. **Fourth panel:** the bone tissue achieves remodeling equilibrium again as time t tends to infinity, and the axes of the three ellipsoids again become coincident.

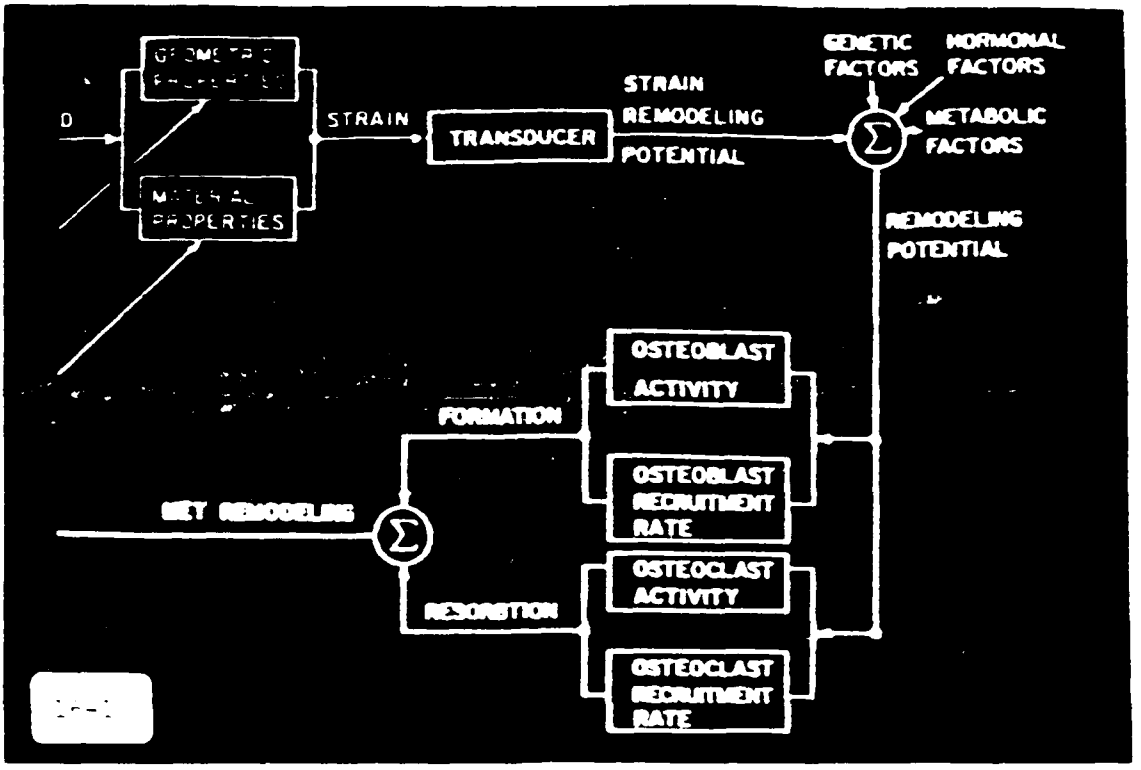
D
STRAIN
TRANSDUCER
STRAIN
REMODELING
POTENTIAL
GENETIC
FACTORS
HORMONAL
FACTORS
METABOLIC
FACTORS
REMODELING
POTENTIAL
OSTEOBLAST
ACTIVITY
FORMATION
OSTEOBLAST
RECRUITMENT
RATE
NET REMODELING
OSTEOCLAST
ACTIVITY
RESORPTION
OSTEOCLAST
RECRUITMENT
RATE

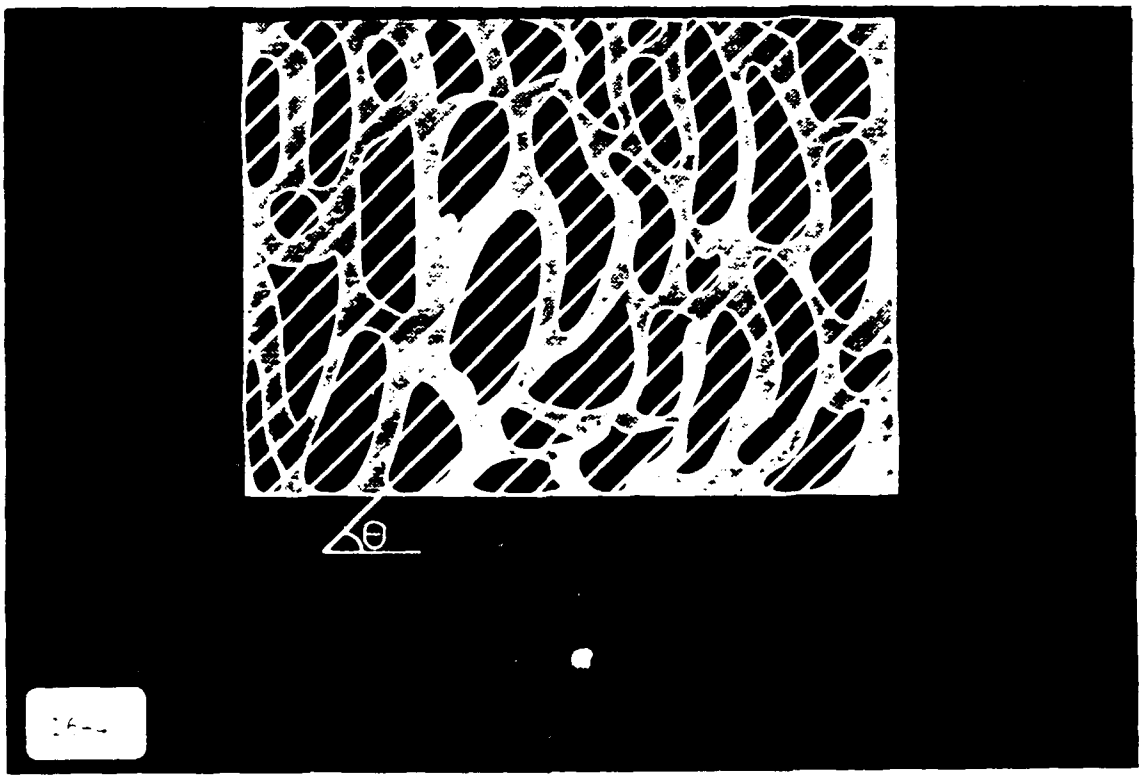
Δθ

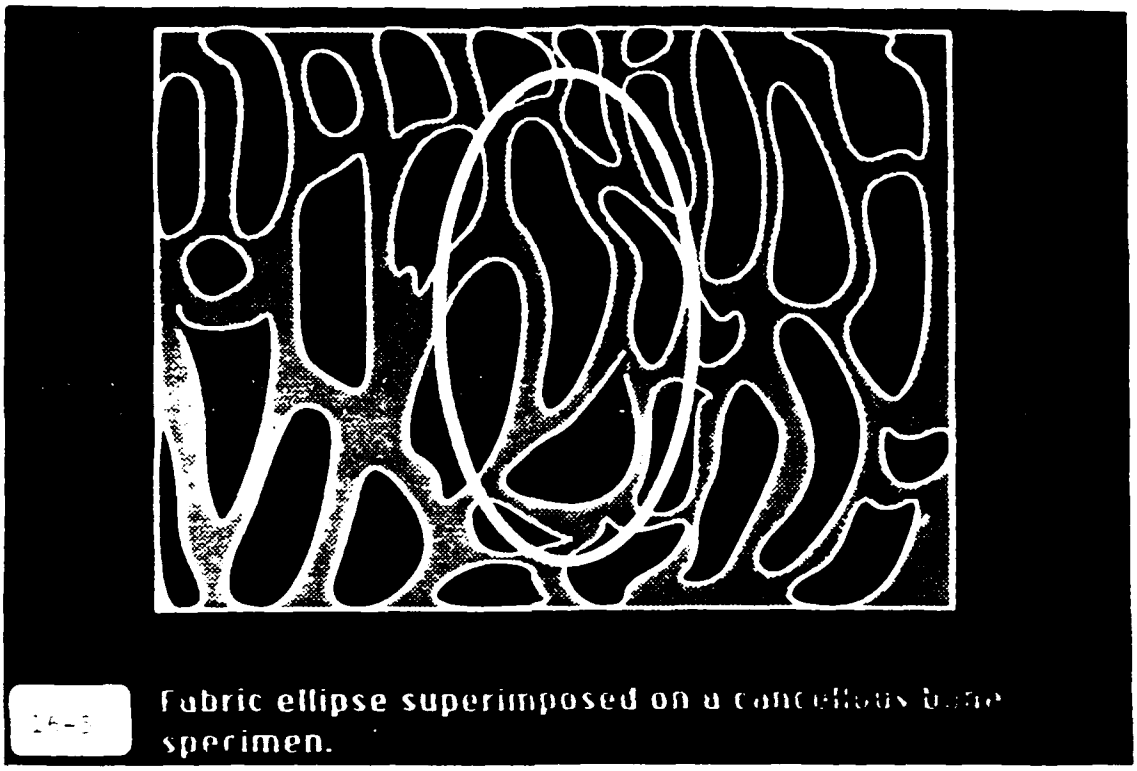

Fabric ellipse superimposed on a cancellous bone specimen.

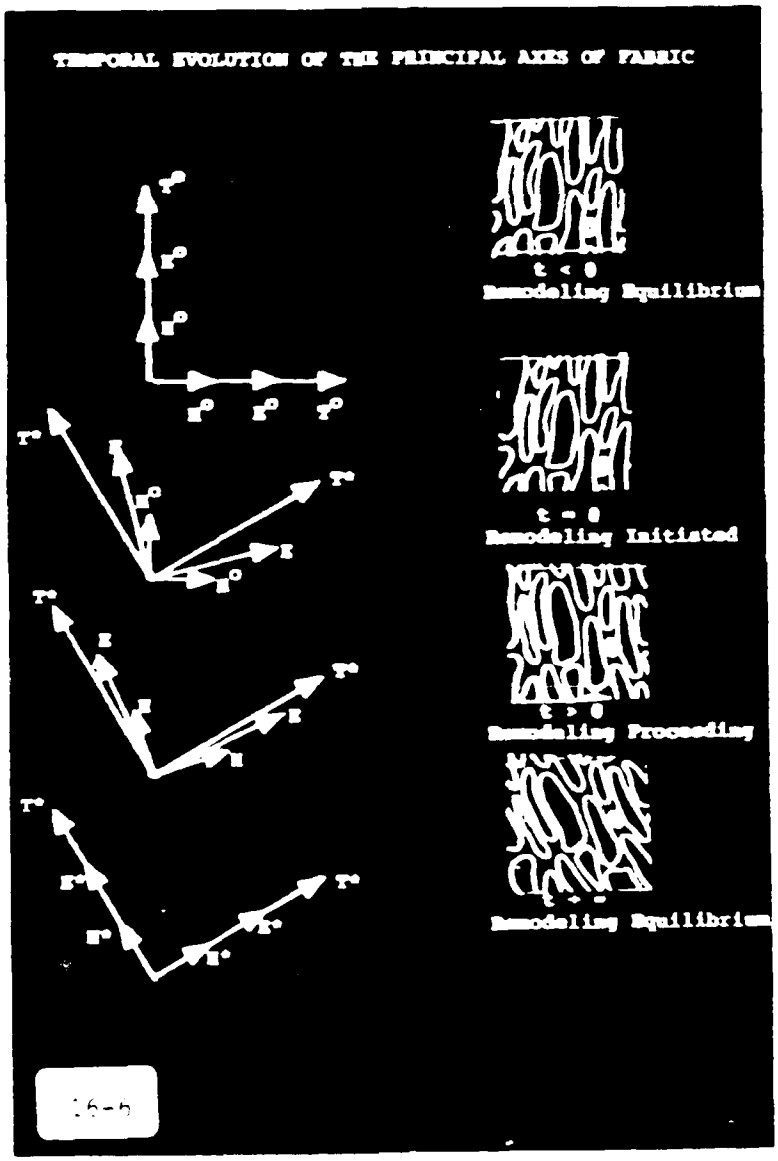

ANISOTROPIC COMPOSITES FOR SOFT AND HARD TISSUE REPLACEMENTS

J. L. Kardos
Materials Research Laboratory and
Department of Chemical Engineering
Washington University
St. Louis, MO 63130

Most of the tissues in the human body are classical composite materials. Indeed, the amazing functionality of many of them is due to their composite structure and their unique ability to handle anisotropic stresses and strains. In the soft tissue area blood vessels and heart valve leaflets are two examples in the cardiovascular system of living layered composites whose different mechanical properties in different directions (anisotropy) allows them to perform reliably under complex states of stress and deformation (1). In the hard tissue area, bone (particularly the long leg bones) is a highly anisotropic composite consisting of collagen reinforced by crystalline fibrous calcium hydroxyapatite.

In our efforts to replace structural tissues with synthetic materials, man has often neglected to design into the replacements the very reason that the originals work so well - anisotropy. While it is true that any material placed into the body must be biologically and chemically compatible with all the body systems, it is equally important that the replacement be a mechanical replica of the living structure, if it is to do the job reliably over long periods of time. Synthetic composites are unique in the spectrum of materials, in that they may be designed and fabricated to exactly match the necessary anisotropy of the living original.

The replacement of diseased arteries with a viable prosthetic structure is a good example of the use of a composite material to replicate both the biological and mechanical performance of a living structural tissue. Initial material selection must be made in conjunction with the structural design. The material must be reasonably compliant, capable of being reinforced anisotropically or of being oriented to produce anisotropy, and resistant to creep under both static and dynamic loading. It must perform without property loss in the rather harsh environment of the cardiovascular system. It must also perform without disturbing its environment, i.e., it

must be non-thrombogenic, and it must not cause unusual deposition of thick layers of cells which could change its flow capacity and its mechanical performance. The design must be one which matches the anisotropic stiffness properties of the natural artery to which it will be attached (2), minimizes the possibility of creep (3), and where possible improves the biocompatability of the material. Mechanical testing protocols must be devised to thoroughly qualify the material and the design for creep resistance, strength (4), fatigue resistance (5), and reliability under performance stress conditions and performance environments. Reliable accelerated test techniques are clearly necessary for design lifetimes in excess of 10 years. An example of an arterial prosthesis development, including the development of accelerated testing protocols, will be reviewed.

REFERENCES

1. R. E. Clark, W. M. Swanson, J. L. Kardos, R. W. Hagen, and R. A. Beauchamp, "Durability of Prosthetic Heart Valves". Annals of Thoracic Surgery, 26, 323 (1978).
2. R. E. Clark, S. Apostolou, and J. L. Kardos, "Mismatch of Mechanical Properties as a Cause of Arterial Prostheses Thrombosis", Surgical Forum, 27, 208 (1976).
3. J. L. Kardos, W. M. Swanson, and R. E. Clark, "Physical Testing of Polymers for Use in Circulatory Assist Devices", Final Report, Contract No. NO1-HV-7-2919, PB81-238834, National Technical Information Service, 5285 Port Royal Rd., Springfield, VA 22151.
4. A. P. Bhate and J. L. Kardos, "A Novel Technique for the Determination of High Frequency Equibiaxial Stress-Deformation Behavior of Viscoelastic Elastomers", Pol. Eng. Sci., 24, 862 (1984).
5. K. P. Gadkaree and J. L. Kardos, "Prediction and Measurement of Fatigue Lifetime Distributions for Elastomeric Biomaterials", J. Appl. Pol. Sci., 29, 3041 (1984).

Figures 1 through 7 added for amplification of the lecture.

Figure 1. Schematic diagram of the aorta blood vessel wall illustrating its multi-ply composite construction; t_i - tunica intima, t_m - tunica media, t_a - tunica adventitia. Note the hoop direction orientation to contain internal pressure but still provide bending flexibility.

Figure 2. Stress concentrations at the bond line caused by stiffness mismatch. Two sheets of Biomer segmented polyetherurethane copolymer lap-joined and stretched longitudinally to 22% strain between crossed polarizers. The top sheet is anisotropic (three times as stiff in the longitudinal direction as in the transverse direction); the bottom sheet is isotropic, having a stiffness equal to that of the upper sheet's transverse direction.

Figure 3. Static creep map for engineering design with biomaterials. The vertical axis is percent strain. Time-temperature superposition principles can be used successfully to predict long-term behavior from short-term experiments. Results are shown here for Biomer in a saline environment at 37°C.

Figure 4. Superimposed static and dynamic creep as a function of frequency and maximum stress level. ξ is the minimum-to-maximum stress ratio during the dynamic test. The static load is maintained at the minimum stress level. Note the frequency effect and the comparison to the static curve. Biomaterials must be tested in this mode if they are to be applied in dynamic loading situations.

Figure 5. An approach to fatigue lifetime prediction for elastomeric biomaterials. Flaws cause an initial distribution of material strength; the initial flaw size distribution can be determined using simple size effect law; flaws then grow according to tearing energy flaw growth criterion; failure occurs as flaws become critically large leading to distribution of lifetimes. (Gadkaree and Kardos, J. Appl. Pol. Sci., 29, 3041 (1984).

Figure 6. Final engineering design equation for fatigue lifetime distribution prediction. Three pairs of constants must be determined from short-term tests. Static tensile tests yield the mean (μ) and variance (σ^2) of the initial material strength distribution. Static tensile tests on cut specimens yield the effect of flaw size on strength (M and N). Short term flaw growth experiments under tensile cyclic loading yield flaw growth law constants (A and b). K is a constant and U is the strain energy density determined from a stress-strain test. (Gadkaree and Kardow, J. Appl. Pol. Sci., 29, 3041 (1984).

Figure 7. Proof testing of final composite artery design. Cyclic biaxial testing at the design loads and beyond is required. From left to right: initial static axial extension of 15% strain is imposed; internal pressure cycling at hoop strains up to 60% strain (shown here); 300% hoop strain to test laminate bonding integrity.

Figure 5 - Schematic diagram of an aorta wall
ti.. tunica intima, tm.: tunica media,
17-1 ta.: tunica adventitia.

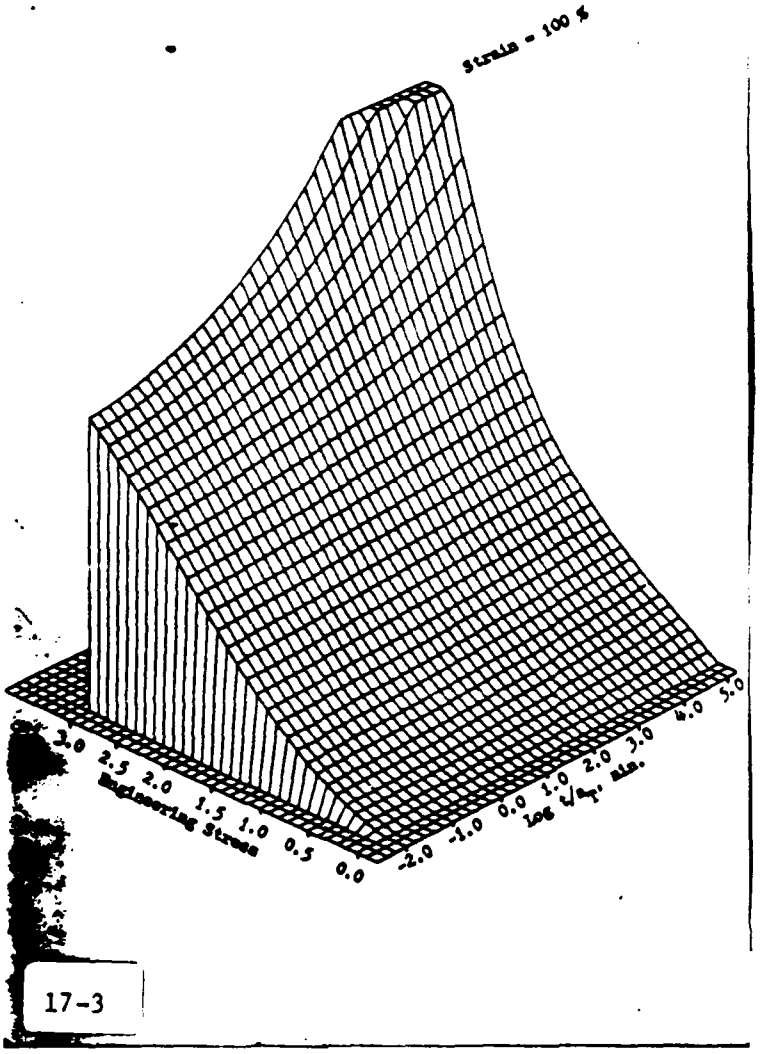
Stress = 100 $
3.0
2.5
2.0
1.5
1.0
0.5
0.0
Engineering Stress
-2.0
-1.0
0.0
1.0
2.0
3.0
4.0
5.0
Log t/$_{sec}$, min.

17-3

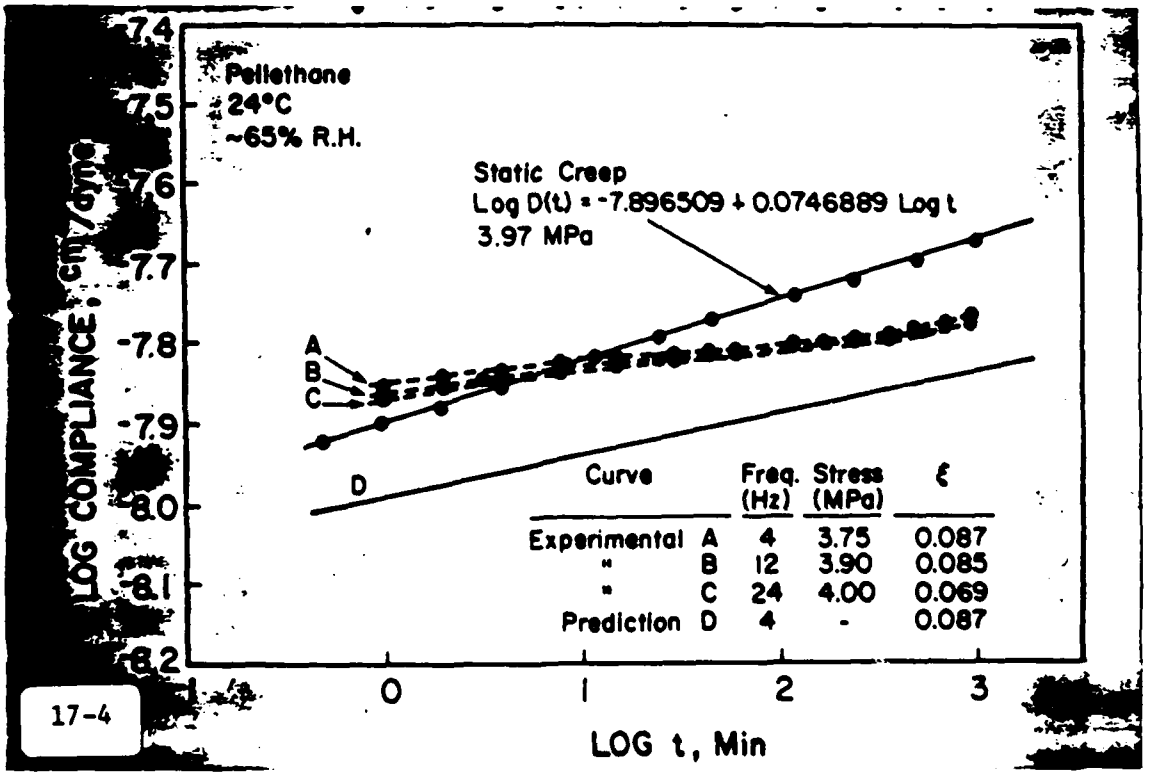
Pellethane
24°C
~65% R.H.
Static Creep
Log D(t) = -7.896509 + 0.0746889 Log t
3.97 MPa
A
B
C
D
LOG COMPLIANCE, cm²/dyne
-7.4
-7.5
-7.6
-7.7
-7.8
-7.9
-8.0
-8.1
-8.2
0
1
2
3
LOG t, Min
Curve | Freq. (Hz) | Stress (MPa) | ε
Experimental A | 4 | 3.75 | 0.087
" B | 12 | 3.90 | 0.085
" C | 24 | 4.00 | 0.069
Prediction D | 4 | - | 0.087

17-4

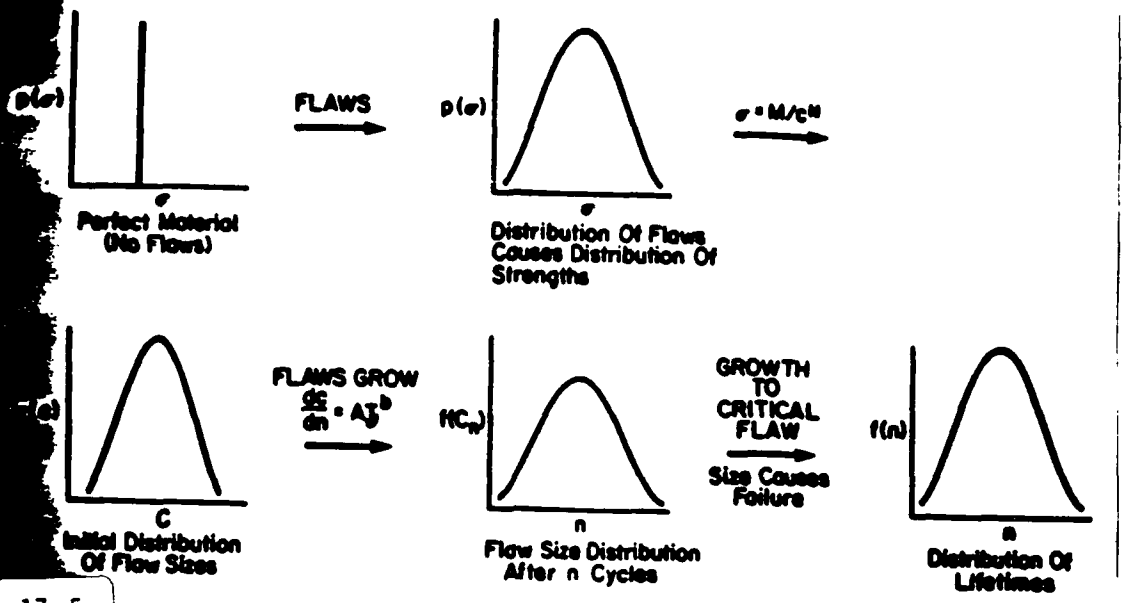

17-5

$$f(n) = \frac{MN}{\sigma\sqrt{2\pi}} \left(\frac{1}{b-1}\right) \frac{n^{(N+1-b)/(b-1)}}{\left(\frac{1}{A(b-1)(2KU)^b}\right)^{N/(b-1)}}$$

$$\exp\left\{-\frac{1}{2}\left\{\left[\frac{M\, n^{N/(b-1)}}{\left(\frac{1}{A(b-1)(2KU)^b}\right)^{N/(b-1)}} - \mu\right] / \sigma\right\}^2\right\}$$

17-6

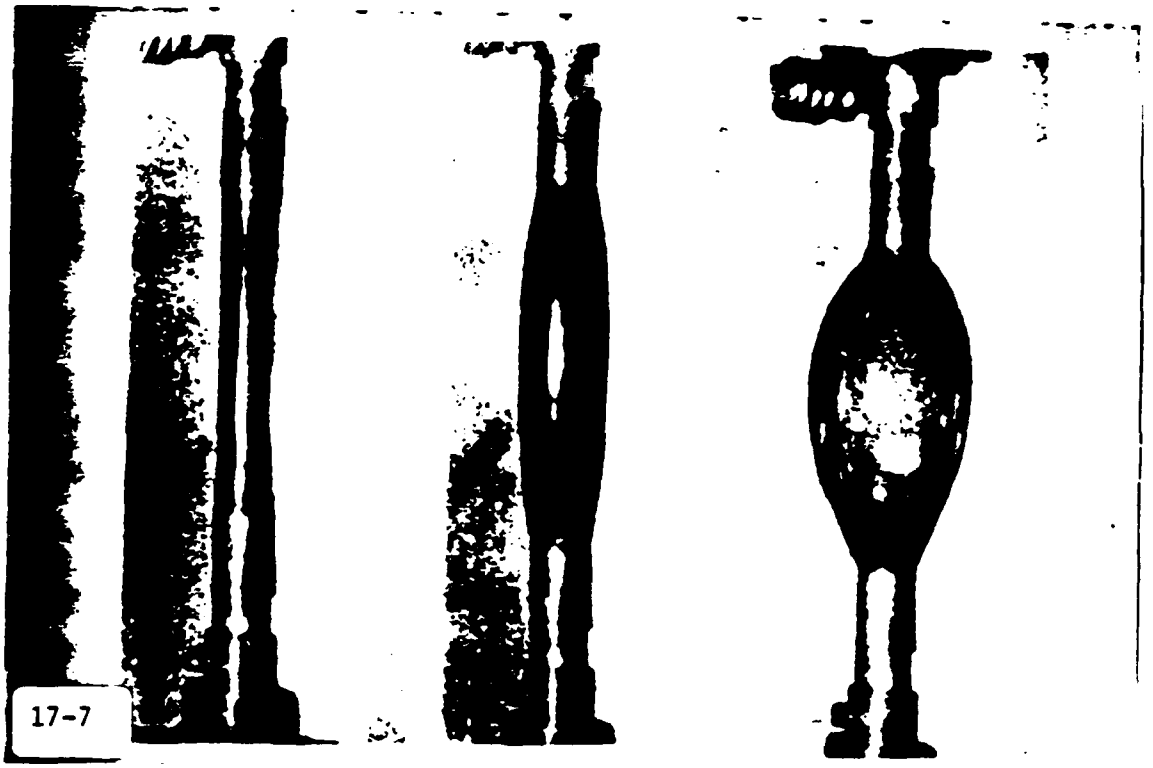

17-7

MICROSTRUCTURE-PROPERTY RELATIONSHIPS IN BIOCOMPOSITES

Ilhan A. Aksay and Mehmet Sarikaya

Department of Materials Science and Engineering, and
Advanced Materials Technology Program,
The Washington Technology Center,
University of Washington, Seattle, WA 98195

Progress is being made in materials processing in improving microstructural control down to the nanometer scale, as materials at this scale exhibit unprecedented properties (such as mechanical, electrical, superconductive, and optical).[1-4] The processing of these synthetic materials is based on the additive principle, in which component phases with varying properties are fused together in an ordered manner to form a multiphase system. Conventionally, these structures can be achieved by phase transformations (precipitation-hardened alloys) or by mechanical mixtures at the microscale level (metal and ceramic matrix composites).[5] More advanced processing involves ion beam techniques (such as molecular beam epitaxy and liquid and vapor deposition)[3,4] in which the microstructure is controlled at the nanometer level. In order to meet the demands of modern technology for better properties, more complex systems have to be developed through more intricate and energy-efficient processing strategies.

The approach taken by living organisms in processing composites is in many ways more controlled than the synthetic methods. In the formation of biological composites, living organisms can design and produce, efficiently, complex microstructures having unique properties at all spatial levels (down to the nanometer scale), and in more controlled ways at the molecular dimension.[6-8] It is desirable, therefore, to produce man-made materials by using processing approaches similar to those used by the living organisms, i.e., by biomimicking. This present research has been initiated to study some of the principles inherent in the processing methods used by organisms in producing composites and their physical properties as related to microstructures. In this short note, we summarize the results of a recent study on the microstructures of the red abalone shell (*Haliotis rufescens*) in relation to its mechanical properties.

A longitudinal cross-section of the abalone shell displays two types of microstructures: an outer prismatic layer and an inner nacreous layer. Two forms of $CaCO_3$, calcite (rhombohedral, $R\bar{3}c$) and aragonite (orthorhombic, Pmnc) constitute the inorganic component of the organic-inorganic composite in the prismatic and the nacreous layers, respectively. The structure and the properties of the nacreous layer are described here, as this is the part which displays a good combination of mechanical properties.[9]

Mechanical properties, i.e., σ_f (fracture strength) and K_{IC} (fracture toughness), have been evaluated in the transverse direction (perpendicular) to the shell plane. They exhibit values of 180 MPa and about 7.0 MPa-$m^{1/2}$, respectively. The study of the crack propagation behavior reveals a high degree of tortuosity, not seen in the more traditional brittle (such as Al_2O_3) and

high toughness (ZrO_2) ceramics,[10] indicating certain toughening mechanisms, such as crack blunting, branching, and "layer pull-out" operating in the shell (Figure 1). A closer examination of the microstructure reveals that cracks mostly advance through the organic layer and with difficulty, as this process is accompanied by sliding of the $CaCO_3$ layers (when there is a shear component of the resolved stress) and by the bridging of the organic ligaments (when there is a normal stress component), as shown in Figures 2 and 3, respectively. It is these last two mechanisms which mostly contribute to the toughening of the shell.

The superior mechanical properties of abalone shell compared to those of the more traditional ceramics and their composites (plotted in Figure 4) comes from its unique "brick and mortar" microstructure. A TEM micrograph (Figure 5) recorded in the transverse direction shows the alternating layers of hexagonal-shaped 0.2-0.5 μm thick aragonite crystals which form the hard component, and the thin (20-50 nm) organic substance in between (lipids and proteins), providing the ductile component of the composite.

Preliminary results on the mechanical properties of B_4C-Al (35%) laminated cermets designed on the basis of the above observations, indicate a 30% increase in the fracture toughness of the composite. This increase in the cermet toughness is attributed to the same toughening mechanisms observed in abalone shell. Further improvement in both strength and toughness is expected with the decrease in the thickness of the composite layers (down to submicrometer levels); in the present case, the smallest thickness of the layers in the cermet laminate is about 10 μm, far too thick to benefit the effects of the lamination. Consequently, the present research is directed to the processing of cermets with submicrometer-layer thicknesses to achieve this goal in conjunction with the studies of the quantitative effects of the organic layer in sea shells.

This research was supported by the Air Force Office of Scientific Research under Grants Nos. AFOSR-87-0114 and AFOSR-89-0496.

1. F. Spaepen, "The Art and Science of Microstructural Control," *Science*, 235 1010 (1987).
2. R. C. Cammarata, "The Supermodulus Effect in Composition Modulated Thin Films," *Scripta Met.*, 20 883 (1980).
3. M. S. Dresselhaus, "Intercalation of Layered Materials," *Materials Research Society Bulletin*, 12 (3) 24 (1987).
4. *Metallic Superlattices: Artificially Strong Materials*, edited by T. Sinjo and T. Takada (Elsevier, Amsterdam, 1987).
5. A. Kelly and R. L. Nicholson, *Strengthening Methods in Crystals*, (Wiley, New York, 1971).
6. H. A. Lowenstam, "Minerals Formed by Organisms," *Science*, 211 1126 (1981).
7. S. Mann, "Mineralization in Biological Systems," *Structure and Bonding*, 54 124 (1983).
8. S. Weiner, "Organization of Extracellularly Mineralized Tissues: A Comparative Study of Biological Crystal Growth," *CRC Critical Reviews in Biochemistry*, 20 [4] 365 (1986).
9. J. D. Currey, "Biological Composites," *J. Materials Educ.*, 9 (1-2) 118 (1987).
10. *Deformation of Ceramic Materials II*, edited by R. C. Tressler and R. C. Bradt (Plenum, New York, 1984).


18-1
10 μm

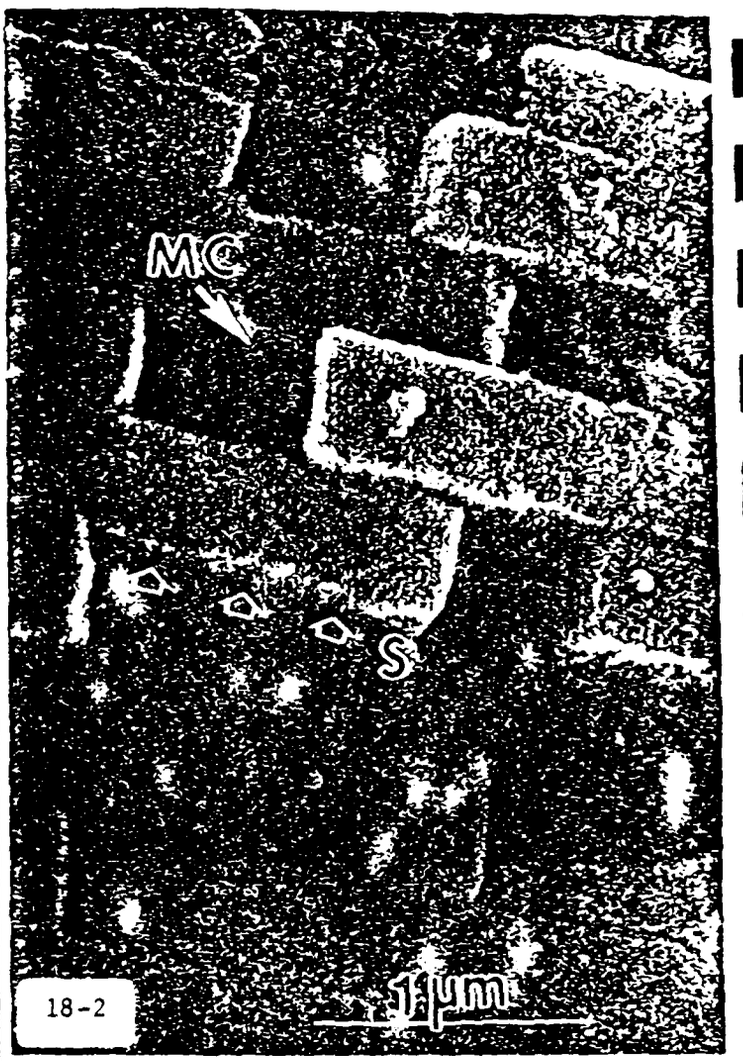
MC
S
18-2
1 μm

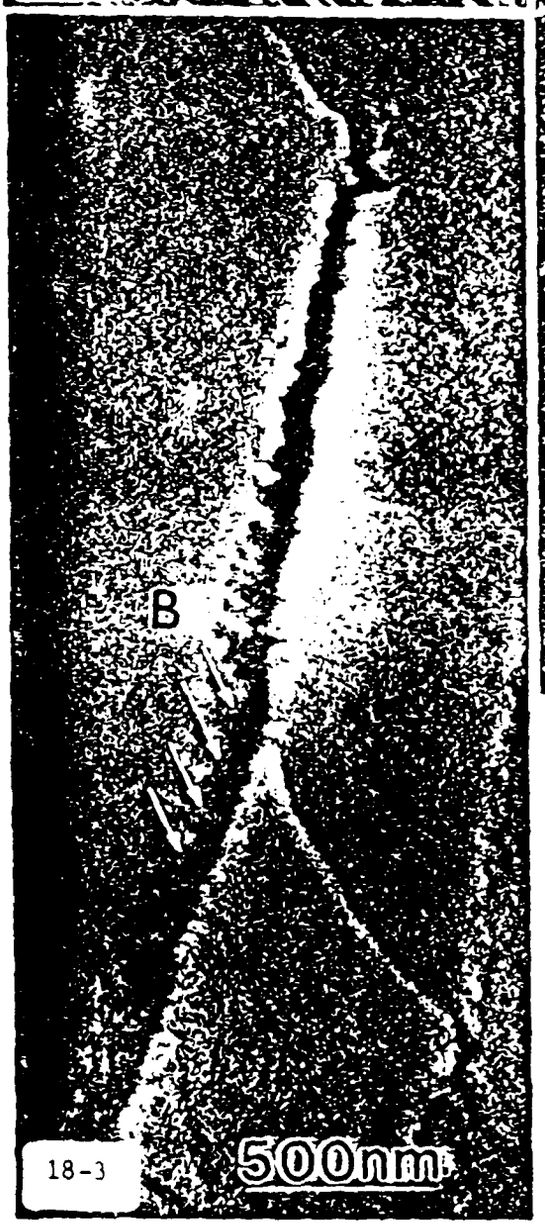
B
18-3
500nm

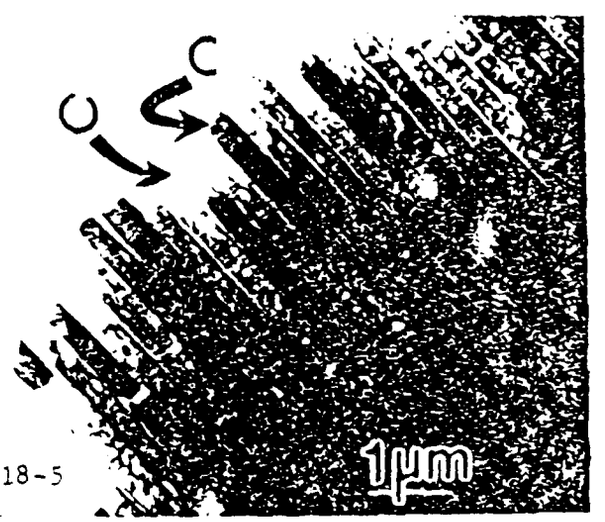
C
C
18-5
1μm

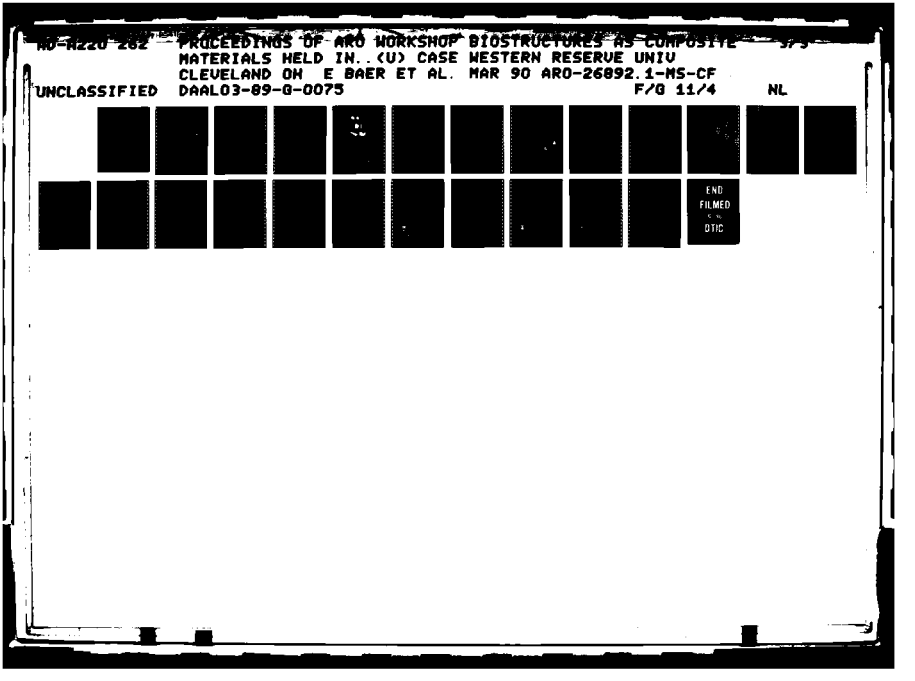
AD-A220 262 PROCEEDINGS OF ARO WORKSHOP BIOSTRUCTURES AS COMPOSITE
MATERIALS HELD IN..(U) CASE WESTERN RESERVE UNIV
CLEVELAND OH E BAER ET AL. MAR 90 ARO-26892.1-MS-CF
UNCLASSIFIED DAAL03-89-G-0075 F/G 11/4 NL
END
FILMED
DTIC

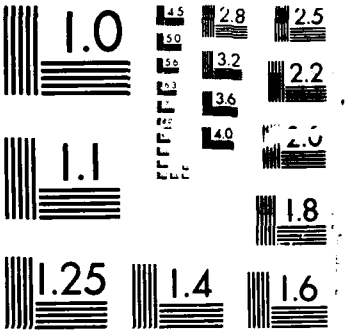
1.0
1.1
1.25
1.4
1.6
1.8
2.2
2.5
2.8
3.2
3.6
4.0
4.5
5.0
5.6

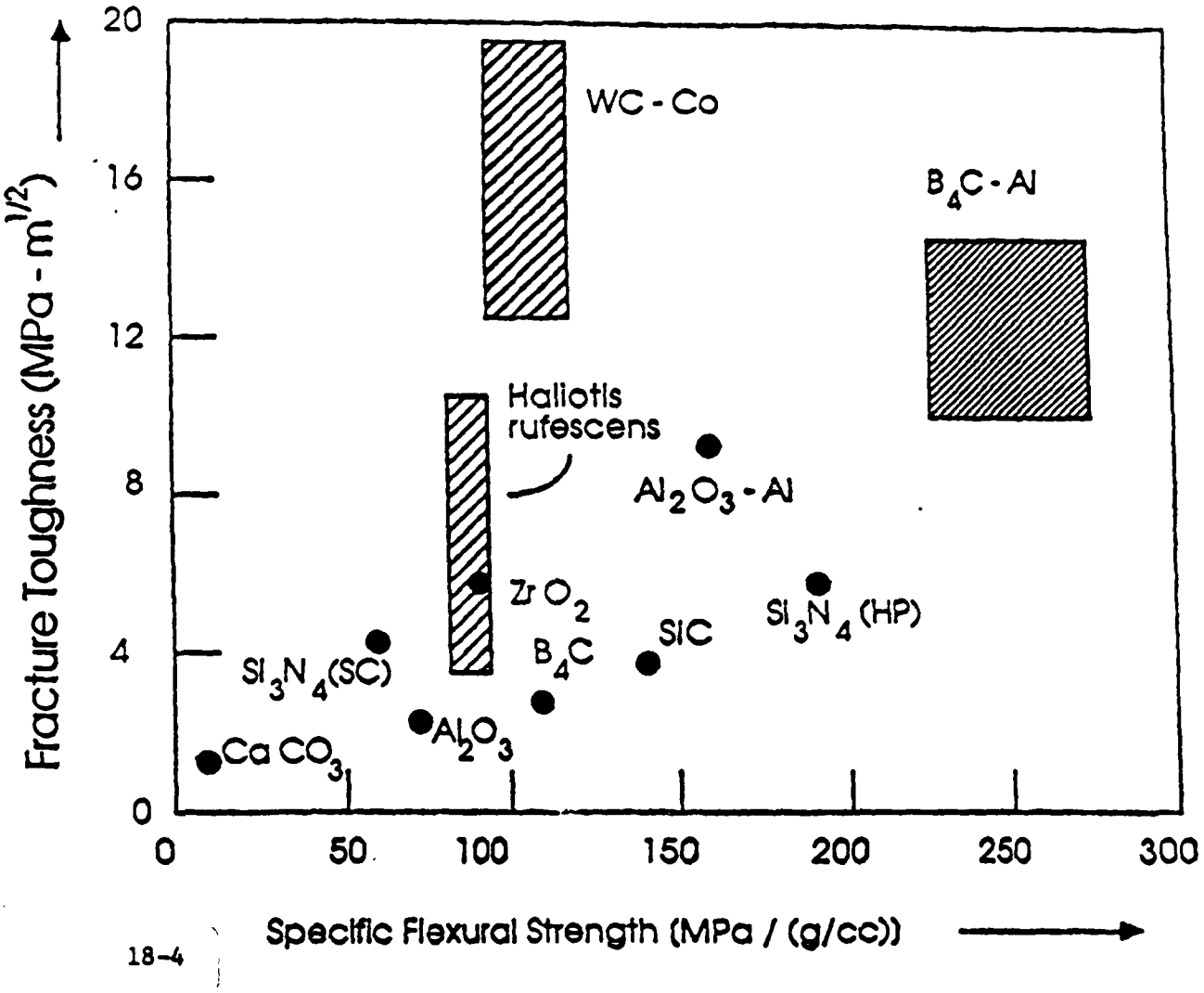
Fracture Toughness (MPa - m^1/2)
20
16
12
8
4
0
WC - Co
B4C - Al
Haliotis rufescens
Al2O3 - Al
ZrO2
Si3N4 (HP)
SiC
B4C
Si3N4 (SC)
Al2O3
Ca CO3
0
50
100
150
200
250
300
Specific Flexural Strength (MPa / (g/cc))

18-4

IMPACT BEHAVIOR OF 3-D COMPOSITES

Frank K. Ko
Fibrous Materials Research Center
Department of Materials Engineering
Drexel University

ABSTRACT

Biological tissues serve as excellent models for the design of highly damage resistant, strong and tough composites for medical or defense applications. A unique feature associated with most of these biological systems, ranging from sharkskin to bone, is their 3-D interconnected network of fibrous 'backbone'. Although we are far from having a synthetic system capable of coming close to the versatility of natural systems, a large family of 3-D fiber architectures are now available for the production of high impact resistant composites.

These 3-D fiber architectures can be produced by proper selection of textile processing techniques such as weaving, knitting, braiding or orthogonal fiber placement (Figure 1). The morphology of these structures can be linear or curvilinear. The structural integrity of the fiber architecture can be varied from low level (as in the orthogonal systems) to a high level of integration (as in the 3-D braids). According to programmed fiber placement sequence, these fibers may be organized into various structural shapes (Figure 2).[1]

3-D composites, exhibit much greater energy absorption than laminates , as demonstrated in the area under the impact response curves (Figure 3). As the level of fiber integration increases, the level of damage tolerance increases (Figure 3b,c)[2] . The insensitivity to impact damage of the 3-D composites was also demonstrated using 3-D braided PEEK/Carbon thermoplastic composites[3], wherein the residual compressive strength of the 3-D composites was shown to be 30 to 50% higher than that of comparable laminates. The most dramatic demonstration of impact tolerance was the ballistic response shown in Figure 4. These 3-D composites exibited the capability to withstand multiple strikes without loss of structural integrity. Similar damage resistant characteristics were also illustrated in 3-D braided FP Al_2O_3/Al-Li metal matrix composites. In comparison to unidirectionally reinforced composites, the 3-D composites exhibited fourfold increases (49 vs. 11 foot-pounds) in crack inhibition and twofold increases (145 vs. 83 ft-lbs) in propagation energy.

---

[1] Ko, F.K. "Three Dimensional Fabrics for Composites," Chapter 5 in Textile Structural Composites, T.W. Chou and F.K. Ko, eds, Elsevier, 1989, pp.129-171

[2] Ko, F.K. and Hartman, D., "Impact Behavior of 2-D and 3-D Glass/Epoxy Composites," SAMPE Journal, July/August, 1986, p.26

[3] Hua, C. and Ko, F.K., "Properties of 3-D Braided Commingled PEEK/Carbon Composites," Proceedings, SAMPE Technical Conference, September 24-26, 1989.

Figure Captions

Fig. 1 3-D Integrated fiber architecture.

Fig. 2 Net shapes produced by 3-D braiding.

Fig. 3 Dropweight impact response of 2-D and 3-D composites.

Fig. 4 Ballistic performance of 3-D braided epoxy resin composites.

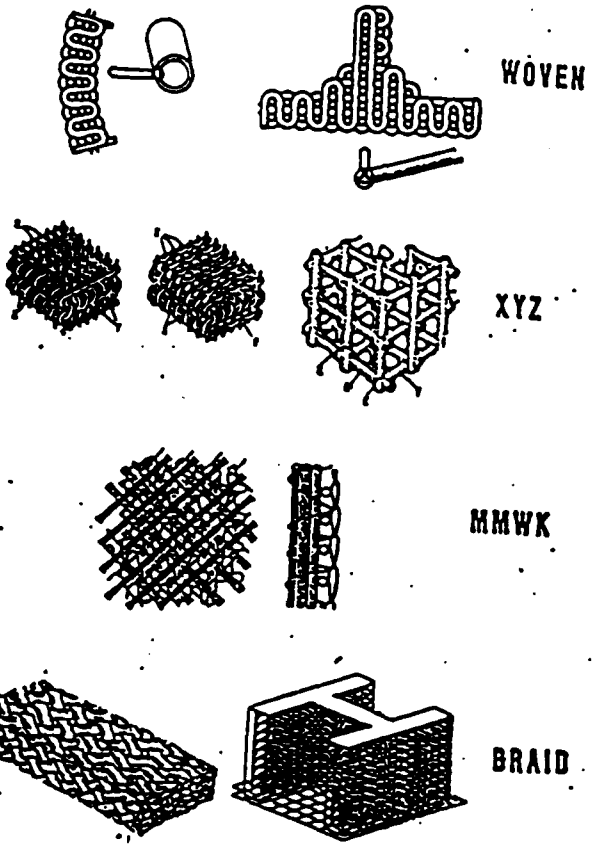

19-1

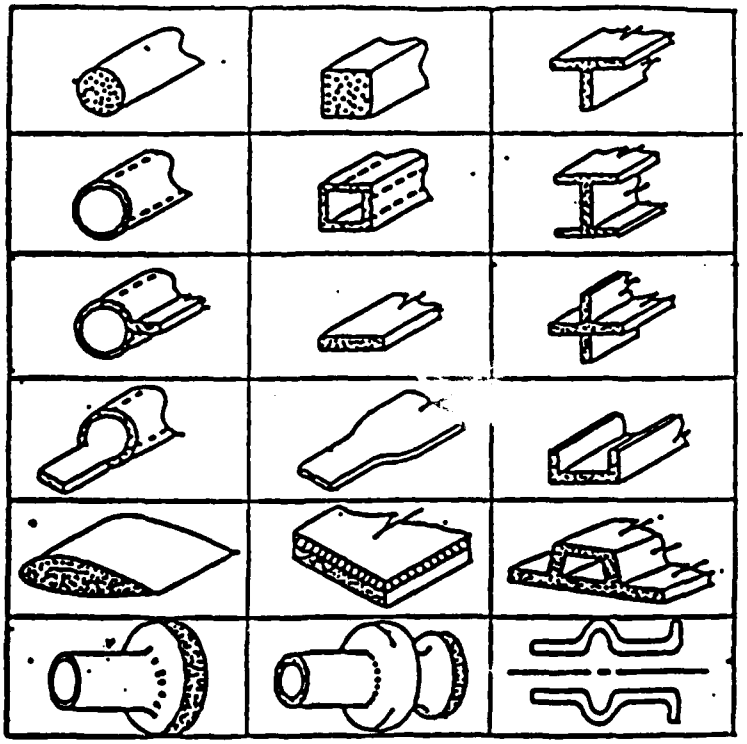

19-2

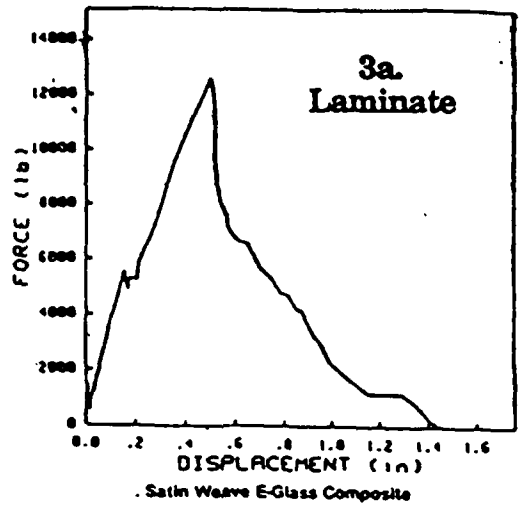

. Satin Weave E-Glass Composite

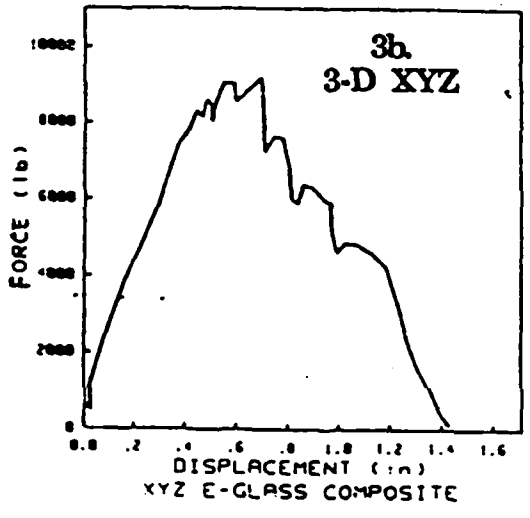

XYZ E-GLASS COMPOSITE

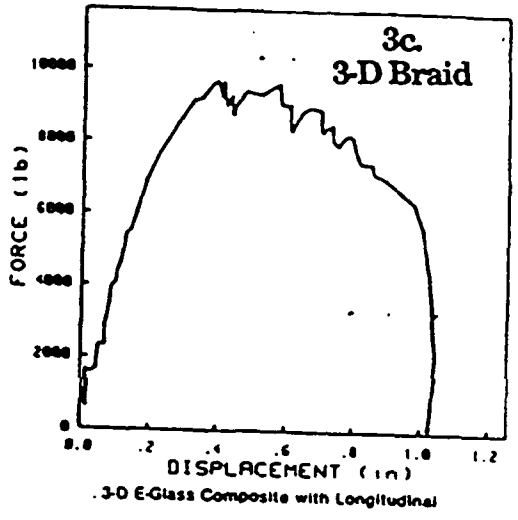

. 3-D E-Glass Composite with Longitudinal

19-3

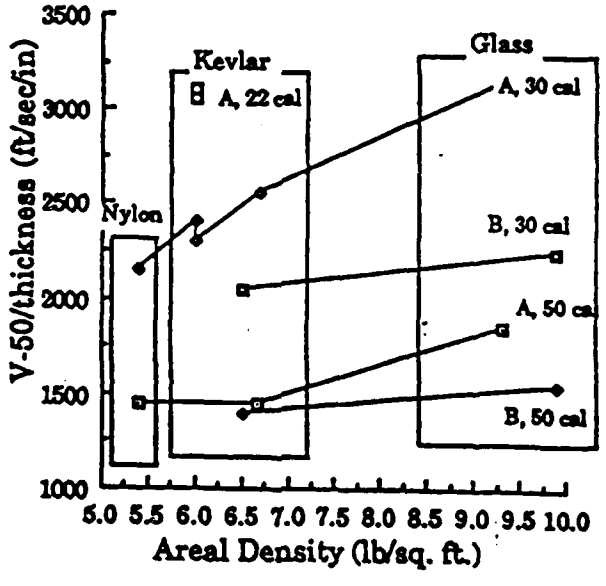

19-4

Figures 5 through 10 added for amplification of the lecture.

Fig. 5 Role of fiber architecture in composites: schematic diagrams of various textile braids.

Fig. 6 Structures and materials currently being used for soft tissue prostheses.

Fig. 7 Structural and mechanical properties of some human organs and tissues.

Fig. 8 Modeling of textile structural composites.

Fig. 9 Impact behavior of 2-D and 3-D glass/epoxy composites.

Fig. 10 (left) Effect of impact energy level on compression after impact strength for 3-D braid commingled and laminated carbon/PEEK composites.
(right) Effect of impact energy on damage area of 3-D braid commingled and laminated carbon/PEEK composites.

THE ROLE OF FIBER ARCHIETCTURE IN COMPOSITES

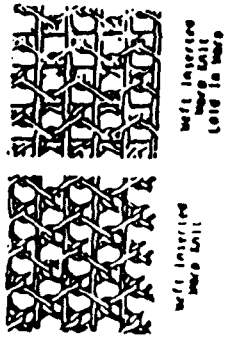

Structual Backbone

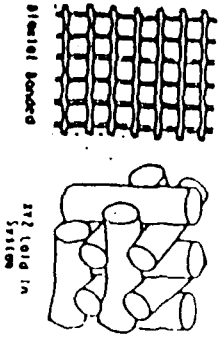

- Control Pore Geometry
- Control Fiber Orientation
- Control Fiber Packing Density (V_f)
- Structural Toughening
- Near Net Shape Manufacturing

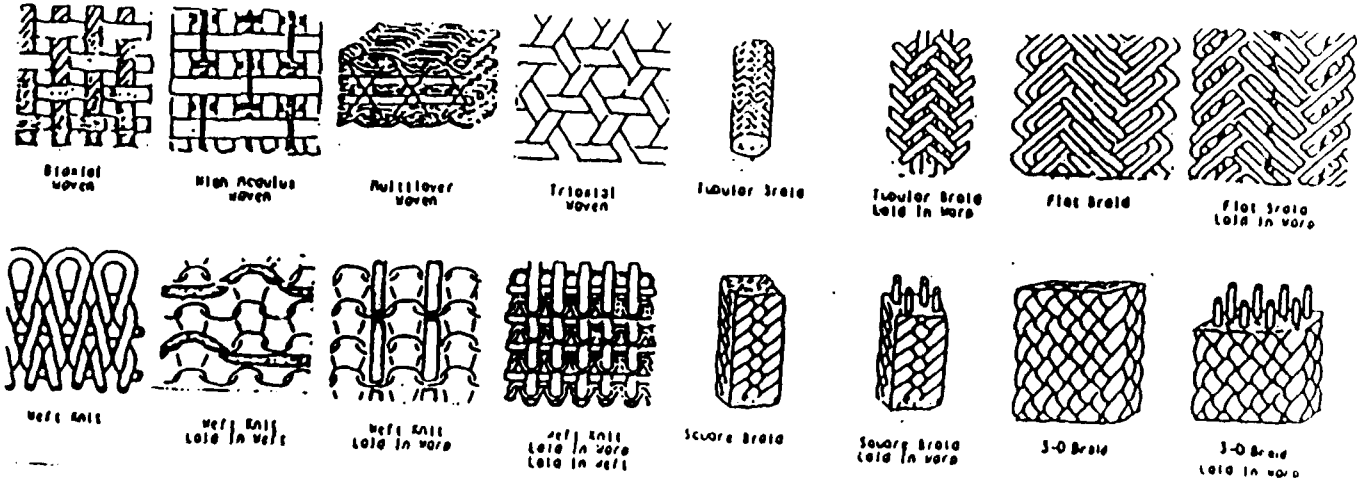

STRUCTURES AND MATERIALS CURRENTLY BEING USED FOR SOFT TISSUE PROSTHESES

APPLICATION	MATERIAL	STRUCTURE	
		yarn	fabric
Arteries	Polyester Dacron 56	textured	weft knit straight tube bifurcation plain woven straight tube
Tendon	Polyester Dacron 56	low twist filament	plain woven narrow tape coated with silicone rubber
Hernia Repair	Polypropylene	monofilament	tricot jersey knit
Esophagus	Regenerated Collagen	multifilament	plain weave
Heart Valve	Polyester Dacron 56	multifilament	plain weave
Patches	Polyester Dacron 56	textured	knitted velour
Sutures	Polyester	monofilament braided	
	Regen. Collagen	monofilament	

STRUCTURAL AND MECHANICAL PROPERTIES OF SOME HUMAN ORGANS AND TISSUES

	TENDON	KNEE LIGAMENT	SKIN	ARTERIES
Fiber Type	Collagen	Collagen	Collagen + Elastin	Elastin + Collagen
Fiber Orientation	parallel	oblique, spiral	random	spiral
Attachment	bone-tendon-muscle-bone	bone-ligament-bone	continuous	other organs
Function	load transmission	load carrying (hold bones together)	protect tissues	blood carrying
Tensile Strength	15-50 kg/mm^2	1.4-3 kg/mm^2*	.4-1 kg/mm^2	~.015 kg/mm^2
Breaking Elongation	4-10 %	15-30 %	50-100 %	9-30 %

MODELLING OF TEXTILE STRUCTURAL COMPOSITES

1. Modelling of the manufacturing process
2. Quantification of the fabric geometry
3. Modelling of the mechanical behavior

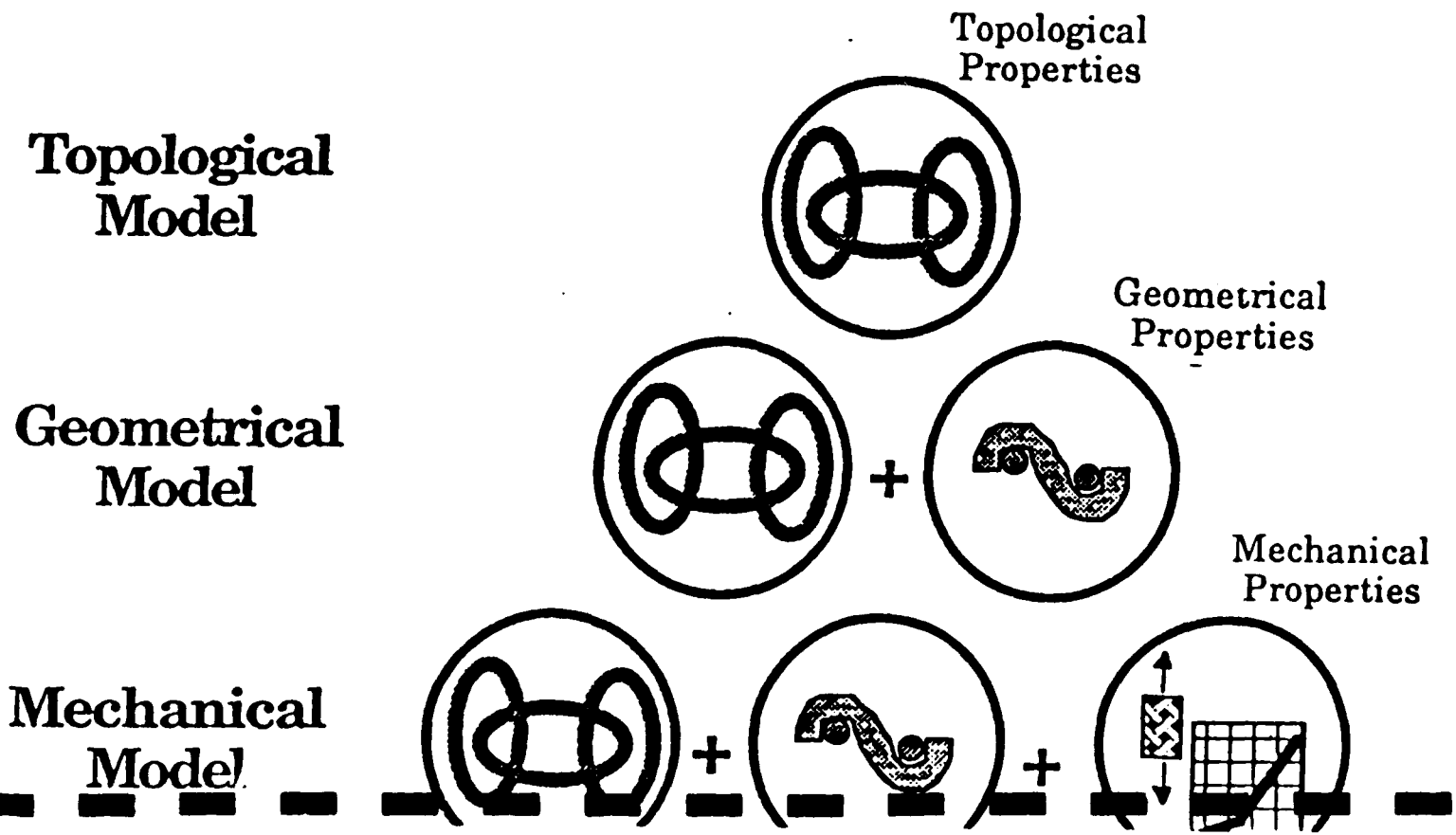

IMPACT BEHAVIOR OF 2-D AND 3-D GLASS/EPOXY COMPOSITES

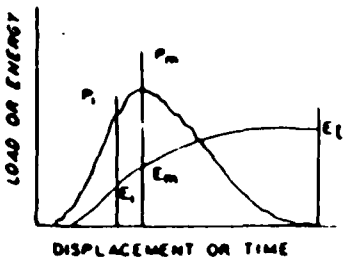

MAJOR POINTS OF INTEREST

P_i, E_i LOAD, ENERGY INCIPIENT DAMAGE POINT (BACK FACE CRACKING)

P_m, E_m LOAD, ENERGY AT MAXIMUM OR FAILURE POINT (THROUGH CRACK)

E_t TOTAL ENERGY (FULL PENETRATION)

E_p $E_t - E_m$, PROPAGATION ENERGY

Fig. 1. Instrumented Impact Testing

Table III.
Instrumented Impact Properties of Fabric Reinforced Composites

Sample		E_i (ft-lb)	E_p (ft-lb)	DI	E_m (ft-lb)	σ_m (psi)	ρ (lb/in^3)	t (in)
E-glass								
105	1x1x1	175 2	478 7	2 732	175 21	230 4	0 07	0 5
106	1x1x1 (L)*	119 8	545 3	4 558	119 84	311 2	0 071	0 516
107	1x1x1 (L)	214 5	424 8	1 981	214 48	395 2	0 072	0 675
108	XYZ	264 9	374 7	1 415	264 9	371 2	0 076	0 5
201	XYZ	174 1	284 4	1 634	458 46	247 2	0 072	0 437
202	Satin Weave	37 2	283 9	7 631	285 82	502 4	0 076	0 5
203	Plain Weave	28 3	344 2	12 181	288 4	459 2	0 074	0 5

ρ = density, DI = ductility index, t = thickness
* Sample split in two

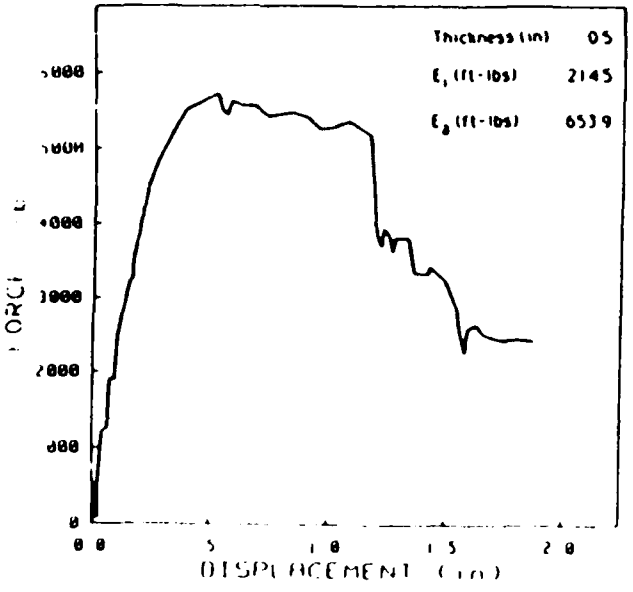

a. 1/0 Braid Glass Composite

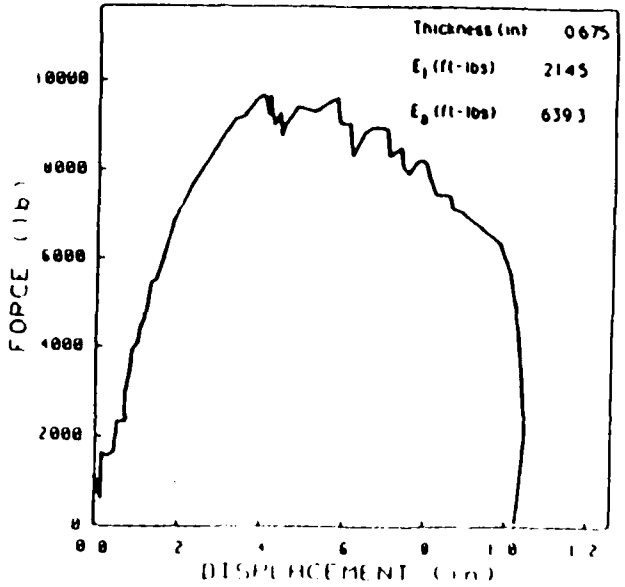

a. 3D E-Glass Composite with Longitudinal

FMRL

MATRIX PLACEMENT BY COMMINGLING

3-D Braided Commingled Carbon/Thermoplastic Composites

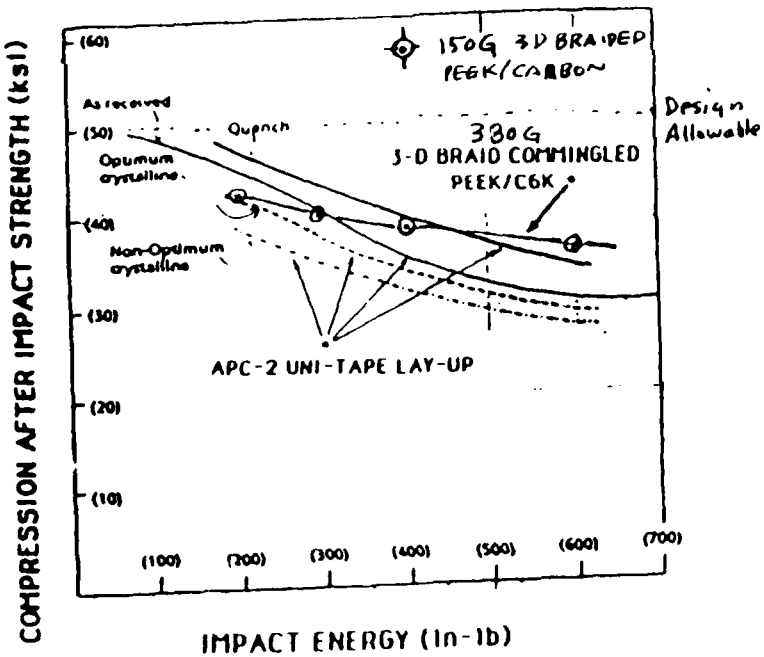

Effect of Impact Energy Level on Compression After Impact Strength for 3-D Braid Commingled and Laminated Carbon/PEEK Composites

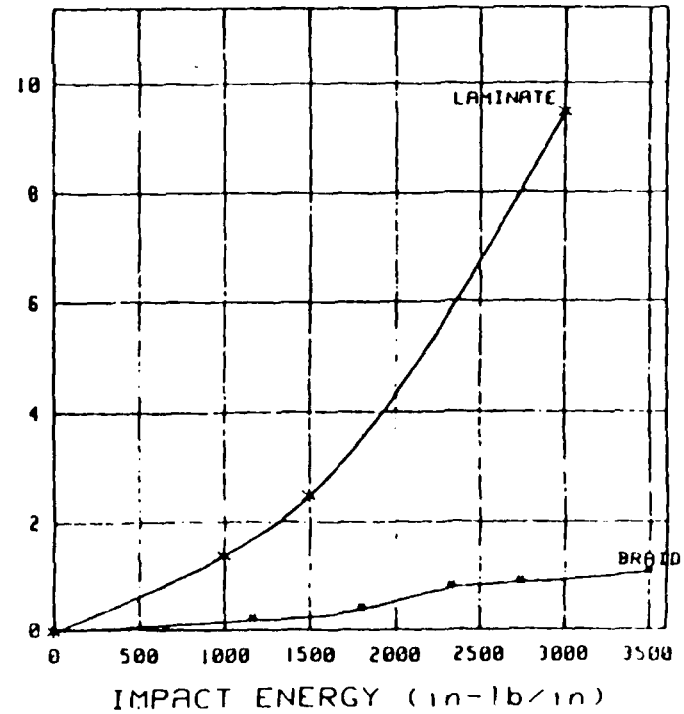

Effect of Impact Energy on Damage Area of 3-D Braid Commingled and Laminated Carbon/PEEK Composites

EMRL

ARO Workshop on "Biostructures as Composite Materials Systems", Cleveland, Ohio.

October 23-25 1989

Summary of group discussion

Members:

Professor W. Bonfield (Chairman)	QMW, University of London.
Professor I. Aksay	University of Washington
Mr. J. Cassidy	CWRU
Dr. R. Farrell	Johns Hopkins APL
Dr. Kaplan	US Army
Dr. L. Klein	CWRU
Dr. D. Wallace	Celtrix Laboratories
Professor W. Williams	CWRU

(1) Research opportunities

Processing of nano-scale composites.
Organisation of complex biological structures by electrical and magnetic fields.
Genetic regulation of polymer synthesis in biological solids.
Mechanisms of self assembly - modelling in collagen.
Modelling of mechanical property-structure relationships for biological tissues.
Control of size of basic building units.
Mechanical properties of ground substance.
Natural joint design and function.
Development of stable tissue-implant interfaces with an enhanced lifetime.
Interaction between different tissues, and the biological system.
Natural adhesives.

(2) Additional topics for possible consideration

Inorganic precursors.
Biomineralisation.
Computer simulation of self organising complex systems.
Resistant coatings (rice husk, micro-organisms).
Macromolecular models.
Biological materials from extreme environments (deep sea, high and low temperatures).
Damage mechanisms and failure modes.
Intelligent materials.
Biosensors.
Mechano receptors.
The tooth as a model system.

(3) Development of analogue materials

Design of multi functional composites.
Modification of existing natural materials to extend/change mechanical behaviour.
Establishment of limits of performance, particularly for time-dependent properties.
Study of repair mechanisms in natural materials and design of self-repairing replacement materials.
Three dimensional visualisation.

Consideration of macro-biological structures (coral reefs) and a general consideration of scaling effects.

(4) Resource requirements

Multi disciplinary sourcing of literature.
National and regional centres for special microscopic and analytical techniques.
Access to national laboratories for biostructures studies.
Development of microscopic techniques for directly examining wet tissues.

(5) Properties - some possibel advances

Comprehensive assessment of the heterogeneity of mechanical/physical properties of biological materials.
Department of spatial stress birefringence.
Gravitational effects on property structure relationships.
Physical basis of negative temperature coefficient of swelling coefficient of cornea.

(6) Rules of complexity

Thermodynamics

Scale and transformation
Surfaces and interfaces.
Adaption

plus

Kinetics

Rates and time constants.

ARO WORKSHOP

BIO-STRUCTURES AS COMPOSITE MATERIALS SYSTEMS

Issues and Opportunities for Future Research

L.J. Gibson

1. Characterization of biological materials

- a wide range of biological materials have been studied to some extent: silks, collagen, cellulose, chitin, cuticle, bone, shells, wood
- there is some understanding of the mechanisms by which some of these materials derive some of their properties
- not clear which materials and properties it would be advantageous to mimic
- need to identify interesting materials and properties
- in addition, need for futher work on understanding mechanisms by which biological materials derive their properties: characterization of microstructure, measurement of a broader range of properties (e.g. mechanical, electrical, magnetic, optical, thermal, acoustic, adhesion, interface properties, transport properties, response to environment) and identification and modelling of the mechanism(s) controlling the property

2. Design of artificial materials

- artitiicial materials may be used as implants in prosthetic devices (e.g. blood vessels, tendon)
- then the goal is to duplicate the behaviour of the natural material that implant is replacing (to avoid introduction of stress concentrations, for example)
- as initial focus, could try to produce artificial materials which mimic the general stress-strain response of many pliant materials (eg. collagen, skin, lung tissue)

- artificial materials may also be made for engineering components in non-biological applications
- then the goal is to design a material with improved properties by exploiting the mechanism by which the natural material derives its properties
- as initial focus, could try to produce an artificial material which mimics some of the crack stopping mechanisms of natural shell materials (eg. cross-lamellar shell or organic/inorganic composite shell structures such as nacre)

- in both instances, the goal is to design appropriate microstructures and to develop processing techniques which mimic the microstructure and/or the mechanism controlling the property in the biological material
- many natural materials integrate their microstructures at various levels, giving hierarchical structures; there is a need for the development of processing techniques which produce integrated hierarchical structures in man-made materials
- in conjunction with the development of processing techniques, there is a need for modelling the behaviour of natural materials and for application of the model's to microstructural design

3. Research on related interdisciplinary topics

- cell biology
- molecular engineering of self-reinforcing composites
- design engineers
- instrumentation: measurement of strain in biological materials

Report of Subcommittee

ARO WORKSHOP on

BIO-STRUCTURES AS COMPOSITE MATERIALS SYSTEMS

at Case Western Reserve University October 23-25, 1989

Subcommittee: Cowin, Fletcher, Hiltner, Kardos, Keith, McElhaney, Schick, and Wainwright (chair).

Our subcommittee felt unanimously that the workshop was a screaming success. The degree to which the papers given were made understandable across subject boundaries was noteworthy and the creative open-mindedness of the participants was outstanding. The breadth of the workshop was satisfyingly great and yet the quality of the speakers was such that many subjects were given in real, useful depth. It is rare indeed that such statements can be made about workshops and conferences! Obviously, the ultimate cause of this fine state of affairs is the percipience and judgment of Professor Eric Baer who knows a lot of smart people in the world, and who knows who will contribute usefully to such a broadly cast workshop.

Our subcommittee sought to list **promising research subjects** that lay in the path ahead, given the background we heard at the workshop:

(1) Biomineralization. This subject was touched on by various speakers and discussants. It is an exciting field in biology today as witnessed by the recent publications of 4 books on the subject in the past 2 years. In particular, the mechanism for controlling the structural hierarchy of mineralized tissues and synthetic materials would be a good subject to address in future. Nannophase and highly oriented ceramics caught our attention. We spent some time thinking that attention paid to invertebrate systems as model systems offered a very broad spectrum of hierarchical systems for study and contemplation. For example, sponges with their diverse array of fiber architecture, calcareous Green and Red seaweeds with interesting cell wall (as in Lorna Gibson's "cellular solids"), and the nearly perfectly oriented calcitic stereome of echinoderms promise to provide useful ideas for synthetics.

(2) **Environmental materials,** in contrast to materials for inside the human body, was an idea introduced by Dr. Kaplan in his brief acount of work going on at Nahant. Since **the environment** is clearly the *cause célèbre* of the brightest undergraduates and many governments now and for the next few years, our thinking should project our new synthetic materials and sytems into that all-important realm. Obvious aerospace materials may fall into this category, but we had in mind things closer to home. Materials that are environmentally smart may well have some very interesting features indeed. Some might have limited life-times and be biodegradable or self-degradable on a wide time scale. It may take us into really new ways of thinking.

(3) **Healing materials** have been on everyone's mind since biologists have been talking to materials scientists and engineers. What are possible mechanisms of healing? One could imagine an institute set up to ask this question! We wondered what possible combination of solids and fluids could allow a local change or healing or adjustment of properties. This is surely an area for the future.

(4) **Switches.** Every process needs a switch to turn it on and off. Perhaps the design of such mechanisms is less for the goup who met at this workshop than it is for electrical engineers. On the other hand, precisely what are switches in biosystems made of? *That* is a question for us. A switch must embody a structure. What is the range of interactions between mechanical stress and the electrochemistry of hierarchical materials? Here is another place where our materials and systems group can profitably interact in the future with electrical engineers.

(5) **Mechanoreceptors and other sensors** are associated with switches in our minds. Steve Cowin brought this up because he had read a stimulating account of recent work by biologists and engineers. Here again, we could well work together with sensory physiologists and electrical engineers to design the right materials for such nifty items. It would be especially nice to think about putting sensors and switches into the hierarchical structure of future materials.

(6) **Other interesting biomaterials and systems.** What can our group learn from the study of **hot spring bacteria** and the many higher organisms that live in the hot vents and reducing H_2S environment on the deep sea floor? **Coral reefs** are the only animal structures that are big enough on the earth's surface to be visible from a satelite. They are made of polycrystalline aragonite by "lowly" animals that harbor single-celled plants (dinoflagellates) inside their cells: the plant-animal symbosis permits the fast growth rates of skeletal material such that it accumulates in sufficient quantities to be important in controlling the circulation of the tropical oceans and the movements of ships. Can man do this by using or immitating biosystems?

ISSUES

1. Gaps in Knowledge

   A. Processing Paths Natural & synthetic
   B. Nucleation & Growth: sites, morphologies, transition states
   C. Kinetics
   D. Crystallographic Relationships
   E. Geometrical shape & size factors
   F. Molecular arrangements & rearrangements

2. Areas not discussed

   A. Fractals
   B. Non-linearity
   C. Surfaces & interfaces
      i. Adhesion
      ii. Layered structures

3. Artificial Materials Design and Construction

   A. Tailored composite systems

4. Other Natural Systems

5. Catalog of Resources

   A. Information
   B. Facilities

6. Properties

Physical & Chemical		Transport	
A.	Mechanical	G.	Mass
B.	Optical	H.	Charge
C.	Electrical	I.	Heat
D.	Magnetic		
E.	Thermal		
F.	Chemical		

7. Rules of Complexity

8. New Instrumentation probes

Appendix III

Proposal for Workshop

The proposed workshop on "Connective Tissues and other Bio-Structures as Hierarchical Composite Materials Systems" will focus on the structure-property relationships for these highly complex composite materials systems. In recent years, synthetic composites are being created to serve in ever more demanding use conditions, and subsequently, the design of the advanced composites of tomorrow will be tailored to function in unique environments. Subsequently, the lessons from biosystems which are highly specific and adaptive, should provide us with futuristic scenerios that may catalyze new concepts and composite designs.

The workshop will be designed to stimulate opportunities and also address problems that arise when materials are exceedingly complex. This necessitates an hierarchical systems approach to the design and synthesis of complex structures involving unique combinations of interacting solids. In some instances, the composite will actually become the structural component or "smart" device. We will discuss the analysis of complex behavior in natural polymeric systems in terms of hierarchies, an approach that interrelates our understanding of structure at various scales. Structural hierarchy is more than a convenient vehicle for description and analysis, and may prove invaluable in the design of new advanced materials. Important and difficult questions to be addressed include the physical and

chemical factors that give rise to relatively discrete levels of structure and the relations that govern their scaling.

The workshop is tentatively scheduled for the autumn of 1989 at Case Western Reserve University in Cleveland, Ohio. Comprehensive presentations by recognized experts in the field will be combined into an overall workshop style format. Discussions will be focussed to identify future scientific and technological priorities and needs.

1. Hierarchical Structure

Overview lectures and discussions of structural hierarchies in biocomposite systems including soft connective tissue, hard connective tissue (bone) and cellulosic structures (wood) will take place at the beginning of the workshop. Particular emphasis will be on the discrete nature (and scales) of hierarchical levels, and the highly specific interactions which must occur between levels. These interactions are necessary so that the overall composite structure can function to meet the high performance requirements of the overall system.

2. Molecular Deisgn and Information in Macromolecules

In order to attempt to understand the origins of hierarchical levels both at the nano and the micro scales, the constitutional and the conformational structure

of the biomacromolecules that are the macromolecular building blocks of connective tissue will be reviewed. In particular we will review the "information" in the fibrous protein, collagen, which is the fundamental building block in all varieties of connective tissue. This will be followed by a dialogue on mucopolysaccharides and glycoproteins which serve as the "glue" joining the hierarchical levels which are composed primarily of collagenous material.

3. Structure Property Relationships in Bio-Composites

We propose to discuss some key questions aimed at an understanding of the evolution of specific properties from the various levels of hierarchy. Specifically the mechanical and optical properties of these "smart" biocomposites will be considered. For example, in tendon we will consider a uniaxially oriented system that functions mechanically primarily in one direction, while in intestine the composite is a complex "lay-up" structure which must function multiaxially. Even with more thought provoking systems such as cornea, which functions as a coupled mechano-optical device, we will attempt to relate the optical properties to hierarchical structure within the cornea.